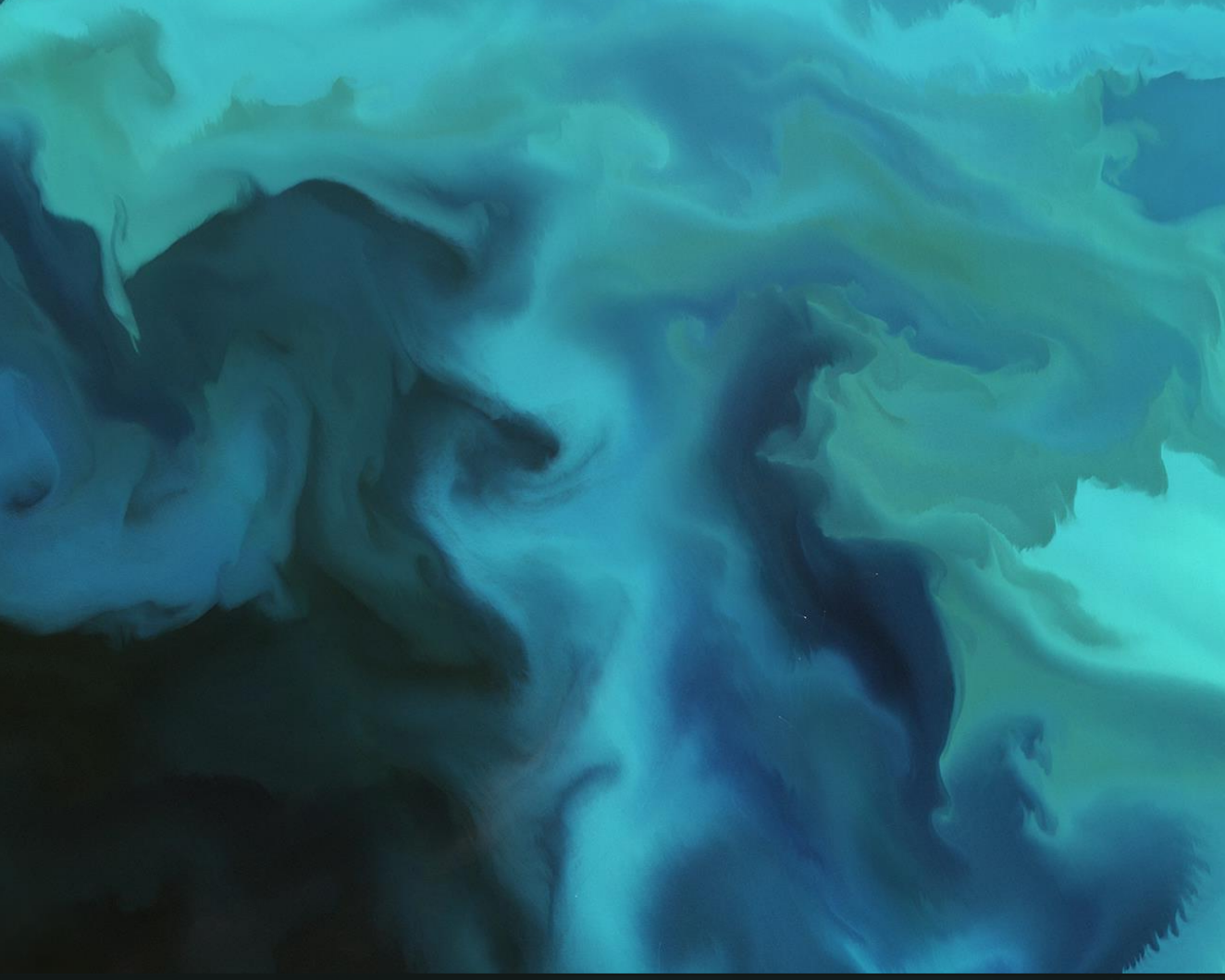

The **Organic Complexation** of **Iron** and **Copper** in **Marine Environments**

Veronica Arnone

Tesis Doctoral

Doctorado en Oceanografía y Cambio Global

Las Palmas de Gran Canaria

2024

ULPGC Universidad de Las Palmas de Gran Canaria | IOCAG Instituto Universitario de Oceanografía y Cambio Global

QUIMA QUÍMICA MARINA ULPGC

GOBIERNO DE ESPAÑA | MINISTERIO DE CIENCIA E INNOVACIÓN

UNIVERSIDAD DE LAS PALMAS DE GRAN CANARIA

ESCUELA DE DOCTORADO

Título de la Tesis

The Organic Complexation of Iron and Copper in Marine Environments

Tesis Doctoral presentada por Dª. **Veronica Arnone** dentro del Programa de Doctorado en Oceanografía y Cambio Global de la Universidad de Las Palmas de Gran Canaria y dirigida por la **Dra. J. Magdalena Santana Casiano** y el **Dr. Aridane González González.**

La Directora El Codirector La Doctoranda

(firma) (firma) (firma)

Las Palmas de Gran Canaria, a de de .

Acknowledgements

El desarrollo de esta Tesis Doctoral no habría sido posible sin el apoyo de mi entorno laboral y familiar, en el que incluyo a amigos y compañeros, que me han acompañado en este largo camino. En primer lugar, me gustaría dar las gracias a mis directores, los Doctores J. Magdalena Santana Casiano y Aridane González González, que han sido guías y mentores de este proyecto. A ellos he de agradecer el apoyo, la motivación y la orientación que me han ofrecido, así como su entusiasmo por la ciencia y las valiosas lecciones que trascendían la química y la oceanografía. En especial, quiero dar las gracias a Aridane por haber sido el pilar de este aprendizaje y por asesorarme sin descanso todos estos años. Gracias por los valiosos conocimientos, los inestimables consejos y por transmitirme el valor del trabajo en equipo. Extiendo los agradecimientos a mi tutor, el Dr. Melchor González Dávila, por la gran ayuda brindada en el desarrollo de este trabajo y las tan necesarias discusiones sobre química.

Mi gratitud se extiende al Ministerio de Ciencia e Innovación (Gobierno de España) ya que el desarrollo de esta Tesis ha sido posible gracias a la financiación concedida (PRE2018-084476), asociada al proyecto ATOPFe (CTM2017-83476-P).

Gracias al grupo QUIMA por acogerme todos estos años y, sobre todo, a todos los compañeros que hicieron más amenas las eternas horas de laboratorio. A Carolina, Adrián, David Curbelo y David González. Gracias por el apoyo, la ayuda y los cafés en compañía. Gracias también a los más nuevos, Adrián Bullón, Laura y Víctor, por recordarme lo feliz que fue el comienzo del camino. Por supuesto a la Dra. Norma Pérez, por los valiosos consejos y las lecciones de paciencia con los equipos. Un especial

agradecimiento a David González, en estos años nuestros caminos se cruzaron en tres momentos y lugares distintos y, en cada uno de ellos, puedo recordar momentos en los que di las gracias por contar con tu apoyo.

Quiero agradecer a la Dra. Géraldine Sarthou y la Dra. Hélène Planquette por hacer posible mi estancia en Brest, por aceptarme y brindarme de todo lo necesario. A Floriane, por estar siempre disponible e intentar ayudarme en todo momento. Y no me olvido del grupo de internacionales de Brest, con sus animadas noches de tacos y sidra. Gracias María, Natalia, José, Marc, Wen-Hsuan y Lucie.

Gracias a todos los amigos que estuvieron ahí en esos momentos de desconexión tan necesarios. A Carmen, Kristuel, Eduardo, Alejandro, Airam, Oihane, Galileo, Gonzalo, Borja, Raibel, Débora, Vero y Romi. A Elisabet y Jorge, gracias por acortar los kilómetros que nos han separado y estar ahí dispuestos a aguantar mis perretas, siempre con una sonrisa y buenos consejos. Y a todos aquellos con los que compartí una parte del camino.

Gracias a mis padres, que me han acompañado y apoyado todos estos años. A ellos que han aguantado mis silencios, mis ausencias y mi estrés de la mejor manera posible. Gracias por enseñarme el valor de una familia unida, que se quiere y se cuida por encima de todo.

Mis últimas líneas son para Héctor. Este camino te cogió de lleno y, sin saberlo, te convertiste en la persona que me animó a seguir. Gracias por romperme los esquemas, por enseñarme que hace falta poco para ser feliz, por entenderme y no entenderme a ratos. Has sido mi mayor apoyo, mi lugar seguro y si he llegado hasta aquí es también gracias a ti.

Summary

Trace metals are required by phytoplankton to form enzymes and proteins involved in photosynthesis, respiration and nutrient assimilation processes. The bioavailability of these trace metals determines ocean productivity and affects the rate of carbon sequestration, which has consequences for O_2 production and CO_2 uptake. Seawater contains natural organic ligands that complex dissolved iron (dFe) and copper (dCu) with important biochemical implications. The solubility, scavenging, bioavailability, and assimilation rates of dFe and dCu are determined by their complexation, which also impacts their residence time in the dissolved phase. Due to the heterogeneity of dissolved organic matter in seawater, identifying Fe and Cu-binding ligands has been challenging. However, it is possible to determine the concentration and binding strength of these compounds through voltammetric measurements.

Iron and copper-binding ligands were measured in different marine environments that have not been extensively studied in terms of organic speciation until now. On one hand, the concentration and binding strength of Fe and Cu-binding ligands were measured in coastal waters around oceanic islands in the Macaronesian region. Coastal surface waters showed higher ligand concentrations than open ocean surface waters. The observed distribution was related to hydrodynamic features that resuspend sediments and promote the biological activity around the islands.

On the other hand, the concentration and binding strength of Cu-binding ligands were studied in the Arctic region. Two studies were conducted, one over the Greenland shelf and Fram Strait, and the other over the central Arctic Ocean. High concentrations of Cu-binding ligands were observed in surface

waters, particularly above the shelf and close to the Greenland coast. The surface exhibited the highest concentration of Cu-binding ligands, which were associated with various sources, including coastal (glacial and coastal water discharge), autochthonous (exudates, organic matter degradation and/or bacterial remineralization), and allochthonous (sea-ice melting and Transpolar Drift export) sources. These sources are related to weaker compounds. In the central Arctic Ocean, Cu-binding ligands exhibit the maximum concentrations in the surface waters of the Amundsen and Makarov Basins and decreasing values towards the Barents Sea. The distribution of these ligands is influenced by water stratification and surface current circulations, especially the Transpolar Drift, which transports water from the Siberian shelves to the central Arctic. The ligands present in surface waters are associated with terrestrial organic matter and humic substances.

All of these studies have shown that the chemical speciation of dFe and dCu in the investigated regions was dominated by the formation of organic complexes, which keep the dissolved species in solution for longer periods of time. The observed concentration and distribution were strongly related to specific sources and influenced by complex water circulation pathways.

This PhD Thesis highlights the significance of investigating ligand concentration and binding strength to determine the residence time, bioavailability of essential trace metals in marine environments, and the properties of the ligands in order to better understand the marine biogeochemical cycles of Fe and Cu.

Thesis Preview

The following PhD Thesis, titled "The organic complexation of dissolved iron and copper in marine environments" was conducted at the Universidad de Las Palmas de Gran Canarias, in the Instituto de Oceanografía y Cambio Global (IOCAG), within the QUIMA group, as part of the Doctoral Program in Oceanography and Global Change (DOYCAG). The study was carried out in the framework of the ATOPFe project (CTM2017-83476-P) funded by the Ministerio de Ciencia e Innovación del Gobierno de España. The research was conducted with the support of an FPI grant (PRE 2018-084476), under the supervision of Dra. J. Magdalena Santana Casiano and Dr. Aridane González González.

The PhD Thesis starts with a detailed introduction that explains the critical aspects of organic complexation of iron and copper in seawater. It also analyses the importance of these trace metals and the factors that determine their organic speciation in the ocean. The subsequent three chapters present the research findings: "Iron and copper complexation in Macaronesian coastal waters" (Marine Chemistry, https://doi.org/10.1016/j.marchem.2022.104087); "Distribution of copper-binding ligands in Fram Strait and influences from the Greenland Shelf (GEOTRACES GN05)" (Science of the Total Environment, https://doi.org/10.1016/j.scitotenv.2023.168162); and "Natural copper-binding ligands in the Arctic Ocean. The influence of the Transpolar Drift (GEOTRACES GN04)" (Frontiers in Marine Science, https://doi.org/10.3389/fmars.2023.1306278). The three scientific publications that are included in the PhD Thesis were published in JCR journals (Q1). The PhD Thesis concludes with a comprehensive overview.

To conform to the regulations established by the Universidad de Las Palmas de Gran Canaria for PhD Thesis (BOULPGC. Art. 22, 27 January 2023), the document includes a summary in Spanish with a general introduction, objectives, and conclusions.

Content

Image: ESA/ Copernicus Sentinel-2A data (2016).

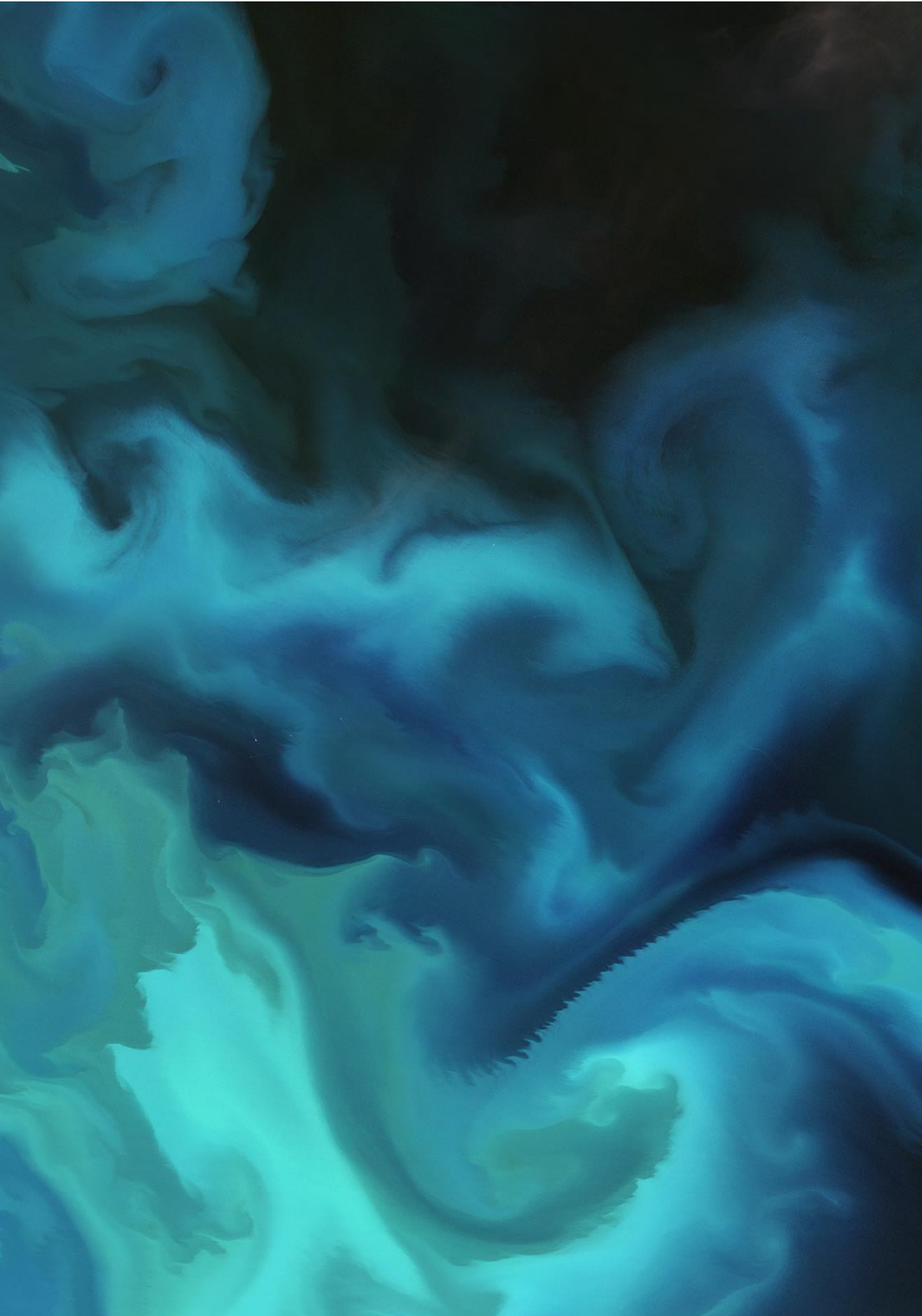

Chapter 1. Introduction

1.1 Trace metals in the ocean

The biogeochemistry of trace metals in seawater has garnered significant attention in the last decades. Numerous studies have explored the relationship between bio-essential trace metals, the carbon cycle, and climate change. Certain trace metals have an intricate interplay with the carbon sequestration in the marine environment due to their role in the phytoplankton growth. The ocean is one of the largest sinks of carbon dioxide (CO_2) and absorbs nearly 26% of CO_2 produced by human activities (Friedlingstein et al., 2023). Phytoplankton performs a significant portion of this uptake and carbon sequestration, requiring multiple nutrients, including numerous trace metals.

Many trace metals in seawater, such as iron (Fe) and copper (Cu), are essential micronutrients whose availability affects ocean productivity and biogeochemistry (Sunda, 1989; Morel and Price, 2003; Boyd and Ellwood, 2010; Tagliabue et al., 2017). Dissolved iron (dFe) and copper (dCu) play a crucial role as co-factors in different physiological functions of phytoplankton (Table 1.1), including photosynthesis, respiration, and nutrient assimilation processes (Twining and Baines, 2013). The availability of dFe and dCu is crucial in primary production and high concentrations of Cu in seawater can have toxic effects and limit phytoplankton growth (Morel et al., 1978; Sunda and Lewis, 1978; Brand et al., 1986). However, the distribution of these metals in the ocean is not uniform (Bruland et al., 2014) and not all the physical and chemical forms in which they are present in seawater can be assimilated (Morel et al., 2008; Morel and Price, 2003). Therefore, it is essential to understand the distribution of these trace metals and the physico-

chemical processes that affect them in order to determine their biogeochemical cycles and their impact on ocean productivity.

Iron is the fourth most abundant component in the Earth's crust (McDonough and Sun, 1995). In oceanic waters, Fe is present at subnanomolar levels due to its low solubility in oxygenated waters (Liu and Millero, 2002). Fe is essential for photosynthesis, respiration and nitrate fixation processes (Table 1.1), so the low level of dFe limit the phytoplankton growth (Boyd et al., 2007; Hutchins and Bruland, 1998). The importance of Fe in oceanic primary production was recognized since the 1930s (Hart, 1934). In the late 1970s, the development of trace-metal clean sampling and analytical methods (Bruland et al., 1979) allowed for successful measurements of dFe concentrations (Gordon et al., 1982; Landing and Bruland, 1987). The role of dFe as potential primary production limiting factor was demonstrated in the 1990s, based on shipboard experiments of Fe-enrichments in natural waters (Martin et al., 1990; Martin and Fitzwater, 1988). Based on that, the “iron hypothesis” postulated by Martin (1990), suggested that during glacial periods the increased input of Fe-rich dust stimulates phytoplankton productivity, due to a major nutrient utilization, and leads to enhanced atmospheric CO_2 drawdown. Enrichment experiments have demonstrated the complexity of the oceanic Fe biogeochemical cycle and the necessity of further research (Boyd et al., 2007; de Baar et al., 2005). Nowadays, dFe is widely recognized as a limiting factor of primary production in the open ocean and upwelling regions (Boyd et al., 2000; de Baar et al., 2005; Hutchins and Bruland, 1998; Martin and Fitzwater, 1988). However, the availability of macro- and micronutrients other than dFe, such as nitrogen, phosphorous or cobalt, can also limit phytoplankton growth (Moore et al., 2013).

Table 1.1. Enzymes and proteins containing trace metals as co-factors (Twining and Baines, 2013).

Metal	Enzymes and Protein	Function
Fe	Cytochromes	Electron transport in photosynthesis and respiration
	Ferredoxin	Electron transport in photosynthesis and N fixation
	Other Fe-S proteins	Electron transport in photosynthesis and respiration
	Nitrate and nitrite reductase	Conversion of nitrate to ammonia
	Chelatase	Porphyrin and phycobiliprotein synthesis
	Nitrogenase	N fixation
	Catalase	Conversion of hydrogen peroxide to water
	Peroxidase	Reduction of reactive oxygen species
	Superoxide	Disproportionation of superoxide to hydrogen peroxide and O_2
Cu	Plastocyanin	Photosynthesis electron transport
	Cytochrome oxidase	Mitochondrial electron transport
	Ascorbate oxidase	Ascorbic acid oxidation and reduction
	Superoxide dismutase	Disproportionation of superoxide to hydrogen peroxide
	Multicopper ferroxidase	High-affinity transmembrane Fe transport

Copper is less abundant than Fe in the Earth crust (McDonough and Sun, 1995) and, similar to dFe, dCu is at subnanomolar concentrations in seawater. Enzymes that contain Cu play a role in photosynthesis, respiration, Fe assimilation, and denitrification processes (Table 1.1, Twining and Baines, 2013). However, Cu has a dual effect on marine microorganisms, as it can be toxic at certain levels and its tolerance varies between species (Sunda and

Lewis, 1978; Brand et al., 1986). Thus, the availability of dCu, both in excess and deficiency, is crucial for phytoplankton development.

The phytoplankton requirement of dFe and dCu varies between species and is affected by other nutrient availability (Ho et al., 2003; Twining and Baines, 2013). For example, Fe is required for nitrate reductase and cells that grow in nitrate-rich waters present a higher Fe demand, as they need to reduce nitrate into ammonium before assimilation (Maldonado and Price, 1996). On the other hand, under Fe-limiting conditions Cu requirements increase, as Cu is involved in the high-affinity Fe transport system (Maldonado et al., 2006). Based on laboratory cultures, the average elemental composition of marine eukaryotic phytoplankton is defined by an extension of the Redfield formula $(C_{124}N_{16}P_1S_{1.3}K_{1.7}Mg_{0.56}Ca_{0.5})_{1000}Sr_5Fe_{7.5}Zn_{0.8}Cu_{0.38}Co_{0.19}Cd_{0.21}Mo_{0.03}$ (Ho et al., 2003). However, substantial differences were detected between studies conducted in laboratory conditions and natural waters related to the composition of the culture media employed (Twining and Baines, 2013).

1.2 Iron and copper speciation in seawater

In seawater, trace metals can exist in different physical and chemical forms, known as speciation, which determines the properties, reactivity, processes, and the behaviour of the elements. Factors, such as seawater temperature, pH, salinity, oxygen, and complexation with organic compounds play a critical role in the bioavailability of these metals in the ocean. According to the Intergovernmental Panel on Climate Change (IPCC) reports on climate change, all these parameters are changing in the ocean (IPCC, 2021) with impacts on trace metals biogeochemical cycles (Hoffmann et al., 2012). In this sense, the GEOTRACES program (https://www.geotraces.org/)

significantly contributed to the current knowledge of trace elements in the ocean. This international programme investigates the biogeochemical cycles and large-scale distribution of trace elements and their isotopes in the marine environment. The scientific community involved in this programme has successfully created an open-access database containing information on the physical and chemical speciation of Fe and Cu in the ocean. This database can be found in the eGEOTRACES Electronic Atlas (https://www.egeotraces.org/).

The **physical speciation** of a trace metal (M) is operationally defined based on the filtration pore size (Gledhill and Buck, 2012). The total seawater trace metals concentration (M_{total}) comprises the particulate (pM, particle collected on filters with 0.45 μm or 0.2 μm pore size) and the dissolved metal (dM, particles size less than 0.2 μm). The dissolved phase can be divided into the colloidal (cM, particle size between 0.02 and 0.2 μm) and soluble fractions (sM, particle size less than 0.02 μm).

$$M_{total} = pM + dM = pM + cM + sM \quad (1.1)$$

Dissolved trace metals are usually collected from seawater using 0.2 μm pore size filters, as recommended by the GEOTRACES protocol (Cutter et al., 2017). The importance of the dissolved fraction is related to the biological activity, as phytoplankton can assimilate dissolved nutrients (Sunda, 1989). The proportion of dM present in the seawater varies according to the pH, the formation of complexes with organic compounds, the concentration of dissolved oxygen, the salinity, and the precipitation into hydroxides (Millero, 2013; Millero et al., 1995). The distribution of dFe and dCu in seawater has been studied in different marine environments (estuaries, coasts, shelf and open waters) and oceans. However, to date there are more studies on the distribution and speciation of Fe than of Cu in seawater.

In terms of **chemical speciation**, trace metals can be classified into organic and inorganic species. The pH, redox potential, ionic strength, and presence of organic compounds are among the factors that affect the chemical status of trace metals. According to Gledhill and Buck (2012), from a chemical perspective trace metals can be categorized as labile inorganic complexes (M', including free metal), organic ligand complexes (ML), and non-labile metals (M_{inert}).

$$M_{total} = M' + ML + M_{inert} \quad (1.2)$$

It is important to highlight the redox speciation of Fe and Cu. Iron exists in seawater as ferrous and ferric ions, Fe(II) and Fe(III), respectively. In oxygenated waters, Fe(II) undergoes oxidation into Fe(III) in a question of minutes, depending on the physico-chemical properties of the seawater (Figure 1.1, Millero et al., 1987; González-Dávila et al., 2005; Santana-Casiano et al., 2005; González-Dávila et al., 2006; González et al., 2010a; Samperio-Ramos et al., 2018a, 2018b). Fe(III) is the dominant and thermodynamically stable form of Fe (Kuma et al., 1996; Millero, 1998). Under oxidising conditions and at a pH of 8, the solubility of Fe(III) is greatly reduced (Liu and Millero, 2002). Fe(III) tends to precipitate and undergoes scavenging; however, the presence of organic ligands keeps Fe in solution for longer period of time (Arreguin et al., 2021; González et al., 2019; Millero et al., 1995). In fact, more than 99% of the dFe is complexed with organic ligands (Gledhill and van den Berg, 1994) and these ligands can accelerate, retard or not affect the Fe(II) oxidation in seawater (Santana-Casiano et al., 2000). At the same time, low concentrations of Fe(II) can be detected in seawater as a result of in situ Fe(III) reduction processes (González-Santana et al., 2023; Sarthou et al., 2011), interaction with metal-binding ligands

(Arreguin et al., 2021; González et al., 2019; Rose and Waite, 2003; Samperio-Ramos et al., 2018a, 2018b; Santana-Casiano et al., 2014, 2010, 2000) and or photochemical reactions (Miller et al., 1995; Waite and Morel, 1984).

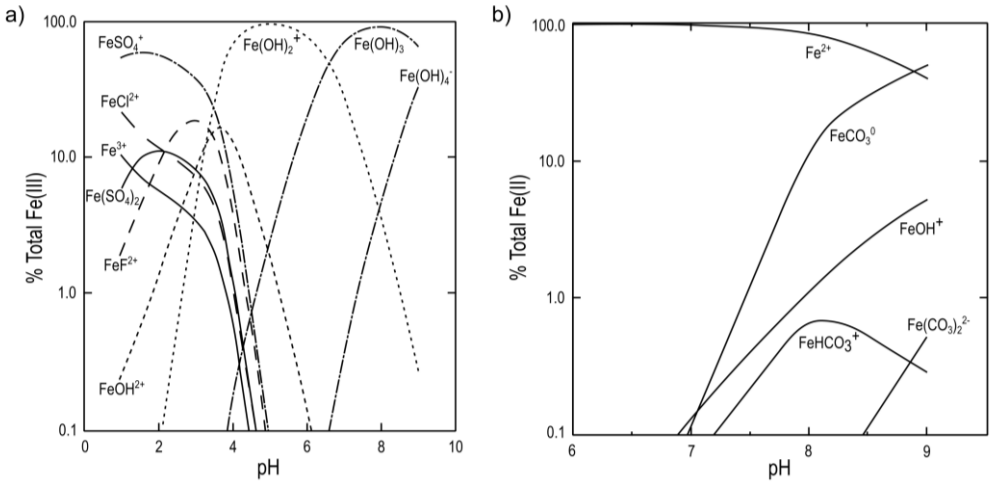

Figure 1.1. Seawater speciation of a) Fe(III) and b) Fe(II), determined at 25ºC and S=35. Figures from Millero et al. (1995).

In seawater, Cu predominantly occurs in two oxidation states: cuprous and cupric cations, Cu(I) and Cu(II), respectively. The more stable and abundant species is Cu(II), while Cu(I) constitutes approximately 5% to 10% of the total Cu content (Moffett and Zika, 1983). Cuprous ions rapidly oxidise in seawater and are influenced by several factors, including oxygenation, temperature, bicarbonate concentration, and interactions with major ions such as Ca^{2+} and Mg^{2+} (González-Dávila et al., 2009; Moffett and Zika, 1983; Pérez-Almeida et al., 2013). Reduction of Cu(II) to Cu(I) take place in surface waters owing to photo-oxidation of dissolved organic matter (DOM, Zika, 1981), and Cu(II) interacts with OH^-, Cl^-, SO_4^{2-} and CO_3^{2-} (Figure 1.2). However, the complexation of Cu(II), as observed with carbonate ions,

inhibits this reduction process, which may lead to increased oxidation rates (Moffett and Zika, 1983). In seawater, more than 99% of dCu is primarily complexed with organic ligands. Only 1% of dCu exists as free Cu^{2+} cations, which can adversely affect cell growth and viability, specifically at high concentrations. Studies conducted on cyanobacteria, coccolithophores and diatom species have revealed a toxicity limit of 10 pM for Cu^{2+} (Sunda and Lewis, 1978; Brand et al., 1986), while concentration lower than 0.001 pM can limit the phytoplankton growth rates (Annett et al., 2008). However, complexed Cu could be accessible to phytoplankton communities and sustain the growth under Cu^{2+} limiting conditions (Annett et al., 2008; Semeniuk et al., 2015).

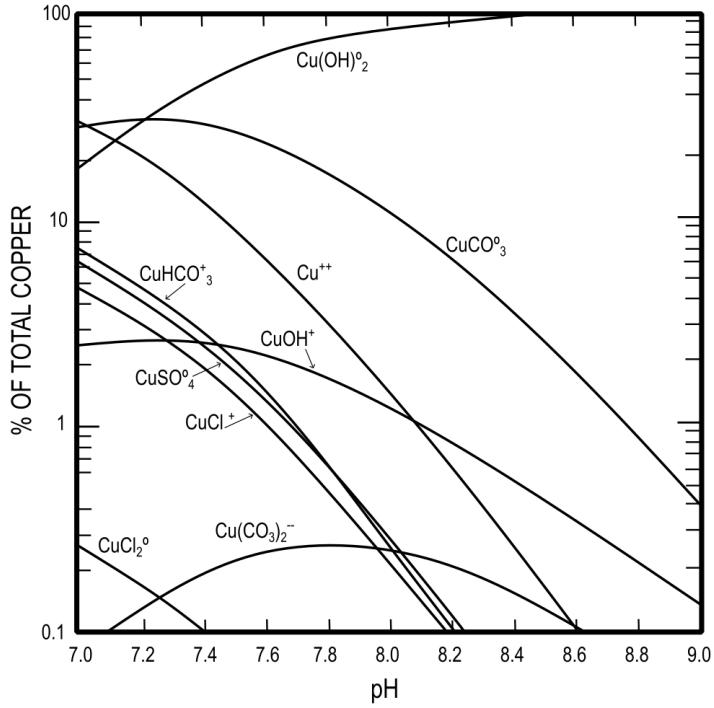

Figure 1.2. Seawater speciation of copper, determined at 25ºC. Figures from Zirino and Yamamoto (1972).

The interaction between Fe and Cu has been studied in terms of redox reactions (Figure 1.3, González et al., 2016; Pérez-Almeida et al., 2019). The presence of Cu(II) and Cu(I) in solution accelerates the oxidation of Fe(II) in seawater due to the interaction of both metals with hydroxyl, H_2O_2, $O_2^{\bullet-}$, and carbonate groups. In turn, Cu(II) is rapidly reduced to Cu(I) in the presence of Fe(II), whereas the oxidation rate of Cu(I) increases in the presence of Fe(III). At the same time, Fe and Cu species can be formed (cuprous and cupric ferrite).

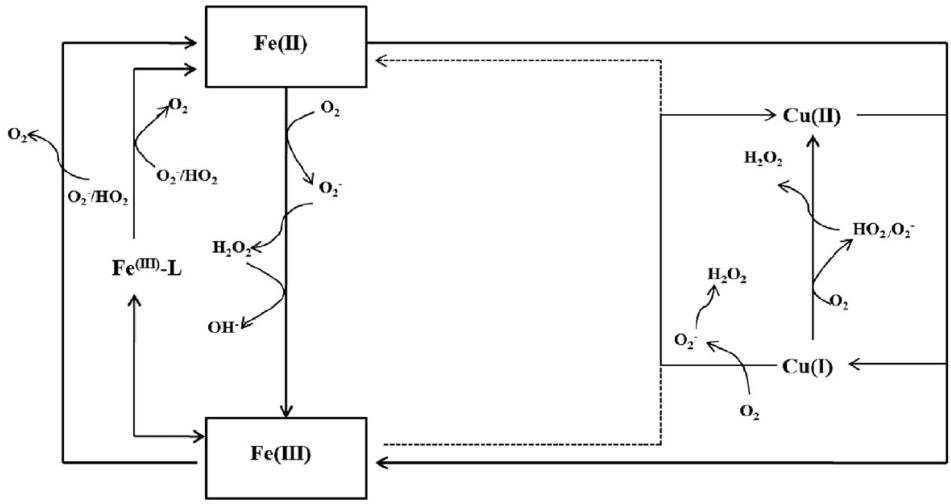

Figure 1.3. Redox reactions and interactions between Fe and Cu in seawater. Figure from González et al. (2016).

As mentioned above, the speciation of both dFe and dCu in seawater is controlled by the formation of complexes with natural organic compounds called ligands. Despite the importance of ligands in Fe and Cu chemistry in the ocean, there is a lack of knowledge about them. Ligands controls Fe solubility, avoiding the formation and precipitation of oxyhydroxide

compounds, and increasing the Fe residence time in the dissolved phase in seawater (Liu and Millero, 2002; Rue and Bruland, 1995). For Cu, the formation of complexes moderates the scavenging rates and diminish the Cu^{2+} concentrations, controlling its toxic effect on phytoplankton species (Brand et al., 1986). Simultaneously, complexed trace metals can be assimilated by phytoplankton thought specific cellular mechanisms (Morel et al., 2008; Semeniuk et al., 2009; Sutak et al., 2020; Walsh et al., 2015).

Ligands represent a heterogeneous group of compounds consisting of a variety of functional groups, some of which are specific for Fe or Cu, while others are capable of complexing both trace metals. The competition between dFe and dCu has been described for different compounds, but this does not mean that they have the same affinity (Abualhaija et al., 2015; Rue and Bruland, 2001). A list of some characterised ligands in the ocean is presented below:

- **Siderophores:** dFe-binding ligands with low molecular weight released by marine bacteria and cyanobacteria under metal stress conditions, particularly under Fe-limiting availability (Rue and Bruland, 1995; Vraspir and Butler, 2009). Siderophores have also been proposed as dCu-binding ligands, but they have not yet been characterized (McKnight and Morel, 1980).

- **Thiols:** organo-sulphur compounds (glutathione, cysteine, arginine, among others) released by marine microorganisms and capable of complexing dCu and dFe (Dupont et al., 2004; Laglera and Monticelli, 2017; Leal et al., 1999). Thiols can be found in estuaries, coastal and open ocean environments, and hydrothermal vents (Dryden et al., 2007; Dupont et al., 2006; Sander et al., 2007; Tang et al., 2000).

- **Humic substances:** includes humic and fulvic acids able to complex both dFe and dCu in seawater, which can be found in estuaries, coastal and open ocean waters (Abualhaija et al., 2015; Gao and Guéguen, 2018; Laglera et al., 2019, 2007; Laglera and van den Berg, 2009; Muller and Batchelli, 2013). Humic substances in seawater are associated with terrestrial or marine origins, both of which are associated with the decomposition of organic matter.

- **Phenols:** compounds able to complex both dFe and dCu (Munin and Edwards-Lévy, 2011), exudates of diatoms and green algae under metal stress conditions (López et al., 2015; Rico et al., 2013; Santana-Casiano et al., 2014). The interaction between different polyphenols and dFe has been determined in laboratory studies (Arreguin et al., 2021; González et al., 2019; Samperio-Ramos et al., 2018c).

- **Methanobactins:** multidentate Cu-binding ligands released by methanotrophic bacteria to meet metabolic requirements (Choi et al., 2006) found in estuaries, open ocean waters, deep sea sediments and hydrothermal vents (Ruacho et al., 2022).

- **Domoic acid:** toxic amino acid released by certain *Pseudo-nitzschia* species, capable of increasing dFe availability and controlling dCu toxicity (Rue and Bruland, 2001).

- **Porphyrins:** Fe-binding ligands contained in algal pigments and released into seawater by exudates or zooplankton grazing (Hutchins et al., 1999).

- **Exopolysaccharides:** ligands produced by eukaryotic phytoplankton, as well as heterotrophic and autotrophic bacteria, capable of complexing

both Fe and Cu (González et al., 2010b; Hassler et al., 2011; Norman et al., 2015).

1.3 Iron and copper biogeochemical cycles

The distribution and abundance of trace metals in the oceans is controlled by a combination of processes involving physico-chemical mechanisms, ocean circulation, sinks and sources (Bruland et al., 2014). Dissolved Fe and dCu share common biogeochemical processes that control their distribution and some specificities that affect one metal more than the other. In general, the variability observed for both trace metals depends on the geographical location and the associated sources (Figure 1.4). Since the formation of complexes with organic binding ligands controls the speciation of both dFe and dCu, different autochthonous and allochthonous sources of Fe and Cu-binding ligands must be taken into account (Gledhill and Buck, 2012; Ruacho et al., 2022).

Coastal regions receive riverine discharge, which supply dFe and dCu to the coastal zone. **Riverine inputs** are irregular due to their non-homogeneous location and varying geographical and temporal flow. These elements are predominantly discharged from rivers in either dissolved or particulate form. However, they are mostly eliminated through flocculation and sedimentation at the river-sea interface, due to the salinity gradient (Sholkovitz, 1978). Approximately 95% of Fe and 40% of Cu were removed during estuarine mixing and exhibit a non-conservative behaviour (Sholkovitz, 1978). Although removal processes do occur, a fraction of these trace metals can still be transported to the ocean. At a global scale, introduce approximately $6.7 \cdot 10^{9}$ mol Cu yr^{-1}, making them the primary source of dCu in the ocean (Richon

and Tagliabue, 2019). In contrast, the amount of dFe introduced, on the other hand, is $2.7 \cdot 10^{10}$ mol Fe yr^{-1} (Jickells et al., 2005). Riverine DOM contains different groups of metal-binding ligands that bind to trace metals, keeping them in solution. However, some of this organic matter also flocculates (Kogut and Voelker, 2001; Buck et al., 2007a; Hollister et al., 2021). Riverine inputs of trace metals and ligands are typically observed in coastal areas, but in the Arctic Ocean the importance of these inputs extends to the open ocean (Guieu et al., 1996; Opsahl et al., 1999; Stedmon et al., 2011; Anderson and Amon, 2015; Charette et al., 2020).

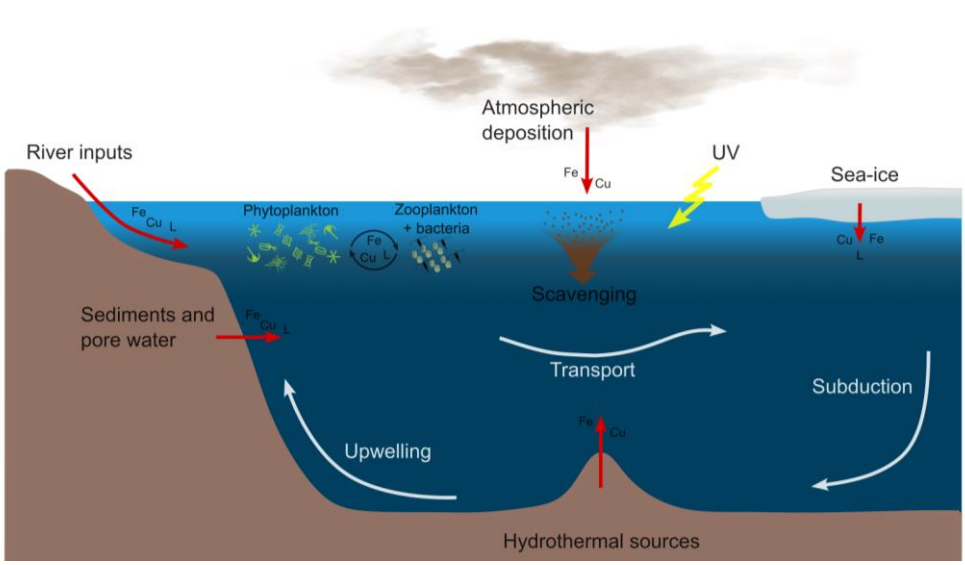

Figure 1.4. Marine biogeochemical cycle of iron (Fe), copper (Cu) and metal-binding ligands (L). Red arrows indicate source mechanisms, while white arrows represent physical transport mechanisms. Figure adapted from Tagliabue et al. (2017) and Ruacho et al. (2022).

Coastal glaciers also discharge freshwater along with significant loads of terrigenous materials, including particulate and dissolved trace metals. Fluxes of dFe and dCu vary considerably between regions, with values reported for

the Greenland Ice Sheet (mean fluxes of $1.3 \cdot 10^9$ mol Fe yr^{-1} and $5.9 \cdot 10^6$ mol Cu yr^{-1}) being much higher than for the Antarctic Ice Sheet (mean fluxes of $1.4 \cdot 10^9$ mol Fe yr^{-1} and $2.9 \cdot 10^6$ mol Cu yr^{-1}, Hawkings et al., 2020). On the other hand, icebergs, which form as glaciers calve, transport materials that were released during melting toward the open ocean. Sea-ice also incorporates sediment, trace metals, organic matter and metal-binding ligands in regions of formation and transports them until melting (Krembs et al., 2002; Tovar-Sánchez et al., 2010; Anderson and Amon, 2015; Lin et al., 2020).

Atmospheric deposition is the largest input of trace metals to the surface waters of the open ocean, occurring through dry or wet deposition with spatial and temporal variability (Bruland et al., 2014). Atmospheric dust has natural and anthropogenic sources that influence the trace metal content and its solubility. On a global scale, the atmospheric deposition contributes on average $2.9 \cdot 10^{11}$ mol Fe yr^{-1} and $2.7 \cdot 10^8$ mol Cu yr^{-1} (Jickells et al., 2005; Richon and Tagliabue, 2019). Oceanic regions located close to the major deserts receives large inputs of dFe from dusts deposition, such as the Northeast Atlantic Ocean (Conway and John, 2014; Jickells et al., 2005). Aerosols of anthropogenic origin have higher Cu contents and solubilities (Little et al., 2014).

Marine sediments, especially near continental margins, are a significant source of Fe and Cu to the overlying water column (Bowie et al., 2002; Heggie et al., 1987). The remineralization of these trace metals from particles has been proposed as the primary source of metals to the surrounding waters. Deep water upwelling is an important source of Fe and Cu to the euphotic zone, particularly at continental margins associated with particle resuspension

(Johnson et al., 1999). This surface enrichment also supports the phytoplankton growth around islands located in high nutrient low chlorophyll (HNLC) regions (Gove et al., 2016). Bottom and shelf sediments also act as a source of ligands to surrounding waters (Gerringa et al., 2008; Ruacho et al., 2020).

Deep waters also receive trace metals from **hydrothermal vents**, whose fluids are enriched in several elements, including Fe and Cu (German and Von Damm, 2004; González-Santana et al., 2020; Tagliabue et al., 2010). However, due to the temperature and pH conditions, most of these metals precipitate close to the source. Cu is removed from the plume faster than Fe due to the precipitation of different materials, although the amount of Fe released is greater than that of Cu (German et al., 1991). Abiotic and biotic processes favour the formation of metal-binding ligands around the hydrothermal systems (Sander and Koschinsky, 2011). However, the contribution of dissolved trace metals is limited and stabilization by organic complexation in the hydrothermal plume is low (Bennett et al., 2008; Dulaquais et al., 2023).

Once Fe and Cu are in surface waters, the phytoplankton growth actively removes dFe and dCu as part of their metabolic requirements, which vary with species and location (Sunda, 1989). Microorganisms have developed strategies to uptake different forms of trace metals, including complexed Fe and Cu species, as well as dissolved ionic species (Figure 1.5). Four different Fe and Cu uptake systems were defined for phytoplankton organisms (Morel et al., 2008; Walsh et al., 2015; Kong and Price, 2020; Sutak et al., 2020): (1) transport of complexed Fe or Cu with specific compounds, such as siderophores or cysteine; (2) transport of Fe^{2+} and Cu^{2+} though divalent metal

ion transporters; (3) transport of Cu^{+} by high-affinity transporters; (4) transport of reduced species (Fe^{2+} and Cu^{+}) after the action of cell surface reductase on free or complexed metal ions.

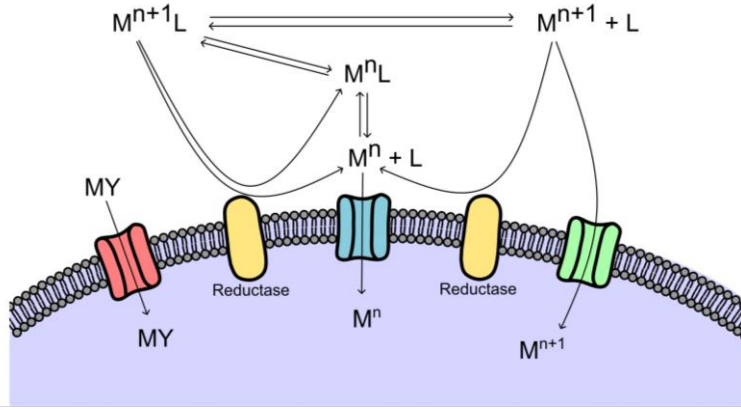

Figure 1.5. Schematic representation of trace metal uptake mechanisms in marine phytoplankton. The metals are divided into four groups: oxidized species (M^{n+1}), which include Fe^{3+} and Cu^{2+}; reduced species (M^{n}), which include Fe^{2+} and Cu^{+}; complexed species ($M^{n}L$ and $M^{n+1}L$); and specific chelated forms (MY). The blue area represents the interior of the cell, and the membrane is depicted in grey. Membrane transport systems are illustrated in pink, blue, and green, and surface reductases are depicted in yellow. Figure adapted from Morel et al. (2008), Walsh et al. (2015), Kong and Price (2020) and Sutak et al. (2020).

The biological use of trace metals results in their transport to the deeper ocean. However, it has been reported that there is a significant recycling of Fe mediated by zooplankton, bacteria and viruses which regenerate dFe in surface waters (Boyd and Ellwood, 2010; Bruland et al., 2014). Phytoplankton, bacteria and cyanobacteria can release organic compounds to increase Fe availability and/or control Cu availability and toxicity. The biological production of metal-binding ligands was evidenced by laboratory experiments and field measurements, where maximum ligand concentrations were related with the highest biomass measurements. Zooplankton grazing,

viral lysis and bacterial remineralization are other passive mechanisms to produce biogenic ligands (Sato et al., 2007; Poorvin et al., 2011). At the same time, the biological activity throughout the water column can decompose metal-binding ligands.

Passive removal processes of trace metals affect both dissolved and particulate fractions and are related to particle settling. The precipitation involves the formation of solids from dissolved phases and mainly occurs in rivers and estuaries, due to strong chemical variations. Within rivers, suspended particles can aggregate and create larger clumps as a result of the pH gradient and the interaction with large organic molecules (Sholkovitz, 1978). The scavenging and the aggregation with sinking particles also remove dFe, dCu and metal-binding ligands from surface water via adsorption onto the surface of particles (Völker and Tagliabue, 2015). These particles, which remain in suspension in the water column, will ultimately settle and accumulate on the sea floor, due to their weight (Bruland et al., 2014). However, these particles may act as a source of trace metals by desorption, in a process known as reversible scavenging (Cheize et al., 2019; Little et al., 2013; Richon and Tagliabue, 2019). In surface waters the solar irradiance can induce photodegradation processes that degrade and/or produce weaker ligands (Barbeau et al., 2001; Barbeau, 2006; Laglera and van den Berg, 2006; Shank et al., 2006).

1.4 Characterization of organic metal-binding ligands

The competitive ligand exchange adsorptive cathodic stripping voltammetry (CLE-ACSV) is a widely used technique for the analysis of dFe and dCu, which also allows the quantification of ligand concentrations and

the determination of the conditional stability constant ($K^{cond}_{M'L}$) formed between trace metals and ligands (Campos and van den Berg, 1994; Croot and Johansson, 2000; Pižeta et al., 2015). This approach involves the competition between natural and known ligands, which are adsorbed onto the mercury drop electrode and undergo a redox reaction. The CLE-ACSV do not provide molecular information about the organic ligand, while the ligand concentration and the conditional stability constant are the result of an average of the mixture of ligands present in the solution. However, commercial standards can be used to quantify specific metal-binding ligands, such as electroactive humic substances and thiols (Laglera et al., 2007; Whitby and van den Berg, 2015). Voltametric methods are widely used due to their sensitivity, which enables them to operate at low concentrations of metal and ligand without requiring sample pretreatment (Middag et al., 2023). Nevertheless, it should be noted that the results obtained with the CLE-ACSV are conditional to the experimental conditions applied. Other techniques, such as chromatographic and mass spectrometry methods, have been proposed for quantifying and characterising metal-binding ligands (Middag et al., 2023).

$$M' + L' \rightleftharpoons ML \tag{1.3}$$

$$K^{cond}_{M'L} = \frac{[ML]}{[M']+[L']} \tag{1.4}$$

Over subsequent years, significant advances were made on Fe and Cu organic speciation. However, the chemical identity of ligands remains unknown (Vraspir and Butler, 2009). Identifying ligands is hindered by the heterogeneity of DOM in seawater and the intricate association formed with trace metals. For that reason, the ligand pool is considered to be a continuum of compounds with different complexing capacities, which are determined by the complexation sites. For this reason, dissolved ligands are classified based

on their complexing capacity determined by the $K^{cond}_{M'L}$, which characterizes the apparent strength of ligands binding sites. This constant is used to operationally divide ligands into strong and weak compound, also called L_1 and L_2. In the case of Fe-binding ligands (L_{Fe}) the log K^{cond}_{Fe3+L}=22 is the value that splits ligands into the two classes, while for Cu-binding ligands (L_{Cu}) is log K^{cond}_{Cu2+L}=13 (Bruland et al., 2000; Gledhill and Buck, 2012).

1.5 Implication of climate change on the biogeochemistry of Fe and Cu in seawater

The speciation, distribution and concentration of Fe and Cu in seawater are influenced by their supply and removal mechanisms, redox chemistry, and environmental conditions. The properties of trace metals and metal-binding ligands in seawater are also impacted by several factors, including temperature, pH, ionic strength, salinity, and light. The changing natural environmental conditions resulting from climate change (IPCC, 2022) have significant implications for trace metal biogeochemistry (Hoffmann et al., 2012; Millero et al., 2009).

The rise in atmospheric CO_2 concentrations has increased ocean temperatures, leading to greater ocean stratification and increased ice melting, which raises sea levels. As a result of changes in oceanic and atmospheric circulation, the weather is affected, with consequences for both atmospheric deposition and riverine inputs (Doney et al., 2012). Additionally, the equilibration of CO_2 concentration between the atmosphere and surface waters leads to a decrease in pH and a reduction in hydroxide (OH^-) and carbonate (CO^{2-}_3) concentrations. These changes have significant biogeochemical implications.

The **inorganic speciation** of trace metals is influenced in different way. Divalent and trivalent metals, such as Fe and Cu, can form complexes with OH^- and CO^{2-}_3. The ocean acidification, which lowers pH levels, promotes the presence of free forms of these metals (Millero et al., 1995; Millero and Hawke, 1992). Additionally, the total concentration of free Fe increases when the pH is lowered, as it enhances the solubility of Fe(III) and slows the oxidation rate of Fe(II) (Millero, 2013; Millero et al., 2009). The oxidation of Fe(II) will also decrease due to the reduction in dissolved O_2 caused by the ocean warming, the enhanced stratification and the expansion of oxygen minimum zones (Keeling et al., 2010). Simultaneously, the increase of sea surface temperatures accelerates the Fe(II) oxidation rates (Millero et al., 1987), while the intensification of surface water stratification would enhance the photochemical reduction of Fe(III) (Kuma et al., 1995).

Ocean acidification also affects the **organic speciation** of trace metals. However, the impact of pH on metal-binding ligands has not been extensively studied due to the heterogeneous nature of the ligands and the results are unclear (Millero et al., 2009). Some studies demonstrate that at lower pH, the concentration of unprotonated binding sites decreases, resulting in less Cu complexation and favouring free metal forms (Gledhill et al., 2015; Millero et al., 2009). Other studies have shown that the pH decrease is associated with higher organic Fe complexation (Hirose, 2011; Stockdale et al., 2016). Finally, the exposure of surface waters to sunlight, which is enhanced by greater water stratification, leads to the photolysis of metal-binding ligands (Barbeau, 2006; Laglera and van den Berg, 2006).

Chemical speciation models were developed to predict the changes in metal speciation with different CO_2 future emission scenarios (Figure 1.6)

(Stockdale et al., 2016). The reaction of organic and inorganic Fe and Cu species in the ocean is complex and challenging to forecast. Nevertheless, it is imperative to define and comprehend these variations, as all these chemical changes have important consequences for the development of the phytoplankton community.

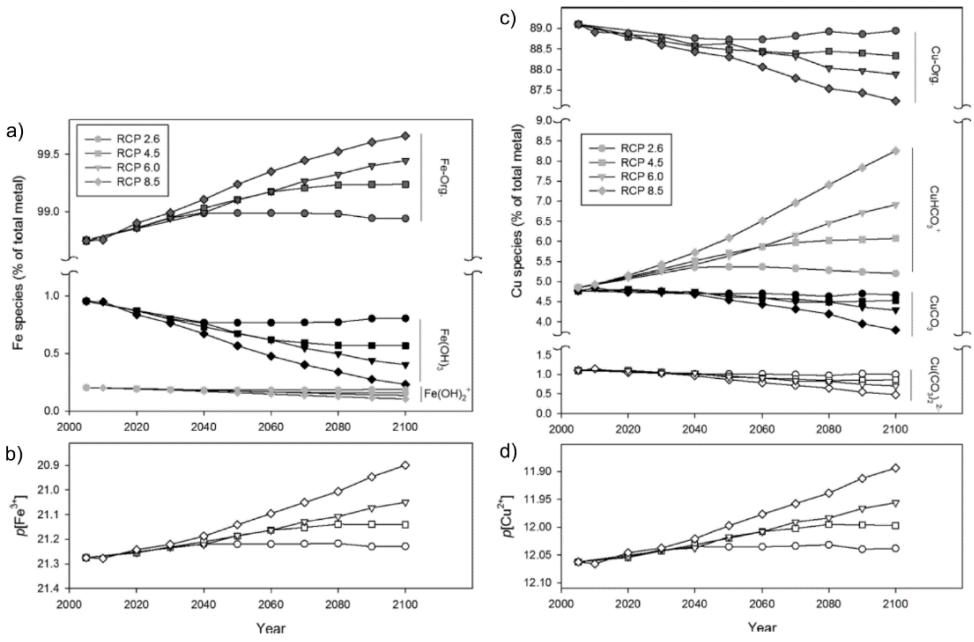

Figure 1.6. Model predictions of trace metal speciation trends until 2100 under four RCP scenarios in seawater. a) Organic and inorganic dominant Fe complexes. b) Concentration of Fe^{3+} (represented as -log[Fe^{3+}]). c) Organic and inorganic dominant Cu complexes. d) Concentration of Cu^{2+} (represented as -log[Cu^{2+}]). Figure from Stockdale et al. (2016).

The impacts of climate change in the ocean vary between regions and basins, with some areas, such as islands and polar regions, being particularly vulnerable to changes (IPCC, 2022). Islands will be affected by changes in weather, ocean circulation, water stratification, and sea level (Gove et al.,

2016; Veron et al., 2019). Tropical and subtropical islands may experience reduced nutrient availability in the future as a result of changes in their biogeochemical cycles and ocean dynamics (Doney, 2010). In addition, rising temperatures will have a significant impact on the polar regions (IPCC, 2022). The Arctic Ocean is experiencing a reduction in sea-ice cover and the thawing of permafrost, which is associated with increased freshwater inputs (Peterson et al., 2002; Schuur et al., 2013, 2015). This increased freshwater input can increase the bioavailability of both trace metals and organic matter (Charette et al., 2020; Frey and McClelland, 2009; Guieu et al., 1996; Stedmon et al., 2011). However, studies investigating the organic speciation of Fe and Cu in oceanic islands and polar regions are limited. Additionally, the complex biochemical and physical interactions in these environments make model predictions uncertain.

1.6 Objectives

As stated above, the study of Fe and Cu speciation in seawater is a key point to understand their distribution in marine environments. Improving our understanding of organic speciation will improve our comprehension of the bioavailability of dFe and dCu and shed light on how the distribution of these micronutrients might be related to primary production and CO_2 sequestration in the ocean.

This PhD Thesis aims to provide insight into the organic speciation of dFe and dCu in poorly studied regions potentially affected by climate change. To achieve this goal, the concentrations of dFe and dCu, together with their respective ligand concentrations and conditional stability constants, have been estimated in oceanic and coastal regions of the Atlantic and Arctic

Oceans. The overall objective has been subdivided into three specific objectives.

Objective 1. Determine the possible effects of oceanic islands on the organic speciation of dFe and dCu in the surrounding surface waters. In order to reach this objective, a quantification and characterisation of dFe and dCu, together with that of the natural binding ligands that complex each trace metal, was carried out in the coastal waters of the Macaronesian islands.

The development of this objective constitutes the Chapter 2, where the organic speciation was evaluated around Cape Verde, Canary Islands and Madeira. This study evaluated the distribution and binding strength of Fe and Cu-binding, elucidating the possible processes (physical and biological) that influence the observed characteristics.

Objective 2. Characterise the distribution of Cu-binding ligands in a region influenced by coastal and oceanic processes. This objective includes the quantification of Cu-binding ligands and the determination of their respective condition stability constants throughout the water column.

This objective is addressed in Chapter 3, which describes Cu-binding ligands in the Greenland shelf area and Fram Strait region and evaluates the influence of ligand export from the Arctic Ocean and inputs from coastal Greenland areas.

Objective 3. Characterise the distribution of Cu-binding ligands in an oceanic region. This objective involves the quantification of Cu-binding ligands and the determination of their respective condition stability constants throughout the water column.

This objective is undertaken in Chapter 4 in a study focusing on the Cu organic speciation in the central Arctic Ocean. Throughout the study region Cu-binding ligands were evaluated in seawater covered and uncovered by sea-ice. The observed distribution was related to riverine sources of organic matter and associated with the export of material through the Fram Strait to the Nordic Seas and the North Atlantic Ocean.

Chapters 5 and 6 provide the general summary with the main conclusions and perspectives for future work.

Chapter 7 contains information on the introduction, objectives and conclusions translated into Spanish.

Image: ESA/Copernicus Sentinel-3 data (2021).

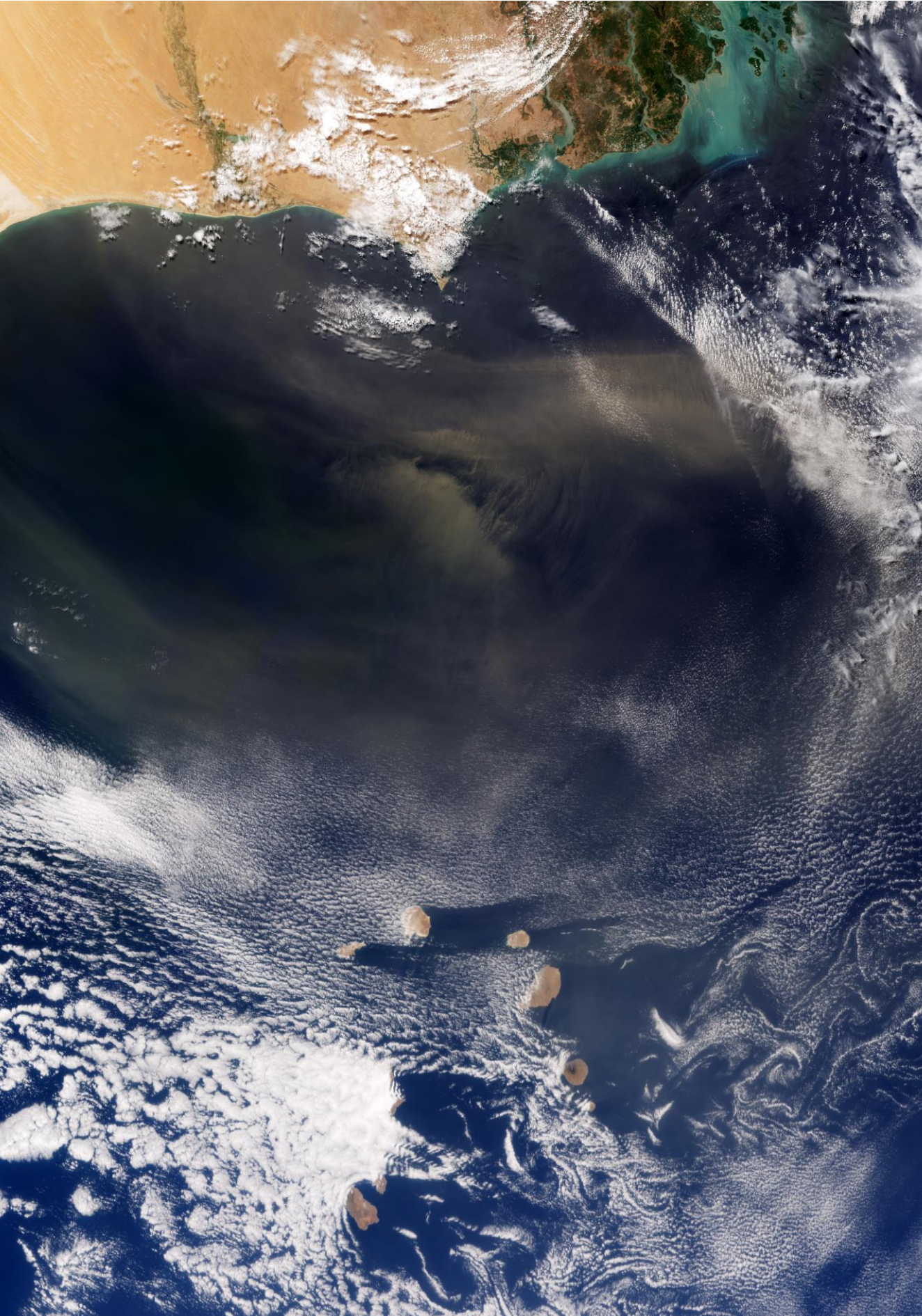

Chapter 2. Iron and copper complexation in Macaronesian coastal waters

Marine Chemistry, 29 January 2022

https://doi.org/10.1016/j.marchem.2022.104087

V. Arnone[a], D. González-Santana[a], M. González-Dávila[a], A.G. González[a], J.M. Santana-Casiano[a]

[a]Instituto de Oceanografía y Cambio Global, IOCAG, Universidad de Las Palmas de Gran Canaria, ULPGC, 35017, Las Palmas de Gran Canaria, Spain.

Abstract

Dissolved iron (dFe) and copper (dCu), the concentration and the conditional stability constants of organic binding ligands (L_{Fe}, L_{Cu}, log K^{cond}_{Fe3+L} and log K^{cond}_{Cu2+L}) were studied in the surface coastal waters of the Macaronesia region (Cape Verde, Canary Islands, and Madeira) using competitive ligand exchange-adsorptive cathodic stripping voltammetry (CLE-ACSV). Two oceanic stations were also studied: the Cape Verde Ocean Observatory (CVOO) and the European Station for Time Series in the Ocean in the Canary Islands (ESTOC). Dissolved Fe varied from 0.46 to 1.32 nM and L_{Fe} concentrations were between 0.56 and 2.96 nM. More than 98% of the total dFe was complexed with conditional stability constants (log K^{cond}_{Fe3+L}) between 20.77 and 21.90 (L_2-type ligands). Dissolved Cu concentrations ranged between 0.07 and 4.03 nM and the amount of L_{Cu} varied between 0.54 and 2.59 nM, with more than 99% of dCu organically complexed. The conditional stability constant (log K^{cond}_{Cu2+L}) showed values between 13.40 and 14.42 (L_1-type).

Due to biological activity and water mixing induced by the wind around the islands, dissolved metals and ligand concentrations were greater at the coastal stations than in oceanic water. Variations were observed between the eastern and western parts of Fogo, Tenerife and Gran Canaria. On the east coasts, the increase in dissolved metals and ligand concentrations were related to wind-induced water mixing. The results of this study will contribute to the knowledge about the impact of coastal areas on the Fe and Cu biogeochemical cycles.

Keywords: Iron, Copper, Organic ligands, Coastal waters, Macaronesian region.

2.1 Introduction

Iron (Fe) and copper (Cu) are essential trace metals for marine microorganisms, as they are involved in many metabolic processes. Iron is essential for photosynthesis, respiration processes (Raven et al., 1999; Morel and Price, 2003) and nitrogen fixation (Moore et al., 2001; Mills et al., 2005) and is used in superoxide dismutase (SOD, Wolfe-Simon et al., 2005), as well as in the nitrate and nitrite reductase processes (Sunda, 1989; Twining and Baines, 2013). Copper is an important constituent in different enzyme systems related to a variety of processes including photosynthetic and mitochondrial electron transport (Sunda, 1989; Peers et al., 2005). However, high concentrations of free cupric ion (Cu^{2+}) are toxic to certain marine organisms and can inhibit phytoplankton growth (Morel et al., 1978; Sunda and Lewis, 1978; Brand et al., 1986). Copper is also a cofactor involved in the Fe transport reaction (Sunda, 1989; Peers et al., 2005).

Iron and Cu are similar in some biogeochemical aspects. Both trace metals are present in seawater in two different oxidation states, and the oxidized species are the most thermodynamically stable in oxic waters (Santana-Casiano et al., 2005; González-Dávila et al., 2009). The formation of organic complexes with dFe and dCu dominates the speciation of both metals (>99%). This may increase Fe solubility, stabilizing it against the oxy-hydroxide formation and precipitation (Rue and Bruland, 1995; Liu and Millero, 2002) and thus increasing its residence time and bioavailability (Kuma et al., 1996; Hutchins et al., 1999; Maldonado and Price, 1999; Buck et al., 2007). Different models show that phytoplankton can use complexed Fe to obtain free metal which is available for biological uptake (Morel et al., 2008). In the case of Cu, organic complexation reduces the scavenging and promotes the

decrease of free Cu^{2+}, controlling its bioavailability and toxicity. A fraction of the Cu-ligand complexes may also contribute to Cu uptake (Annett et al., 2008; Semeniuk et al., 2009, 2015). The Fe and Cu-binding ligands (L_{Fe} and L_{Cu}) present different sources such as: rupture of cells after grazing (Sato et al., 2007), viral lysis (Poorvin et al., 2011), transformation of organic matter (Gerringa et al., 2006), phytoplankton exudates (Rico et al., 2013; Santana-Casiano et al., 2014) and sediments (Gerringa et al., 2008). The L_{Fe} and L_{Cu} are classified according to the value of the conditional stability constants (log K^{cond}_{Fe3+L} and log K^{cond}_{Cu2+L}). These ligands can be considered to be strong (L_1) or weak (L_2), where log K^{cond}_{Fe3+L} = 22 divides L_1 and L_2-type of Fe-binding ligands (Gledhill and Buck, 2012). For Cu, the value which splits ligands type corresponds to log K^{cond}_{Cu2+L} = 13 (Bruland et al., 2000; Buck and Bruland, 2005).

In the Atlantic Ocean surface waters, dFe concentrations range between 0.1 and 0.8 nM (Boye et al., 2006; Rijkenberg et al., 2008) with variations between different areas of the ocean depending on Fe sources, mesoscale processes and primary production. In the North Atlantic oceanic region, between 71% and 87% of surface dFe comes from the aeolian deposition of Saharan dust (Conway and John, 2014). However, Fe solubilization from aeolian input is low (~1.7%, Baker et al., 2006) and previous work has shown the concentration of dFe increase by 0.05 – 0.10 nM after a dust event (Rijkenberg et al., 2008, 2012). Surface dCu concentrations vary between 0.7 and 5.9 nM (Buckley and van den Berg, 1986; Saager et al., 1997). The presence of Saharan dust does not influence the concentration of dCu in the North Atlantic surface waters (Jacquot and Moffett, 2015).

The Fe speciation in the oceanic and upwelling region of the Northeast Atlantic Ocean has been previously studied (Gledhill and van den Berg, 1994; Boye et al., 2003, 2006; Gerringa et al., 2006; Rijkenberg et al., 2008, 2012; Thuróczy et al., 2010; Buck et al., 2015). These investigations showed variable values of log K^{cond}_{Fe3+L} (18.8 – 22.85) and L_{Fe} concentration ranging from 0.82 to 4.08 nM. However, Cu speciation in the open ocean of the Atlantic Ocean has been poorly studied. Research has mainly focused on polar waters (Buck et al., 2010; Bundy et al., 2013; Heller and Croot, 2015), Pacific oceanic waters (Coale and Bruland, 1990; Whitby et al., 2018; Ruacho et al., 2020) and coastal environments influenced by rivers (Abualhaija et al., 2015; Gledhill et al., 2015). Few speciation studies have been conducted in the Atlantic Ocean (Buckley and van den Berg, 1986; Moffett et al., 1990; Jacquot and Moffett, 2015). For the North Atlantic Ocean, a log K^{cond}_{Cu2+L} of 13.6±0.5 and a L_{Cu} of 2.6±0.8 nM have been reported (Jacquot and Moffett, 2015).

The surrounding waters of oceanic islands are characterized by very complex and dynamic environments where a high concentration of phytoplankton biomass is typically observed (Blain et al., 2001, 2007). Various studies (Blain et al., 2001, 2007, 2008; Gerringa et al., 2008) in the vicinity of the Kerguelen Islands (Southern Ocean) have shown that different processes act as a source of micronutrients, particulate Fe (Bowie et al., 2015) and dFe-ligands (Monteiro and Orren, 1985; Gerringa et al., 2008) and thus promote phytoplankton growth. Different dFe sources can be found, such as the horizontal advection, the vertical mixing, the isopycnal mixing, the atmospheric dust deposition and the consequent dissolution from lithogenic particulate Fe (Blain et al., 2008). However, regeneration from biogenic material and the input from the sediments are the most important sources of

dFe above the plateau (Elrod et al., 2004; Blain et al., 2008). Due to the importance of Fe supply in the phytoplankton production and CO_2 sequestration, numerous studies have been carried out in islands of the Southern Ocean (Blain et al., 2001, 2007, 2008; Planquette et al., 2007; Gerringa et al., 2008; Robinson et al., 2016) and around the Pacific Ocean (Gordon et al., 1998; Kondo et al., 2007; Raapoto et al., 2019). However, the contribution of micronutrients and organic ligands from islands in other oceanic regions is still poorly understood.

The Macaronesia region in the Northeast Atlantic Ocean is a large area from the Cape Verde archipelago to the Azores islands, dominated by many processes such as mesoscale eddies, filaments and coastal upwelling (Caldeira et al., 2002; Sangrà et al., 2009; Pelegrí et al., 2017). The complex hydrodynamic affects the distribution of metals and ligands in both oceanic and nearshore areas. Across the region, temperature increases and precipitation decreases towards the Equator (Mehlmann et al., 2020). The interaction between the orography and trade winds controls the weather of each island and the region between them. There is no riverine input to the coastal waters. However, when it rains, there is non-continuous input through runoff and ravines subject to the rainfall regime, which is variable and very scarce on some islands. The chemical speciation of Fe could be influenced by these sporadic contributions and also by the great input of atmospheric dust deposition from the Sahara desert and Sahel region (Duce and Tindale, 1991; Gelado-Caballero et al., 2012; López-García et al., 2021). Another factor that could influence Fe and Cu speciation are the anthropogenic sources. In each archipelago there are power plants and desalination plants, which together with wastewater can alter the chemical composition of coastal waters.

During early spring 2019, dFe and dCu speciation were measured in coastal surface waters in three different archipelagos in the Macaronesia region (Cape Verde, Canary Islands and Madeira). The concentration of dFe and dCu, and the concentration and characteristics of Fe and Cu-binding ligands were measured by Competitive Ligand Exchange-Adsorptive Cathodic Stripping Voltammetry (CLE-ACSV). The results from this research will show the first dataset on dFe and dCu speciation in the coastal waters of the Macaronesia Islands, increasing our knowledge of the Fe and Cu biogeochemical cycles.

2.2 Materials and Methods

2.2.1 Sampling strategy

The POS533 cruise took place during early spring (from February 29 to March 19, 2019) on board the *R/V* Poseidon in the eastern Atlantic Ocean, along the Macaronesian archipelagos (Cape Verde, Canary Islands and Madeira). Seawater samples were taken in coastal and oceanic stations by following a path from south to north (Figure 2.1), starting from Cape Verde and finishing in Madeira.

The exact location of each station is shown in Figure 2.2. In the Cape Verde region (Figure 2.2a), samples were taken in coastal waters near the islands of Santo Antão (St. 1), São Nicolau (St. 4), Fogo (St. 6), Santiago (St. 9), Maio (St. 11), Boa Vista (St. 13), Sal (St. 14) and São Vicente (St. 16). One oceanic station (St. 17) was sampled at the Cape Verde Ocean Observatory (CVOO) located north of the archipelago.

In the Canary Islands (Figure 2.2b), the coasts of El Hierro (St. 21), La Gomera (St. 25), Tenerife (St. 31, 32 and 34) and Gran Canaria (St. 39, 40 and 42) were sampled. One station was located between the islands of El Hierro and La Gomera (St. 23) and one between Tenerife and Gran Canaria (St. 37). An oceanic station was positioned at the European Station for Time Series in the Ocean in the Canary Islands (ESTOC), located north of the archipelago.

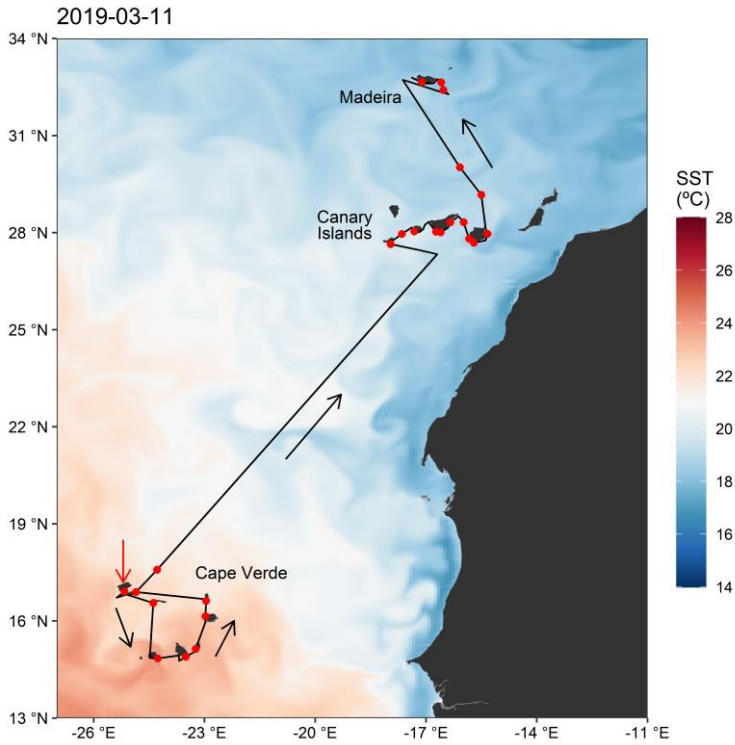

Figure 2.1. Representation of POS533 cruise track (black line) over a sea surface temperature image (COPERNICUS product) of March 11 (2019). The cruise took place between February 29 and March 19 (2019). The sampling started in Cape Verde (St. 1, red arrow) and ended in Madeira. The station locations are marked by red dots.

Another set of coastal samples were obtained in the Salvages Islands (St. 45, Figure 2.2b), Desertas Islands (St. 52, Figure 2.2c), in the channel between

Desertas Islands and Madeira (St. 54, Figure 2.2c) and in the south of Madeira (St. 63, Figure 2.2c).

2.2.2 Sampling

Seawater samples for dFe, dCu and ligand (L_{Fe} and L_{Cu}) measurements were collected at 20 m depth at coastal and oceanic stations (Figure 2.2) using a trace metal clean PFA Teflon diaphragm pump connected to PFA Teflon tubing, and filtered online (0.2µm Acropack Supor®, 6.4 mm MNPT/ 6.4 – 12.7 mm). During sampling, the acid-cleaned low-density polyethylene (LDPE) bottles were triple rinsed with the seawater sample before filling the bottle, double bagged and kept in the dark at -20ºC. For each metal, 250 ml of seawater was sampled in separate bottles. The procedure followed the protocol described by Cutter et al. (2010) and Buck et al. (2012).

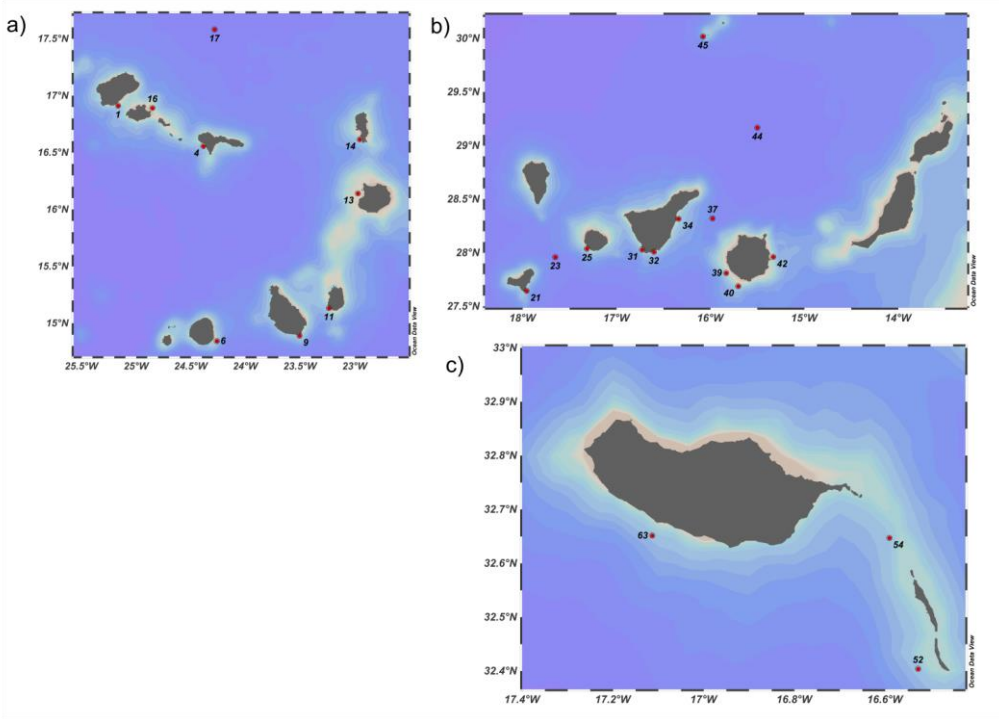

Figure 2.2. Sampling locations along the cruise POS533 in the three regions Madeira (a), Canary Islands (b) and Cape Verde (c).

For hydrographic information, temperature and salinity data were recorded from a CTD coupled to the rosette. The pH (total scale) was measured using the UV-Vis spectrophotometric technique (Clayton and Byrne, 1993) with m-cresol purple as an indicator with a standard deviation of ±0.002 (González-Dávila et al., 2003). Dissolved oxygen was measured on board by using the Winkler Titration (Grasshoff et al., 1999). Nutrients used for the statistical analysis, were collected in 14 ml polyethylene tubes to determine the content of nitrate and nitrite (NO_3^-+NO_2^-), phosphate (PO_4^{3-}) and silicates ($Si(OH)_4$) performing the spectrophotometric analysis (Grasshoff et al., 1999) with a QuAAtro auto-analyser (SEAL Analytical, UK).

2.2.3 Instrumentation and reagents

Iron and Cu stock solutions were prepared weekly from standard solutions for atomic absorption spectrometry (Fluka), diluted with MQ-water and acidified with 100 µL ultrapure 12.8 M HCl.

A 1.0 M stock buffer of EPPS (N-(2-hydroxyethyl)piperazine-N′; 2-propanesulfonic acid; *Sigma-Aldrich*) was prepared in 1.0 M ultrapure NH_4OH (VWR) at pH 8.2. Possibly remaining metals were removed from the buffer solution by adding 100 µM of MnO_2, stirred overnight and filtrated through an acid-clean 0.45 µm filter (Campos and van den Berg, 1994).

For the Fe analysis, a 0.01 M stock solution of TAC (2-(2-thiazolylazo)-p-cresol; Sigma-Aldrich) was prepared in methanol (Sigma-Aldrich). For Cu analysis, a 0.01 M solution of SA (salicylaldoxime; Sigma-Aldrich) was prepared in 0.1 M ultrapure HCl. All stock solutions were kept in the fridge when they were not in use (darkness and 8°C).

The dFe and dCu concentrations and the speciation were measured by CLE-ACSV on an Epsilon voltammeter (Basi, Inc) connected with a hanging mercury drop electrode (CGME, Basi, Inc). The reference electrode was Ag/AgCl with a salt bridge filled with 3M KCl, with a platinum auxiliary electrode. The solution was mixed during the deposition time and purged by bubbling with high purity nitrogen. The first two drops of the mercury drop electrode were always discarded, and the third mercury drop was used. Voltammetric conditioned cells (PTFE) were always used.

2.2.4 dFe and dCu concentration

Dissolved Fe concentrations were determined by CLE-ACSV with ligand competition against TAC (Croot and Johansson, 2000) using the method of standard additions. An aliquot (10 ml) of the seawater sample was UV-irradiated for 4 h in a quartz tube, then 20 µL of TAC and 100 µL of 1M EPPS were added. The differential pulse stripping voltammetry (DPSV) conditions for Fe measurements were: deposition potential at -410 mV for 120 sec, quiet time for 5 sec, initial potential at -410 mV and final potential at -600 mV. The step was 2 mV, pulse width of 10 ms, pulse period of 100 ms and pulse amplitude of 50 mV.

The dCu concentration was determined by using SA as a competitive ligand (Campos and van den Berg, 1994) with the standard addition method. The samples were prepared with 20 µL of 0.01M SA and 100 µL of 1M EPPS. The DPSV conditions for Cu measurements were: deposition potential at -50 mV for 100 sec, quiet time for 10 sec, initial potential at -150 mV and final potential at -600 mV. The step was 4 mV, pulse width of 50 ms, pulse period of 200 ms and pulse amplitude of 50 mV.

2.2.5 dFe and dCu speciation

For the determination of dFe complexation, 10 mL samples were pipetted into 15 Teflon bottles, 100 µL of EPPS (final concentration 10^{-2} M) and different concentrations of Fe were added (from 0 to 10 nM). After a 1h equilibration period, 10 µL of TAC (final concentration 10 µM) was added and left to equilibrate overnight (Croot and Johansson, 2000). The titration series were measured in a Teflon cell, with two +0 Fe additions and more than 10 titration points (Garnier et al., 2004; Gledhill and Buck, 2012).

The procedure used to determine the dCu speciation was the same but using 10 µL of SA (final concentration 10 µM, Campos and van den Berg, 1994). Under the buffer conditions for those determinations, the inorganic metal side reaction coefficients are $\alpha_{Cu'}$=32 (Pižeta et al., 2015) and $\alpha_{Fe'}=10^{10}$ (Hudson et al., 1992), respectively, controlled by the pH, temperature and salinity of the sample.

The dCu and dFe speciation in seawater, the dCu and dFe-binding ligands (L_{Cu} and L_{Fe}), and the conditional stability constants (K^{cond}_{CuLi} and K^{cond}_{FeLi}) were computed using the ProMCC software (Omanović et al., 2015). One ligand class model fitted the experimental values. All the stability constants determined and indicated in the paper are conditional to the experimental seawater conditions for the samples. The dFe and dCu speciation and concentration data are accessible in the database PANGAEA (Santana-Casiano and Quack, 2021).

2.2.6 Theory

Considering the dissolved phase (<0.2 μm), the dissolved concentration of a metal (dM), both for Fe and Cu, in a natural seawater sample can be defined as:

$$dM = [M'] + [ML] \tag{2.1}$$

Where [M´] represents the labile metal concentration, defined as the sum of all inorganic species including M^{n+}. [ML] is the concentration of metal complexed with organic ligands (L). The reaction between M´ and the labile natural binding ligands (L´) can be expressed as:

$$M' + L' \rightleftharpoons ML \tag{2.2}$$

The conditional stability constant of the formed complex ($K^{cond}_{M'L}$) describes the strength of a binding ligand and is calculated from:

$$K^{cond}_{M'L} = \frac{[ML]}{[M'][L']} \tag{2.3}$$

[M´] is related with $[M^{n+}]$ by the inorganic side reaction coefficient ($\alpha_{M'}$):

$$[M'] = \alpha_{M'} \cdot [M^{n+}] \tag{2.4}$$

In terms of ionic metal (M^{n+}), the conditional stability constant can be calculated from:

$$K^{cond}_{M^{n+}L} = \alpha_{M'} \cdot K^{cond}_{M'L} \tag{2.5}$$

The reactivity of the metal, M, with the natural binding ligands (f_{ML}) describes the complexation capacity of dissolved ligands to be bound with M (Gledhill and Gerringa, 2017). This coefficient can be estimated in respect to M´ and M^{n+} as expressed below:

$$f_{M'L} = K_{M'L}^{cond} \cdot [L_M] \quad (2.6)$$

$$f_{M+L} = K_{M^{n+}L}^{cond} \cdot [L_M] \quad (2.7)$$

The excess ligand (eL_M) represents the concentration of free M-binding sites (Thuróczy et al., 2011a) and indicates the saturation state of ligands. The eL_M was defined as:

$$[eL_M] = [L_M] - [dM] \quad (2.8)$$

The L_M/dM ratio indicates the saturation state of the natural ligand and values close to 1 designate that most of the ligands are bound with the metal. For Fe, ratios near 1 indicate a high potential for metal precipitation, while higher values denote a great potential for metal solubilization (Thuróczy et al., 2011a).

To determine the speciation of M through CLE-ACSV, it is necessary to add a well-characterized ligand (AL) that reacts with M and competes with ML to form a new complex (MAL). The MAL is an electroactive complex that can be adsorbed onto the mercury drop and undergo a reduction. Further details on the determination of the speciation of Fe by using TAC can be found in (Croot and Johansson, 2000). For the speciation of Cu, further information can be found in Campos and van den Berg (1994).

The "detection window" or analytical window determines the concentration of the ligands and the conditional stability constant that can be estimated with the titration. The side reaction coefficient of the MAL complex (α_{MAL}) represents the centre of the detection window (D), which is defined as the product of the AL concentration (AL) and the conditional stability constant for the MAL complex. The higher the α_{MAL} value, the greater its ability to form complexes and compete with other ligands. This allows

stronger complexes to be detected (with higher $K^{cond}_{M'L}$ or K^{cond}_{Mn+L} values) but results in a lower concentration of ligands (Campos and van den Berg, 1994; Buck et al., 2012). For Fe, the analytical window is defined as:

$$\alpha_{Fe(TAC)_2} = \beta^{cond}_{Fe(TAC)_2} \cdot [TAC]^2 = D \quad (2.9)$$

For a TAC concentration of 10 µM, $\beta^{cond}_{Fe(TAC)2}$ takes a value of $10^{12.4}$ (Croot and Johansson, 2000) then $\alpha_{Fe(TAC)2}$=251. For Cu, the detection window is given by:

$$\alpha_{CuSA} = K^{cond}_{CuSA} \cdot [SA] + \beta^{cond}_{Cu(SA)_2} \cdot [SA]^2 = D \quad (2.10)$$

Where both stability constants were calculated as a function of salinity, S (Campos and van den Berg, 1994):

$$\log K^{cond}_{CuSA} = 10.12 - 0.37 \cdot \log S \quad (2.11)$$

$$\log \beta^{cond}_{Cu(SA)_2} = 15.78 - 0.53 \cdot \log S \quad (2.12)$$

Considering a 10 µM concentration of SA and sample salinity, α_{CuSA} presented values between 5.09 and 5.10.

2.2.7 Statistical analysis

The data were analysed by Principal Components Analysis (PCA) using the PAST software. The PCA analysis (Figure 2.3) was applied, considering the following variables: temperature, salinity, fluorescence, turbulence, dFe, dCu, NO_3^-+NO_2^-, PO_4^{3-} and $Si(OH)_4$. Since the variables have different units, the programme's tool has been used to normalise the data by considering their standard deviation.

2.3 Results

2.3.1 Hydrographic characterization

Hydrographic, oxygen and pH data for each station are depicted in Table 2.1, and the description of the hydrographic conditions was recently reported by Mehlmann et al. (2020). The Macaronesia region presented a south to north sea surface temperature (SST) gradient (Figure 2.1 from satellite image). The maximum SST was measured at the Cape Verde stations with average values of 22.33±0.47ºC and minimum SST in Madeira (18.60±0.18ºC). Around the Canary Islands, the mean SST was 19.18±0.39ºC.

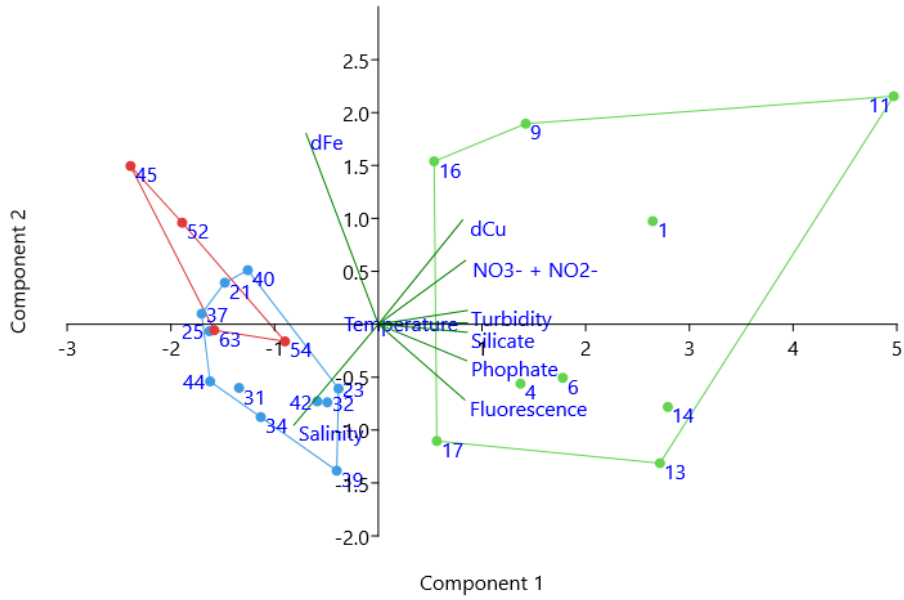

Figure 2.3. Results of PCA analysis realized considering temperature, salinity, fluorescence, turbidity, dissolved Fe (dFe), dissolved Cu (dCu) and nutrients (nitrate and nitrate, phosphate, and silicates) for the Macaronesia region. Green dots represent Cape Verde stations, blue dots Canary Island stations and with red colour Madeira samples.

Sea surface salinity (SSS) values (Table 2.1) at Cape Verde were the lowest throughout the studied area, with values between 35.93 and 36.52. In the Canary Islands and Madeira the SSS were practically constant with mean values of 36.80±0.06 and 36.72±0.04, respectively. A gradient in dissolved oxygen concentration was also measured (Table 2.1), with concentrations around 214.5±4.7 μmol kg^{-1} in the Cape Verde region, values of 228.3±2.1 μmol kg^{-1} in the Canary Islands and 230.6±1.0 μmol kg^{-1} around Madeira. The average pH at the studied stations was 8.07±0.02 with the lowest values in the Cape Verde islands (8.05) and the highest (8.09) around the Madeira archipelago.

The fluorescence (not calibrated) decreases from south to north and it was given in an arbitrary unit (a.u.) approximately equal to mg m^{-3} of chlorophyll. Higher average concentrations were recorded in the Cape Verde archipelago (0.58±0.31 a.u.), intermediate values in the Canary Islands (0.33±0.19 a.u.) and lower amounts in the Madeira archipelago (0.15±0.10 a.u.). At Cape Verde, stations 13 and 14 presented maximum fluorescence concentrations at 20 m depth (1.07 and 0.85 a.u., respectively) while the lowest value was observed at St. 17 (0.13 a.u.). In the Canaries, maximum values were recorded at St. 39 (0.65 a.u.) and 32 (0.56 a.u.) and the minimum at St. 37 (0.07 a.u.). Finally, in the Madeira archipelago the highest, fluorescence was observed at St. 54 (0.29 a.u.) and the lowest at St. 63 (0.09 a.u.).

The turbidity (Table 2.1) along the region ranged between 0.01 and 0.34 NTU. At Cape Verde, maximum values were recorded at St. 13 and 14 (mean value 0.28±0.08 NTU) while all other stations presented a mean value of 0.03±0.001 NTU. In the Canary Islands, maximum values of turbidity were found at St. 39, 40 and 42 (mean value= 0.043±0.01 NTU) the other station

presented lower values, around 0.02±0.01 NTU. Finally, the Madeira region showed turbidity around 0.02±0.01 NTU.

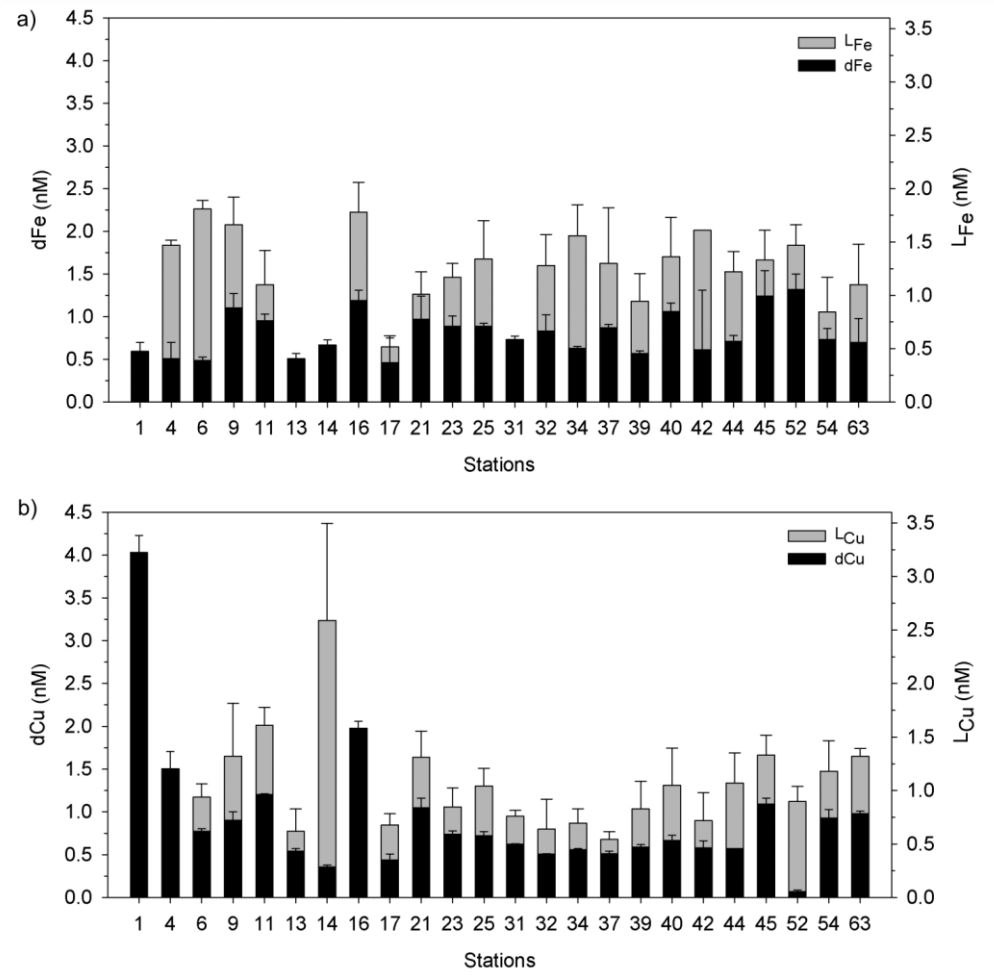

Figure 2.4. a) Concentration of dissolved Fe (dFe, nM) and Fe-binding ligands (L_{Fe}, nM). b) Concentration of dissolved Cu (dCu, nM) and Cu-binding ligands (L_{Cu}, nM). Stations from 1 to 17 were in the Cape Verde region, from 21 to 44 in the Canary Islands, and from 45 to 63 in Madeira.

2.3.2 Iron speciation

The dFe speciation is shown in Table 2.2. The dFe concentration ranged from 0.46 to 1.32 nM (mean value 0.80±0.25 nM) for all the regions (Figure 2.4). Only four stations (St. 1, 13, 14 and 31) showed saturated ligand titrations, and the dFe speciation was not computed within the detection windows used in the investigation. At Cape Verde, the mean dFe concentration was 0.72±0.28 nM and the maximum values were recorded at stations 9, 11 and 16 (1.08±0.12 nM). The other stations showed lower concentrations (0.54±0.08 nM). In the case of the Canary Islands, the mean dFe concentration was 0.80±0.16 nM. The minimum concentration was found at St. 39 (0.57±0.03 nM) and the maximum at St. 40 (1.06±0.10 nM). At Madeira, St. 63 (0.70±0.28 nM) showed a dFe concentration similar to St. 54 (0.73±0.13 nM), located between Madeira and Desertas Islands. At Desertas (St. 45) and Salvages Islands (St. 52) the dFe concentrations were similar (1.28±0.06 nM). Considering that the Madeira archipelago comprises the islands of Salvages, Desertas and Madeira, the mean dFe for the area was 1.00±0.33 nM. The oceanic stations (St. 17 CVOO, St. 44 ESTOC) presented different dFe concentrations, being lower in CVOO (St. 17, dFe=0.46±0.29 nM) than in ESTOC (St. 44, dFe=0.71±0.07 nM).

The L_{Fe} concentrations in the whole studied area (Figure 2.4 and Table 2.2) showed an average concentration of 1.29±0.32 nM. In the Cape Verde Islands (mean L_{Fe}=1.39±0.50 nM) the lowest concentration was found at the oceanic station (St. 17, 0.52±0.11 nM) and the maximum at St. 6 (1.81±0.08 nM). In the Canary Islands, the mean L_{Fe} concentration was 1.28±0.21 nM with a maximum at St. 42 (L_{Fe}=1.61±0.58 nM) and minimum at St. 39 (L_{Fe}=0.94±0.26 nM). In the Madeira archipelago, the mean L_{Fe} concentration

was 1.19±0.27 nM. At St. 63, L_{Fe} presented a concentration of 1.10±0.38 nM, while the maximum was observed at St. 52 and 45 (1.40±0.10 nM). The L_{Fe} at the oceanic stations showed a concentration of 0.52±0.11 nM at CVOO (St. 17), which increased to 1.22±0.19 nM at ESTOC (St. 44).

Throughout the studied region, log K^{cond}_{Fe3+L} (Table 2.2) varied between 20.77 and 21.90 (mean value 21.45±0.29). The different archipelagos showed similar mean log K^{cond}_{Fe3+L}, and the oceanic stations presented values that fell within the range of the coastal stations. Based on the two ligands classification, all the samples corresponded to an L_2 ligand type with log K^{cond}_{Fe3+L}<22.

The Fe', Fe^{3+}, FeL and eL_{Fe} parameters were estimated based on the dFe and L_{Fe} concentration. The average Fe' concentration showed lower concentrations in Cape Verde (7.04±5.52 pM), intermediate concentrations in the Canary Islands (11.77±9.28 pM) and higher amounts in the Madeira archipelago (19.08±9.47 pM). More than 98% of Fe' was organically complexed (Table 2.2), with the lowest percentages at St. 21 (south of El Hierro) and St. 54 (between Madeira and Desertas) at ~96.4%. The mean FeL concentration for the entire studied region was 0.82±0.25 nM with values oscillating between 0.45 nM and 1.30 nM. The mean FeL was 0.78±0.33 nM in Cape Verde, 0.79±0.16 nM in the Canary Islands and 0.98±0.33 nM in the Madeira archipelago.

The solubility of Fe(III) oxy-hydroxide, was estimated taking into account the *in situ* values of pH, temperature and salinity (Liu and Millero, 1999). This is the predominant Fe(III) species at pH 8 and presented an overall mean concentration of 0.018±0.001 nM. The solubility product of $Fe(OH)_3$, log

$K^*_{Fe(OH)3}$, took values between 3.9 and 4.2 while the hydrolysis constant for the same species, log β^*_3, ranged from -14.7 to -14.9.

2.3.3 dCu speciation

The dCu speciation data are shown in Table 2.3 and Figure 2.4. Natural ligands were saturated in dCu for stations 1, 4 and 16. As observed for Fe, Cu parameters also showed variations between and within the regions. Throughout the studied area, dCu ranged between 0.07 nM and 4.03 nM (mean concentration 0.91±0.77 nM). Cape Verde presented the greatest variability of dCu with concentrations between 0.36 and 4.03 nM (mean concentration 1.30±1.15 nM). Stations 1, 4 and 16 showed the highest dCu concentrations (4.03±0.20 nM, 1.51±0.20 nM and 1.98±0.08 nM, respectively) within this area. The stations were close to one another and located towards the northwest of Cape Verde. Minimum dCu concentrations (~0.45±0.09 nM) were recorded at the northeast stations (St. 13, 14 and 17).

In the Canary archipelago, the average dCu concentration was 0.65±0.15 nM and the maximum was found at St. 21 (1.05±0.11 nM), while the rest of the stations showed similar concentrations (0.61±0.08 nM). In the case of Madeira, St. 63 showed a dCu concentration similar to St. 54 (0.98±0.03 nM and 0.93±0.10 nM, respectively). The lowest concentration was observed in the Desertas Islands (St. 52, dCu=0.07±0.02 nM) and the highest in the Salvages Islands (St. 45, dCu=1.09±0.17 nM). The mean concentration observed in the Madeira archipelago was 0.77±0.47 nM. As indicated for Fe, station 45 presented dCu concentrations similar to the Madeira stations than to the Canaries. dCu concentrations at the oceanic stations slightly increased from south to north, with 0.44±0.07 nM at St. 17 and 0.57±0.01 nM at St. 44.

Table 2.1. Location, temperature (ºC), salinity, pH (total scale), dissolved oxygen concentration (µmol kg^{-1}) and fluorescence (a.u.) for each station measured at 20 m depth. Also included are nutrient concentrations (nitrites and nitrates, phosphates and silicates measured in µmol l^{-1}) obtained at around 20 m depth.

	Station	Latitude (°N)	Longitude (°E)	Temperature (°C)	Salinity	pH	O_2 (µmol kg^{-1})	Fluorescence (a.u.)	$NO_3^- + NO_2^-$ (µmol l^{-1})	PO_4^{3-} (µmol l^{-1})	$Si(OH)_4$ (µmol l^{-1})	Turbidity (NTU)
Cape Verde	1	16.9107	−25.1662	22.54	36.47	7.98	215.04	0.40	0.02	0.13	0.91	0.04
	4	16.5556	−24.3860	22.37	36.36	8.05	210.90	0.65	0.13	0.09	0.28	0.03
	6	14.8430	−24.2627	22.59	36.20	8.06	211.86	0.49	0.80	0.13	0.58	0.03
	9	14.8913	−23.5069	22.53	36.08	8.04	208.75	0.23	1.35	0.15	0.83	0.02
	11	15.1332	−23.2371	23.15	35.93	8.07	210.43	0.25	4.48	0.37	1.64	0.03
	13	16.1407	−22.9727	21.70	36.25	8.06	219.42	1.07	0.34	0.16	0.17	0.22
	14	16.6154	−22.9557	21.61	36.35	8.06	217.65	0.85	0.45	0.19	0.23	0.34
	16	16.8915	−24.8518	22.21	36.50	8.07	213.67	0.57	0.27	0.13	0.09	0.03
	17	17.5811	−24.2831	22.25	36.52	8.06	222.98	0.14	0.12	0.19	0.30	0.03
Canary Islands	21	27.6439	−17.9579	19.46	36.89	8.07	225.45	0.22	0.15	0.06	0.03	–
	23	27.9591	−17.6529	19.48	36.85	8.07	225.30	0.65	0.38	0.16	0.07	0.02
	25	28.0375	−17.3157	19.71	36.89	8.07	225.64	0.21	0.03	0.05	0.10	0.01
	31	28.0279	−16.7275	19.92	36.87	8.07	228.27	0.28	–	–	–	0.03
	32	28.0085	−16.6023	19.06	36.79	8.07	228.25	0.56	0.07	0.13	0.40	0.03
	34	28.3165	−16.3394	18.90	36.76	8.07	229.38	0.30	0.01	0.08	0.11	0.02
	37	28.3200	−15.9779	18.95	36.78	–	229.17	0.06	0.10	0.08	0.03	–
	39	27.8105	−15.8317	18.86	36.75	8.09	231.03	0.65	0.04	0.07	0.27	0.04
	40	27.6872	−15.7041	18.97	36.76	8.06	227.43	0.27	0.15	0.07	0.36	0.04
	42	27.9610	−15.3309	18.70	36.72	8.08	230.27	0.23	–	–	–	0.05
Madeira	44	29.1669	−15.5004	19.01	36.79	8.08	230.83	0.22	0.02	0.06	0.13	0.02
	45	30.0175	−16.0790	18.75	36.77	8.08	231.37	0.11	0.02	0.02	0.12	0.01
	52	32.4041	−16.5272	18.54	36.69	8.09	229.03	0.02	0.23	0.06	0.27	0.01
	54	32.6471	−16.5905	18.37	36.67	8.09	230.91	0.29	0.19	0.06	0.19	–
	63	32.6514	−17.1136	18.73	36.74	8.07	230.94	0.09	0.21	0.05	0.19	0.03

The L_{Cu} (Table 2.3 and Figure 2.4) for the entire studied region presented an average concentration of 1.05±0.46 nM with values between 0.54 nM and 2.59 nM. At Cape Verde, the mean concentration was 1.29±0.74 nM and the maximum (St. 14, 2.59±0.91 nM) and minimum (St. 13, 0.62±0.21 nM) were located at two nearby stations. In the Canary Islands, the mean L_{Cu} concentration was 0.86±0.23 nM, the highest value was measured at St. 21 (1.31±0.25 nM) and the lowest at St. 37 (0.54±0.07 nM). In Madeira, St. 63 (1.32±0.07 nM) presented a concentration higher than the one reported at St. 54 (1.18±0.29 nM) and south to Desertas Islands (St. 52, 0.90±0.14 nM), but similar to St. 45 (1.33±0.19 nM). The mean L_{Cu} within the Madeira archipelago was 1.18±0.20 nM. Regarding the oceanic stations (mean L_{Cu}=0.87±0.28 nM), St. 17 presented a lower concentration (0.68±0.11 nM) than St. 44 (1.07±0.28 nM).

In the Macaronesian region, log K^{cond}_{Cu2+L} varied between 13.40 and 14.42 (mean value 13.92±0.33, Table 2.3). In Cape Verde, the mean log K^{cond}_{Cu2+L} was 13.85±0.41. Around the Canaries, the average value was 13.89±0.30 with maximum at St. 37 (14.40±0.13). In the Madeira archipelago, log K^{cond}_{Cu2+L} showed a mean value of 14.10±0.28. As regards the oceanic stations, St. 17 presented a higher log K^{cond}_{Cu2+L} (14.22±0.16) than St. 44 (13.54±0.20). All stations showed log K^{cond}_{Cu2+L} values higher than 13, corresponding to L_1-type ligands.

The Cu′ concentrations ranged between 0.14 and 5.70 pM (average of 1.59±1.40 pM). The mean Cu′ concentration observed in Cape Verde (1.77±2.11 pM) was similar to that obtained in the Canary Islands (1.73±1.20 pM), and both of them were higher than the observed in the Madeira

archipelago (0.93±0.43 pM). The Cu^{2+} concentration ranged between 0.004 pM and 0.18 pM with an average value of 0.05±0.04 pM.

The CuL concentrations (mean global value 0.74±0.38 nM) indicated that more than 99% of Cu' was complexed (an exception was St. 52 at 97.7%). In Cape Verde, CuL ranged between 0.36 and 1.20 nM (average 0.88±0.56 nM). In the Canary region (average 0.60±0.08 nM), the maximum was found at St. 21 (1.05 nM), the minimum at St. 32 and 37 (0.51 nM). Except for St. 52 (0.07 nM), the values recorded in Madeira (average 1.00±0.08 nM) presented CuL concentrations higher than Cape Verde and the Canary Islands. The oceanic stations presented concentrations of 0.44 nM (St. 17) and 0.57 nM (St. 44).

The PCA analysis was conducted including all the stations. In the analysis (Figure 2.3), the stations were considered as bulk data as well as clustered by archipelagos with similarities between Canary Island and Madeira samples. The PC1 explained 92.9% of the variance. Samples were split into stations that presented higher nutrient availability (NO_3^-+NO_2^-, $Si(OH)_4$ and PO_4^{3-}, Table 2.1), dCu, temperature, turbidity and fluorescence on positive scores, that correspond with Cape Verde samples. Salinity and dFe concentration had negative scores and contain the Canary Islands and Madeira samples. Then PC1 mostly reflects the south to north gradient observed with a transition from more nutrient-rich to oligotrophic waters. This could indicate that the source of dFe is different from that of dCu and the rest of the nutrients.

The PC2 explained 7.1% of the variance, the strongest positive coefficients were related with dFe and dCu while the negatives with salinity and fluorescence. This distribution could be related to biological utilisation of dFe

Table 2.2. Dissolved Fe concentrations (dFe, nM) and dFe speciation for all the studied stations. Labile Fe (Fe', in pM), free inorganic Fe (pFe^{3+}) expressed as -log[Fe^{3+}] in M, Fe-binding ligands (L_{Fe}, in nM), excess of ligands (eL_{Fe}, in nM calculated as the difference between L_{Fe} and dFe), organically bound Fe (FeL, in nM), percentage of the metal organically complexed (%FeL), stability constant referred to Fe^{3+} (log $K^{cond}_{Fe^{3+}L}$) and the reactivity of the metal-binding ligands in respect to the Fe^{3+} (log $\alpha_{Fe^{3+}L}$). "nd" means that the natural ligands were saturated in dFe.

	Station	dFe(nM)	Fe′ (pM)	pFe^{3+}	L_{Fe} (nM)	eL_{Fe} (nM)	FeL (nM)	%FeL	log $K^{cond}_{Fe^{3+}L}$	log $\alpha_{Fe^{3+}L}$
	1	0.60 ± 0.10	nd	nd	nd	nd	nd	nd	nd	nd
	4	0.51 ± 0.19	2.28 ± 0.07	21.64 ± 23.17	1.47 ± 0.05	0.96	0.51	99.55	21.36 ± 0.01	12.53
	6	0.49 ± 0.04	1.14 ± 0.16	21.94 ± 22.79	1.81 ± 0.08	1.32	0.49	99.77	21.87 ± 0.46	13.13
	9	1.10 ± 0.17	11.7 ± 1.28	20.93 ± 21.89	1.66 ± 0.26	0.56	1.09	98.94	21.21 ± 0.19	12.43
Cape Verde	11	0.95 ± 0.08	14.3 ± 9.38	20.84 ± 21.03	1.10 ± 0.32	0.15	0.94	98.49	21.60 ± 0.34	12.64
	13	0.51 ± 0.06	nd	nd	nd	nd	nd	nd	nd	nd
	14	0.67 ± 0.06	nd	nd	nd	nd	nd	nd	nd	nd
	16	1.19 ± 0.12	3.25 ± 0.41	21.49 ± 22.39	1.78 ± 0.28	0.59	1.19	99.73	21.79 ± 0.21	13.04
	17	0.46 ± 0.29	9.56 ± 0.33	21.02 ± 22.48	0.52 ± 0.11	0.06	0.45	97.92	21.85 ± 0.38	12.56
	21	0.97 ± 0.27	31.9 ± 8.86	20.50 ± 21.05	1.01 ± 0.21	0.04	0.94	96.71	21.59 ± 0.23	12.59
	23	0.89 ± 0.12	8.68 ± 0.70	21.06 ± 22.16	1.17 ± 0.13	0.28	0.88	99.02	21.54 ± 0.11	12.61
	25	0.89 ± 0.03	7.47 ± 0.20	21.13 ± 22.70	1.34 ± 0.36	0.45	0.88	99.16	21.41 ± 0.26	12.54
	31	0.73 ± 0.04	nd	nd	nd	nd	nd	nd	nd	nd
	32	0.83 ± 0.19	5.67 ± 1.30	21.25 ± 21.89	1.28 ± 0.29	0.45	0.82	99.32	21.51 ± 0.32	12.62
Canary Islands	34	0.63 ± 0.02	5.18 ± 0.41	21.29 ± 22.39	1.56 ± 0.29	0.93	0.63	99.18	21.11 ± 0.17	12.31
	37	0.87 ± 0.04	11.5 ± 7.58	20.94 ± 21.12	1.30 ± 0.52	0.43	0.86	98.68	21.23 ± 0.37	12.34
	39	0.57 ± 0.03	5.73 ± 1.32	21.24 ± 21.88	0.94 ± 0.26	0.37	0.56	98.99	21.41 ± 0.29	12.39
	40	1.06 ± 0.10	25.50 ± 7.27	20.59 ± 21.14	1.36 ± 0.37	0.30	1.03	97.59	21.09 ± 0.22	12.23
	42	0.61 ± 0.07	10.00 ± 1.79	21.00 ± 21.75	1.61 ± 0.58	1.00	0.60	98.36	20.77 ± 0.27	11.98
	44	0.71 ± 0.07	6.02 ± 0.58	21.22 ± 22.23	1.22 ± 0.19	0.51	0.70	99.15	21.36 ± 0.20	12.44
	45	1.24 ± 0.30	14.4 ± 10.30	20.84 ± 20.99	1.33 ± 0.28	0.09	1.23	98.84	21.90 ± 0.48	13.03
Madeira	52	1.32 ± 0.18	15.70 ± 5.26	20.80 ± 21.28	1.47 ± 0.19	0.15	1.30	98.81	21.70 ± 0.46	12.87
	54	0.73 ± 0.13	28.60 ± 11.80	20.54 ± 20.93	0.84 ± 0.33	0.11	0.70	96.08	21.24 ± 0.37	12.16
	63	0.70 ± 0.28	5.62 ± 2.90	21.25 ± 21.54	1.10 ± 0.38	0.40	0.69	99.20	21.49 ± 0.35	12.53

and dCu, but could also indicate a correlation between dCu and NO_3^-+NO_2^- and turbidity.

Through this analysis, Cape Verde is the region with the greatest dispersion, where St. 1, 9, 11 and 16 were different from the rest of the stations. However, the Canary Islands and Madeira samples are more aggregated.

2.4 Discussion

2.4.1 Island environment and processes

The metal distributions around the islands are affected by complex hydrographic dynamics and processes such as horizontal advection, vertical mixing, regenerations from sinking particles and resuspension from shelf sediments (Blain et al., 2008). Furthermore, for the Canary Islands and Madeira, a strong mesoscale variability was observed due to the interaction between the prevailing winds and currents with the landmasses (Caldeira et al., 2002; Sangrà et al., 2005; Caldeira and Sangrà, 2012). Islands act as barriers with differences in flow current perturbation and wind share between east and west (Sangrà et al., 2009). As a consequence, the mixing process which takes place in these waters also differs.

As the presence of microorganisms is also relevant in terms of metal speciation, it is important to remark that the mesoscale variability generated in the vicinity of oceanic islands also influences the phytoplankton community. On the island of Gran Canaria, the effect of wind stress on biological production has previously been studied (Basterretxea et al., 2002; Arístegui and Montero, 2005). It was observed that on the flanks and

downstream of the island an enhancement of biological production was associated with wind induced water upwelling (divergent boundary) or downwelling (convergent boundary).

The studied region, archipelagic waters, is also particularly complex to describe due to the variety of chemical processes that could take place. Firstly, surface waters are subject to photoreduction reactions affecting both metals and organic compounds. The photochemical reaction can occur by direct light absorption followed by a charge transfer between ligand and metal or by the production of radical species. As a result, the amount of metals in the solution could increase, the ligands may decompose or the binding sites could be modified or lost, resulting in a ligand binding strength decrease (Moffett and Zika, 1987; Barbeau, 2006). These processes can enhance the bioavailability and reactivity of metals and may occur in solution or on the particle surface. In fact, the presence of suspended particulate matter decreases the concentration of surface metals due to the scavenging process. In the open ocean surface waters, the presence of particles is related to biological sources or dust deposition. In coastal areas, the particles could also be related to runoff, ravines inputs and suspended sediments, as well as anthropogenic sources. Other molecular aggregates may undergo scavenging. Within the dissolved fraction, the colloidal phase may contain both metal species and ligands. The formation of larger colloidal aggregates may increase the transport of metals to deeper layers and decrease their bioavailability (Wu et al., 2001). In addition, in coastal areas, human activities such as sewage discharge, power and desalination plants and industries could alter the chemistry of coastal water.

Table 2.3. Dissolved Cu concentrations (nM) and dCu speciation for all the studied stations. Labile Cu (Cu', in pM), free inorganic Cu (Cu^{2+}, in pM), Cu-binding ligands (L_{Cu}, in nM), excess of ligands (Excess of L_{Cu}, in nM calculated as the difference between L_{Cu} and dCu), organically bound Cu (CuL, in nM), percentage of the metal organically complexed (%CuL), conditional stability constant for Cu^{2+} (log K^{cond}_{Cu2+L}), the reactivity of the metal-binding ligands in respect to Cu^{2+} (log α_{Cu2+L}). "nd" means that the natural ligands were saturated in dCu.

	Station	dCu (nM)	Cu(pM)	Cu^{2+} (pM)	L_{Cu} (nM)	eL_{Cu} (nM)	CuL (nM)	%CuL	log K^{cond}_{Cu2+L}	log α_{Cu2+L}
	1	4.03 ± 0.20	nd	nd	nd	nd	nd	nd	nd	nd
	4	1.51 ± 0.20	nd	nd	nd	nd	nd	nd	nd	nd
	6	0.78 ± 0.03	5.70 ± 0.75	0.18 ± 0.02	0.94 ± 0.12	0.16	0.77	99.27	13.40 ± 0.08	4.37
	9	0.90 ± 0.10	2.29 ± 0.40	0.07 ± 0.01	1.32 ± 0.49	0.42	0.90	99.75	13.48 ± 0.30	4.60
Cape Verde	11	1.20 ± 0.01	0.45 ± 0.04	0.01 ± 0.001	1.61 ± 0.17	0.40	1.20	99.96	14.33 ± 0.12	5.54
	13	0.54 ± 0.03	1.71 ± 0.52	0.05 ± 0.02	0.62 ± 0.21	0.08	0.54	99.68	14.09 ± 0.39	4.88
	14	0.36 ± 0.02	0.14 ± 0.02	0.004 ± 0.001	2.59 ± 0.91	2.24	0.36	99.96	13.58 ± 0.31	4.99
	16	1.98 ± 0.08	nd	nd	nd	nd	nd	nd	nd	nd
	17	0.44 ± 0.07	0.32 ± 0.04	0.01 ± 0.001	0.68 ± 0.11	0.24	0.44	99.93	14.22 ± 0.16	5.05
	21	1.05 ± 0.11	1.38 ± 0.14	0.04 ± 0.004	1.31 ± 0.25	0.26	1.05	99.87	13.97 ± 0.21	5.08
	23	0.74 ± 0.04	1.77 ± 0.31	0.06 ± 0.01	0.85 ± 0.18	0.11	0.74	99.76	14.08 ± 0.33	5.01
	25	0.72 ± 0.05	0.44 ± 0.06	0.01 ± 0.001	1.04 ± 0.17	0.32	0.72	99.94	14.21 ± 0.18	5.23
	31	0.63 ± 0.003	1.77 ± 0.25	0.06 ± 0.01	0.76 ± 0.05	0.14	0.62	99.72	13.91 ± 0.16	4.79
	32	0.51 ± 0.01	1.45 ± 0.06	0.05 ± 0.002	0.64 ± 0.28	0.13	0.51	99.71	13.91 ± 0.35	4.72
Canary Islands	34	0.56 ± 0.01	1.43 ± 0.71	0.04 ± 0.02	0.70 ± 0.14	0.14	0.56	99.74	13.96 ± 0.17	4.80
	37	0.51 ± 0.03	1.86 ± 0.17	0.06 ± 0.01	0.54 ± 0.07	0.03	0.51	99.64	14.40 ± 0.13	5.14
	39	0.59 ± 0.03	1.32 ± 0.15	0.04 ± 0.005	0.83 ± 0.26	0.24	0.59	99.78	13.77 ± 0.31	4.69
	40	0.67 ± 0.06	1.40 ± 0.09	0.04 ± 0.003	1.05 ± 0.35	0.38	0.67	99.79	13.60 ± 0.31	4.62
	42	0.58 ± 0.08	5.14 ± 0.53	0.16 ± 0.02	0.72 ± 0.26	0.14	0.58	99.12	13.40 ± 0.27	4.25
	44	0.57 ± 0002	1.03 ± 1.61	0.03 ± 0.05	1.07 ± 0.28	0.50	0.57	99.82	13.54 ± 0.20	4.57
	45	1.09 ± 0.07	0.55 ± 0.17	0.02 ± 0.01	1.33 ± 0.19	0.24	1.09	99.95	14.42 ± 0.22	5.54
Madeira	52	0.07 ± 0.02	1.52 ± 0.20	0.05 ± 0.01	0.90 ± 0.14	0.83	0.07	97.72	13.78 ± 0.12	4.73
	54	0.93 ± 0.10	0.72 ± 0.17	0.02 ± 0.01	1.18 ± 0.29	0.25	0.93	99.92	14.21 ± 0.36	5.28
	63	0.98 ± 0.03	0.94 ± 0.10	0.03 ± 0.003	1.32 ± 0.07	0.34	0.98	99.90	13.99 ± 0.30	5.11

All these processes result in a very complex and heterogeneous set of compounds that constitute the ligand pool present in the seawater. Different assumptions have to be taken into account to apply the CLE-ACSV technique and obtain information about the bulk ligand concentration and characterization (Gerringa et al., 2014). In addition, pH, temperature, salinity and the chosen competitive ligand are key parameters. For this reason, the term "conditional" is used to indicate the stability constants determined by voltammetry under the selected experimental conditions.

2.4.2 dFe speciation

The surface concentrations of dFe measured along the Macaronesian coastal region (mean dFe=0.80±0.25 nM) were comparable with the results obtained in the whole Atlantic Ocean with values between 0.13 and 1.80 nM (Gledhill and van den Berg, 1994; Rijkenberg et al., 2012; Buck et al., 2015; Hatta et al., 2015). The oceanic stations (St. 17 and 44) showed dFe concentrations similar to those reported by other studies in the same region (Boye et al., 2006; Buck et al., 2015). In Cape Verde, the highest concentrations were observed at St. 9 and 11, the south-easternmost samples of the region, along with higher concentrations of NO_3^-+NO_2^- and $Si(OH)_4$. For these stations, Mehlmann et al. (2020) reported a wind speed (25.5 m s^{-1}) higher than the one observed in other locations (~9.8 m s^{-1}). Windy conditions can enhance the vertical diffusive mixing and supply dFe to the surface water from waters below (Rijkenberg et al., 2012) and from the sediment (Gerringa et al., 2008) as well as from the island due to the proximity of the coast. These resuspended sediments can favour the sequestration of dFe to deep waters via scavenging or be a source of Fe^{2+} if the particles undergo photoreduction

processes in surface waters (Wells and Mayer, 1991). Two studies with transects from the oceanic region to the African coastal margin reported a trend with increasing dFe concentrations toward the coast (Rijkenberg et al., 2012; Hatta et al., 2015). In the study at hand, there were no evidences of contributions of dFe from the African dust, and the observed variations were associated with local processes.

The measured L_{Fe} concentrations (0.52 – 1.81 nM) were in good agreement with the literature for the Atlantic Ocean (Gledhill and van den Berg, 1994; Boye et al., 2003, 2006; Gerringa et al., 2006; Rijkenberg et al., 2008; Thuróczy et al., 2010; Buck et al., 2015). Most of these investigations showed a variation of L_{Fe} between 0.8 and 2 nM and different ligand sources were suggested (biological production, organic matter remineralization, benthic fluxes and dust deposition). No clear relationship was observed between the L_{Fe} and the fluorescence peaks detected during the cruise, where stations with high L_{Fe} concentrations did not correspond with high fluorescence. Minimum L_{Fe} at St.17 was associated with oceanic waters. For coastal stations, a relationship was observed between wind conditions, biological activity and water depth with the concentration of L_{Fe}. The effect of the wind on the water mixing and the resuspension of dFe and L_{Fe} can be important at the shallower stations and could be coupled with a biological enhancement. Stations 1, 13 and 14 presented shallow depths (63 m, 35 m and 31 m, respectively), and had the highest turbidity and saturated titration curves, which could be associated with resuspension of L_{Fe} from bottom sediments. Station 6 presented high L_{Fe}, low dFe concentrations, windy conditions, high fluorescence and high concentrations of NO_3^-+NO_2^- and $Si(OH)_4$. At this location, both turbulence (induced by wind) and biological activity may control the ligand and metal concentrations. The east coasts of Tenerife and

Gran Canaria (St. 34 and 42) were characterized by windy conditions, high L_{Fe}, low dFe but low fluorescence concentrations. These locations (St. 34 and 42) were close to urbanized areas where the anthropogenic ligand sources (sewage discharge, desalination plants and industries) along with the water mixing induced by the wind could explain the L_{Fe} and dFe values. Station 39, situated in the southwest part of Gran Canaria, showed low L_{Fe}, low dFe and high concentrations of fluorescence and $Si(OH)_4$. Arístegui et al. (1997) reported an enhancement of primary production on the west coast of Gran Canaria, associated with both wind stirring and local water upwelling, which could explain the decrease of dFe due to biological uptake. On the other hand, at St. 25, 31 and 32, as reported for the coast of Gran Canaria (Arístegui et al., 1997; Basterretxea et al., 2002; Arístegui and Montero, 2005), convergent or divergent fronts could be present along either side of the wake region and produce water sinking or upwelling, respectively, which could influence the metal and ligand distribution.

The dFe and L_{Fe} concentrations were linearly correlated (Figure 2.5). The ratio L_{Fe}/dFe indicates the saturation state of ligands and, whether precipitation is favoured or not (Thuróczy et al., 2011a). This behaviour highlights the role of ligands in stabilising dFe in surface water. All stations (except stations 1, 13, 14 and 31 that presented saturated titration curves) showed a ratio higher than 1 as reported for coastal areas and marginal seas (Kondo et al., 2007; Mellett and Buck, 2020) and could be related with a similar origin of dFe and L_{Fe}. Higher ratios were observed at stations 4, 6, 34 and 42, where L_{Fe} concentrations were greater than dFe (eL_{Fe} values were close to or greater than 1 nM). Stations 4 (L_{Fe}/dFe=2.88) and 6 (L_{Fe}/dFe=3.72) presented relatively high fluorescence values (0.65 and 0.49 a.u., respectively), which could indicate a biological production of ligands.

Thuróczy et al. (2011a) reported a ratio of around 4.4 for surface waters with high phytoplankton activity. Stations 34 (L_{Fe}/dFe=2.48) and 42 (L_{Fe}/dFe=2.64) ratios were related to water mixing induced by the wind. Figure 2.5 shows how these stations differ from the other samples.

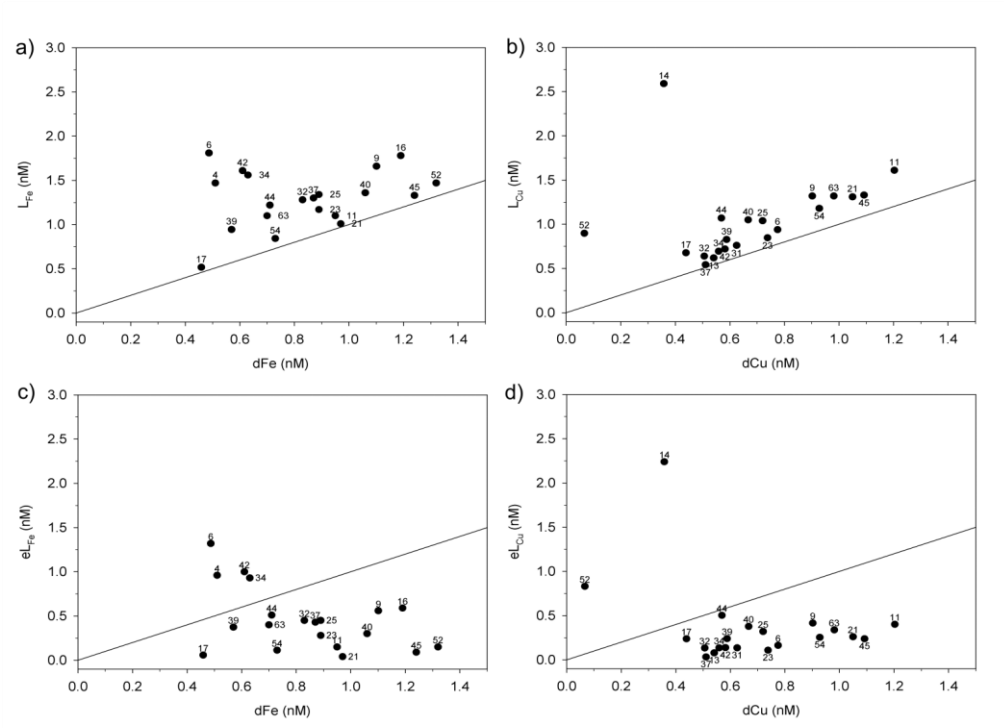

Figure 2.5. Correlation between ligand and dissolved metal concentrations for Fe (a) and Cu (b). Relationship between excess ligand and dissolved metal concentration for Fe (c) and Cu (d). The solid line represents a 1:1 relationship.

The log K^{cond}_{Fe3+L} obtained in this work (21.45±0.29) was in the range of values (18.8 – 22.85) reported in the literature for oceanic waters in this region (Gledhill and van den Berg, 1994; Boye et al., 2003, 2006; Gerringa et al., 2006; Rijkenberg et al., 2008, 2012; Thuróczy et al., 2010; Buck et al., 2015). As detected in the Macaronesia region, only one ligand type was normally

measured in the Northeast Atlantic region (Boye et al., 2003, 2006; Gerringa et al., 2006; Rijkenberg et al., 2008; Thuróczy et al., 2010), L_1 or L_2. Buck et al. (2015) reported data for a second ligand class, probably associated with the use of a larger detection window (25 μM SA). Our samples presented log K^{cond}_{Fe3+L} values lower than 22 (L_2-type) in agreement with the literature on the region (Gerringa et al., 2007; Thuróczy et al., 2010). On the other hand, the lower value reported at St. 42 matched with the results reported by (Boye et al., 2003, 2006). Voltammetry results do not provide information about the nature of the compounds detected, but they do allow us to compare the conditional constants obtained with those of compounds already identified through incubation experiments or processes. Siderophores have been detected in surface water with log K^{cond}_{Fe3+L} values between 21 and 24 (Witter et al., 2000; Bundy et al., 2018) in regions with atmospheric dust deposition. Humic Substances have also been detected with strong ligand constants (Laglera and van den Berg, 2009; Laglera et al., 2011). The presence of weaker ligands (log $K^{cond}_{Fe3+L}<22$) has been related to the grazing of phytoplankton by zooplankton and with the bacterial remineralization of organic sinking particles (Sato et al., 2007; Poorvin et al., 2011). In addition, Witter et al. (2000), González et al. (2019) and Arreguin et al. (2021) also reported the complexing capacity of individual ligands in seawater (i.e. catechin, sinapic acid, gallic acid, gentisic acid, apoferritin, alterobactin, desferrioxamine, enterobactin and ferrichrome) in a wide range, from L_1 to L_2-type ligands.

The variability observed for Fe' (range between 1.14 and 31.90 pM) was slightly higher than that described for the surface oceanic waters of the Northeast Atlantic Ocean (Gledhill and van den Berg, 1994; Boye et al., 2003, 2006), where concentration between 1.4 and 26.9 pM were obtained. The Fe'

concentration gradient with the lowest values at Cape Verde and highest at Madeira follow the trend observed in the excess ligand concentration. Most of the FeL concentrations (0.45 – 1.30 nM) were similar to the values indicated for the oceanic region (Gledhill and van den Berg, 1994; Boye et al., 2003, 2006), which presented concentrations between 0.54 and 1.77 nM.

The obtained theoretical concentration of $Fe(OH)_3$ (0.018±0.001 nM) was higher than the observed concentration of Fe^{3+}(between 10^{-21} and 10^{-22} M). The precipitation of hydroxides was not favoured due to the low concentration of Fe^{3+}. It has been demonstrated that the presence of organic binding ligands increases the solubility of Fe (Kuma et al., 1996; Liu and Millero, 1999).

The average $\log f_{Fe^{3+}L}$ obtained along the Macaronesia region (12.62±0.43, Table 2.2) agreed with the results reported for the Northeast Atlantic surface waters (Thuróczy et al., 2010; Buck et al., 2015; Gerringa et al., 2017), with values between 12 and 13.7. Higher $\log f_{Fe^{3+}L}$ values indicate a higher capacity of the ligand to bind dFe.

2.4.3 dCu speciation

The measured dCu surface concentration in the Macaronesia region (mean value 0.91±0.77 nM) was comparable with the results reported for the Atlantic Ocean (Kremling, 1985; Kramer, 1986; Saager et al., 1997; Jacquot and Moffett, 2015; Roshan and Wu, 2015). The maximum measured dCu concentration, at St. 1 (4.03±0.20 nM), was in the range of the values reported by (Buckley and van den Berg (1986) for the surface water in the same region (3.6 – 5.9 nM). The Cape Verde stations presented the highest dCu variability.

The highest concentrations were found around the northwestern islands (St. 1, 4 and 16), corresponding with a relatively high surface fluorescence (>0.40 a.u.). Furthermore, the northeastern stations (St. 1, 4 and 16) should be the ones most affected by the currents arriving from the Canary Islands, and by the mixing processes which occur in the Cape Verde Frontal Zone (Peña-Izquierdo et al., 2012; Pelegrí et al., 2017) but could also be accentuated by the strong winds near St. 1 (Mehlmann et al., 2020). Jacquot and Moffett, (2015) suggested that the sediments and shelf can be a source of dCu for the region between Cape Verde and Mauritania. However, the shallowest stations (St. 13 and 14) presented the lowest dCu concentration along with the oceanic station (St. 17). The chemical properties of the sediment determine the effect on the surrounding waters, but also the biological activities can change the amounts of dCu and L_{Cu} present in surface waters. The small increase in concentration registered between the Canary Islands (dCu= 0.65±0.15 nM) and Madeira (dCu= 0.77±0.47 nM) was reflected in the results of Jacquot and Moffett (2015) and Roshan and Wu (2015).

The correlation between dCu and salinity (Figure 2.6) observed in the Macaronesia region was compared with the results reported in the western North Atlantic Ocean for oceanic waters (Jacquot and Moffett, 2015; Roshan and Wu, 2015). The Madeira data were observed to be within the range described by these authors; Cape Verde values (excluding stations 1, 4 and 16) followed a different trend, while the Canary Islands data presented a different distribution. Roshan and Wu (2015) associate the linearity between the parameters with a long residence time of dCu in the surface mixed layer. Deviations observed in our data could be related to the processes that differentiate coastal from oceanic waters described above, where St. 1, 4 and

16 are the most affected by the mixing of the waters in the Cape Verde Frontal Zone.

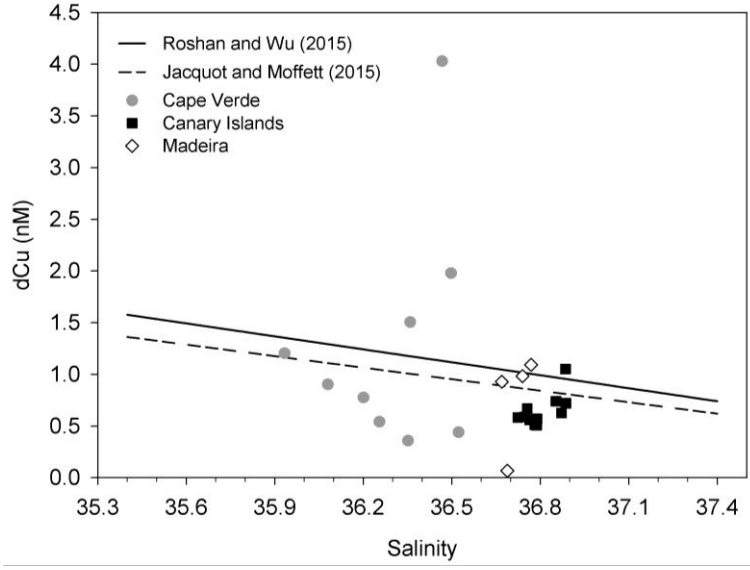

Figure 2.6. Dissolved Cu (dCu, nM) vs. salinity for Cape Verde region (grey circles), Canary Islands (black squares) and Madeira (empty rhombuses). Stations 1, 4 and 16 were not included. The correlation reported by Roshan and Wu (2015) was dCu=-2.35 S+39.1 (R^2=0.97) while the trend described by Jacquot and Moffett (2015) was dCu=-0.37 S+14.6 (R^2=0.80).

The L_{Cu} concentrations recorded throughout the Macaronesia archipelagos (mean L_{Cu}=1.05±0.46 nM) were lower than the ones obtained by Jacquot and Moffett (2015) for the oceanic area, whose results between Mauritania and Portugal (~35 m depth) presented values between 2 and 3.69 nM. As indicated for L_{Fe}, at St. 13 and 14, the biological activity could explain the lowest (St.13, 0.62±0.21 nM) and highest (St.14, 2.59±0.91 nM) L_{Cu} concentrations observed in the Cape Verde region. Both stations presented low dCu concentrations and the highest fluorescence and turbidity value. Furthermore, these locations were shallow and the contribution of L_{Cu} from the bottom

sediments should also be considered. Low L_{Cu}, dCu and fluorescence values observed at CVOO (St. 17) and in open waters between Tenerife and Gran Canaria (St. 37) supports the hypothesis that coastal waters represent a source of dCu and Cu-ligands for the nearby areas by biological activity and/or by the contribution from the sediments and the coast. As suggested for L_{Fe}, windy conditions can increase the water mixing and favour the resuspension from benthic sediments (Jacquot and Moffett, 2015) and explain the high L_{Cu} concentrations reported at St. 9 (1.32±0.49 nM), 11 (1.61±0.17 nM) and 21 (1.31±0.24 nM). Stations 9 and 11 also presented high concentrations of NO_3^- +NO_2^- and $Si(OH)_4$ which could also imply an input of nutrients and ligands from deeper waters associated with mixing processes.

Based on these results, a linear multiple regression was applied to determine which environmental variables were related to the concentration of ligands in seawater. For L_{Fe} no significant (p-value>0.05) correlations were observed. However, L_{Cu} concentration was correlated with water turbidity, NO_3^-+NO_2^- concentration and fluorescence, following the equation below:

$$L_{Cu} = 1.173 + 0.147 \cdot [NO_3^- + NO_2^-] + 6.104 \cdot \text{Turbidity} - 1.292 \cdot \text{Fluorescence} \quad (2.13)$$

The determination coefficient (R^2) of the linear model presented a value of 0.7, with a standard error or estimation of 0.3 nM and the variability of L_{Cu} associated with the parameters is significant (p-value < 0.05).

The linear model explains almost 70% of the variability observed in the coastal waters of the Macaronesia islands. Within this fit, the role of turbidity outweighs the effect of fluorescence and NO_3^-+NO_2^- concentration. Turbidity is an important factor that differentiates coastal from oceanic regions, as the distance from the coast decreases, this variable can increase due to both

terrigenous input and bottom sediment mobilisation. Fluorescence can be related to primary production, which is generally higher in coastal regions than in oceanic waters. On the other hand, the presence of NO_3^-+NO_2^- could be related to higher productivity, anthropogenic sources and, consequently, organic ligands. Among the variety of substances that form dissolved organic matter are amino acids, which can react and bind to dissolved metals (Benner, 2011; Devez et al., 2015).

The concentration of L_{Cu} and dCu were positively correlated (Figure 2.5). The ratio L_{Cu}/dCu, representing the saturation state of the ligands with Cu, was always higher than 1. On the other hand, the relation between eL_{Cu} and dCu concentrations indicates that at St. 14 and 52 the concentrations of ligands were much higher than at the other stations. The biological production (St. 14) and the water mixing with resuspension from the sediment (St. 52) could increase L_{Cu} concentrations.

The log K^{cond}_{Cu2+L} obtained in this study (13.92±0.33) corresponds with L_1-type ligands (log K^{cond}_{Cu2+L}>13). The results were comparable with data reported by other authors in the same region (Jacquot and Moffett, 2015; log K^{cond}_{Cu2+L}=13.57±0.48). Coastal stations presented log K^{cond}_{Cu2+L} values between 13.40 and 14.42, higher than the ones observed in the nearshore waters of the West Florida Shelf (Mellett and Buck, 2020), whose values range between 13.09 and 13.31 and where riverine inputs of ligands were detected. Inshore waters of the Bermudas (Oldham et al., 2014) presented two ligand classes (log K^{cond}_{Cu2+L1}= 14 – 15.1 and log K^{cond}_{Cu2+L2}=12.6 – 14.1), and the environment was affected by different anthropogenic activities. For offshore waters, Mellett and Buck (2020) also reported a single ligand type (log K^{cond}_{Cu2+L} = 13.85 – 13.91) with values more similar to those obtained in

the Macaronesia region for both coastal and oceanic waters. In offshore surface waters near the Bermudas (Oldham et al., 2014) two ligand classes were detected with log K^{cond}_{Cu2+L1}= 15.1 – 14 and log K^{cond}_{Cu2+L2}=13.7 – 12.6. Also, in the continental slope of the northeast Pacific, Whitby et al. (2018) observed two ligand types in oceanic (log K^{cond}_{Cu2+L1}= 15.5 and log K^{cond}_{Cu2+L2}=12.9) and nearshore stations (log K^{cond}_{Cu2+L1}= 15.5 and log K^{cond}_{Cu2+L2}=12.6). For the Sargasso Sea, Moffett et al. (1990) suggest that strong ligands are related to a recent biological origin rather than to refractory humic substances.

The amounts of Cu' and Cu^{2+} (1.59±1.40 pM and 0.05±0.04 pM, the respective mean concentrations) were very low compared to the dCu concentrations (0.91±0.76 nM). Free Cu can be toxic and inhibit the growth of phytoplankton. The toxicity depends on each organism, but it is estimated that at concentrations higher than 10 pM, some phytoplankton and cyanobacteria species reduce the growth rate (Sunda and Lewis, 1978; Brand et al., 1986; Coale and Bruland, 1990). However, if the free Cu concentration is too low (below 0.01 pM), it is insufficient to allow the acquisition of Fe by marine organisms (Peers et al., 2005; Maldonado et al., 2006). The Cu^{2+} concentrations observed in the Macaronesia region did not exceed the toxicity values but could limit the growth of phytoplankton due to Cu^{2+} deficiency, as reported for oceanic waters (Moffett and Dupont, 2007; Jacquot and Moffett, 2015). Most of the dCu concentrations were observed as CuL, with more than 99% of dCu bound with ligands, as reported in the literature (Coale and Bruland, 1990; Buck and Bruland, 2005; Moffett and Dupont, 2007; Whitby et al., 2018)

Throughout the Macaronesia region, log f_{Cu2+L} ranges between 4.25 and 5.54 (average value 4.90±0.34). Higher values indicate a higher capacity of the ligand to bind dCu. While the average value was lower than the one observed in nearshore waters of the West Florida Shelf (5.15 – 5.10) described by Mellett and Buck (2020), the range observed in the Macaronesia region was wider. The West Florida offshore waters presented values more similar to those obtained at St.17 (log f_{Cu2+L}=5.05).

When comparing the speciation results of Fe with those of Cu, it was observed that the maximums and minimums of dFe and dCu or L_{Fe} and L_{Cu} were not measured at the same stations. The sources of metals and ligands were not always the same between stations, as well as the processes which removed them from surface water, especially in coastal waters where several processes are taking place at the same time. For example, the chemical properties of the sediments, the organisms which form the phytoplankton community or the dynamic process, are not the same in the region. However, at many stations (10 over 24), the ranges of concentrations of L_{Fe} and L_{Cu} were similar. Buck et al. (2015) and Jacquot and Moffett (2015) suggested for the North Atlantic Ocean that the ligands could have a similar source or at least a part of L_{Fe} was not specific for Fe. The same was also suggested for the West Florida Shelf waters (Mellett and Buck, 2020). At the stations where the biological activity and the wind stress were not important, other factors could explain the presence of high values of dissolved metal and ligands. The horizontal advection, the isopycnal mixing and the dissolution from lithogenic particles (Blain et al., 2008) are processes which alter the speciation of metals in coastal waters but their effects cannot be demonstrated with the available data.

2.5. Conclusions

The knowledge about the iron and copper speciation in the coastal waters is quite important to be able to understand the global biogeochemical cycles of Fe and Cu. Among the Atlantic Ocean, the surrounding waters of Macaronesia islands are relevant to the role of the Atlantic circulation. They are close to the upwelling and within the subtropical gyre. Regarding Fe speciation, dFe was found in excess of L_{Fe} concentrations, and a complexation percentage higher than 98% was observed. Only one ligand (concentrations ranging between 0.56 and 2.96 nM) was detected with log K^{cond}_{Fe3+L} values lower than 22 (L_2-type). On the other hand, strong Cu-complexing ligands dominate dCu speciation. More than 99% of dCu was complexed by strong ligands (L_1-type) of log K^{cond}_{Cu2+L}=13.92±0.33 and only one complex was detected at concentrations varying between 0.54 and 2.59 nM. As a consequence of the high complexation, the concentration of Cu^{2+} (0.004-0.18 pM) was below the toxicity limit but could inhibit the growth of certain phytoplankton species. This distribution of dFe and dCu seems to be related to the hydrographic parameters (temperature, salinity, turbidity, fluorescence and nutrient concentration), while the content of L_{Cu} was mostly related to the turbidity, fluorescence and NO_3^-+NO_2^- concentrations that were fitted to a multilinear regression equation.

Throughout the study region, dFe and dCu presented different distributions of extreme values. However, the concentration ranges of L_{Fe} and L_{Cu} overlapped at many stations even if the maximums and minimums were obtained at different locations.

The chemistry of Fe and Cu is also dependent on the wind-mediated mixing processes and fluorescence. A relationship was observed between the

maximum and minimum values obtained and the presence of strong winds and high fluorescence, both for dFe and dCu concentrations, as well as for L_{Fe} and L_{Cu} concentrations. Differences between coastal and oceanic concentrations of dissolved metals and ligands were observed in the regions of the Canary Islands and Cape Verde.

According to the current investigation, the coastal stations present a higher concentration of dissolved metals and ligands than the oceanic stations. Therefore, coastal waters of the Macaronesia region could be a source of metals and ligands, possibly associated with the resuspension of sediments by the action of currents and wind and the biological activity. The data reported in this study improve our knowledge about the Fe and Cu biogeochemical cycles in coastal waters.

Acknowledgments

We want to express our gratitude to Dr. Birgit Quack from GEOMAR for inviting us to participate in the AIMAC project. Thanks to the Master and crew of *R/V Poseidon* for support during the cruise. Special thanks go to Rui Caldeira, Cátia Azevedo, Claudio Cardoso, Ricardo Faria and Jesus Reis from the Oceanic Observatory of Madeira for the CTD-deployments and data. To acknowledge the GEOMAR funds for POS533 and Kastriot Qelaj for the nutrient analysis. This study received funding from the European Union's Horizon 2020 research and innovation program under grant agreement No 820989 (project COMFORT, Our common future ocean in the Earth system–quantifying coupled cycles of carbon, oxygen, and nutrients for determining and achieving safe operating spaces with respect to tipping points). We also acknowledge the financial support for the ATOPFe project (CTM2017-

83476-P) from the Ministerio de Ciencia e Innovación (Spain). Veronica Arnone's participation was funded by the PhD grant (PRE 2018-084476). The participation of Aridane G. González was within the Programa de Cooperación INTERREG V-A España-Portugal MAC (Madeira-Azores-Canarias) 2014e2020 (PLANCLIMAC project).

Image: USGS/ESA/ Landsat-8 satellite's Operational Land Imager (2013).

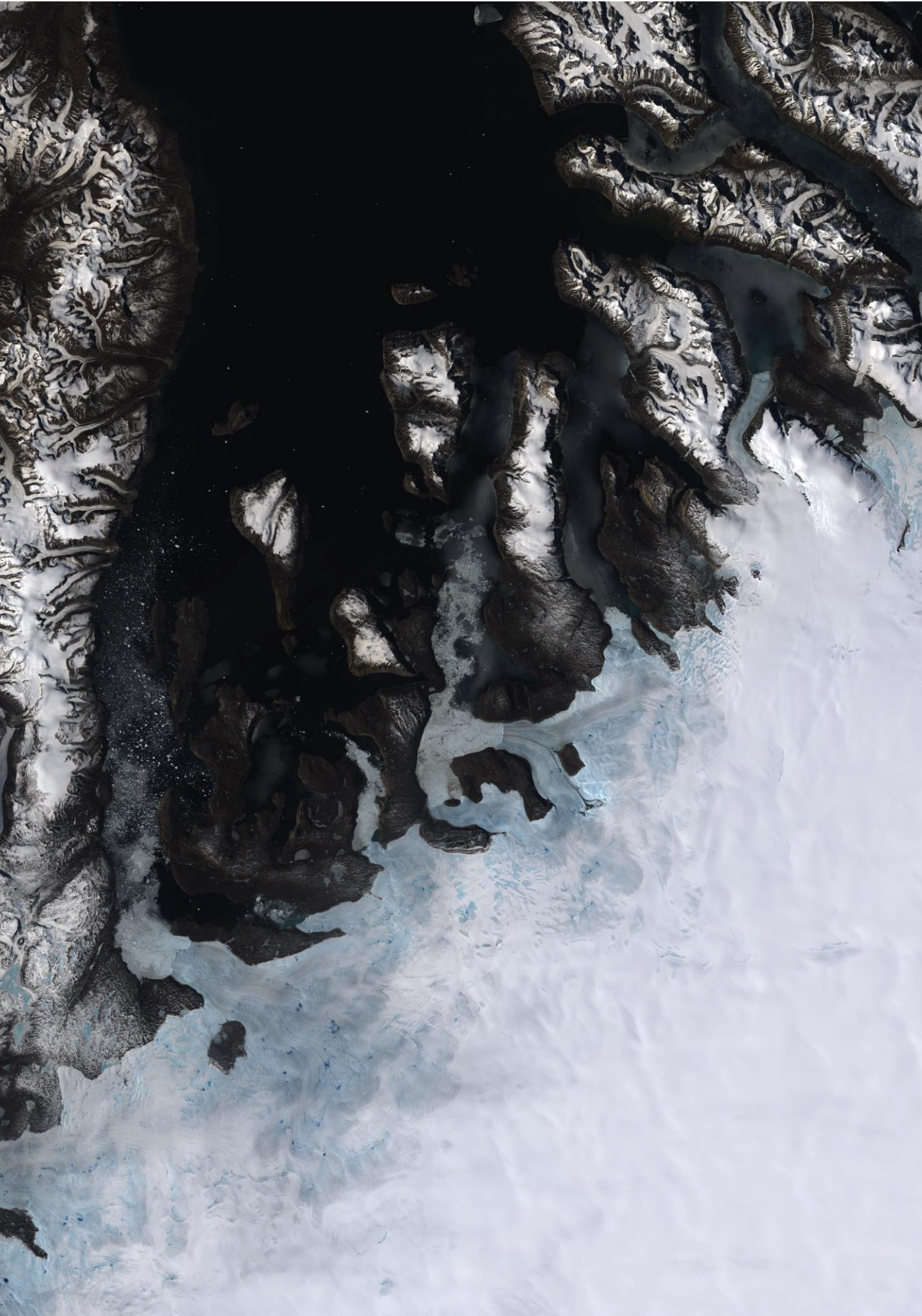

Chapter 3. Distribution of copper-binding ligands in Fram Strait and influences from the Greenland shelf (GEOTRACES GN05)

Science of the Total Environment, 25 October 2023

https://doi.org/10.1016/j.scitotenv.2023.168162

V. Arnone[a], J. M. Santana-Casiano[a], M. González-Dávila[a], G. Sarthou[b], S. Krisch[c], P. Lodeiro[d], E.P. Achterberg[c], A.G. González[a]

[a]Instituto de Oceanografía y Cambio Global, IOCAG, Universidad de Las Palmas de Gran Canaria, ULPGC, Spain.

[b]Univ Brest, CNRS, IRD, Ifremer, LEMAR, F-29280 Plouzané, France.

[c]GEOMAR Helmholtz Centre for Ocean Research Kiel, 24148 Kiel, Germany.

[d]Department of Chemistry, University of Lleida – AGROTECNIO-CERCA Center, Rovira Roure 191, 25198, Lleida, Spain.

Abstract

The Fram Strait represents the major gateway of Arctic Ocean waters towards the Nordic Seas and North Atlantic Ocean and is a key region to study the impact of climate change on biogeochemical cycles. In the region, information about trace metal speciation, such as copper, is scarce. This manuscript presents the concentrations and conditional stability constants of copper-binding ligands (L_{Cu} and log K^{cond}_{Cu2+L}) in the water column of Fram Strait and the Greenland shelf (GEOTRACES cruise GN05). Cu-binding ligands were analysed by Competitive Ligand Exchange-Adsorptive Cathodic Stripping Voltammetry (CLE-ACSV) using salicylaldoxime (SA) as competitive ligand. Based on water masses and the hydrodynamic influences, three provinces were considered (coast, shelf, and Fram Strait) and differences were observed between regions and water masses. The strongest variability was observed in surface waters, with increasing L_{Cu} concentrations (mean values: Fram Strait=2.6±1.0 nM; shelf=5.2±1.3 nM; coast= 6.4±0.8 nM) and decreasing log K^{cond}_{Cu2+L} values (mean values: Fram Strait=15.7±0.3; shelf=15.2±0.3; coast=14.8±0.3) towards the west. The surface L_{Cu} concentrations obtained above the Greenland shelf indicate a supply from the coastal environment to the Polar Surface Water (PSW) which is an addition to the ligand exported from the central Arctic to Fram Strait. The significant differences (in terms of L_{Cu} and log K^{cond}_{Cu2+L}) between shelf and coastal samples were explained considering the processes which modify ligand concentrations and binding strengths, such as biological activity in sea-ice, phytoplankton bloom in surface waters, bacterial degradation, and meltwater discharge from 79NG glacier terminus. Overall, the ligand concentration exceeded those of dissolved Cu (dCu) and kept the free copper (Cu^{2+}) concentrations at femtomolar levels (0.13 – 21.13 fM). This indicates

that Cu^{2+} toxicity limits were not reached and dCu levels were stabilized in surface waters by organic complexes, which favoured its transport to the Nordic Seas and North Atlantic Ocean and the development of microorganism.

Keywords: Copper, Organic Cu-binding ligands, Voltammetric method, Fram Strait, Northeast Greenland shelf.

3.1 Introduction

The Arctic region is highly vulnerable to the impact of climate change, with the warming of this polar area being two to three times faster than the global average (IPCC, 2022). The decrease of sea-ice coverage, associated with regional warming, increases light penetration and enhances phytoplankton growth in nutrient-rich waters (Arrigo et al., 2008). The decreasing sea-ice coverage changes the carbon uptake (Cai et al., 2010), modifies the ocean currents (Wang et al., 2020) and decreases (-15% per decade) the transport of ice-rafted materials from the Siberian shelves towards the Nordic Seas (Krumpen et al., 2019). Furthermore, the increase in riverine runoff (Peterson et al., 2002; Feng et al., 2021) and the permafrost thawing (Schuur et al., 2013, 2015) causes a rapid increase in organic matter discharge (Frey and McClelland, 2009; Stedmon et al., 2011). These inputs contain trace metals (Guieu et al., 1996; Charette et al., 2020) and metal-binding ligands (Slagter et al., 2017), essential for numerous biogeochemical processes, including the phytoplankton growth (Twining and Baines, 2013). Trace metals bioavailability is determined by speciation, which is strongly influenced by the formation of complexes with organic molecules, referred to as ligands, that constitute a heterogeneous group of compounds with distinct

functional groups. Ligands are involved in trace metal assimilation and distribution by limiting scavenging processes and influencing dissolution and precipitation rates. The consequences of climate change are still largely unknown but could impact the biogeochemical cycles of bio-essential trace metals, such as copper (Sunda, 1989; Peers et al., 2005; Maldonado et al., 2006), including their organic speciation.

Copper (Cu) is an essential micronutrient required for numerous metabolic functions in phytoplankton development (Twining and Baines, 2013). The free cupric ion (Cu^{2+}), on the other hand, is toxic at relatively high concentrations and could inhibit phytoplankton growth rates (Brand et al., 1986). The organic speciation of Cu in seawater, its bioavailability and toxicity, is strongly controlled by the formation of complexes with organic Cu-binding ligands (L_{Cu}). These ligands are classified based on the conditional stability constant (K^{cond}_{Cu2+L}, Buck and Bruland, 2005) into strong (L_1, log K^{cond}_{Cu2+L}=13–16) and weak ligand classes (L_2, log K^{cond}_{Cu2+L}=11–13), which provide information about the binding strength but not about molecular characterization of the organic compounds. Nevertheless, different functional groups have been identified as Cu-binding ligands, such as exopolysaccharides (log K^{cond}_{Cu2+L}<8, Lombardi et al., 2005), humic substances (log K^{cond}_{Cu2+L}=10–12, Kogut and Voelker, 2001; Whitby and van den Berg, 2015), thiols (log K^{cond}_{Cu2+L}=11–16, Walsh and Ahner, 2013) and methanobactins (log K^{cond}_{Cu2+L}>14, Choi et al., 2006). However, there is a lack of information on the oceanic distribution and nature of Cu speciation, particularly in the Arctic region with limited data on Cu-binding ligand concentrations reported for Canadian Arctic waters (Nixon et al., 2019), the sub-arctic North Pacific (Moffett and Dupont, 2007; Whitby et al., 2018;

Wong et al., 2021) and the North Atlantic Ocean (Kramer, 1986; Gourain, 2020).

In the Arctic Ocean, the supply of metal-binding ligands is largely related to terrestrial sources that introduce DOM throughout river discharges (Opsahl et al., 1999; Amon, 2003; Benner et al., 2005; Guéguen et al., 2007). About 10% of global riverine discharge of freshwater arrives in the Arctic (Benner et al., 2005). Freshwater and shelf-derived material from the Eurasian region, including metal-binding ligands (Slagter et al., 2017, 2019; Laglera et al., 2019; Ardiningsih et al., 2020; Krisch et al., 2022), are transported towards the central Arctic by the Transpolar Drift (TPD, Gordienko and Laktionov, 1969) and subsequently through Fram Strait and towards the Nordic Seas and North Atlantic Ocean (Ardiningsih et al., 2020; Williford et al., 2022). About 18–26% of the terrigenous DOM that reaches the Arctic is exported to the Nordic Seas by the TPD, which is associated with the East Greenland Current (EGC, Benner et al., 2005). This export potentially impacts the global carbon cycle, cycling of other elements, and biological production. Additional sources of organic matter and metal-binding ligands in the Arctic region are sediments (Davis and Benner, 2005; Goñi et al., 2013), phytoplankton or microbial production (Benner et al., 2005), and sea-ice melt (Charette et al., 2020). Considering that Arctic waters spend 2-3 years travelling from the Siberian shelves to the Fram Strait (Pfirman et al., 1997), during this transit the organic matter is subject to modifications related to sea-ice melt or formation, shelf-sea interactions, flocculation, biological DOM degradation, photooxidation and sediment release from ice (Charette et al., 2020; Slagter et al., 2017).

Within the high-latitude region, the Fram Strait is the major gateway of water from the Arctic to the Atlantic Ocean (Rudels, 2019). It is a key region to understand the impact of climate change on biogeochemical cycles. The region is a source of dissolved trace metals (Krisch et al., 2022), metal-binding ligands (Ardiningsih et al., 2020) and DOM (Granskog et al., 2012) to the Nordic seas and towards the North Atlantic Ocean, due to a pronounced Arctic export. In addition, the Arctic surface water transports large amounts of dissolved trace metals (Gerringa et al., 2021a) and DOM (Opsahl et al., 1999; Amon, 2003; Davis and Benner, 2005; Guéguen et al., 2007) with fluvial origin. The Fram Strait also receives waters from the Atlantic Ocean that have lower concentrations of Fe-binding ligands (Ardiningsih et al., 2020) and dissolved trace metal than Arctic surface waters (Krisch et al., 2022), and DOM related to marine origin (Granskog et al., 2012). The western region of Fram Strait receives large volumes of freshwater due to the melting along the coastal margins of the Greenland Ice Sheet which can be an important source of metal-binding ligands to the ocean. The Nioghalvfjerdsfjorden Glacier (79NG), located in the study area, is one of the major outlets of the North-East Greenland Ice Stream (NEGIS), which drains 12% of the Greenland Ice Sheet area (Rignot and Mouginot, 2012). The meltwater flux corresponds to 14.2 ± 0.96 km^3yr^{-1} (Wilson et al., 2017) and contributes (up to 13%) to the coloured DOM (CDOM) concentrations in coastal waters (Stedmon et al., 2011) and Fe-binding ligands (Ardiningsih et al., 2020). However, the contribution of dissolved micronutrients is lower than 2% of the total micronutrient transported across the Fram Strait (Krisch et al., 2022).

In this study, data of Cu-binding ligand concentrations and conditional stability constants (L_{Cu} and log K^{cond}_{Cu2+L}) in Fram Strait and over the

northeast Greenland shelf are presented and related to the water masses in the region, in order to identify possible sources of Cu-binding ligands. This study will provide critical information on the controls of Cu cycling in a region that is experiencing rapid changes.

3.2 Methods

3.2.1 Sampling

Samples were collected during a GEOTRACES cruise (GN05) on the RV Polarstern (PS100) during the boreal summer (from July 22nd to September 1st, 2016). The water column was sampled along the northeast Greenland Shelf, near the 79NG glacier terminus and across the Fram Strait (Figure 3.1). Details about the cruise can be found in the expedition report (Kanzow, 2016). Seawater for trace metal analysis was taken following GEOTRACES sampling procedure (Cutter et al., 2010) with a trace metal clean rosette and the GO-FLO bottles (Ocean Test Equipment). Right after recovery, the rosette was transferred into an over-pressured clean container (class 100) and the water was filtered (Acropak 0.8/0.2 µm pore size) into 125 mL low-density polyethylene (LDPE) bottles. The bottles were cleaned following GEOTRACES protocols (Cutter et al., 2010) and, after sampling, stored at -20ºC.

Conductivity, temperature and depth were measured with a Sea-Bird CTD (SBE 911plus) installed on the trace metal clean rosette frame. Macronutrient data (NO^-_3, NO^-_2, PO_4^{3-}, $Si(OH)_4$) obtained from the trace metal clean rosette were reported by Graeve et al. (2019).

3.2.2 Analysis of Cu-binding ligands by CLE-ACSV

The dCu concentrations have been measured and reported by Krisch et al. (2022). They were measured by high-resolution inductively coupled plasma-mass spectrometry (HR-ICP-MS) following solid-phase extraction after preconcentration using an automated SeaFAST system (SC-4 DX SeaFAST pico; ESI) (Rapp et al., 2017).

The concentration of Cu-binding ligands (L_{Cu}) and the conditional stability constants (K^{cond}_{Cu2+L}) were determined using the Competitive Ligand Exchange-Adsorptive Cathodic Stripping Voltammetry (CLE-ACSV) with SA as competitive ligand (Campos and van den Berg, 1994). Accordingly, 1 M boric acid was prepared in 0.3 M ammonia as buffer (pH 8.2), 0.01 M solution of salicylaldoxime (SA) was prepared in 0.1 M suprapure HCl and Cu stock solutions (Fluka), were used. Possibly remaining metals were removed from the buffer solution by adding 100 µM of MnO_2, stirred overnight and filtered through an acid-clean 0.45 µm filter (van den Berg, 1982). To guarantee the chemical properties, both SA and Cu stock solutions were prepared every other week and together with the buffer were kept in the fridge (at 8ºC and darkness) when they were not in use. Briefly, 10 mL samples were pipetted into 10 PTFE vials (22 ml volume), 100 µL of buffer (final concentration 10^{-2} M) and different concentrations of Cu were added (from 0 to 10 or 15 nM). A few samples were analysed with higher Cu addition, up to 20 nM, but no differences were found in the Cu-binding ligand determination. After a 1 h equilibration period, 10 µL of SA (final concentration 10 µM) was added and left to equilibrate overnight. The measurements were performed using a Hanging Mercury Drop Electrode (VA663 stand Metrohm), an Ag/AgCl reference electrode with a KCl salt

bridge (3 M) and a glassy carbon counter electrode. Following 120 s nitrogen gas purge, a deposition potential of – 0.2 V was applied for 180 s. After 10 s of equilibration, a differential pulse scan was applied from – 0.2 to – 0.5 V, with a step potential 3 mV, modulation amplitude 49.95 mV, interval time 0.1 s and modulation time of 0.05 s. Data fitting was performed with PromCC software (Omanović et al., 2015) using the "complete fitting" for one ligand (Appendix Figure A.1). For each titration curve, the sensitivity was determined by internal calibration, from the last titration points (4 or 5) which presented linearity. This method assumes that in the linear portion of the titration curve, all ligands were titrated. In some samples, to ensure that all ligands had been fully titrated, two Cu additions were made to the last titration point (with 4 or 8 nM of Cu) and measured immediately. These additions were not used during data treatment.

The side reaction coefficient for CuSA (α_{CuSA}) and the inorganic metal ($\alpha_{Cu'}$) was calculated for each seawater sample to consider the salinity variability (Campos and van den Berg, 1994). The α_{CuSA}, represents the centre of the detection window (D) and its value is a function of the SA concentration and the salinity (S), that affects the conditional stability constants for CuSA 1:1 and 1:2 complexes ($\log K^{cond}_{CuSA}$, $\log \beta^{cond}_{Cu(SA)2}$), as expressed below:

$$\alpha_{\mathrm{CuSA}} = \mathrm{K}^{\mathrm{cond}}_{\mathrm{CuSA}} \cdot [\mathrm{SA}] + \beta^{\mathrm{cond}}_{\mathrm{Cu(SA)_2}} \cdot [\mathrm{SA}]^2 = \mathrm{D} \quad (3.1)$$

$$\log \mathrm{K}^{\mathrm{cond}}_{\mathrm{CuSA}} = 10.12 - 0.37 \cdot \log \mathrm{S} \quad (3.2)$$

$$\log \beta^{\mathrm{cond}}_{\mathrm{Cu(SA)_2}} = 15.78 - 0.53 \cdot \log \mathrm{S} \quad (3.3)$$

The $\alpha_{Cu'}$ is defined by the stability constants (β^{cond}_{CuXi}) of the complexes formed between Cu and the major seawater ions (X_i), and the acidity Cu constant ($\beta^{cond}_{Cu(OH)i}$) at seawater ionic strength, as defined by:

$$\alpha_{Cu'} = 1 + \sum\left(\beta^{cond}_{CuX_i} \cdot [X]^i\right) + \sum\left(\beta^{cond}_{Cu(OH)_i}/[H^+]^i\right) \quad (3.4)$$

In this case, given the salinity range (29.87 – 35.14) the log α_{CuSA} varied between 5.10 and 5.14 while the $\alpha_{Cu'}$ ranged from 28 to 30. This variability did not produce important modifications on the detection windows.

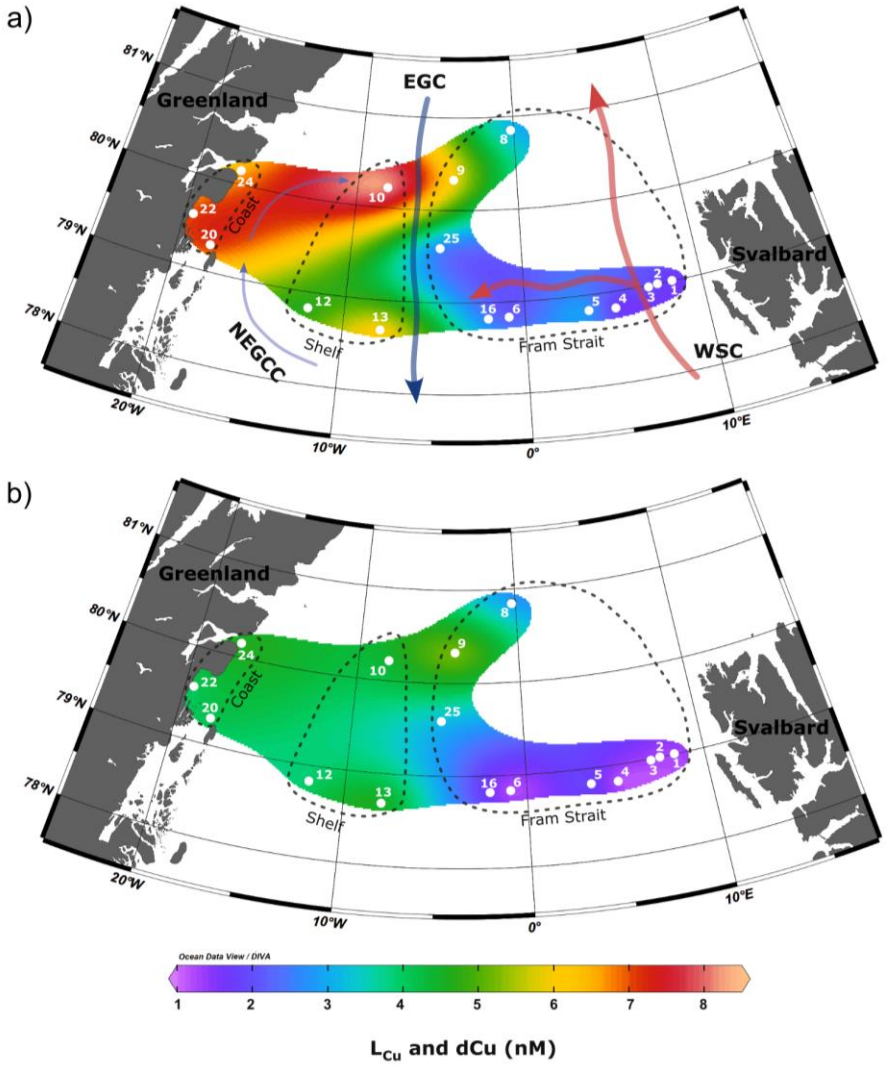

Figure 3.1. Map of the study area and surface distribution of a) Cu-binding ligands (L_{Cu}, in nM) and b) dissolved Cu (dCu, in nM). The information about dCu has been reported by Krisch et al. (2022). Station location during GEOTRACES expeditions

GN05 (2016) in Fram Strait and schematic flowpaths of major currents are shown. The West Spitsbergen Current (WSC) was depicted in red and the East Greenland Current (EGC) in blue. Above the Greenland Shelf, thin blue arrows indicate the circulation of the North-East Greenland Coastal Current (NEGCC). Three zones have been differentiated in the study, enclosed by dashed line and from east to west denoted as: Fram Strait, shelf and coast.

3.2.3 Statistical analysis

Statistical analysis was applied to determine whether there are significant differences in physical properties (temperature, salinity), macronutrient concentrations (NO^-_3, NO^-_2, PO_4^{3-}, $Si(OH)_4$), dCu concentrations and parameters associated with Cu-binding ligands (concentrations of L_{Cu}, eL_{Cu}, Cu' and Cu^{2+}, as well as log K^{cond}_{Cu2+L} and log α_{Cu2+L}) between regions and water masses. Since the variables displayed a non-normal distribution and heteroscedasticity, a Kruskal-Wallis test (Kruskal and Wallis, 1952) was applied to determine significant differences between regions (Appendix Table A.1) and water masses (Appendix Table A.2). For parameters that presented significant differences (p-value<0.05), a Conover test (Conover and Iman, 1979) was applied to elucidate which groups (regions or water mass) were different.

3.3 Results

3.3.1 Hydrographic description

The main current and water mass distributions in the region have been described elsewhere (Rudels et al., 2005; Laukert et al., 2017) and shortly summarised here (Figure 3.1 and 3.2). Different water masses were defined based on potential temperatures (θ) and potential densities (referred to 0 and

500 dbar of pressure, σ_0 and σ_{500} respectively). The relatively warm (potential temperature θ>2ºC) and saline (S>35) Atlantic Water (AW, 27.7<σ_0<27.97) is carried northwards by the West Spitsbergen Current (WSC) in the upper 500 m depth on the eastern part of the Fram Strait. On the western side, the East Greenland Current (EGC) flows southward and brings cold ($\theta\leq$0ºC) and less saline (S<34.5) Polar Surface Water (PSW, $\sigma_0\leq$27.7) to the Atlantic Ocean, above 200 m depth (Laukert et al., 2017). The interaction of both current systems within the Fram Strait creates the Recirculated Atlantic Water (RAW, θ>0ºC, σ_0>27.97, σ_0<30.444), which flows southward with the WSC at ~500 m (Rudels et al., 2005). Mostly on the western Fram Strait, the Arctic Atlantic Water (AAW, 0<$\theta\leq$2ºC, 27.7<σ_0<29.97) flows southward between 150 and 300 m depth. In Fram Strait, the Arctic Intermediate Water (AIW, $\theta\leq$0ºC, σ_0>27.97, $\sigma_0\leq$30.444) flows between 700 and 1500 m depth. Due to the small number of observations in this study, Deep Water (DW, $\sigma_0\geq$30.444) included different water masses (Upper Polar Deep Water, UPDW; and Nordic Seas Deep Water, NDW) with potential temperatures between -0.89 and -0.66ºC, potential densities (σ_o) that ranged from 27.72 to 28.10 kg m^{-3}, and salinities between 34.91 and 34.93 (Rudels et al., 2005). Above the Greenland shelf, two main troughs in the seafloor determined the oceanic circulation and produced an anticyclonic surface circulation. Part of the water is carried by the EGC and returned through the WSC, flows northward along the Norske Trough to reach the 79NG glacier. It then continues into the Westwind Trough, which is the North-East Greenland Coastal Current (NEGCC) and presents a ‘‘C’’-shaped distribution (Schaffer et al., 2017).

According with the results, three different zones were established based on the station bottom depth and the water masses. The Fram Strait region includes stations 1, 2, 3, 4, 5, 6, 8, 9, 16 and 25 whose depths exceed 790 m.

This area was affected by the WSC current on the east and the EGC on the west, close to the shelf break, and the water masses found were: PSW, AAW, AIW, AW, RAW and DW. The shelf region comprises stations 10, 12 and 13 with bottom depths deeper than 170 m. The water masses identified here were the PSW and the AAW. Finally, the coastal region was influenced by the NEGCC, including stations 20, 22 and 24 (bottom depth >178 m) and present PSW and AAW.

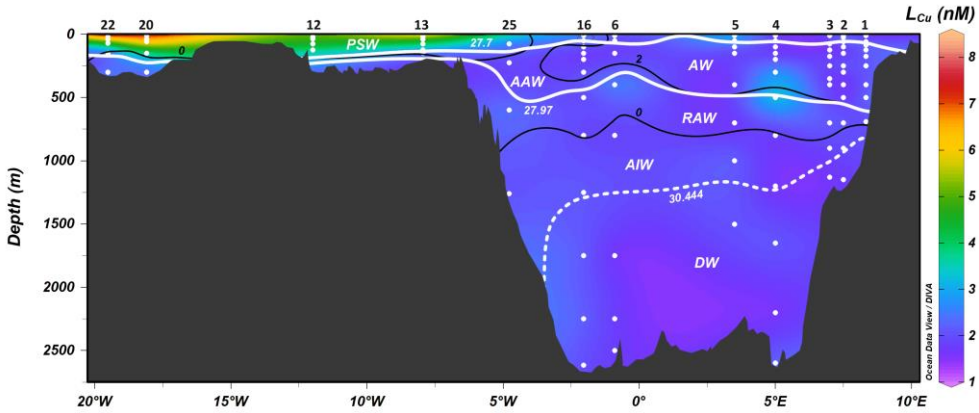

Figure 3.2. Vertical distribution of Cu-binding ligands (L_{Cu} in nM) along a longitudinal transect from Svalbard to Greenland shelves. Potential temperature was depicted by black contour lines, potential density anomaly by white solid lines while dashed white line indicate the potential density anomaly of 30.444 estimated considering 500 dbar of pressure. Six water masses were identified: Polar Surface Water (PSW), Atlantic Water (AW), Recirculated Atlantic Water (RAW), Arctic Atlantic Water (AAW), Arctic Intermediate Water (AIW) and Deep Water (DW).

3.3.2 Cu-binding ligand distribution

For the determination of L_{Cu} in the seawater samples, two and one-ligand fitting was attempted; however, only one class of ligand was detected in each titration curve. The L_{Cu} concentrations in the study area ranged from 1.4 to 8.2 nM (Table 3.1), with the highest values present in the surface waters (<100

m depth, Figure 3.2 and Appendix Table A.1). The L_{Cu} concentrations showed a longitudinal trend with increasing values towards the Greenland coast (Figure 3.1 and 3.2). Differences between stations located in Fram Strait, on the shelf and close to the coast were observed, with significant (p-value<0.05) higher concentrations within the last two groups. On the shelf, L_{Cu} varied between 1.7 and 8.2 nM with higher concentrations at the surface with a local maximum (30 m depth) at St. 10 (8.2 nM). Coastal samples presented a L_{Cu} that range from 2.4 to 7.1 nM, with increasing concentrations observed at the surface waters. Fram Strait L_{Cu} varied between 1.4 and 6.0 nM.

In detail, the surface (<100 m depth) variability of L_{Cu} (1.4 – 8.2 nM) was higher than in deeper waters (L_{Cu} range 1.6 – 3.3 nM, at >100 m depth). In surface samples (Appendix Table A.1) the observed L_{Cu} concentrations at the coast (mean value 6.4±0.8 nM) and the shelf (mean value 5.2±1.3 nM) presented significant differences (p-value<0.05, Appendix Table A.4.b). However, below 100 m depth (Appendix Table A.2), the L_{Cu} showed similar values with concentrations of 2.0±0.4 nM in Fram Strait, 2.6±0.7 nM on the Greenland shelf and 2.7±0.6 nM near the coast, without significant differences between shelf and coastal stations (p-value>0.05, Appendix Table A.4.c).

Station 9 (included in the Fram Strait group and with a bottom depth of 2544 m), located close to the shelf break, had L_{Cu} concentrations between 1.8 and 6.0 nM. This station showed a pronounced surface maximum and a minimum at depth, a distribution similar to the stations located on the shelf but differing from those located on the eastern Fram Strait.

Table 3.1. Summary of results for dissolved copper binding ligand parameters calculated for the coast, shelf and Fram Strait regions. Minimum, maximum, mean with standard deviation (±1σ) and median were reported.

Region	Stations		dCu (nM)	L_{Cu} (nM)	eL_{Cu} (nM)	log K^{cond}_{Cu2+L}	log α_{Cu2+L}	Cu^{2+} (fM)	Cu' (pM)	%CuL	L_{Cu}/dCu
Coast	20, 22, 24	Min	1.7	2.4	0.4	14.5	6.2	1.4	38.1	99.99	1.2
		Max	4.7	7.1	3.04	15.3	7.1	12.5	361.2	100	1.8
		Mean	3.5 ± 1.1	5.1 ± 1.9	1.60 ± 0.94	14.9 ± 0.3	6.6 ± 0.3	3.8 ± 2.8	111.1 ± 80.3	100.00 ± 0.0	1.4 ± 0.2
		Median	4.1	5.8	1.45	14.9	6.5	3.3	95.2	100	1.4
Shelf	10, 12, 13	Min	1.6	1.7	0.14	14.8	6.4	1.2	33.9	99.98	1.1
		Max	4.6	8.2	3.76	15.7	7.3	7.9	237.0	100	1.9
		Mean	3.0 ± 1.1	4.1 ± 1.7	1.05 ± 0.83	15.2 ± 0.3	6.8 ± 0.3	2.7 ± 1.8	78.7 ± 53.8	100.00 ± 0.0	1.3 ± 0.2
		Median	3.2	4.2	0.94	15.2	6.7	1.8	53.3	100	1.3
Fram Strait	1, 2, 3, 4, 5, 6, 8, 9, 16, 25	Min	1.2	1.4	0.03	14.3	5.8	0.1	3.9	99.96	1.0
		Max	5.2	6.0	1.84	16.3	7.7	21.1	633.8	100	2.2
		Mean	1.6 ± 0.5	2.2 ± 0.6	0.58 ± 0.34	15.5 ± 0.3	6.9 ± 0.3	1.7 ± 3.0	50.7 ± 87.6	100.00 ± 0.01	1.4 ± 0.2
		Median	1.5	2.0	0.57	15.6	6.9	0.8	23.8	100	1.4

In the study region, the dCu speciation was dominated by organic complexation. The L_{Cu} concentrations were always in excess with respect to dCu (Tables 1, A1, A2 and A3), as indicated by the excess ligand concentration ($eL_{Cu} = L_{Cu} - dCu$). Notice that both L_{Cu} and eL_{Cu} depend strongly on the detection window applied. The eL_{Cu} ranged from 0.03 nM to 3.8 nM, with higher concentrations observed at the shelf and coastal stations. This indicates that the detected L_{Cu} were not fully saturated with dCu in solution.

Coastal and shelf eL_{Cu} concentrations were significantly different to those from Fram Strait waters (p-value<0.05, Appendix Table A.4), but deeper waters (>100 m) appeared to be similar among the regions (p-value>0.05). The relationship between L_{Cu} and eL_{Cu} was linear (Figure 3.3a) with a slight difference observed between surface samples <100 m, located close to the coast, on the shelf and at St. 9, and deeper samples (>100 m depth samples) from all the regions. The difference between surface and deep samples may indicate an extra source of L_{Cu} in surface waters that were not observed in the case of dCu. The distribution of L_{Cu} follows the pattern described for dCu (Appendix Figure A.2) with more than 99.9% being organically complexed. Briefly, the concentration of dCu ranged from 1.2 to 5.2 nM (Table 3.1). Coastal and shelf stations presented a similar dCu concentration range (1.7 – 4.7 nM and 1.8 – 4.6 nM, respectively). The Fram Strait presented dCu concentrations between 1.2 and 2.5 nM, except St. 9 which showed a higher concentration range (1.5 – 5.2 nM) with a maximum at the surface. Dissolved Cu concentrations were strongly coupled to L_{Cu} (Figure 3.3b) with a slightly higher correlation observed on the shelf (R^2=0.83, p-value<0.05) and near the coast (R^2=0.86, p-value<0.05) than in Fram Strait (R^2=0.69, p-value<0.05). Samples with concentrations of L_{Cu} higher than 4 nM and dCu higher than

3.5 nM correspond to surface samples (<100 m depth) located close to the coast, on the shelf but also include St. 9.

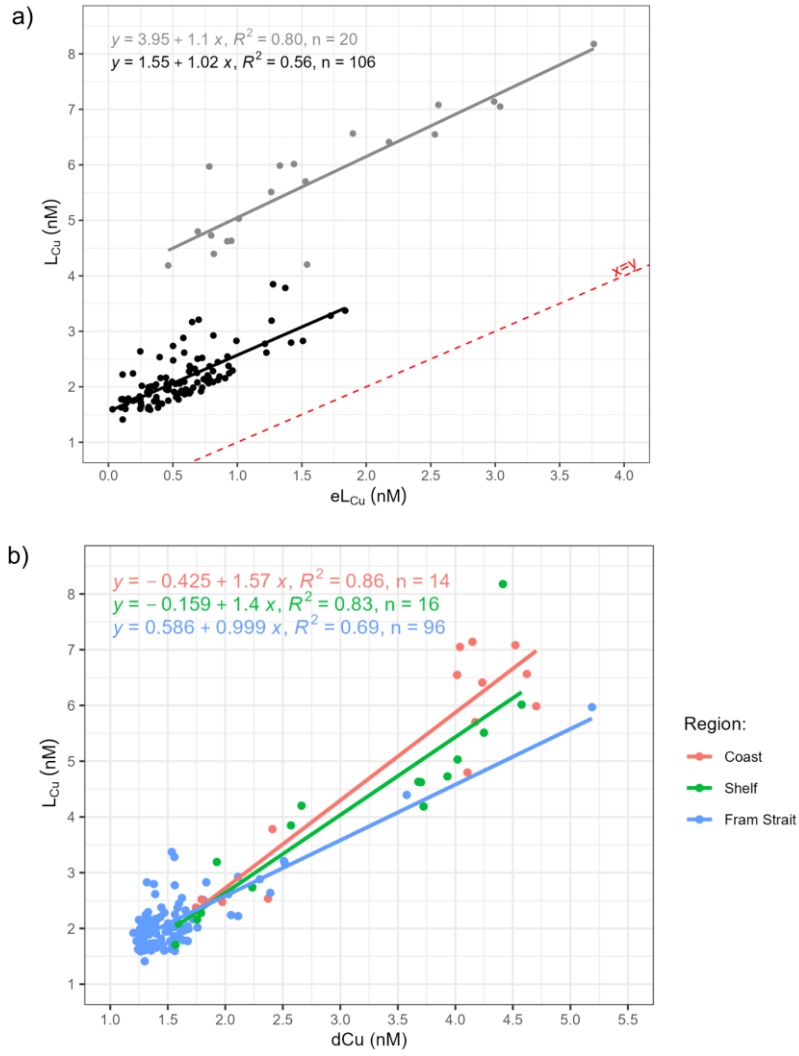

Figure 3.3. a) Correlation between copper-binding ligand (L_{Cu}) and the excess ligand ($eL_{Cu} = L_{Cu} - dCu$) concentrations, both of them in nM. Surface samples (<100m depth) located close to the coast (St. 20, 22 and 24), above the shelf (10, 12 and 13) and at St. 9 were represented in grey (R^2=0.80, p-value=$1.212e^{-7}$, n=20). Black dots (R^2=0.56, p-value< $2.2e^{-16}$, n=106) include samples deeper than 75m from all the regions. The correlation between parameters was shown with solid lines. b) Correlation between copper-binding ligand (L_{Cu}) and dCu concentration (nM) with linear correlation estimated for coastal (R^2=0.86, p-value= $1.48e^{-6}$, n=14), shelf

(R^2=0.83, p-value=1.08e^{-6}, n=16) and Fram Strait (R^2=0.69, p-value<2.2e^{-16}, n=96) samples.

Significant correlations (R^2=0.84, p-value<0.05) were observed between L_{Cu} concentration and salinity (Figure 3.4). The region presents a salinity gradient between 29.87 and 35.14 where the lower salinities presented the highest L_{Cu} concentrations.

The relationship between the concentration of Cu-binding ligands and the class of ligands with the different water masses could help to identify potential sources. Table A.3 and Figure 3.5 present the concentration of L_{Cu} as a function of the water masses and location. In terms of water masses, significant differences were detected among stations located in the Fram Strait, the shelf and coastal waters. The highest L_{Cu} concentrations were found in PSW and the lowest in AW. In Fram Strait, the six water masses showed different L_{Cu} concentrations. The lowest L_{Cu} concentrations were observed in waters that come from the Atlantic Ocean (AW=2.0±0.3 nM) and deep waters (DW=1.9±0.2 nM). Fram Strait surface waters that contained waters from the Arctic Ocean showed higher L_{Cu} concentrations (PSW=3.2±1.1 nM and RAW=2.3±0.5 nM). In the Fram Strait area, significant differences (p-value<0.05), in terms of L_{Cu}, were observed between PSW and AW, AIW, RAW and DW. Shelf stations presented two water masses with L_{Cu} concentrations in PSW (4.7±1.4 nM) higher than those observed in AAW (2.1±0.3 nM). Cu-binding ligand differences between the water masses were significant (p-values<0.05). Close to the coast, the mean L_{Cu} concentration observed on PSW (5.5±1.7 nM) was higher than in AAW (2.5±0.1 nM) with significant differences (p-values<0.05). Water masses presented different concentrations of eL_{Cu}. The highest variabilities and concentrations were observed in PSW near the coast (mean eL_{Cu}=1.8±0.9 nM) and on the shelf

(mean eL_{Cu}=1.3±0.9 nM), with the maximum eL_{Cu} value (3.8 nM) observed at St. 10 (30 m depth). Concentrations were also significantly different between AAW and PSW above the Greenland shelf (p-value<0.05). The eastern Fram Strait showed the lowest variabilities (eL_{Cu} ranged from 0.03 to 1.8 nM) with minimum concentrations observed in DW and maximum in RAW. In this area, significant differences (p-value<0.05) were observed between DW and AW, PSW and RAW.

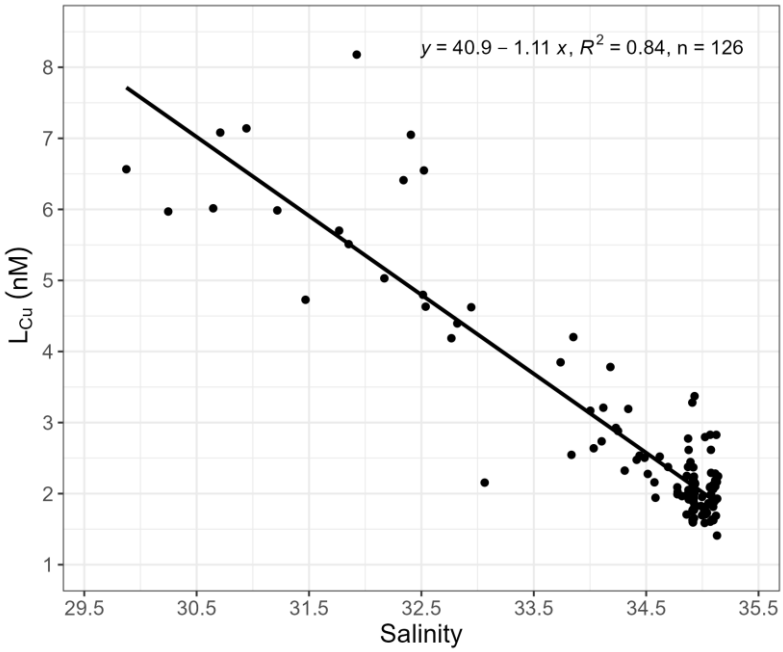

Figure 3.4. Copper-binding ligand (L_{Cu}) concentration (nM) against salinity with a linear fitting applied on all samples collected along the study area (R^2=0.84, p-value<$2.2e^{-16}$, n=126). Samples with salinity lower than 33 differ significantly (p-value= $4.418e^{-12}$) from samples with higher salinity.

3.3.3 Cu-binding ligand strengths

The conditional stability constants of L_{Cu} (log K^{cond}_{Cu2+L}), which describes the strength of ligands, presented values between 14.2 and 16.3 (Table 3.1).

The ligands detected in the entire region were classified as strong Cu-binding ligands, or L_1 class (Bruland et al., 2000; Buck and Bruland, 2005). The log K^{cond}_{Cu2+L} calculated is strongly conditioned by the detection window applied in each study. However, this current investigation has been conducted with the same detection windows as other oceanic publications, where both weak and strong ligands were detected (Laglera and van den Berg, 2003; Bundy et al., 2013; Abualhaija et al., 2015; Whitby and van den Berg, 2015; Whitby et al., 2018; Hollister et al., 2021; Wiwit et al., 2021). Values of log K^{cond}_{Cu2+L} observed along the three defined regions (Table 3.1 and Figure 3.5) decrease towards the west (mean values Fram Strait= 15.5±0.3, shelf=15.2±0.3 and coast=14.9±0.3). In Fram Strait, log K^{cond}_{Cu2+L} was significantly different (p-value<0.05, Appendix Table A.4) than those observed on the shelf and in the coastal area. Most of this variability was observed in surface samples (Fram Strait=15.6±0.3.; shelf=15.22±0.3; coast=14.8±0.3; Appendix Table A.1). Below 100 m depth, the log K^{cond}_{Cu2+L} presented lower variability with a mean value of 15.5±0.4 (Fram Strait=15.5±0.3.; shelf=15.0±0.2; coast=15.2±0.2; Appendix Table A.2). No significant differences (p-value>0.05) were observed between water masses inside each region (Appendix Table A.5).

The reactivity of the natural Cu-binding ligands (α_{Cu2+L}) describes the capacity of dissolved ligands to be bound with Cu and is the product of the K^{cond}_{Cu2+L} and L_{Cu} (Gledhill and Gerringa, 2017). In the study area, log α_{Cu2+L} varied between 5.8 and 7.7 (Table 3.1, Figure 3.5). Lower values were observed close to the coast (6.6±0.3), intermediate values on the shelf (6.8±0.3) and higher values in Fram Strait (6.9±0.3). Significant differences (p-value<0.05) were only observed between Fram Strait and the coast. Within each region, there were no statistical (p-value>0.05) differences between water masses (Appendix Table A.5).

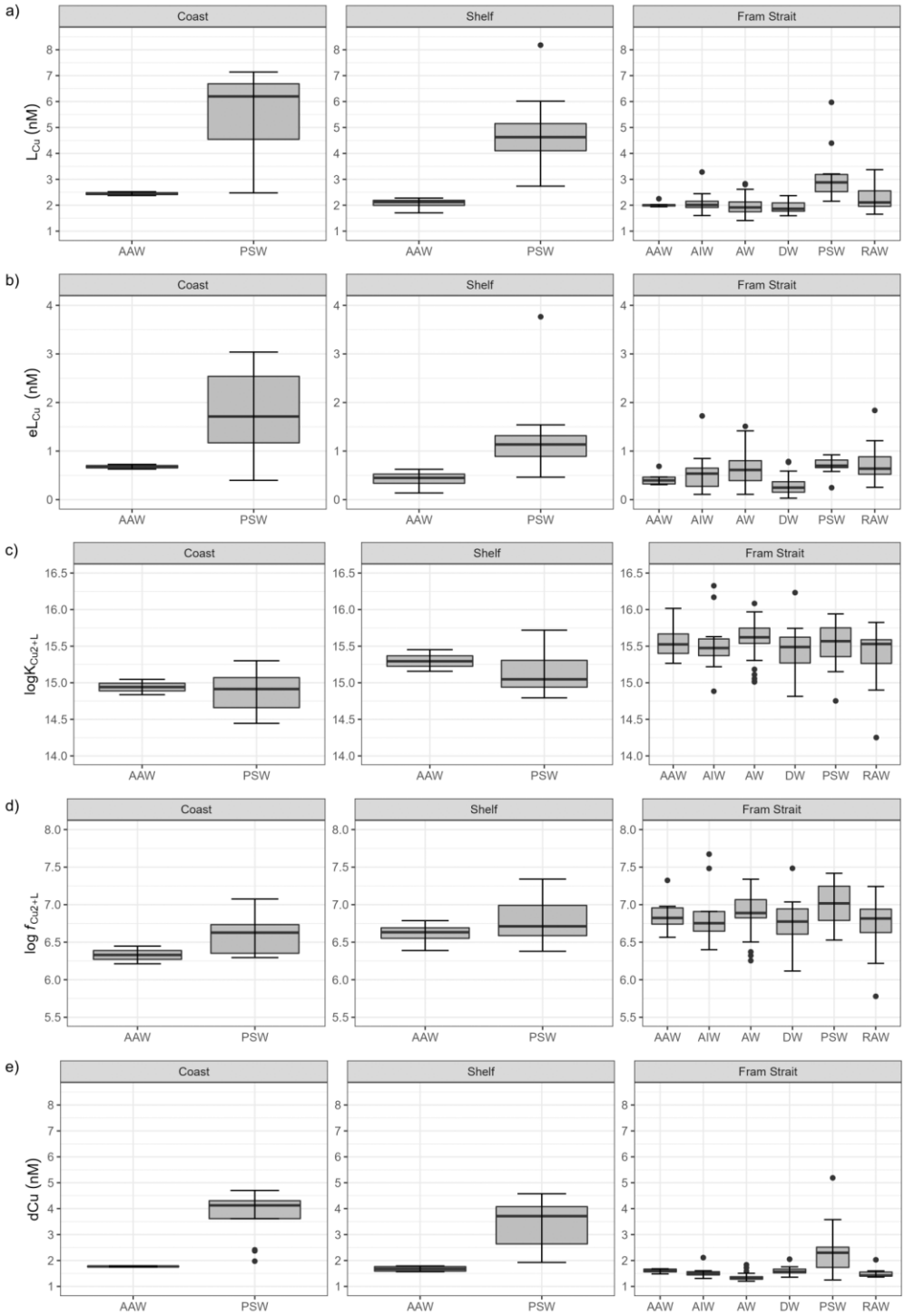
a)
Coast
Shelf
Fram Strait
L_{Cu} (nM)
AAW
PSW
AIW
AW
DW
RAW
b)
eL_{Cu} (nM)
c)
$logK_{Cu2+L}$
d)
log f_{Cu2+L}
e)
dCu (nM)

Figure 3.5. Boxplots of the concentration of L_{Cu} (a), eL_{Cu} (b), log K_{Cu2+L} (c), log f_{Cu2+L} (d), and dCu (e) from the station located on the Fram Strait, above the shelf and close to the coast categorized by water mass (Polar Surface Water, PSW, Atlantic Water, AW, Recirculated Atlantic Water, RAW, Arctic Atlantic Water, AAW, Arctic Intermediate Water, AIW, and Deep Water, DW). Circles indicate the outliers.

3.3.4 Nutrient distribution and Cu-binding ligands relationship

The concentration of macronutrients (NO^-_3+NO^-_2, PO_4^{3-} and $Si(OH)_4$) in the study region were correlated with ligand concentrations (Figure 3.6). Macronutrient concentrations were reported by Graeve et al. (2019) and described for the Fram Strait (Krisch et al., 2020, 2021; Tuerena et al., 2021). Briefly, differences in nutrient concentrations were observed between the eastern and western Fram Strait. Macronutrient concentrations increase at depth and the highest values were found in DW (NO^-_3+NO^-_2= 12.32±2.05 µM, PO_4^{3-}= 0.84±0.18 µM, $Si(OH)_4$= 9.46±2.15 µM). Surface water masses showed different nutrient behaviours from west to east, the PSW presented relatively high concentrations of PO_4^{3-} (0.61 ±0.17 µM) and $Si(OH)_4$ (4.74±1.38 µM) but low NO^-_3+NO^-_2 (4.26±3.42 µM) compared to AW (NO^-_3+NO^-_2=9.34± 3.96 µM, PO_4^{3-}= 0.66±0.24 µM, $Si(OH)_4$= 3.79±1.59µM). In Fram Strait, NO^-_3+NO^-_2 and PO_4^{3-} in PSW showed significant differences from the AIW and DW concentrations. However, $Si(OH)_4$ concentrations in Fram Strait presented significant differences between different water masses (Appendix Table A.5). Close to the coast, the 79NG did not release significant amounts of nutrients.

The relationship between L_{Cu} and macronutrient concentrations was evaluated with linear fitting models (Figure 3.6). Significant negative relationship was observed between both L_{Cu} and NO^-_3+NO^-_2 as well as between L_{Cu} and PO_4^{3-} levels. In the study region, no significant (p-

value>0.05) relationships were observed between Cu-binding ligand parameters (L_{Cu} and log K^{cond}_{Cu2+L}) and fluorescence.

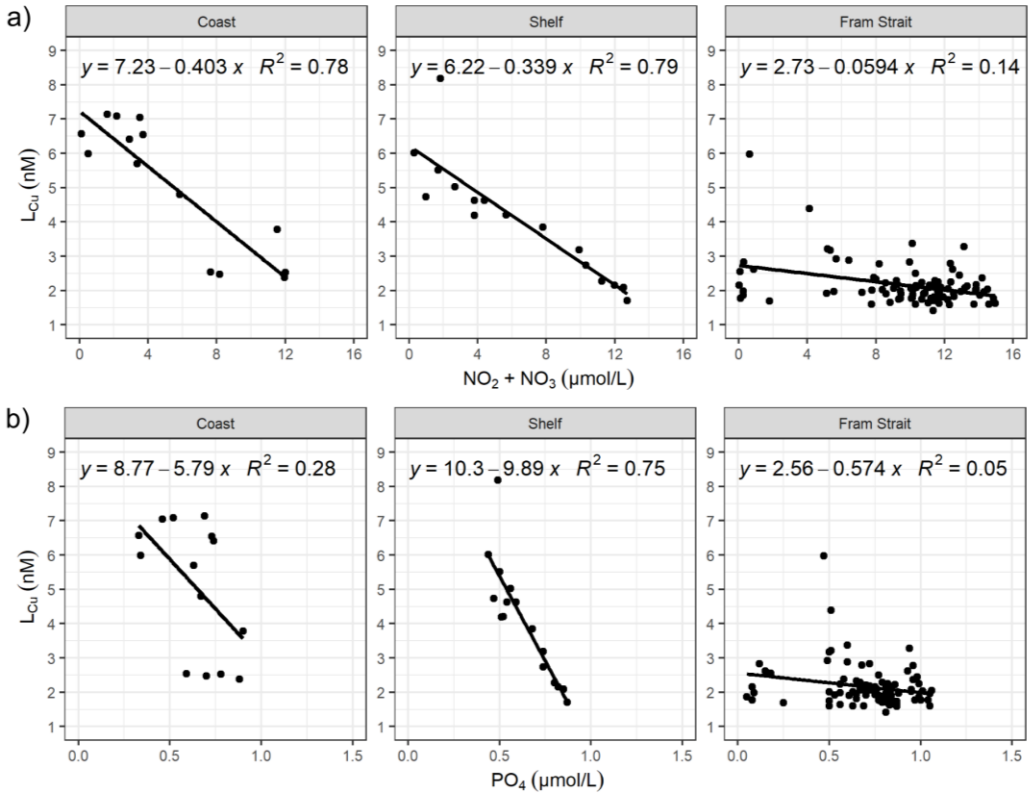

Figure 3.6. Variability of Cu-binding ligand (LCu in nM) with respect to (a) nitrate and nitrite, and (b) phosphate concentrations (µmol/L). The number of samples (n) vary by region: 14 observations on the coast, 16 above the shelf and 95 in Fram Strait.

3.4 Discussion

3.4.1 Copper complexation in the region

Most of the L_{Cu} concentrations observed in coastal and oceanic waters in the study region (1.4 – 8.2 nM) falls within the values typically reported in

the open ocean (1 – 6 nM, Ruacho et al., 2022). However, the vertical distribution of L_{Cu} above the Greenland shelf contrasts with that obtained in the eastern Fram Strait, as well as the concentrations observed in oceanic and coastal waters, which exhibit increasing values with depth (Ruacho et al., 2022). The L_{Cu} concentrations observed in the eastern Fram Strait (1.2 – 5.2 nM) were similar to the values reported for strong ligands (L_1=0.8 – 5 nM) in the North Atlantic (2 – 2.5 µM SA, Gourain, 2020; Jacquot and Moffett, 2015) and the North Pacific Ocean (5 and 10 µM SA, Whitby et al., 2018; Wiwit et al., 2021; Wong et al., 2021). The surface maximum of L_{Cu} concentration reported for the Greenland shelf and coast (>7 nM) exceeds surface values observed in the open ocean (~1 nM, Ruacho et al., 2022) and remains lower than concentrations detected in estuarine environments. In estuaries, a substantial quantity of L_1 (ranging from 1 to 33 nM) and L_2 (ranging from 14 to 300 nM) ligand classes were detected (2.5 and 10 µM SA, Laglera and van den Berg, 2003; Muller and Batchelli, 2013). In other polar regions, such as the Canadian Arctic Archipelago and Baffin Bay, as well as Antarctic surface waters (Bundy et al., 2013; Nixon et al., 2019), L_{Cu} concentrations of up to 4 nM were observed, a level lower than those observed on the Greenland shelf and coast (1.7 – 8.2 nM and 2.4 – 7.2 nM, respectively). However, similar to the Greenland shelf, the Canadian Arctic Archipelago and Baffin Bay also exhibited a surface maximum of L_{Cu} concentration associated with the biological production of L_{Cu} in surface waters. It is important to highlight that the method applied for ligand detection by Nixon et al. (2019) was immobilized Cu(II)-ion affinity chromatography and does not inform about the ligand binding strength.

The log K^{cond}_{Cu2+L} obtained in this study (14.3 –16.3) corresponds to strong binding ligands (log K^{cond}_{Cu2+L}>13, Buck and Bruland, 2005), exceeding the

values between 12 and 14.8 reported for the North Atlantic Ocean (Jacquot and Moffett, 2015; Gourain, 2020). The North Pacific Ocean exhibited log K^{cond}_{Cu2+L} values for L_1 class ligands between 13.2 and 15.6 (Whitby et al., 2018; Wiwit et al., 2021; Wong et al., 2021), which were more similar to the results obtained in the study area. The log K^{cond}_{Cu2+L} values can be used to correlate the detected ligands with possible sources, which will be discussed in the next section.

It is important to remark that the results obtained using the voltametric method are conditioned by the detection window applied. Concentrations of SA higher than 2.5 μM favour the detection of stronger ligands, while lower concentrations enable the detection of weaker compounds (Campos and van den Berg, 1994). The detection window applied in this study (10 μM SA) allowed the detection of strong ligands; however, in other regions, the same detection window enabled the measure of both strong and weak ligands (Laglera and van den Berg, 2003; Whitby et al., 2018; Wiwit et al., 2021). In natural waters, exists a continuum of ligands with varying strengths that may be detected or not based on the experimental conditions. For this reason, the non-detection of weak ligands does not indicate their absence in the Arctic region. In addition, the use of the internal calibration method to establish the sensitivity is suitable for determining strong ligands, while it potentially reduces the detection of weak ligands (Pižeta et al., 2015). The presence and non-detection of weaker ligands (Campos and van den Berg, 1994), as well as the adsorption of organic compounds onto the Hg drop electrode (Kogut and Voelker, 2003), could impact the measurements of ligand concentration and binding strength. Furthermore, it is important to highlight that the log K^{cond}_{Cu2+L} obtained through voltammetry represents the average binding capacity of the ligand pool in each sample. Consequently, the presence of

various natural ligand classes influences the determination of the conditional stability constant (Miller and Bruland, 1997).

3.4.2 Sources and sinks of Cu-binding ligands

Different mechanisms could explain the L_{Cu} concentrations and stability constants reported along the Fram Strait region, as well as the surface longitudinal variability reported.

Water mass circulation and influence from the TPD

The complex circulation patterns existing in Fram Strait (Rudels et al., 2005; Laukert et al., 2017; Schaffer et al., 2017) strongly influence the physico-chemical characteristics of waters, especially at the surface where most of the significant variabilities were measured.

The similarities in L_{Cu} concentration between the eastern Fram Strait and the North Atlantic can be attributed to the influence of the WSC, which brings Atlantic waters to the eastern part of the strait (Rudels et al., 2005). North Atlantic surface waters are characterised by low ligand concentrations (Jacquot and Moffett, 2015; Gourain, 2020; Ruacho et al., 2022) and relatively lower DOM levels compared to Arctic waters (Nguyen et al., 2022).

The high surface L_{Cu} concentrations reported for the shelf (~8 nM) and the maximum observed at St. 9 (~5 nM) could be related to the TPD, as suggested for Fe-binding ligands (Ardiningsih et al., 2020). The PSW observed above the Greenland shelf is related to the TPD and transported into the region by the EGC (Rudels et al., 2005). In the Arctic Ocean, the TPD carries high concentrations of DOM and trace metals from the Siberian shelves and rivers

(Opsahl et al., 1999; Amon, 2003; Benner et al., 2005; Guéguen et al., 2007; Gerringa et al., 2021a), including metal-binding ligands. To the extent of our knowledge, there is no information about Cu complexation from Siberian rivers. High concentrations of humic-like substances were observed inside the TPD (Gao and Guéguen, 2018; Gamrani et al., 2023) and correlated with Fe-binding ligands (Laglera et al., 2019; Slagter et al., 2019). This correlation was also detected in Fram Strait, where higher concentrations of Fe-binding ligands were observed above the Greenland shelf (Ardiningsih et al., 2020). Humic substances are not Fe-specific ligands and have been shown to complex Cu (Abualhaija et al., 2015), suggesting that a portion of the L_{Cu} pool may contain humic substances with riverine origin, as reported elsewhere (Kogut and Voelker, 2001; Whitby and van den Berg, 2015; Whitby et al., 2018; Hollister et al., 2021). Copper-binding humic substances detected in estuarine environments showed log K^{cond}_{Cu2+L} values between 14.9 and 15.9 (Muller and Batchelli, 2013) and do not explain the full range of log K^{cond}_{Cu2+L} (14.3 – 16.3) observed in the study area. The conditional stability constants observed in Fram Strait were also higher than the values of 12.1 reported for humic acids of different oceanic regions (Whitby and van den Berg, 2015). Other substances different from humics can be part of the L_{Cu} pool detected. For example, a portion of the riverine DOM transported towards the Fram Strait also contains thiol substances (Gao and Guéguen, 2018). Thiols have been identified as Cu-binding ligands in estuarine environments with variable conditional stability constants between 12 and 15 (Laglera and van den Berg, 2003; Whitby et al., 2017). In addition, laboratory studies with marine alga under copper stress conditions revealed conditional stability constants for Cu-binding ligands between 11.2 and 13 (Leal et al., 1999; Dupont et al., 2004; Walsh and Ahner, 2013). Then, thiols with the highest conditional stability

constants could account for a part of the L_{Cu} pool detected in the study area. The input of riverine material into the study region can be supported by the relationship between L_{Cu} concentrations and salinity (Figure 3.4). The correlation was observed exclusively within PSW, where samples with lower salinity exhibited the highest concentrations. Siberian rivers also discharge large quantities of dCu that are not scavenged on the shelf, enabling its transport to the Fram Strait by the TPD (Charette et al., 2020). This input of dCu is expected to be complexed by organic matter transported through the rivers, as observed in other coastal regions (van den Berg et al., 1987; Hoffmann et al., 2007; Muller and Batchelli, 2013; Williford et al., 2022). The strong complexation of dCu enables its transport within the Arctic Ocean and through the Fram Strait. The export of complexed Cu could be important in the regions that present Fe limitation, such as the south of Greenland and the Irminger Basin (Hopwood et al., 2018). As under Fe-limitation, some diatoms have higher Cu-requirements (Maldonado et al., 2006), this export of Cu-organically complexed from the Arctic Ocean towards the Nordic Seas and North Atlantic could support phytoplankton growth.

However, it must be noted that the coastal and shelf waters exhibited a lower dCu reactivity compared to the eastern Fram Strait, related to the longitudinal decrease of log K^{cond}_{Cu2+L} towards the west and the decline of log α_{Cu2+L} values (Table 3.1). In contrast to L_{Cu} and log K^{cond}_{Cu2+L}, log α_{Cu2+L} showed no significant variability between regions and water masses because the westward increase of L_{Cu} was countered by the decrease in log K^{cond}_{Cu2+L}.

Contributions from ice and glacial margins

The surface layer of Fram Strait may also receive freshwater from sea-ice and the 79NG terminus. The highest concentrations of L_{Cu} and dCu were

observed in surface waters above the shelf and close to the Greenland coast, an area that presented different sea-ice arrangements (data reported by König-Langlo, 2016). Sea-ice may act as a source of organic matter, trace metals, macronutrients, and sediments that were trapped in the ice when it was formed and released during melting (Thomas et al., 1995; Tovar-Sánchez et al., 2010; Evans and Nishioka, 2019). The sea-ice trace metal composition and size fractioning are a function of the location where the ice was formed, the age, the structure, and the processes that occur inside, such as biological degradation and reduction processes (Thomas et al., 1995; Tovar-Sánchez et al., 2010; Evans and Nishioka, 2019). A study carried out in the northwest of Svalbard revealed that the content of Cu in sea-ice (range from 30.4 to 67 nM) was much higher than that observed in seawater, with concentrations around 5 nM (Tovar-Sánchez et al., 2010). The first-year ice detected in the study region should contain lower nutrients and trace metal concentrations than multiyear Arctic ice (Tovar-Sánchez et al., 2010); however, part of the dCu detected in the western Fram Strait may come from the ice. On the other hand, the DOM observed in the northwest of Svalbard is more related to the biological production of protein-like substances (Zabłocka et al., 2020). Thus, part of the L_{Cu} and dCu observed in the western Fram Strait could be related to the ice. The biological production will be discussed in the following section.

Part of the observed coastal maximums of L_{Cu} and dCu could be related to the subglacial discharge of freshwater that may introduce nutrients, DOM, and trace metals into surface waters (Aciego et al., 2015; Cape et al., 2019; Hopwood et al., 2020; Krause et al., 2021). The release of DOM with glacial meltwater is 1 – 2 orders of magnitude lower than the inputs from Arctic rivers. However, it is likely more bioavailable due to its lower aromatic

composition (Hopwood et al., 2020). The release of DOM might contribute to the L_{Cu} pool and may explain why, along the study area, the L_{Cu} concentrations increased towards the west while log K^{cond}_{Cu2+L} decreased. The longitudinal increase in L_{Cu} was stronger than dCu, an extra or more intense source of L_{Cu} compared to dCu is thus suggested (Figure 3.3b). The contribution of dCu through subglacial discharge must be limited, as observed if we compare the concentration observed in coastal surface waters (maximum of 4.7 nM) with that reported for the central Arctic (~7 nM, Gerringa et al., 2021a). However, studies made in different Greenlandic glaciers indicate that up to 2.5 nM of dCu could be released through glacial discharge (Krause et al., 2021).

The general decreasing relationship between L_{Cu} and NO^-_3+NO^-_2 and PO_4^{3-} (Figure 3.6) observed on the shelf and coastal samples reinforce the hypothesis of coastal inputs of Cu-binding ligands. The highest L_{Cu} was related to the lowest NO^-_3+NO^-_2 concentrations at coastal and shelf samples and low PO_4^{3-} concentrations on the shelf (Figure 3.6). The linear relationship observed concerning salinity (Appendix Figure A.4) in coastal (R^2=0.86) and shelf (R^2=0.93) waters for NO^-_3+NO^-_2 and on the shelf for PO_4^{3-} (R^2=0.82) indicate a low supply of these nutrients from Greenland glacial meltwater (Meire et al., 2016; Krisch et al., 2020, 2021; Tuerena et al., 2021) compared to the overwhelming supply of dCu and dCu-binding ligand from the central Arctic with the Transpolar Drift. This decrease in macronutrient concentrations with salinity could be related to a dilution of seawater properties due to the input of freshwater (Krause et al., 2021) that at the same time is adding Cu-binding ligands into the Fram Strait.

The extra supply of Cu-binding ligands in the coastal region could be exported to the shelf area by the NEGCC (Schaffer et al., 2017). This would explain the surface maximum of ligands observed at St. 10 (8.18 nM) and the corresponding log K^{cond}_{Cu2+L} (14.84).

Influence of biological activity

The phytoplankton community (mainly diatoms and bacteria) may contribute to Cu-binding ligands, as observed for the surface waters of the central Arctic and the Canadian Arctic Archipelago (Davis and Benner, 2005; Nixon et al., 2019; Williford et al., 2022). Phytoplankton blooms were described in Fram Strait (Lester et al., 2021) and could release L_{Cu} into the surface waters (Leal et al., 1999). This could contribute to the L_{Cu} pool detected in this study, as suggested for Fe-binding ligands (Ardiningsih et al., 2020). The algal sea-ice community produces high concentrations (26.2 ± 3.9 nM) of strong Cu-binding ligands (log K^{cond}_{Cu2+L} =15.2 ± 0.3), as described by Bundy et al. (2013) for the Antarctic Peninsula. These values were higher than those reported above the Greenland shelf surface waters (L_{Cu}=5.2±1.3 nM; log K^{cond}_{Cu2+L}=15.2±0.3) but notice that sea-ice samples were not analysed. The characteristics of these Cu-binding ligands can be affected by melting, as the salinity is much lower than that of pore water. In addition, weak ligands such as exopolymer substances (EPS) may also present conditional stability constants lower than 10 (Ruacho et al., 2022). These substances were detected in Fram Strait sea-ice (Meiners et al., 2003) and described as Cu-binding ligands, exudates under Cu-stress conditions and extreme temperature and salinity (Krembs et al., 2002; Riedel et al., 2006; Lin et al., 2020). The EPS were suggested as part of the Fe-binding ligand pool in the Greenland shelf (Ardiningsih et al., 2020).

As mentioned above, log K^{cond}_{Cu2+L} showed decreasing values close to the Greenland coast, which produced lower log α_{Cu2+L} values (Table 3.1) and higher Cu^{2+} concentration (Table 3.1). In general terms, the Cu^{2+} concentration reported here (0.13 – 21.13 fM) does not exceed the toxicity limits (10 pM) established for different cyanobacteria, coccolithophores, and diatoms species (Sunda and Lewis, 1978; Brand et al., 1986). However, the concentration of Cu^{2+} reported could reduce phytoplankton growth and reproduction rates (Brand et al., 1986; Peers et al., 2005). Under Cu-limiting conditions, phytoplankton may actively release metal-binding ligands into the medium to acquire Cu (Walsh et al., 2015). Phytoplankton exudates may contain relatively weaker Cu-binding ligands, such as thiols with log K^{cond}_{Cu2+L} between 12 and 15 (Leal et al., 1999), which could contribute to the observed decrease in log K^{cond}_{Cu2+L}.

Sinks of Cu-binding ligands

In the study region, different mechanisms may reduce or transform Cu-binding ligands in seawater. As the concentration of Cu^{2+}, in terms of pCu^{2+} (pCu^{2+}=–log[Cu^{2+}]), was between 13.6 and 15.89, some phytoplankton species could experience Cu-limitation (Peers et al., 2005; Maldonado et al., 2006; Annett et al., 2008). Under Cu-deficient conditions, phytoplankton and diatoms fulfil their requirements through the release of strong and weak complexes (log K^{cond}_{Cu2+L} =13.5 – 16, Semeniuk et al., 2015). Organic matter and metal-binding ligands could be transformed by microbial degradation (Paulsen et al., 2019) and photodegradation processes (Benner et al., 2005). The photodegradation of metal-binding ligands by solar irradiation in surface waters decreases the complexing capacity of Cu-binding ligands (Shank et al., 2006) and increases the Cu^{2+} bioavailability. The persistent sea-ice

coverage in the Arctic limits the effect of solar irradiation, but ice-free surface waters may be subject to this degradation process and modify the ligand characteristics.

3.4.3 Future projections

The effects that climate change may have on trace metal speciation in the region are unknown. The higher Arctic riverine discharge of organic matter (Frey and McClelland, 2009; Stedmon et al., 2011) could increase the release of strong metal-binding ligands (Slagter et al., 2017) and trace metals (Guieu et al., 1996) into the surface waters of the Arctic Ocean. This could lead to an increase in L_{Cu} concentration on the Greenland shelf and coast and a higher export of Cu towards the Nordic Seas and North Atlantic Ocean, as suggested for Fe (Ardiningsih et al., 2020). On the other hand, the thinning and retreat of 79NG ice tongue could produce higher meltwater discharge (Krisch et al., 2021) with stronger dissolved trace metal and DOM release close to the glacier terminus, which could alter the Cu-binding ligand concentrations. However, the reduction of sea-ice coverage may increase light penetration, the phytoplankton growth (Arrigo et al., 2008) as well as the photo-oxidation processes (Bélanger et al., 2006), with potential effects on Cu-binding ligand concentrations, utilisation, and nature. Finally, the intensification of the Atlantic water supply into the Fram Strait (Wang et al., 2020), alters the composition and productivity of the phytoplankton community (Ardyna and Arrigo, 2020) and consequently, the Cu-binding ligands.

According to the literature, an increase in seawater Cu^{2+} due to ocean acidification (Zuehlke and Kester, 1983; Millero et al., 2009; Gledhill et al., 2015), as well as the photooxidation processes (Shank et al., 2006). In

addition, the decrease in pH is also expected to affect the Cu complexation (Gledhill et al., 2015). In the study region, the observed Cu^{2+} concentrations (0.13 – 21.13 fM) were low, possibly even limiting (Brand et al., 1986; Peers et al., 2005), and the Cu-binding ligand concentrations were high (1.4 – 8.2 nM). Accordingly, the toxic levels of Cu^{2+} for microorganisms are not easily achieved in the area under the projected changes in pH (Fransner et al., 2022). Finally, it is important to notice that the concentration of Cu along the Greenland coast could be influenced by mining activity in the region in the future (Søndergaard and Mosbech, 2022), which can be encouraged by the loss of ice coverage in terrestrial regions.

3.5 Conclusions

The current investigation presents the first data set of Cu-binding ligand concentrations (L_{Cu}) and the conditional stability constants (log K^{cond}_{Cu2+L}) for the Arctic region of Fram Strait, including the northeast Greenland shelf and coastal area. Three different zones have been identified along the region, from east to west designated as Fram Strait, the NE Greenland Shelf and the Greenlandic coast. The L_{Cu} concentrations indicate a longitudinal trend with increasing values towards the west, especially in surface waters. Since the most elevated levels of L_{Cu} were detected near the 79NG glacier terminus, the coastal-to-ocean trend suggested that a portion of Cu-binding ligands of the Greenland shelf comes from the coastal sites and all the processes involved in the surrounding areas. The log K^{cond}_{Cu2+L} indicates the presence of strong binding ligands (L_1) and decreases towards the west. The organic matter degradation and/or bacterial remineralization, together with a minor contribution from coastal meltwater discharge, was suggested as the

predominant processes that affect the L_{Cu} concentrations and characteristics in coastal waters. Shelf stations presented intermediate values between coastal and eastern Fram Strait samples due to the combined effect of coastal inputs and ligands exported from the central Arctic via the Transpolar Drift (TPD). The Greenland shelf has distinct phenomena that determine the Cu-binding ligands characteristics, such as the interaction of the two currents (EGC and NEGCC), the presence of sea-ice and the biological activity (in sea-ice or phytoplankton blooms). The eastern Fram Strait presented the lowest L_{Cu} concentrations with results comparable to the North Atlantic Ocean.

The voltammetric technique does not provide information about the nature of organic ligands but allows us to determine the concentration and binding properties. The presence of excreted organic ligands by marine phytoplankton or sea-ice diatoms and degraded organic moieties was suggested to form the Cu-binding ligand pool, especially in coastal waters. However, it is to be expected that this pool of ligands in the region also contains humic substances with terrestrial origin. In addition, the presence of strong ligands keeps the Cu^{2+} at fM levels and allows the transport of Cu towards the Nordic Seas and North Atlantic Ocean.

In light of climate change and global warming, Arctic future projections indicate a complex physical, chemical, and biological alteration of oceanic conditions. The biogeochemical responses are unclear and could have significant impacts on the biogeochemical cycle of trace metals, such as Cu. To understand how trace metals will behave, further investigation into the distribution, nature, and transformation of organic ligands in the Fram Strait and surrounding regions is necessary. This work represents a starting point

for future studies to determine how climate change is going to affect copper speciation, and how the Fram Strait Atlantification may alter ligand concentration and copper toxicity.

Acknowledgements

The authors would like to thank captain Schwarze and his crew of the RV Polarstern, the chief scientist Torsten Kanzow and all other participants, for their effort and support during sample collection. We also acknowledge the financial support for the ATOPFe project (CTM2017-83476-P) from the Ministerio de Ciencia e Innovación (Spain). VA participation was funded by the PhD grant (PRE 2018-084476). AGG participation was partially funded by LabexMER International Postdoctoral Program for providing fellowship and Laboratoire d'Excellence LabexMer (ANR-10-LABX-19). Data can be found online at https://doi.pangaea.de/10.1594/PANGAEA.959511.

Image:S. Hendricks/AWI. SMOS.

Chapter 4. Natural Copper-Binding Ligands in the Arctic Ocean. The Influence of the Transpolar Drift (GEOTRACES GN04)

Frontiers in Marine Science, 12 December 2023

https://doi.org/10.3389/fmars.2023.1306278

V. Arnone[a], J. M. Santana-Casiano[a], M. González-Dávila[a], H. Planquette[b], G. Sarthou[b], L.J.A. Gerringa[c], A.G. González[a]

[a]Instituto de Oceanografía y Cambio Global, IOCAG, Universidad de Las Palmas de Gran Canaria, ULPGC, Spain.

[b]Univ Brest, CNRS, IRD, Ifremer, LEMAR, F-29280 Plouzané, France.

[c]Department of Ocean Systems, Royal Netherlands Institute for Sea Research, NIOZ, Den Hoorn, Netherlands.

Abstract

The Arctic Ocean is a unique biogeochemical environment characterized by low salinity surface waters, extensive sea-ice coverage, high riverine inputs, large shelf extension and the long residence time of deep waters. These characteristics determine the distribution of dissolved bio-essential trace metals, such as copper (Cu), and the dissolved organic-binding ligands capable of complexing it. This work reports the concentrations and conditional stability constants of dissolved Cu-binding ligands (L_{Cu} and log K^{cond}_{Cu2+L}) measured in samples from the Polarstern (PS94) expedition, as part of the international GEOTRACES program (cruise GN04). Full-depth profile stations from the Barents Sea, Nansen Basin, Amundsen Basin and Makarov Basin were analysed by competitive ligand exchange-adsorptive cathodic stripping voltammetry (CLE-AdCSV). The basins and water masses presented a wide range of L_{Cu} concentrations (range: 1.40 – 7.91 nM) and log K^{cond}_{Cu2+L} values (range: 13.83 – 16.01). The highest variability of Cu-binding ligand concentrations was observed in surface waters (≤200 m), and mean concentrations increased from the Barents Sea and Nansen Basin (2.15±0.31 nM and 1.93±0.35 nM, respectively) to the Amundsen (3.84±1.69 nM) and Makarov Basins (4.40± 2.03 nM). The influence of the Transpolar Drift (TDP) flow path was observed in the Amundsen and Makarov Basins, especially on Cu-binding ligand concentrations (L_{Cu} range: 3.96 – 7.91 nM). In contrast, deep waters (>200 m) showed no significant differences between basins and water masses in terms of L_{Cu} concentrations (range: 1.45 – 2.78 nM) and log K^{cond}_{Cu2+L} (range: 14.02 – 15.46). The presence of strong Cu-binding ligands (log K^{cond}_{Cu2+L}>13) in surface waters stabilises the excess of dissolved copper (dCu) transported in the TPD and favours its export to the Fram Strait and Nordic Seas.

Keywords: copper, copper-binding ligands, voltammetric method, Arctic Ocean, Transpolar Drift.

4.1 Introduction

The Arctic Ocean is characterized by a perennial sea-ice coverage and presents one of the most extensive continental shelf areas, with important consequences for ocean chemistry. The shelf covers more than 50% of the total area (Jakobsson, 2002) and is associated with a strong release of terrestrial freshwater (Opsahl et al., 1999). Around 10% of global riverine discharge arrives in the Arctic (Benner et al., 2005) and introduces macronutrients (Cauwet and Sidorov, 1996), trace metals (Middag et al., 2011; Colombo et al., 2019; Charette et al., 2020; Gerringa et al., 2021a; Jensen et al., 2022), dissolved organic matter (DOM, Opsahl et al., 1999; Stedmon et al., 2011) and dissolved metal-binding ligands (Slagter et al., 2017; Laglera et al., 2019). These substances, together with sediments, can be retained in sea-ice and released during its melting (Dethleff et al., 2000; Tovar-Sánchez et al., 2010; Anderson and Amon, 2015; Jensen et al., 2021). The surface Arctic Ocean is also affected by the water input from the Nordic Seas, Atlantic Ocean, and Pacific Ocean with a complex circulation pattern (Bluhm et al., 2015). The Transpolar Drift (TPD) is a significant surface current that allows the transport of riverine and shelf-derived material, along with sea-ice, from the Eurasian shelves to the central Arctic (Amundsen and Makarov Basins, Charette et al., 2020). Additionally, it allows for the export of these materials to the Nordic Seas and North Atlantic Ocean through the Fram Strait (Gordienko and Laktionov, 1969). The circulation and properties of intermediate and deep Arctic waters are conditioned by the system of ridges

and shelves. The ventilation of deep waters is limited, and the exchange only occurs via Fram Strait (Schauer, 2004). The export of Arctic waters and sea-ice to the Nordic Seas stimulates biological activity (Amon, 2003). Subsequently, changes in the Arctic water properties due to climate change may impact the biogeochemistry of other adjacent oceanic regions.

Climate change has already caused significant modifications in Arctic conditions. The observed temperature increases (0.6ºC per decade between 1981 and 2020) in the Arctic Ocean were associated with the decrease of sea-ice coverage and higher light penetration (IPCC, 2022), can enhance the phytoplankton growth (Arrigo et al., 2008). Then, under ice-free conditions, the CO_2 uptake and sequestrations increase (Arrigo et al., 2008). The increased input of freshwater is also modifying the hydrodynamics of the currents in the area and the potential export of Arctic waters (Krumpen et al., 2019). In addition, the permafrost thawing (Schuur et al., 2013, 2015) and the higher freshwater inputs (Peterson et al., 2002) increase the discharge of DOM (Frey and McClelland, 2009; Stedmon et al., 2011), including dissolved metal-binding ligands (Slagter et al., 2017; Laglera et al., 2019), and dissolved trace metals in the Arctic basins (Guieu et al., 1996).

The bioavailability of trace metals is one of the limiting factors that determine primary production in the ocean. Copper (Cu) is required in different biological processes essential for phytoplankton growth (Twining and Baines, 2013), and can be assimilated as free cupric ion (Cu^{2+}) and through complexes with strong binding ligands (Sunda and Lewis, 1978; Semeniuk et al., 2015). However, elevated concentrations of Cu^{2+} can be toxic for certain phytoplankton species (Brand et al., 1986). In seawater, Cu bioavailability and toxicity are controlled by the formation of complexes with

dissolved organic binding ligands (Brand et al., 1986). Copper-binding ligands (L_{Cu}) are a heterogeneous group of compounds (e.g., thiols, humic substances, exopolysaccharides, and methanobactins), that remain largely unidentified. Ligands are classified according to their conditional stability constant respect to the Cu^{2+} ion (log K^{cond}_{Cu2+L}) into strong (L_1 class) or weak ligands (L_2 class), being 13 the value that differentiates the two groups (Bruland et al., 2000; Buck and Bruland, 2005), that are in a good agreement with Ruacho et al. (2022). The biogeochemical cycle of Cu in the Arctic Ocean is still largely unexplored. While riverine runoff was proposed as the primary source of dissolved Cu (dCu) in the Arctic Ocean (Charette et al., 2020; Gerringa et al., 2021a; Jensen et al., 2022), the existing knowledge about Cu organic speciation in the study region and nearby areas are limited (Kramer, 1986; Moffett and Dupont, 2007; Whitby et al., 2018; Nixon et al., 2019; Gourain, 2020; Wong et al., 2021; Arnone et al., 2023). Information about L_{Cu} concentrations was reported for the Canadian Arctic waters (Nixon et al., 2019), the sub-arctic North Pacific (Moffett and Dupont, 2007; Whitby et al., 2018; Wong et al., 2021), the Fram Strait and Greenland shelf(Arnone et al., 2023), and for nearby areas in the North Atlantic Ocean (Kramer, 1986; Gourain, 2020).

To characterize the Cu organic speciation in the central Arctic Ocean, this study evaluates for the first time the dissolved Cu-binding ligand concentrations and the conditional stability constants (L_{Cu} and log K^{cond}_{Cu2+L}) in this oceanographic region. Samples were collected during the TransArcII expedition (GEOTRACES GN04), between August 15th and October 17th 2015, onboard the *RV Polarstern* (PS94). Information about Cu-binding ligands in the Arctic Ocean improve our knowledge about the Cu biogeochemical cycle and the potential export to other oceanic areas.

4.2 Material and Methods

4.2.1 Sampling

During the PS94 TransArc II cruise (GEOTRACES GN04), onboard the icebreaker R/V *Polarstern*, a total of 23 stations were sampled between August 15th and October 17th, 2015 (Figure 4.1a). The cruise covered several basins, including the Barents Sea, Nansen Basin, Amundsen Basin and Makarov Basin, where water samples were collected through full-depth profiles (Schauer, 2016). An ultra-clean CTD (UCCTD) rosette (Rijkenberg et al., 2015) was employed for sample collection, following the GEOTRACES protocols (Cutter et al., 2014). After recovery, the UCCTD system was pushed into an ISO Class 6 clean room container, where samples were filtered over <0.2 µm Sartobran 300 cartridges (Sartorius), under pressure of filtered N_2 (0.7 bar). The sampled 125 mL low-density polyethylene (LDPE) bottles, which were cleaned with hydrochloric acid (HCl) according to the GEOTRACES protocols (Cutter et al., 2014), were rinsed 3-4 times with seawater before filling. After filling, they were stored at -20ºC.

Data of conductivity, temperature and depth, measured with a SEABIRD 911 CTD, can be found in PANGAEA for both UCCTD (Ober et al., 2016) and CTD data (Rabe et al., 2016). A standard rosette sampling system (CTD), equipped with a fluorometer for chlorophyll-a fluorescence, was also deployed at the same stations than the UCCTD.

4.2.2 Nutrients

Unfiltered seawater for macronutrient analysis was sampled from the UCCTD. The analysis of nitrate, phosphate and silicate was performed onboard with a Technicon TRAACS 800 continuous flow auto analyzer as described by (Slagter et al., 2017; Rijkenberg et al., 2018). Data were reported by van Ooijen et al. (2016).

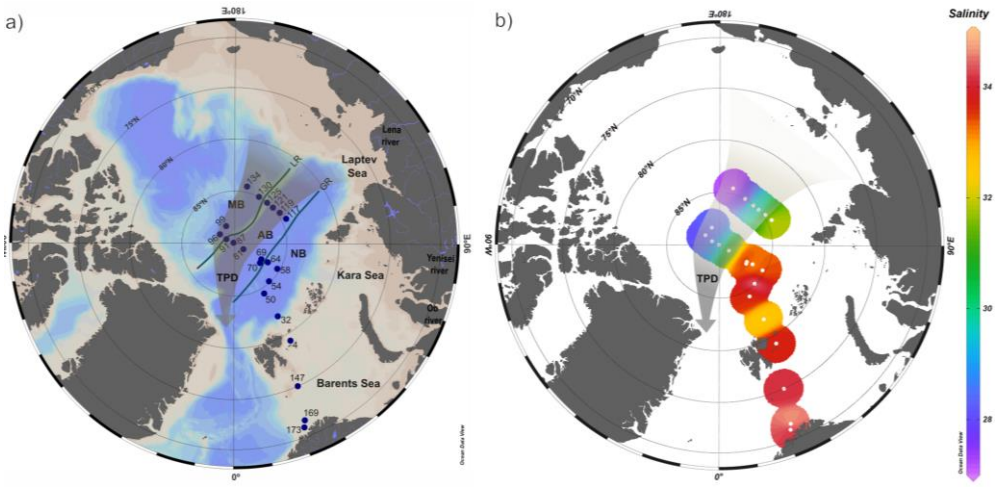

Figure 4.1. a) Map of the study area with the station positions (blue dots). The central Arctic basins crossed during the cruise were indicated as: Nansen Basin (NB), Amundsen Basin (AB) and Makarov Basin (MB). The Gakkel Ridge (GR) divides the NB from the AB while the Lomonosov Ridge (LR) divides the AB form the MB, both of them depicted with solid lines. b) Surface salinity distribution. The brownish arrow indicates the approximate location of the Transpolar Drift (TPD).

4.2.3 Total dissolved Cu analysis

The concentration of dCu was measured with a high-resolution inductively coupled plasma-mass spectrometry (HR-ICPMS element 2, Thermo Finnigan) after pre-concentration (seaFAST) and matrix removal. The analytical error in the determination of dCu range from 0.004 to 0.02 nM (Gerringa et al.,

2021a). More information about dissolved trace metal analysis and results can be found in Gerringa et al. (2021a), as well as, in the PANGAEA database (Gerringa et al., 2021b).

4.2.4 Voltammetric analysis

The L_{Cu} concentration and log K^{cond}_{Cu2+L} values were determined by competitive ligand exchange-adsorptive cathodic stripping voltammetry (CLE-AdCSV) using salicylaldoxime (SA) as competing ligand (Campos and van den Berg, 1994). The 0.01 M SA was prepared in 0.1 M suprapure HCl. The buffer, 1 M boric acid (H_3BO_3) prepared in 0.3 M ammonia (NH_3) and adjusted at pH 8.2, was cleaned with an overnight equilibration with 100 µM manganese dioxide (MnO_2, Sigma-Aldrich) and then filtered by 0.2 µm filter (van den Berg, 1982). Copper stock solutions (Fluka) were made in 0.1% suprapure HCl. To ensure the chemical properties, the reagents were prepared weakly and kept in the fridge (at 8ºC and in darkness) when they were not in use.

For titration procedure, 10 mL seawater aliquots were pipetted into 11 PTFE vials (22 mL volume), and 100 µL of buffer (final concentration 10^{-2} M) was added before discrete Cu(II) additions (0, 0.1, 0.3, 0.6, 0.9, 1.4, 2.3, 4, 6 and 8 nM of Cu). After 1 hour of equilibration, 10 µL of SA (final concentration 10 µM) was added. A minimum of 8 hours of equilibration was allowed before analysis. Few samples were analysed with higher Cu addition, up to 20 nM, but no differences were found in the Cu-binding ligand determination. Titrations were measured with a Hanging Mercury Drop Electrode (VA663 stand Metrohm), a Ag/AgCl reference electrode with a KCl salt bridge (3 M) and a glassy carbon counter electrode. Briefly, a 120s

nitrogen purge was employed to remove oxygen interference, a deposition potential of – 0.2 V was applied for 60 s. After 10 s of equilibration, a differential pulse scan was applied from – 0.2 to – 0.5 V, with a step potential 4 mV, modulation amplitude 49.95 mV, interval time 0.1 s and modulation time of 0.04 s. Data fitting was performed with PromCC software (Omanović et al., 2015) using the "complete fitting" for one ligand class and the sensitivity was determined by internal calibration from the last titration points (4 or 5) which presented linearity. This method assumed that in the linear portion of the titration curve, all ligands were titrated within the detection window (D) of the method (Equation 4.1). To confirm complete titration of all ligands in certain samples, two Cu additions were made at the final titration point (with either 4 or 8 nM of Cu) and promptly measured. It is important to note that these supplemental additions were excluded from data analysis. One ligand class model was fitted the experimental values.

The side reaction coefficient for the Cu and SA complexes (α_{CuSA}) establishes the centre of D (Equation 4.1), and it depends on the concentration of SA and the salinity of the sample (Campos and van den Berg, 1994). For each sample the α_{CuSA} and its conditional stability constants (log K^{cond}_{CuSA}, log $\beta^{cond}_{Cu(SA)2}$) were estimated as follows:

$$\alpha_{\mathrm{CuSA}} = \mathrm{K}^{\mathrm{cond}}_{\mathrm{CuSA}} \cdot [\mathrm{SA}] + \beta^{\mathrm{cond}}_{\mathrm{Cu(SA)_2}} \cdot [\mathrm{SA}]^2 \quad (4.1)$$

$$\log \mathrm{K}^{\mathrm{cond}}_{\mathrm{CuSA}} = 10.12 - 0.37 \cdot \log \mathrm{S} \quad (4.2)$$

$$\log \beta^{\mathrm{cond}}_{\mathrm{Cu(SA)_2}} = 15.78 - 0.53 \cdot \log \mathrm{S} \quad (4.3)$$

In this study, the value of log α_{CuSA} ranged from 5.10 to 5.16, which represents the centre of D. The window extended one to two orders of magnitude above and below the centre (Apte et al., 1988), and included values

between 3.10 and 7.16. The side reaction coefficient for inorganic metal ($\alpha_{Cu'}$) also varies with the salinity (range between 26 and 30). It was calculated considering the major seawater ions (X_i) concentrations and stability constants (β^{cond}_{CuXi}) and the acidity Cu constant ($\beta^{cond}_{Cu(OH)i}$) at seawater ionic strength (Campos and van den Berg, 1994), as expressed below:

$$\alpha_{Cu'} = 1 + \sum\left(\beta^{cond}_{CuX_i} \cdot [X]^i\right) + \sum\left(\beta^{cond}_{Cu(OH)_i}/[H^+]^i\right) \quad (4.4)$$

For data treatment with PromCC, $\alpha_{Cu'}$, log K^{cond}_{CuSA} and log $\beta^{cond}_{Cu(SA)2}$ values were considered for each sample due to the high variability of salinity between depths and stations.

Using the concentration of dCu and the PromCC results (Cu^{2+}, L_{Cu}, and the log K^{cond}_{Cu2+L}) different parameters were estimated, such as the concentrations of labile Cu (Cu'= $Cu^{2+} \cdot \alpha_{Cu'}$, sum of all inorganic species), labile ligand (Cu'L = dCu – Cu') and excess ligand (eL_{Cu} = L_{Cu} – Cu'L, concentration of ligand not bound to Cu). The reactivity between L_{Cu} and dCu (f_{Cu2+L}) is calculated by the product between L_{Cu} and K^{cond}_{Cu2+L} (Gledhill and Gerringa, 2017; Arnone et al., 2022). For an accurate detection of ligands, this reactivity needs to be within the D range. The analytical error reported for L_{Cu} and log K^{cond}_{Cu2+L}, based on seawater voltammetry test, were 0.092 nM and 0.054, respectively.

4.2.5 Statistical analysis

Significant differences between physical properties (temperature and salinity), macronutrient concentrations (nitrate, phosphate and silicate), dCu concentrations and Cu-binding ligands parameters (concentrations of L_{Cu}, eL_{Cu}, Cu' and Cu^{2+}, as well as log K^{cond}_{Cu2+L} and log f_{Cu2+L}) were determined.

A Kruskal-Wallis test (Kruskal and Wallis, 1952) coupled with a Conover test (Conover and Iman, 1979) was applied to investigate differences between groups (basins, water masses), considering p-values < 0.05 as significant. This test was chosen due to the non-normal distribution and heteroscedasticity properties observed in Cu-speciation data.

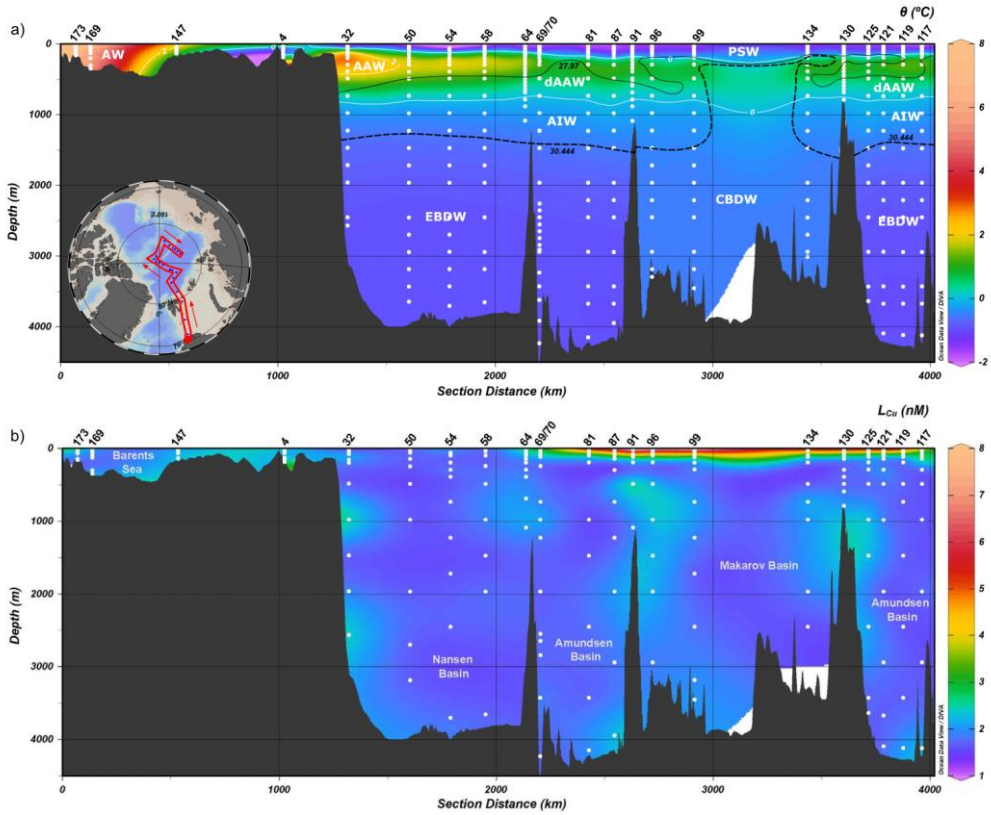

Figure 4.2. Distribution of (a) potential temperature (θ, in ºC) and (b) copper-binding ligands concentration (L_{Cu}) in the Arctic Ocean, including all stations. The temperature transect contains isolines for θ at 0ºC and 2ºC (white solid line), potential density anomaly (σ_θ, 0 dbar) 27.97 (black solid line), and potential density anomaly ($\sigma_{0.5}$, 500 dbar) 30.444 (black dashed line). Seven water masses were defined following Rudels (2019): Polar Surface Water (PSW, θ<0ºC, σ_0<27.97 kg m^{-3}), Atlantic Water (AW), Arctic Atlantic Water (AAW, 0<θ≤2ºC, 27.7<σ_0<29.97 kg m^{-3}), dense Arctic Atlantic Water (dAAW, θ>0ºC, σ_0>29.97 kg m^{-3}, $\sigma_{0.5}$<30.444 kg m^{-3}), Arctic Intermediate Water (AIW, θ<0ºC, σ_0>29.97 kg m^{-3}, $\sigma_{0.5}$<30.444 kg m^{-3}),Canadian Basin Deep Water (CBDW, $\sigma_{0.5}$>30.444 kg m^{-3}, $\sigma_{1.5}$<30.142 kg m^{-3}) and Eurasian Basin Deep Water (EBDW, $\sigma_{1.5}$>30.142 kg m^{-3}).

4.3 Results

4.3.1 Hydrography

The Cu-binding ligand distribution in the Arctic Ocean must be understood in the context of the hydrographic conditions. Therefore, the content and characteristics of L_{Cu} were discussed for each water mass and basin. Arctic Ocean hydrography was described elsewhere (Bluhm et al., 2015; Rudels, 2019), and summarized in other works from PS94 cruise (Slagter et al., 2017; Rijkenberg et al., 2018; Gerringa et al., 2021a). Seven different water masses were identified (Figure 4.2 caption) according to Rudels (2019): Polar Surface Water (PSW), Atlantic Water (AW), Arctic Atlantic Water (AAW), dense Arctic Atlantic Water (dAAW), Arctic Intermediate Water (AIW), Canadian Basin Deep Water (CBDW) and Eurasian Basin Deep Water (EBDW). The PSW in the central Arctic Ocean is strongly influenced by the TPD, whose boundary was defined based on *in-situ* Chromophoric Dissolved Organic Matter (CDOM) fluorescence characteristics. Following the definition of the TPD made by Slagter et al. (2017) for the same cruise, surface waters (<55 or 77 m) from St. 81 to 99 and from St. 119 to 134 were inside the TPD (*in-situ* CDOM fluorescence>0.5 a.u.), both downstream and upstream, respectively. On the other side, waters up to 200 m depth from St. 58 to 99 and from St. 117 to 134 (*in-situ* CDOM fluorescence<0.5 a.u.) were outside the TPD.

Surface waters in the central Arctic were covered by sea-ice. Different ice arrangements were observed in terms of thickness and age (Appendix Figure B.1, König-Langlo, 2015). Close-pack ice conditions were observed between St. 32 and 134 with different stage development. First-year ice with a thickness of less than 70 cm was observed at St. 32 and with thicknesses

between 70 and 120 cm between St. 50 and 58 and at St. 117 and 134. From St. 64 to 96 medium and thick ice was observed, corresponding with a first-year with some old ice (>2m thick). Station 99 presented medium first-year ice.

Along the cruise track, the temperature (Appendix Figure B.2) varied between -1.81 and 8.94ºC. Its profile changed between basins; temperatures higher than 2.78ºC, corresponding to AW, were restricted to the Barents Sea and increased further toward the south. The profiles in Nansen, Amundsen and Makarov Basins were similar, the surface minimum was followed by increasing temperatures until ~250 m depth after which the temperature decreased from 250 m to 1500 m. Finally, temperatures below 1500 m were constant (mean temperature: -0.65 ± 0.13ºC). The maximum temperature in the Nansen Basin at ~250 m (AW temperature 2.78ºC) was higher than in the Amundsen and Makarov Basins (AAW temperature 1.21ºC and 1.11ºC, respectively). The salinity also exhibited surface minima (Figure 4.1b; Appendix Figure B.2) increasing until ~ 250 m, after which it remained constant (34.92 ± 0.04). The surface salinity decreases from the Barents Sea (33.75) via the Nansen and Amundsen Basins to the Makarov Basin (27.18).

The macronutrient (phosphate, nitrate and silicate) distribution was described elsewhere (Slagter et al., 2017; Rijkenberg et al., 2018) and briefly summarized here. Macronutrients presented typical nutrient profiles (Appendix Figure B.2), with a rapid increase in concentrations from 0 to 200 m depth, followed by a comparatively gradual increase from 200 to 2000 m.

Table 4.1. Summary of range (minimum and maximum), mean and standard deviation (SD) and median of Cu speciation parameters considering the full depth profile ("Global study area"), surface waters (≤ 200 m) and deep waters (> 200 m). The number of samples (n) was included in the first column. Dissolved Cu data were reported by Gerringa et al. (2021b).

		dCu (nM)	L_{Cu} (nM)	$logK^{cond}_{Cu2+L}$	$\log \alpha_{Cu2+L}$	eL_{Cu} (nM)	L_{Cu}/dCu	%CuL	Cu' (pM)	Cu^{2+} (pM)
Global study area (n=226)	Min	1.2	1.4	13.83	5.31	0	1	99.52	0.03	0.0008
	Max	7.34	7.91	16.01	7.25	1.89	2.07	100	13.47	0.4209
	Mean±SD	2.26 ± 1.36	2.56 ± 1.42	14.79 ± 0.35	6.15 ± 0.35	0.30 ± 0.25	1.16 ± 0.14	99.95 ± 0.08	1.16 ± 1.85	0.04 ± 0.06
	Median	1.63	2.05	14.78	6.15	0.25	1.12	99.98	0.48	0.015
Surface waters (n=122)	Min	1.2	1.4	13.83	5.31	0.02	1.01	99.57	0.03	0.0008
	Max	7.34	7.91	16.01	7.25	1.89	2.07	100	13.47	0.4209
	Mean±SD	2.83 ± 1.65	3.16 ± 1.70	14.82 ± 0.39	6.27 ± 0.35	0.33 ± 0.27	1.15 ± 0.14	99.96 ± 0.07	1.25 ± 2.18	0.04 ± 0.07
	Median	2.1	2.46	14.79	6.31	0.27	1.11	99.98	0.44	0.0138
Deep waters (n=104)	Min	1.34	1.45	14.02	5.39	0	1	99.52	0.04	0.0014
	Max	1.93	2.78	15.46	6.75	1.11	1.67	100	7.53	0.2353
	Mean±SD	1.58 ± 0.07	1.85 ± 0.25	14.74 ± 0.29	6.01 ± 0.29	0.27 ± 0.23	1.17 ± 0.15	99.93 ± 0.09	1.05 ± 1.38	0.03 ± 0.04
	Median	1.57	1.79	14.76	6.01	0.22	1.14	99.96	0.55	0.0171

Below 2000 m depth, concentrations remained relatively constant. Phosphate concentrations ranged from 0.08 to 1.04 µM, silicate varied between 0.3 and 1.04 µM, while nitrate ranged from 0.04 to 15.06 µM. The basins showed a similar distribution and concentration range without significant differences, except for the first 200 m depth in the Amundsen and Makarov basins, where concentrations (between 6 and 13.58 µM) were higher than in the other basins.

4.3.2 Dissolved Cu-binding ligands

General overview of the studied area

The vertical profiles of L_{Cu} and dCu (Figure 4.2b and 4.3) presented similar patterns with higher variability at surface waters (≤200 m) and more constant concentrations below 200 m (deep waters), with some subsurface maximums. The L_{Cu} concentrations varied between 1.40 and 7.91 nM (Table 4.1) in the first 200 m depth and between 1.45 and 2.78 nM in deeper waters (Figure 4.2b). The concentration of dCu ranged from 1.20 to 7.34 nM in surface waters and from 1.34 to 1.93 nM in deeper waters (Appendix Figure B.3a, Gerringa et al., 2021a). The L_{Cu} concentrations always exceed the dCu with more the 99.52% of dCu complexed (Figure 4.3). Only strong or L_1 ligands were detected using the classification of Bruland et al. (2000) and Buck and Bruland (2005), where L_1 class present log K^{cond}_{Cu2+L} >13 (Appendix Figure B.4). In the surface waters log K^{cond}_{Cu2+L} variability was higher (13.83 – 16.01) than those in deeper waters (14.02 – 15.46). The detection window applied strongly influences the L_{Cu} and K^{cond}_{Cu2+L} detected. The detection window employed in the current investigation was the same one used in other oceanic publications, where both weak and strong ligands were detected

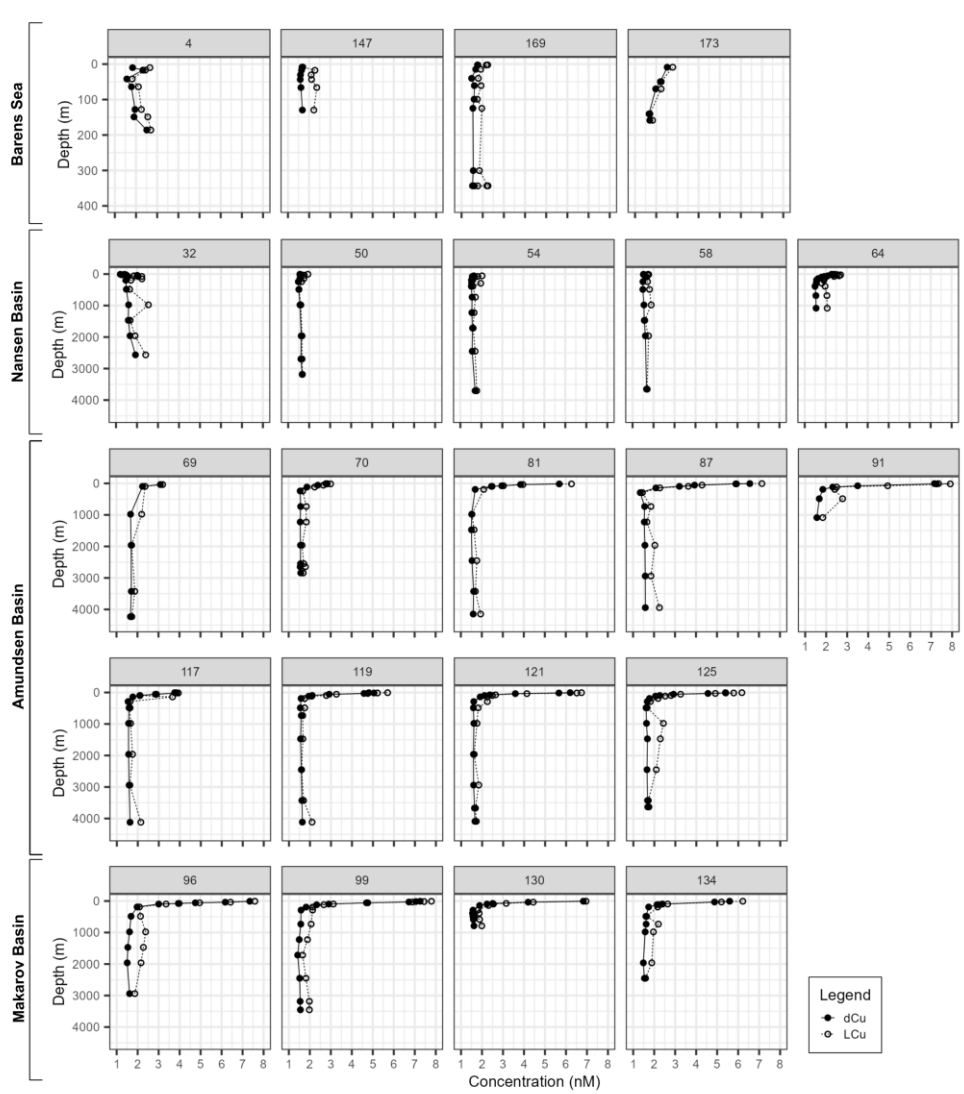

Figure 4.3. Depth profile of dissolved Cu (dCu, black circles with solid lines) and Cu-binding ligand concentrations (L_{Cu}, open circles with dashed lines) depicted per station and grouped by seas and basins. Both parameters represented in nM units. Barents Sea profiles represented with a different vertical scale. Dissolved Cu data were reported by Gerringa et al. (2021b).

(Laglera and van den Berg, 2003; Bundy et al., 2013; Abualhaija et al., 2015; Whitby and van den Berg, 2015; Whitby et al., 2018; Hollister et al., 2021; Wiwit et al., 2021). The presence of Cu-binding ligands keeps the free cupric ion (Cu^{2+}) concentrations between 0.0008 and 0.42 pM, that is below the toxic levels of 10 pM (Sunda and Lewis, 1978; Brand et al., 1986). The reactivity of the ligands, represented by log α_{Cu2+L}, varied between 5.31 and 7.25 at the surface and between 5.39 and 6.75 in deeper waters.

To understand the potential impact of regional variabilities, such as hydrography and water properties (physical, chemical, and biological), on Cu speciation, we evaluate the variation in L_{Cu} across different basins, both in the presence of the TPD and within water masses (both surface and deep waters).

Surface waters

Surface waters of the Arctic Ocean presented the higher L_{Cu} variability (Figure 4.4 and Table 4.2) with concentrations increasing from the Barents Sea and Nansen Basin (mean L_{Cu} 2.15±0.31 nM and 1.93±0.35 nM, respectively) toward the Amundsen and Makarov Basins (mean L_{Cu} 3.84±1.69 nM and 4.40±2.03 nM, respectively). Barents Sea stations were located above a shallow shelf (bottom depth range: 152 – 358 m) and did not show significant vertical L_{Cu} variations. The Nansen Basin exhibited uniform L_{Cu} concentrations (range: 1.71 – 2.23 nM), except at St. 64 showing relatively high surface concentrations (maximum 2.71 nM). The Amundsen and Makarov Basins showed the widest L_{Cu} concentration range (1.75 – 7.91 nM and 2.09 – 7.79 nM, respectively), with more than 7 nM observed at stations 87, 91, 96 and 99. In surface waters, the log K^{cond}_{Cu2+L} ranged from 13.83 to 16.01 but values higher than 15.44 were only observed along the

Barents Sea (range: 13.96 – 16.01). The other basins showed a log K^{cond}_{Cu2+L} range from 13.83 to 15.44. The statistical analysis of L_{Cu} concentrations between basins revealed that differences between the Barents Sea and the Nansen Basin, as well as between Amundsen and Makarov Basins, were not statistically significant (p-value>0.05, Table 4.3a). However, significant differences (p-value<0.05, Table 4.3a) were observed when comparing L_{Cu} concentrations from Barents Sea to Amundsen and Makarov Basins, as well as when comparing L_{Cu} concentrations from the Nansen Basin to Amundsen and Makarov Basins.

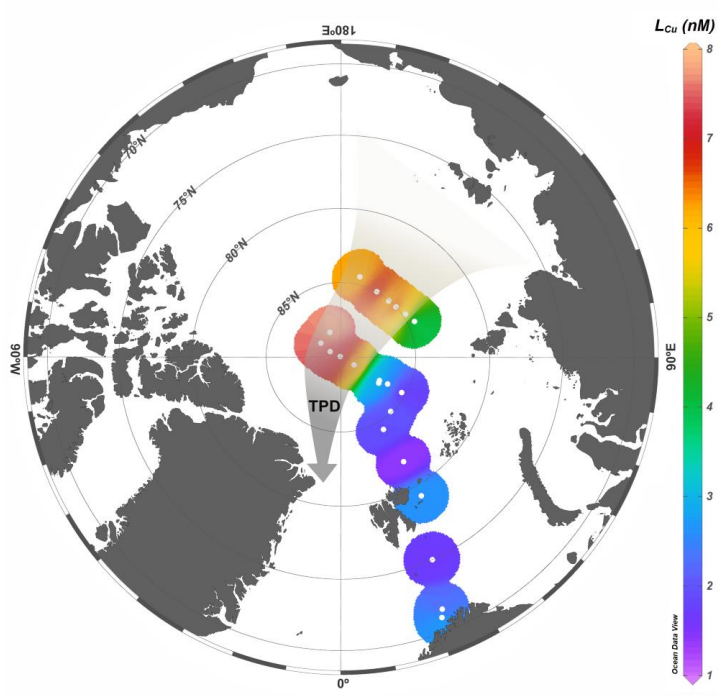

Figure 4.4. Surface distribution of dissolved Cu-binding ligand (L_{Cu}) concentrations (nM) in the first 10 m depth. The TPD path depicted with the brownish arrow.

According to the definition of Rudels (2019), three water masses (Figure 4.2) were identified in the surface waters of the Arctic Ocean that are

interesting to understand the L_{Cu} distribution. The PSW and AAW were observed along the whole cruise track, while the AW was restricted to the Barents Sea and Nansen Basin. The highest concentrations of L_{Cu} (Table 4.1 and Appendix Figure B.5) were measured in PSW (range: 1.40 – 7.91 nM, mean: 3.60 ± 1.85 nM) and the lowest in AW (range: 1.70 – 2.78 nM, mean: 2.09 ± 0.31 nM). However, log K^{cond}_{Cu2+L} and log f_{Cu2+L} values were higher in AW (15.21± 0.45 and 6.53± 0.44, respectively) than in PSW (14.74 ± 0.32 and 6.24 ± 0.29). This produced a higher concentration range of Cu^{2+} in PSW (0.002 – 0.421 pM) than in AW (0.001 – 0.056 pM, Appendix Table B.1). The L_{Cu} concentrations in AAW (range: 1.58 – 3.65 nM, mean: 2.22 ± 0.47 nM), stability constants (14.79 ± 0.40) and log f_{Cu2+L} values (6.13 ± 0.37 nM) were intermediate between those of the PSW and AW. Inside the PSW, lower L_{Cu} concentrations were observed in the Nansen Basin (L_{Cu}=1.94 ± 0.38 nM) and higher in the Amundsen Basin (L_{Cu}= 4.02 ± 1.69 nM) and the Makarov Basin (L_{Cu}= 4.74 ± 1.96 nM).

Based on *in-situ* CDOM fluorescence characteristics, the pathway of TPD can be differentiated in the PSW (Slagter et al., 2017). It is unclear whether station 134 is inside or outside the TPD (Gerringa et al., 2021a; Slagter et al., 2017). However, since the observed L_{Cu} and dCu concentrations are similar to the stations certainly affected by the TPD, station 134 has been included within the TPD pathway. Significant L_{Cu} differences (p-value<0.05, Table 4.3b) were observed among waters inside and outside the TPD. The L_{Cu} concentrations (Table 4.2) inside the TPD (mean: 5.87 ± 1.22 nM) were higher than outside (mean: 2.56 ± 0.56 nM). The same significant difference was observed for dCu inside (mean: 5.46 ± 1.21 nM) and outside the path (mean: 2.25 ± 0.55 nM). The concentrations of dCu y L_{Cu} showed a linear relationship in surface waters inside and outside the TPD, together with

surface coastal samples from stations 4 and 173 (Figure 4.5a). The differences in log K^{cond}_{Cu2+L} and Cu^{2+} concentrations inside and outside the TPD were small but significant (Table 4.2 and Table 4.3b). Other parameters, such as log f_{Cu2+L} (range: 5.40 – 7.16) and the eL_{Cu} concentrations (range: 0.02 – 1.89 nM) did not show significant variations between inside and outside the TPD. The correlation between L_{Cu} and eL_{Cu} observed in surface waters inside and outside the TPD, including coastal samples, did not follow the linear relationship observed in deep and Barents Sea waters (both shallow and deep, Figure 4.5b). No differences were observed inside the TPD between upstream and downstream stations (Supplementary Figure 6).

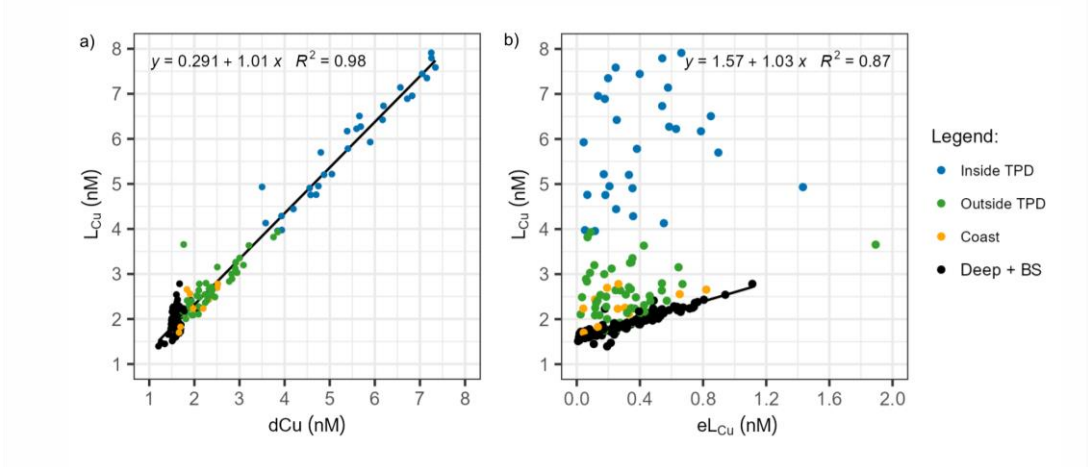

Figure 4.5. a) Correlation between dissolved Cu (dCu) and Cu-binding ligands (L_{Cu}) concentrations in nM. The solid line indicates a linear relationship observed in surface waters, encompassing coastal, inside and outside TPD samples. b) Correlation between L_{Cu} and the excess ligand ($eL_{Cu} = L_{Cu} – Cu'L$) concentrations in nM. The solid line depicts the linear relationship observed in deep and Barents Sea waters, both surface and deep, excluding St. 4 and 173. Data from all basins and seas were included and both relationships were significant (p-value < $2.2e^{-16}$). Different sample groups are color-coded, considering depth, basins, and influences from the TPD and coastal areas. Blue dots represent surface water samples taken inside the TPD from St. 81 to 99 and St. 119 to 134. Green dots denote samples taken outside the TPD (≤200 meters depth) from St. 58 to 99 and St. 117 to 134, including water below the TPD pathway. Yellow bots indicate coastal samples (≤200 meters depth) from St. 4 and 173. Black dots encapsulate deep waters (>200 meters depth) from all basins and Barents Sea samples, excluding St. 4 and 173.

Surface waters L_{Cu} concentrations in Amundsen and Makarov Basins presented significant (p-value<0.05) linear negative relationships with salinity and nitrate concentrations (Figure 4.6). A positive relationship was observed with silicate concentrations. A correlation was also observed between L_{Cu} concentrations, the absorbance parameters of Chromophoric and Fluorescence Dissolved Organic Matter (CDOM and FDOM, respectively) in surface waters (Figure 4.7). For that, the absorbance at 254 nm and 300 nm was collected from data reported by Slagter et al. (2017) and available in PANGAEA (Gerringa et al., 2021b). In surface waters, no linear relationships were observed between L_{Cu} and other parameters such as phosphates, temperature, or fluorescence (data not shown).

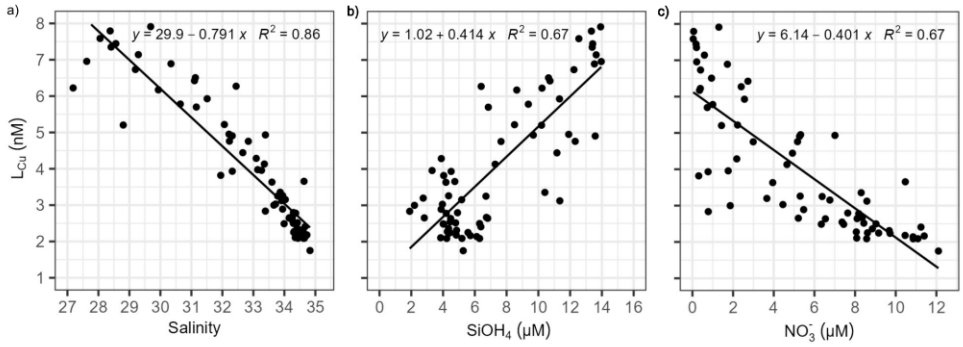

Figure 4.6. Copper-binding ligand (L_{Cu}) concentration (nM) against (a) salinity, (b) silicate ($SiOH_4$, in µM) and (c) nitrate (NO_3^-, in µM) for surface samples (≤200 m) located in the Amundsen and Makarov Basins. Waters inside and outside the TPD were included. The chart area includes the linear fitting applied for each couple of parameters, the relationships established were significant (p-value < $2.2e^{-16}$). Silicate and nitrate concentration data were reported by van Ooijen et al. (2016).

Table 4.2. Summary of range (minimum and maximum), mean and standard deviation (SD) and median of Cu speciation parameters for surface samples (≤ 200 m) of different basins. Barents Sea (St. 4, 147, 169 and 173), Nansen Basin (St. 32, 50 54, 58, 64), Amundsen Basin (St. 69, 70, 81, 87, 91, 117, 119, 121, 125) and Makarov Basin (St. 91, 96, 99, 130, 134). The number of samples (n) was included in the first column. Dissolved Cu data were reported by Gerringa et al. (2021b). The TPD was defined following Slagter *et al.* (2017).

Surface		dCu (nM)	L_{Cu} (nM)	$logK^{cond}_{Cu2+L}$	$\log \alpha_{Cu2+L}$	eL_{Cu} (nM)	L_{Cu}/dCu	%CuL	Cu' (pM)	Cu^{2+} (pM)
Barents Sea (n=25)	Min	1.48	1.7	13.96	5.31	0.04	1.02	99.88	0.03	0.001
	Max	2.52	2.78	16.01	7.25	0.82	1.46	100	2.24	0.07
	Mean±SD	1.80±0.29	2.15±0.31	15.17±0.47	6.50±0.45	0.35±0.22	1.20±0.13	99.98±0.03	0.36±0.59	0.01±0.02
	Median	1.68	2.17	15.25	6.59	0.31	1.18	99.99	0.14	0.004
Nansen Basin (n=28)	Min	1.2	1.4	14.16	5.51	0.02	1.01	99.57	0.07	0.002
	Max	2.39	2.71	15.44	6.67	0.71	1.47	100	6.85	0.214
	Mean±SD	1.68±0.30	1.93±0.35	14.80±0.34	6.08±0.31	0.25±0.16	1.15±0.10	99.95±0.08	0.77±1.32	0.02±0.04
	Median	1.57	1.84	14.82	6.06	0.22	1.15	99.98	0.37	0.012
Amundsen Basin (n=46)	Min	1.58	1.75	13.83	5.4	0.02	1.01	99.57	0.13	0.004
	Max	7.25	7.91	15.34	7.16	1.89	2.07	100	12.31	0.385
	Mean±SD	3.46±1.62	3.84±1.69	14.75±0.30	6.29±0.29	0.39±0.36	1.14±0.17	99.96±0.07	1.42±2.29	0.04±0.07
	Median	2.91	3.22	14.78	6.34	0.35	1.09	99.98	0.66	0.021
Makarov Basin (n=23)	Min	1.74	2.09	14.04	5.76	0.05	1.01	99.66	0.11	0.003
	Max	7.34	7.79	15.24	6.57	0.64	1.26	99.99	13.47	0.421
	Mean±SD	4.10±2.02	4.40±2.03	14.62±0.30	6.22±0.23	0.30±0.16	1.09±0.07	99.95±0.07	2.44±3.18	0.08±0.10
	Median	3.94	3.98	14.66	6.26	0.25	1.07	99.97	0.87	0.027
Inside TPD (n=29)	Min	3.5	3.96	14.04	5.87	0.04	1.01	99.66	0.17	0.004
	Max	7.34	7.91	15.34	7.16	1.43	1.41	100	5.42	0.421
	Mean±SD	5.46 ± 1.21	5.87 ± 1.22	14.58 ± 0.29	6.34 ± 0.28	0.41 ± 0.31	1.08 ± 0.08	99.95 ± 0.07	1.09 ± 1.35	0.09 ± 0.10
	Median	5.4	5.93	14.61	6.33	0.35	1.07	99.97	0.85	0.048
Outside TPD (n=52)	Min	1.52	1.68	13.83	5.4	0.02	1.01	99.57	0.13	0.003
	Max	3.85	3.93	15.44	6.67	1.89	2.07	99.99	13.47	0.282
	Mean±SD	2.25 ± 0.55	2.56 ± 0.56	14.79 ± 0.31	6.18 ± 0.28	0.30 ± 0.28	1.15 ± 0.16	99.96 ± 0.06	4.16 ± 3.85	0.03 ± 0.05
	Median	2.12	2.49	14.77	6.2	0.27	1.12	99.98	3	0.013

Deep waters

Copper complexation showed less variability in deeper waters that in surface ones. No significant differences were detected in deep waters between water masses or basins, and no significant relationships existed between L_{Cu} and temperature, salinity or macronutrient concentrations. In deep waters (Table 4.1, Appendix Figure B.5), the concentrations of L_{Cu} varied between 1.45 and 2.78 nM (mean: 1.85 ± 0.25 nM) similar to the variability of dCu (range: 1.34 - 1.93 nM, mean: 1.58 ± 0.07 nM). However, the relationship between L_{Cu} and dCu in deep water is not linear (Figure 4.5). The L_{Cu} concentration only showed a linear relationship with eL_{Cu} concentration (Figure 4.5), this correlation was not observed in surface waters. The mean value of log K^{cond}_{Cu2+L} was 14.74 ± 0.29 while log f_{Cu2+L} was 6.01 ± 0.29. The concentrations of Cu^{2+} varied between 0.001 and 0.24 pM.

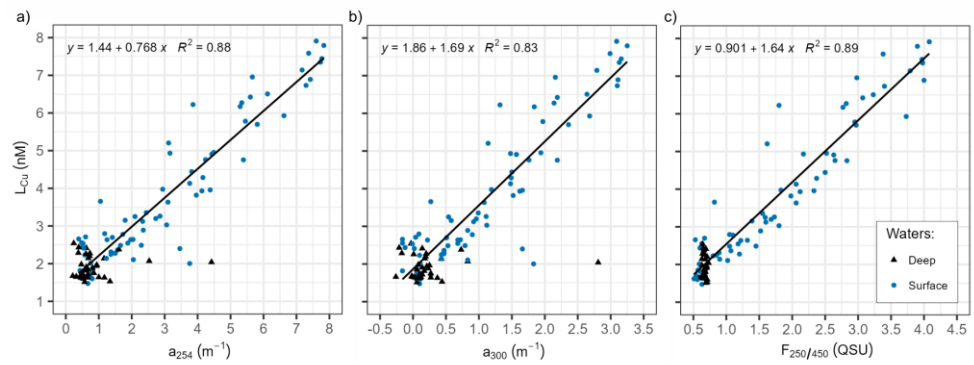

Figure 4.7. Correlation between dissolved copper-binding ligand (L_{Cu}) concentration (nM) and different Chromophoric Dissolved Organic Matter (CDOM) absorbances, at 1 nm resolution with a Spectramax M2 multimode spectrophotometer (Molecular Devices), equipped with a 1 cm path length quartz cell (SUPRASIL®, Hellma Analytics). Data and methodology description can be found in Slagter et al. (2017). The L_{Cu} concentrations were depicted against a) the absorption measured at 254 nm (a_{254}, in m^{-1}); the absorption measured at 300 nm (a_{300}, in m^{-1}); and c) the fluorescent fraction of DOM (FDOM), measured at 450 nm under excitation in 250 nm ($F_{250/450}$, expressed in Quinine Sulphate Units QSU).

In deep waters, L_{Cu} concentrations generally decrease with depth, with some exceptions. Stations 32, 91, 96 and 125 exhibited relatively higher concentrations between 500 and 1000 m depth compared to the rest of deep waters (Figure 4.2 and 4.3).

Cu-binding ligands model for central Arctic surface waters

A linear regression model (R^2= 0.94, p-value <$2.2e^{-16}$) was developed to estimate how the L_{Cu} concentrations vary with other parameters. Different combinations of variables were evaluated (temperature, salinity, oxygen, fluorescence, nitrate, silicate and phosphate) considering all basins and depths. The models presented only good correlations in PSW (equation 4.5) in surface waters inside and outside the TPD path (from station 58 to 134). Therefore, Barents Sea and part of Nansen Basin stations were excluded from model development and the proposed model is contributing to the estimation of Cu-binding ligands in the areas with the presence of PSW. The model was tested with different parameter combinations (Appendix Tables B.2 and B.3), where the Equation 4.5 was obtained as the best fitting according to the Bayesian Information Criterion (Sakamoto et al., 1986). Then, L_{Cu} concentration can be estimated by:

$$L_{Cu} = 10.87321 - 0.244 \cdot \text{Salinity} + 0.25263 \cdot \text{SiOH}_4 - 0.1519 \cdot \text{NO}_3^- \quad (4.5)$$

where the silicate ($SiOH_4$) and nitrate (NO^-_3) were in µM. Accordingly, this equation estimate the concentration of L_{Cu} in the PSW of the central Arctic Ocean. The predicted and measured L_{Cu} concentrations were represented in Figure 4.8.

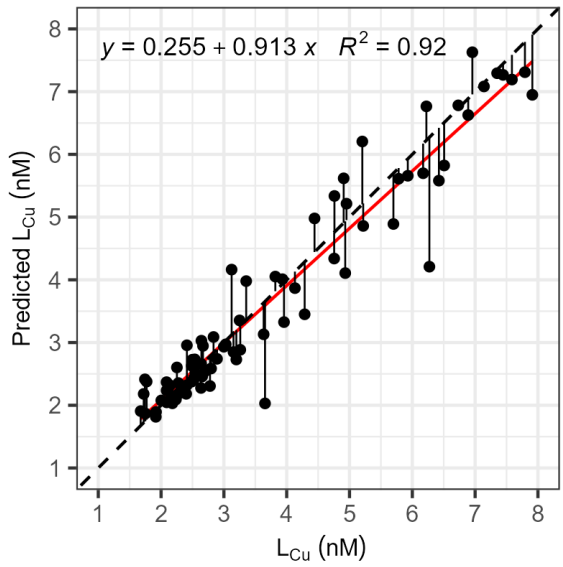

Figure 4.8. Relationship between the concentrations, in nM, of copper-binding ligands measured in seawater (L_{Cu}) and predicted (Predicted L_{Cu}) with equation 4.5. Predicted concentrations were calculated considering temperature, silicate and nitrate concentrations measured during the cruise. The black dashed line represents the 1:1 relationship between the two parameters and deviations from the perfect fitting were indicated by solid black line. The linear relation between the two parameters was indicated by the red solid line (R^2=0.94, p-value < $2.2e^{-16}$).

To provide an idea of how, on the basis of the model, L_{Cu} would be distributed in the Central Arctic, macronutrient and salinity surface data (≤ 200 m) from four cruises between 1995 and 2015 (PANGAEA database) were considered, including the study at hand (Wisotzki and Bakker, 2008; Kattner, 2011; Bakker, 2014). To ensure consistency among the samples collected during various oceanographic cruises, i.e. to confirm that the variables used were affected by the same processes, the dispersion of salinity with that of temperature and nutrients was checked (Appendix Figure B.7). Furthermore, water masses different than the PSW were identified and removed. The data were collected under ice-coverage conditions and were used to calculate L_{Cu}

concentrations. The predicted surface concentration of L_{Cu} ranged between 1.12 and 7.76 nM. High predicted concentrations (between 6 and 7 nM) resulted in all cruises that covered the shelf area, while in the central Arctic L_{Cu} up to 7 nM were observed only in 2015.

4.4 Discussion

4.4.1 Surface water distribution of Cu-binding ligands

During the PS94 cruise, the distribution of L_{Cu} in the Amundsen and Makarov Basins was found to differ significantly between surface and deep waters. This study found that the TPD was a substantial source of L_{Cu} for the central Arctic surface waters (Tables 4.1 and 4.2). Overall, the surface L_{Cu} concentrations were higher than the average concentration for open ocean surface waters (~1 nM, Ruacho et al., 2022).

In the Barents Sea and Nansen Basin, the surface L_{Cu} concentrations (0.8 – 5 nM) were within the range observed in the surface North Atlantic waters (2 – 2.5 µM of SA, Jacquot and Moffett, 2015; Gourain, 2020). The Barents Sea presented relatively low salinities and temperatures (Appendix Figure B.2), which indicate a freshwater input from precipitation, coastal runoff, and sea-ice melt (Rudels, 2012). This input of freshwater may increased the AW L_{Cu} concentrations and, at the same time, act as a source of trace metals, such as dCu, dCo, dMn and dNi (Gerringa et al., 2021a). The input of L_{Cu} trough coastal freshwater explains the relatively higher content of L_{Cu} observed at Stations 4 and 173 (Figure 4.3 and 4.5a). The shelf sediments also act as a source of trace metals, while the primary production and the scavenging are the main removal mechanisms (Gerringa et al., 2021a), which may also

impact the L_{Cu} concentrations. Strong similarities were observed with the AW of the eastern Fram Strait (mean L_{Cu}=1.99 ± 0.34 nM, Arnone et al., 2023). Both regions could have a similar contribution of freshwater from the Svalbard coasts that modify the surface water characteristics. In terms of conditional stability constants, strong Cu-binding ligands were measured (log K^{cond}_{Cu2+L} >13), or L_1 class (Bruland et al., 2000; Buck and Bruland, 2005). The Barents Sea log K^{cond}_{Cu2+L} (mean: 15.17 ± 0.47) was more similar to the eastern Fram Strait (mean log K^{cond}_{Cu2+L}=15.60 ± 0.26, Arnone et al., 2023) than the North Atlantic Ocean (range log K^{cond}_{Cu2+L}=12 – 14.5, Jacquot and Moffett, 2015; Gourain, 2020). The similarities between the Barents Sea and the eastern Fram Strait indicate a common source of ligands, possibly originating from the shelf or phytoplankton exudates. Furthermore, the applied detection window was the same in both regions, facilitating comparison and contributing to the observed similarities.

In the Nansen Basin, L_{Cu} concentrations were similar to those of the Barents Sea and the relatively lower log K^{cond}_{Cu2+L} was possibly resulted from the influence of PSW. The maximum surface L_{Cu} concentrations observed in the PSW of Amundsen and Makarov Basins (6 – 7 nM) were higher than the maximum surface concentration (<5 nM) reported for strong ligands in the North Atlantic and North Pacific Oceans (Jacquot and Moffett, 2015; Whitby et al., 2018; Gourain, 2020; Wong et al., 2021). However, a similar surface maximum was reported for PSW in coastal and shelf Greenland waters (L_{Cu} = 7 – 8 nM, Arnone et al., 2023). High surface L_{Cu} concentrations (up to 33 nM) exist in estuarine environments where greater concentrations, were observed in fresher waters (Laglera and van den Berg, 2003; Muller and Batchelli, 2013). The surface waters log K^{cond}_{Cu2+L} detected in the Amundsen and Makarov Basins (range: 13.83 – 15.34) were higher than in the North

Table 4.3. Statistical analysis. Significant differences in surface waters (≤ 200 m) were determined with a Kruskal-Wallis analysis and a Conover test. The analysis was carried out to determine differences between (a) basins and (b) samples inside and outside the TPD path. The TPD was defined following Slagter et al. (2017). P-values lower than 0.05 indicate significant differences (highlighted in bold).

(a)

Parameter	Kruskal-Wallis test			Conover's test (p-value)					
	$\chi 2$	df	p-value	Nansen-Barents	Amundsen-Barents	Makarov-Barents	Amundsen-Nansen	Makarov-Nansen	Makarov-Amundsen
Temperature (°C)	44.790	3	**1.03E-09**	**6.02E-09**	**4.92E-12**	**4.56E-07**	0.841	0.841	0.396
Salinity	33.980	3	**2.00E-07**	0.09	**1.16E-06**	**5.46E-07**	**0.002**	**0.001**	0.278
Fluorescence (au)	3.388	3	0.336	0.481	1	1	1	1	1
O_2 (µM)	13.218	3	**0.004**	**0.004**	**0.008**	**0.041**	1	1	1
NO^{-}_{3} (µM)	4.676	3	0.197	1	0.517	0.892	0.517	0.892	1
PO^{3-}_{4} (µM)	19.314	3	**2.35E-04**	1	0.997	**0.012**	0.997	**2.78E-04**	**1.88E-04**
$Si(OH)_4$ (µM)	56.128	3	**3.94E-12**	0.436	**7.25E-06**	**2.25E-11**	**2.3E-08**	**4.19E-14**	**2.01E-04**
dCu (nM)	66.653	3	**2.22E-14**	0.104	**2.72E-10**	**2.68E-10**	**8.72E-16**	**4.71E-15**	0.234
L_{Cu} (nM)	63.252	3	**1.19E-13**	**0.073**	**3.69E-09**	**6.64E-09**	**4.67E-15**	**1.04E-13**	**0.395**
eL_{Cu} (nM)	3.069	3	0.381	0.714	1	1	0.697	1	1
Cu' (pM)	28.776	3	**2.50E-06**	**0.014**	**8.71E-06**	**1.17E-06**	0.153	**0.02**	0.177
Cu^{2+} (pM)	28.776	3	**2.50E-06**	**0.014**	**8.71E-06**	**1.17E-06**	0.153	**0.02**	0.177
$\log K^{cond}_{Cu2+L}$	24.294	3	**2.17E-05**	**0.003**	**1.51E-04**	**6.66E-06**	0.594	0.18	0.229
$\log f_{Cu2+L}$	20.817	3	**1.15E-04**	**2.43E-05**	0.0501	**0.015**	**0.015**	0.218	0.287

(b)

Parameter	Kruskal-Wallis test			Conover's test (p-value)
	$\chi 2$	df	p-value	Inside-Outside TPD
Temperature (°C)	5.778	1	**0.0162**	**0.0153**
Salinity	51.573	1	**6.90E-13**	**<2e-16**
Fluorescence (au)	15.566	1	**0.0001**	**3.10E-05**
O_2 (µmol/l)	17.008	1	**3.72E-05**	**1.11E-05**
NO^{-}_{3} (µmol/l)	34.702	1	**3.84E-09**	**2.13E-11**
PO^{3-}_{4} (µmol/l)	0.159	1	0.6903	0.6929
$Si(OH)_4$ (µmol/l)	40.002	1	**2.54E-10**	**1.38E-13**
dCu (nM)	54.441	1	**1.60E-13**	**<2e-16**
L_{Cu} (nM)	55.171	1	**1.11E-13**	**<2e-16**
eL_{Cu} (nM)	2.805	1	0.0942	0.0942
Cu' (pM)	15.218	1	**0.0001**	**4.70E-05**
Cu^{2+} (pM)	15.218	1	**0.0001**	**4.70E-05**
$\log K^{cond}_{Cu2+L}$	9.087	1	**0.0026**	**0.0021**
$\log f_{Cu2+L}$	3.9598	1	**0.0466**	**0.0459**

Atlantic Ocean (range: 12 – 14.5, Jacquot and Moffett, 2015; Gourain, 2020) and generally lower than in the Centre and Northeast Pacific (range: 15 and 16.5, Whitby et al., 2018; Wong et al., 2021). More similar values were reported for the PSW in the coastal and shelf Greenland (range: 14.45 and 15.72, Arnone et al., 2023).

In the Makarov Basin, Pacific waters were reported as a source of dCu that comes from the Bering shelf sediments (Jensen et al., 2022). Furthermore, Pacific waters also act as a minor source of marine CDOM to the Arctic Ocean (Guéguen et al., 2007; Anderson and Amon, 2015). Then, the maximum concentrations of L_{Cu} and dCu reported in the Makarov Basin can be due to a contribution from Pacific waters. The input of DOM through Pacific water was reported in the Canadian Arctic Archipelago and Baffing Bay. In this

area, a maximum surface concentration of L_{Cu} around 4 nM was observed and was associated with a coastal and a biological source (Nixon et al., 2019). However, the class of these ligands is unknown as the technique applied by Nixon et al. (2019) is chromatographic and does not report the binding strengths.

The maximum concentration of Cu^{2+} (up to 0.42 pM) was observed in surface water, which was higher than those observed in Fram Strait and Greenland shelf (0.003 – 12.45 fM, Arnone et al., 2023) and comparable to the reported in the North Atlantic Ocean (0.02 – 0.74 pM, Gourain, 2020). These maximum concentrations remained below the toxicity limit of 10 pM established for cyanobacteria, coccolithophores, and diatoms (Sunda and Lewis, 1978; Brand et al., 1986). Concentrations of Cu^{2+} below 0.016 pM may not support the growth and reproduction rates of phytoplankton (Annett et al., 2008). However, complexed Cu can also be assimilated (Semeniuk et al., 2015). The phytoplankton growth limitation of Cu^{2+} can become more significant in regions with Fe-limitation, such as the Nansen Basin (Rijkenberg et al., 2018), due to the higher Cu-demand of phytoplankton (Annett et al., 2008). The biological utilization of free and complexed Cu can also explain why the maximum concentrations in AW were lower than in PSW, as the phytoplankton growth in the Atlantic Ocean was higher than in the Arctic ice-covered zone (Vernet et al., 2019).

4.4.2 The role of the TPD in the L_{Cu} distribution

The L_{Cu} distribution is related to the TPD flow path, whose core was above the Amundsen and Makarov Basins (Slagter et al., 2017). The TPD played a crucial role in the lateral transport of riverine and shelf-derived material

within the Arctic Ocean and influenced water chemistry (Figure 4.4 and 4.5). In surface waters, the concentrations of L_{Cu} inside the TPD (mean: 5.87 ± 1.22 nM) were higher than that outside the TPD (mean: 2.56 ± 0.56 nM), and these, in turn, was higher than the ones recorded in deep waters (mean: 1.85 ± 0.25 nM). This indicates that the TPD transports high concentrations of L_{Cu} to the central Arctic, particularly in the first 55 – 80 m depth. However, there is a vertical extension of the TPD effect that impacts up to 200 m depth (Figure 4.5a). The TPD also transport high concentrations of trace metals (dCu, dFe, dNi, dCo, dZn and dMn), silicate, phosphate, CDOM and Fe-binding ligands (Slagter et al., 2017; Rijkenberg et al., 2018; Charette et al., 2020; Gerringa et al., 2021a). The absence of L_{Cu} differences between samples upstream and downstream of the TPD could be related to the high stability and the limited removal and modification processes. The sea-ice coverage, the relatively low biological activity and the low temperatures may contribute to the longer stability of the L_{Cu} ligands which facilitate their export towards the Fram Strait and Nordic Seas.

The salinity and nutrient content of the water masses (Figure 4.6) were used to clarify possible sources of L_{Cu}. As mentioned, the TPD water come from the Siberian Shelves and may receive L_{Cu} from rivers, coastal processes and ice-melting. The riverine source of L_{Cu} in the PSW and the TPD is confirmed by the significant negative relationship with salinity. This relationship indicates a conservative mixing behaviour, which was generally observed in estuarine environment (Laglera and van den Berg, 2003; Shank et al., 2004; Hollister et al., 2021). Siberian rivers introduce large amounts of silicates into the shelf waters, which explains the positive relationship established between L_{Cu} and silicate concentrations. However, the waters of the Siberian Shelf are characterized by low nitrate concentrations due to high

biological activity and lower nitrate input from rivers during summer (Kattner et al., 1999). The contribution of Siberian rivers to the water chemistry in the central Arctic was found to vary between stations and depths (Paffrath et al., 2021), potentially accounting for the observed differences in metal and ligands concentrations. At stations 81, 96, 117, and 125 a significant influence from the Lena River was observed within the first 30 meters of depth, followed by the detection of influences from the Yenisei and/or Ob Rivers below this depth (Paffrath et al., 2021). The highest surface L_{Cu} (>6 nM) and dCu (>5.6 nM) concentrations observed in the Amundsen and Makarov Basins can be related to the Lena River influence. Compared to other polar environments, the L_{Cu} concentrations inside the TPD (3.96 – 7.91 nM) were higher than the values obtained on the Antarctic Peninsula (25 µM SA, Bundy et al., 2013). There, strong ligands showed maximum concentrations generally below 5 nM, except for ice (~16 nM) and algal sea ice (~26 nM) measurements.

The TPD also influence the Cu^{2+}, the concentration range inside was higher than outside the TPD (Table 4.2). The saturation state of L_{Cu} can explain this difference, inside the TPD the concentration of L_{Cu} was higher that outside but these were more saturated, which favours the higher concentration of Cu^{2+}.

Surface waters in the Central Arctic, with high levels of complexed Cu, can be transported to southern regions by TPD. Previous studies have demonstrated that the TPD transports trace metals (Chen et al., 2022; Krisch et al., 2022), terrigenous DOM (Benner et al., 2005), and Fe-binding ligands (Ardiningsih et al., 2020, 2021) to the Fram Strait and the Nordic Seas. The export of L_{Cu} and dCu to the Nordic Seas may explain the high L_{Cu}

concentrations measured in surface waters over the Greenland shelf (Arnone et al., 2023). The export is favoured by high L_{Cu} concentrations and ligand strength, and this process may be crucial in the southern areas of Greenland and the Irminger Basin where iron limitation exists (Hopwood et al., 2018). This is because certain organisms, such as diatoms, have higher Cu requirements in Fe-limited conditions (Maldonado et al., 2006). Then the L_{Cu} export could support the phytoplankton growth.

4.4.3 Cu-binding ligands in deep waters

Deep waters in the Amundsen and Makarov Basins seem isolated from the surface; L_{Cu} and dCu transport into the deep waters appears to be absent. This is confirmed by the significant differences between surface and deep dCu and L_{Cu} concentrations, and log *f* values and can be explained by the strong water stratification and deep scavenging. Similar behavior was observed in the Si cycle and was associated with a limited export of particles from surface waters (Liguori et al., 2020).

The L_{Cu} concentrations and properties in deep waters did not differ significantly in deep waters results from the hydrographic characteristics, including oceanic ridges and extensive continental shelves, which limit deep water renewal. In the central Arctic Ocean the exchange of deep water only occurs through the Fram Strait (Tomczak and Godfrey, 2001). For this reason, deep waters in the Eurasian and Canadian Basin present very long residence times (250 – 450 years, Schlosser et al., 1997), which significantly influence the properties of seawater. Prolonged residence times extend scavenging durations, which potentially decrease the concentrations of L_{Cu} and dCu in deep waters. Furthermore, deep waters presented lower complexation,

binding strength, and reactivity than surface waters, which favour scavenging and removal of dCu. At the same time, inputs from bottom sediments were limited. This may explain why deep waters did not present an increase in L_{Cu} and dCu concentrations with depth, as observed in other oceans (Ruacho et al., 2022). Scavenging could remove more dCu than L_{Cu}, as observed in the loss of linearity between the two parameters observed in the deep water (Figure 4.5b). Low concentrations of dFe, dMn, and Fe-binding ligands were observed in deep Arctic waters associated with long exposure to scavenging processes, together with limited deep sources The effect of prolonged deep scavenging in the central Arctic Ocean was described for dFe, Fe-binding ligands, and dMn (Middag et al., 2011; Thuróczy et al., 2011b; Klunder et al., 2012; Slagter et al., 2017; Rijkenberg et al., 2018; Gerringa et al., 2021a).

The deep water L_{Cu} concentrations (range: 1.45 – 2.78 nM, mean: 1.85±0.25 nM) were lower than the concentrations of up to 7 nM observed in other oceans deep waters (Ruacho et al., 2022). A good agreement was observed with the L_{Cu} reported in deep waters of the eastern Fram Strait (1.6 – 3.4 nM, Arnone et al., 2023) and the concentration range for the deep North Atlantic Ocean (Jacquot and Moffett, 2015). These authors measured concentrations of L_{Cu} in the deep Atlantic waters between 1 and 3 nM, with a local bottom maximum (~5 nM) associated with hydrothermal or bottom sediment sources. In the North Atlantic between 40 ºN and 60 ºN, the L_{Cu} concentrations mostly fall below 4 nM with a maximum of around 8 nM associated with bottom sources (Gourain, 2020). Along the Mid-Atlantic ridge concentrations below 5 nM were observed without hydrothermal sources (Gourain, 2020). The local deep maximum (around 1000 m) observed along the cruise track (Stations 32, 91, 96 and 125) can be related to sediment resuspension from the continental slope or ridges. These maxima were not

related to hydrothermal activity, which was observed at greater depths (3000 m) along the Gakkel Ridge (Rijkenberg et al., 2018). The concentration of strong L_{Cu} in deep subarctic Pacific waters was relatively low (3 nM, Coale and Bruland, 1990; Whitby et al., 2018; Wong et al., 2021). However, the entrance of deep Pacific waters through the Bering Strait is not expected.

4.4.4 Cu-binding ligand nature

The voltammetric method does not allows the identification of metal-binding ligands chemical structures, in turn ligands are classified based on log K^{cond}_{Cu2+L} values. Strong L_{Cu} (log K^{cond}_{Cu2+L} > 13, Buck and Bruland, 2005) were detected throughout the study region and can be attributed to various compounds including humics, thiols, methanobactins and exopolysaccharides (Ruacho et al., 2022, and references therein).

The log K^{cond}_{Cu2+L} values observed in the study area (range: 13.83 – 16.01, Table 4.1) were close to the range of terrestrial humic substances reported in estuaries (range: 14.9 – 15.9, Muller and Batchelli, 2013). Humics substances with riverine origin were detected in the central Arctic waters (Gao and Guéguen, 2018; Gamrani et al., 2023) and described as part of the Fe-binding ligands pool in the central Arctic and Fram Strait waters (Slagter et al., 2017, 2019; Rijkenberg et al., 2018; Laglera et al., 2019; Ardiningsih et al., 2020). Since humics can complex both Fe and Cu (Abualhaija et al., 2015), it is reasonable to propose that a fraction of the L_{Cu} pool in the study area comprises humic substances, as suggested for Fram Strait and Greenland shelf waters (Arnone et al., 2023). The presence of humic-like substances in the study area was reflected in the different CDOM absorbances (absorbances at 254 and 300 nm), particularly in surface waters in the Makarov and

Amundsen basins (Slagter et al., 2017). The positive relationship observed between L_{Cu} concentrations and absorbance parameters in surface waters (Figure 4.7) confirms the contribution of humic substances to the L_{Cu} pool. These organic compounds have a riverine origin (Stedmon et al., 2011), but can be also produced in situ as has been indicated for the case of Fe-binding ligands in the same region (Slagter et al., 2017) via microbial action, local DOM production, deposition by ice rafted sediments, etc. Thiols could also account for L_{Cu}, as they were identified in Arctic waters (Gao and Guéguen, 2018) and described as Cu-binding ligands in estuarine environments with log K^{cond}_{Cu2+L} values between 12 and 15 (Laglera and van den Berg, 2003; Whitby et al., 2017).

In the study region, a contribution of L_{Cu} from the biological activity may also occur. In Arctic surface waters, diatoms dominate the phytoplankton community (Uhlig et al., 2019), which can release Cu-binding ligands (Davis and Benner, 2005; Nixon et al., 2019; Williford et al., 2022). Cultures experiments revealed that diatoms produce weak L_{Cu} (log K^{cond}_{Cu2+L} = 8 – 12, Lorenzo et al., 2007, and references therein), and, in field measurements made in Arctic sea-ice, exopolymer substances (EPS) were identified as sea-ice diatoms L_{Cu} exudates (Krembs et al., 2002; Lin et al., 2020). EPS substances were suggested as Cu and Fe-binding ligands in the Greenland shelf (Ardiningsih et al., 2020; Arnone et al., 2023). However, these weak ligands were not observed along the cruise track. The algal sea-ice community can also release high concentrations (26.15 ± 3.88 nM) of strong L_{Cu} (log K^{cond}_{Cu2+L} =15.15 ± 0.25), as observed in the Antarctic Peninsula (Bundy et al., 2013). Bacteria were also suggested as L_{Cu} producers, in particular methanotrophic bacteria can produce strong binding strengths (log

K^{cond}_{Cu2+L}>14), which can be present below the sea-ice inside the TPD where high methane concentrations were observed (Damm et al., 2018).

As TPD acts as the main source of L_{Cu} in the central Arctic Ocean, the composition of the ligands should present riverine organic matter. Therefore, a large part of the L_{Cu} pool could be humic substances or thiols. During the transport from the Siberian shelves to the central Arctic processes the photodegradation and microbial degradation may transform L_{Cu} and decrease their log f_{Cu2+L} (Davis and Benner, 2005; Shank et al., 2006; Paulsen et al., 2019). The role of hydrography in L_{Cu} distributions can even be greater than that of biological and/or photochemical processes, as observed for CDOM (Anderson and Amon, 2015). A small contribution of L_{Cu} may come from Atlantic and Pacific waters. Cu-binding ligands in the North Atlantic Ocean were mainly related to biological production and hydrothermal inputs (Jacquot and Moffett, 2015; Gourain, 2020), while in the Pacific Ocean were associated with marine exudates, organic matter degradation and riverine inputs (Semeniuk et al., 2015; Whitby et al., 2018).

4.4.5 Modelling the Cu-binding ligands in the TPD area

The parameters included in the linear model correlate the water properties with their origin and enable the description of L_{Cu} concentrations in surface waters influenced by the TPD. The waters transported by the TPD comes mainly from the Siberian shelves and are characterized by low salinity, high silicate and low nitrate concentrations due to the influence of riverine discharge and biological uptake (Kattner et al., 1999).

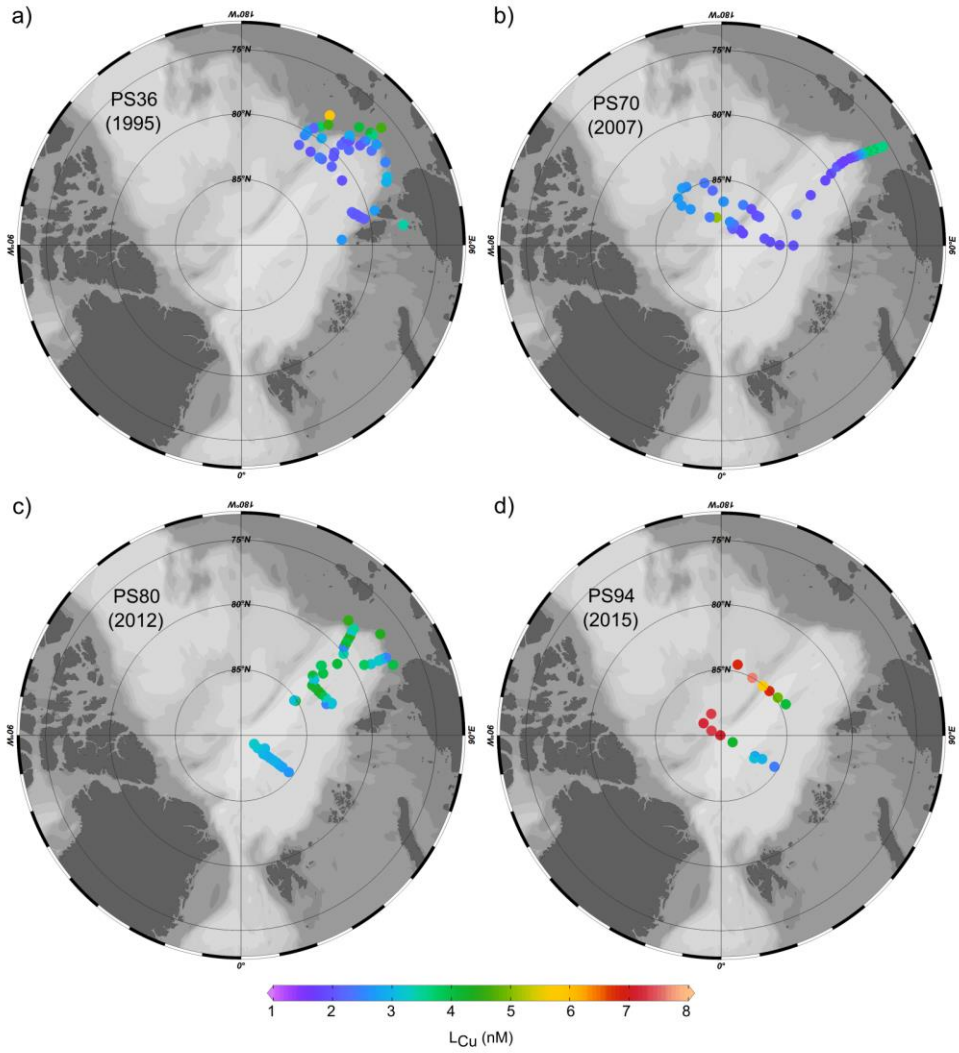

Figure 4.9. Surface distribution of L_{Cu} concentration in the Arctic Ocean estimated with equation 4.5 with data from PANGAEA. Data from three different cruises were compiled: a) PS36 (Kattner, 2011), b) PS70 (Wisotzki and Bakker, 2008), c) PS80 (Bakker, 2014) and d) PS94 (the current study). All of them were conducted between July and September onboard the RV Polarstern.

The predicted concentrations of L_{Cu} exhibited a strong correlation with the measured L_{Cu} values (Figure 4.8). Deviations from the 1:1 relationship

indicate the influence of other processes affecting the distribution of L_{Cu}, which were not accounted for in equation 4.5. These processes include biological production and utilization, microbial degradation, ice sequestrations and release of organic matter, among others. While more complex models would provide a more accurate description of the study area, they could compromise overall generality and applicability, especially in the Arctic Ocean, where multiple sources significantly contribute to each basin or water mass. It must be noted that the model was developed with data collected under the ice coverage and affected by the TPD, resulting in certain consequences. At first, the presence of sea-ice can modify the salinity and influence the biological activity, impacting nitrate and silicate concentrations. Secondly, as in the TPD the majority of ligands come from coastal regions, making this model is not suitable for areas where *in-situ* ligand production is prevalent. Therefore, it is important to proceed carefully when applying the model in ice-free waters or with bloom conditions, as this could lead to errors in estimating ligand concentrations.

The predicted L_{Cu} concentrations (Figure 4.9) were consistent with the previous organic matter studies conducted in the central Arctic Ocean. The shelves contain high organic matter concentrations due to the influence of riverine inputs (Opsahl et al., 1999; Anderson and Amon, 2015), which can explain the high L_{Cu} concentrations (between 6 and 7 nM). While the high L_{Cu} concentrations in the central Arctic (up to 7 nM) were associated with the transport through the TPD (Gordienko and Laktionov, 1969). The variability in L_{Cu} concentrations between 1995 and 2015 can be attributed to natural alterations in water characteristics linked to years with varying river discharges and TPD velocities. Conversely, it may be due to amplified river discharges (Peterson et al., 2002; Schuur et al., 2013, 2015; Feng et al., 2021)

and TPD velocities (Krumpen et al., 2019) linked to climate change, resulting in higher ligand inputs that are then transported to the central Arctic Ocean by the TPD.

The proposed equation provides an estimate of the Cu-binding ligands present in surface water and could offers insight into their temporal evolution of ligands transported by the TPD, if the model is applied to historical data from the Central Arctic surface water. However, the equation require validation and different L_{Cu} concentrations measured in the TPD are necessary. Furthermore, this model could be improved by incorporating other seawater variables (such as pH) and biological activity (such as chlorophyll concentration), which require good data resolution and coverage. Finally, data and parameters associated with rivers, estuaries and continental shelves should be incorporated and validated to extrapolate the model to other Arctic areas.

4.4.6 Future scenarios related to Cu-binding ligands

The effect of climate change on the Arctic Ocean (IPCC, 2022) and the global trace metal biogeochemistry have been reported (Hoffmann et al., 2012). However, little is known about the effect on Cu speciation in the Arctic environment. In seawater, the pH and temperature affect trace metal speciation, altering the solubility, the adsorption onto particles and the reaction rates (Hoffmann et al., 2012). Changes in seawater pH, associated with higher CO_2 concentrations, decrease the organic Cu complexation and favours the inorganic species, with an increase in Cu^{2+} (Millero et al., 2009; Gledhill et al., 2015). The results indicate that the toxicity limit established for different phytoplankton species was not reached (Sunda and Lewis, 1978;

Brand et al., 1986). However, according to the projected changes in pH and the assumed effect on Cu^{2+} availability (Stockdale et al., 2016; Fransner et al., 2022), in the Arctic waters more Cu^{2+} will be bioavailable and the toxicity limits are not expected to be exceeded as the concentration of L_{Cu} will also increase.

The temperature increase leads to permafrost thawing (Schuur et al., 2013, 2015) and strengthening riverine discharge (Peterson et al., 2002; Feng et al., 2021). Higher inputs of riverine freshwater, trace metals, organic matter, and strong binding ligands will arrive at surface Arctic waters (Guieu et al., 1996; Frey and McClelland, 2009; Stedmon et al., 2011; Slagter et al., 2017; Laglera et al., 2019; Charette et al., 2020). Therefore, more dCu and L_{Cu} could be released. Simultaneously, sea-ice thickness and coverage will decrease due to increased temperature and AW contributions in the Arctic Ocean (Belter et al., 2021). As a result, at first, higher solar irradiance produces photo-oxidation processes (Bélanger et al., 2006) which could degrade ligands, decrease their complexing capacity and increase the Cu^{2+} concentrations (Shank et al., 2006). The effects of Cu bioavailability and assimilation can be the opposite. Increasing Cu^{2+} concentrations may either improve its acquisition or cause toxicity, while a reduction in complexing capacity could negatively impact organisms that obtain Cu from strong complexes (Semeniuk et al., 2015). Secondly, the enhanced light penetration could lead to longer growing seasons and a higher primary production (Arrigo et al., 2008), which can alter the amount of L_{Cu} and dCu in surface waters (due to assimilation or release). Changes in phytoplankton community composition could also alter the nature of the ligands excreted.

As reported by Krumpen et al. (2019) and the references therein, the ice dynamic in the Arctic has already changed. Less sea-ice is formed in the Siberian shelves, the ice coverage is getting thinner, the TPD speed increases, and more melting occurs in marginal areas and the central Arctic. At the same time, there is less export of ice to the Fram Strait and much of ice-rafted materials are lost during the transport, which could affect the transport of dCu and L_{Cu}. The melting leads to an accumulation of material (e.g., sediments, organic matter and contaminants) in the central Arctic. Finally, decreased sea-ice thickness facilitates the proliferation of phytoplankton beneath, because sediment loading decreases and light availability increases, with potential impact on dCu and L_{Cu}.

Due to the presence of opposite mechanisms capable of increasing or decreasing Cu-binding ligands, a comprehensive exploration of the distribution and characteristics of these compounds in the Arctic Ocean becomes imperative to understand the impact of climate change on Cu-organic speciation. Moreover, as it remains unclear which of these mechanisms will dominate in the future, the magnitude of these processes must be meticulously evaluated in future modelling.

4.5 Conclusions

In the Arctic Ocean, the Cu-organic speciation is clearly influenced by the hydrography. A strong vertical and longitudinal variability of L_{Cu} and log K^{cond}_{Cu2+L} was observed in surface waters (≤ 200 m), with maximum concentrations in the first few metres of depth and toward the central Arctic Ocean. Surface waters differ significantly from deep waters, and maximum L_{Cu} concentrations were constrained into the PSW. This water mass is

transported from the Siberian shelves to the central Arctic by the TPD and receives large inputs of terrestrial riverine organic matter and trace metals. The TPD act as the main source of L_{Cu} in the Amundsen and Makarov Basins and determines its distribution in the Arctic Ocean.

In the Amundsen and Makarov Basins, deep Arctic waters appear to be isolated from the surface, as much lower concentrations were observed than at the surface. This phenomenon can be attributed to the pronounced stratification of surface waters, constraining vertical mixing, and the scavenging processes within deep waters.

Strong Cu-binding ligands, L_1 class, were detected in the Arctic Ocean, mainly associated with terrestrial organic matter released from Siberian rivers. Terrestrial humic substances and thiols were suggested as the main component of the L_{Cu} pool detected; however, the nature of the ligands cannot be determined with voltammetric techniques. A small input of ligands by phytoplankton and bacterial production was also suggested inside and outside the TPD path. The high concentrations of these strong ligands maintain Cu^{2+} concentrations at pM levels, not exceeding toxicity levels but may produce a Cu deficit in organisms with higher requirements or under Fe-limiting conditions.

TPD plays a key role in organic Cu speciation in the Arctic Ocean. The presence of strong complexes facilitates the transport of Cu towards the Fram Strait and the North Atlantic Ocean, potentially supporting primary production in surface waters with limited bioavailable Cu. However, the effect of climate change on Cu speciation in the Arctic is complex. To understand future scenarios, more research is needed on the biogeochemical

cycle of Cu in the region. This study presents the baseline for future Cu organic complexation studies in the Arctic Ocean.

Acknowledgements

The authors would like to thank the captain Schwarze and the crew of the RV Polarstern on expedition PS94, the chief scientist Ursula Schauer and all other cruise participants.

Funding

We also acknowledge the financial support for the ATOPFe project (CTM2017-83476-P) from the Ministerio de Ciencia e Innovación (Spain). VA participation was funded by the PhD grant (PRE 2018-084476). The analysis of samples was supported by ISblue project, Interdisciplinary graduate school for the blue planet (ANR-17-EURE-0015) and co-funded by a grant from the French government under the program "Investissements d'Avenir" embedded in France 2030. Our participation in this GEOTRACES expedition was funded by Netherlands Organization for Scientific Research (NOW) under contract number 822.01.018 to L. J. A. Gerringa.

Image: ESA/ Copernicus Sentinel-2 data (2021).

Chapter 5. Conclusions

This dissertation presents significant findings on the organic complexation of Fe and Cu in different oceanic and coastal environments that have received limited research attention regarding trace metal organic speciation.

Firstly, in the Chapter 2 we analysed the potential impact of Macaronesia's oceanic islands on Fe and Cu complexation in surface waters. The key results are as follows:

- Coastal areas around oceanic islands in the Macaronesia archipelago (Cape Verde, Canary Islands and Madeira) present higher surface concentrations of dFe and dCu, as well as their corresponding metal-binding ligands, than the surrounding oceanic waters. This revealed that the coastal island regions could act as a source of this elements to the open ocean.
- The hydrodynamic characteristics in the study area influence the distribution of dFe and dCu, as well as their organic speciation. The biological activity and the sediment resuspension were suggested has the main source mechanisms, associated with the incidence of wind and currents.
- The voltametric analysis revelated the dominance of strong binding ligands, which control the speciation of both dFe and dCu, as well as the toxicity of Cu^{2+}.
- The distribution of Cu-binding ligands was related to the concentration of nitrate and nitrite, the fluorescence and the water turbidity with the development of linear equation.

The Chapter 3 focused on the organic complexation of Cu in coastal and oceanic waters in the Fram Strait and Greenland shelf region. This area is of biogeochemical significance due to its links between the Arctic Ocean and North Atlantic Ocean, as well as the interaction between coastal and oceanic dynamics and the environmental variability resulting from climate change. The key findings of this study are:

- The Cu-binding ligand concentration present a longitudinal trend, with increasing values from open ocean Fram Strait area to the Greenland coast. It suggested a source of ligands from the glacier terminus and the process that occurred in coastal waters.

- The conditional stability constant of ligands indicated the presence of strong ligands with keeps the Cu^{2+} concentration below the toxicity limits. The constants presented decreasing values from open ocean Fram Strait area to the Greenland coast, associated with the organic matter degradation and/or bacterial remineralization, and the coastal meltwater discharge.

- The vertical profile of Cu-binding ligands above the Greenland shelf differs from the distribution observed in other coastal and shelf areas not affected by river discharge, and from the open ocean waters, including the Fram Strait. Maximum surface concentrations were confined to the Polar Surface Waters, suggesting a combination of coastal inputs together with an export of ligands from the central Arctic Ocean by the Transpolar Drift.

- The high concentration of complexed dCu with strong binding ligands in Polar Surface Waters above the Greenland shelf enable

the transport of dCu toward southern regions of the Nordic Seas and North Atlantic Ocean. A phenomenon which supports phytoplankton growth in regions with Fe limiting conditions.

Finally, the Chapter 4 describes the organic complexation of Cu in the central Arctic Ocean and the Barents Sea, an area that has not been previously investigated. It was found that:

- The Makarov and Amundsen basins showed surface concentrations of Cu-binding ligands higher than those observed in the Barents Sea and other open ocean regions. The maximum was constrained in the Polar Surface Waters and associated with the transport of waters from the Siberian shelves by the Transpolar Drift.
- The strong stratification of the waters and the limited mixing prevent the transport of Cu-binding ligands from the surface to the deep ocean and enable the export of ligands toward the Fram Strait by the Transpolar Drift.
- Strong binding ligands were detected in surface water and associated with terrestrial organic matter and humic substances released by rivers. However, a portion of the ligand pool could have received contributions from sea-ice plankton production and bacterial degradation. The presence of this strong binding ligands maintains Cu^{2+} at non-toxic concentration.
- A relationship between Cu-binding ligands concentrations, silicate and nitrate concentration, together with the salinity was defined for the Polar Surface Waters in the Amundsen and Makarov basins. he

linear equation enables the quantification of Cu-binding ligands in surface water of the central Arctic Ocean.

Image: ESA/Envisat (2008-2009).

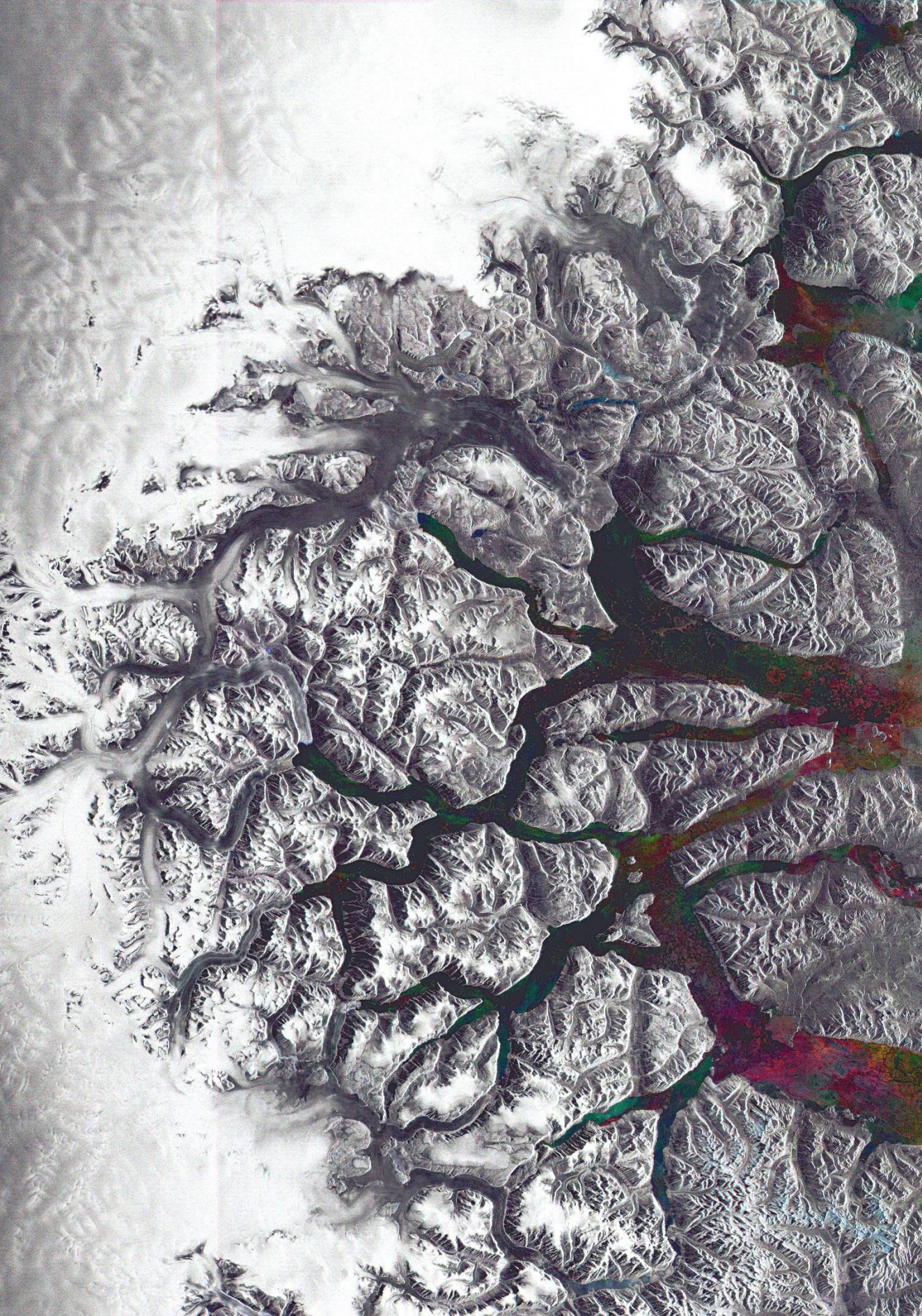

Chapter 6. Future Research

The findings presented in this PhD Thesis represent an initial investigation into the complexation of Fe and Cu in various marine environments that have been poorly studied to date. Nevertheless, numerous unanswered questions need to be addressed in future research to better understand the biogeochemical cycling of Fe and Cu in the ocean, especially in sensitive and vulnerable areas due to climate change.

The methodology employed in this PhD Thesis does not enable us to determine the composition of the observed ligand pool. It is of interest to incorporate additional methodologies capable of identifying and isolating different groups of organic compounds within the ligand pool. This can be achieved by techniques able to measure individual compounds or through the interaction of Fe and Cu with individual ligands.

The Macaronesia study highlighted the importance of water mixing processes in the resuspension of ligands and metals, based on surface data. To establish and explore the potential sources of these substances, a comprehensive study of the entire water column across different islands and watersheds must be conducted in order to better understand the "island" effect on Fe and Cu metal chemistry. Furthermore, incorporating additional oceanic stations in the study can further facilitate comparisons.

This Thesis presents novel findings on the dispersion of Cu ligands in the Central Arctic and Fram Strait. The significance of the Transpolar Drift in transferring complexed Cu in both the Arctic Basin and to the North Seas has been established. Ligands detected in the Central Arctic have been linked to the coastal origins of Siberian rivers. Nonetheless, information regarding the

behaviour and distribution of ligands in this region is unknown. To achieve a more comprehensive understanding of the behaviour of ligands in the region, it is essential to conduct further studies on Cu compounds in the Siberian shelf, coastal zones, and estuaries.

The impact of climate change on the organic speciation of dFe and dCu in the marine environment is not entirely clear, as discussed in Chapters 3 and 4. Further assessment is required to understand the evolution of these chemical species and their potential impact on phytoplankton development. It is necessary to evaluate the distribution of trace metals and their ligands to gain a better understanding. Studies could be conducted to evaluate the intra- and inter-annual variability of these parameters. These findings could then be applied to enhance the predictive capability of models. In addition, experimental research in needed in order to measure the change of different Fe and Cu-binding ligands at conditions that simulate the climate change scenarios for the next century.

Image: ESA/Envisat MERIS (2011).

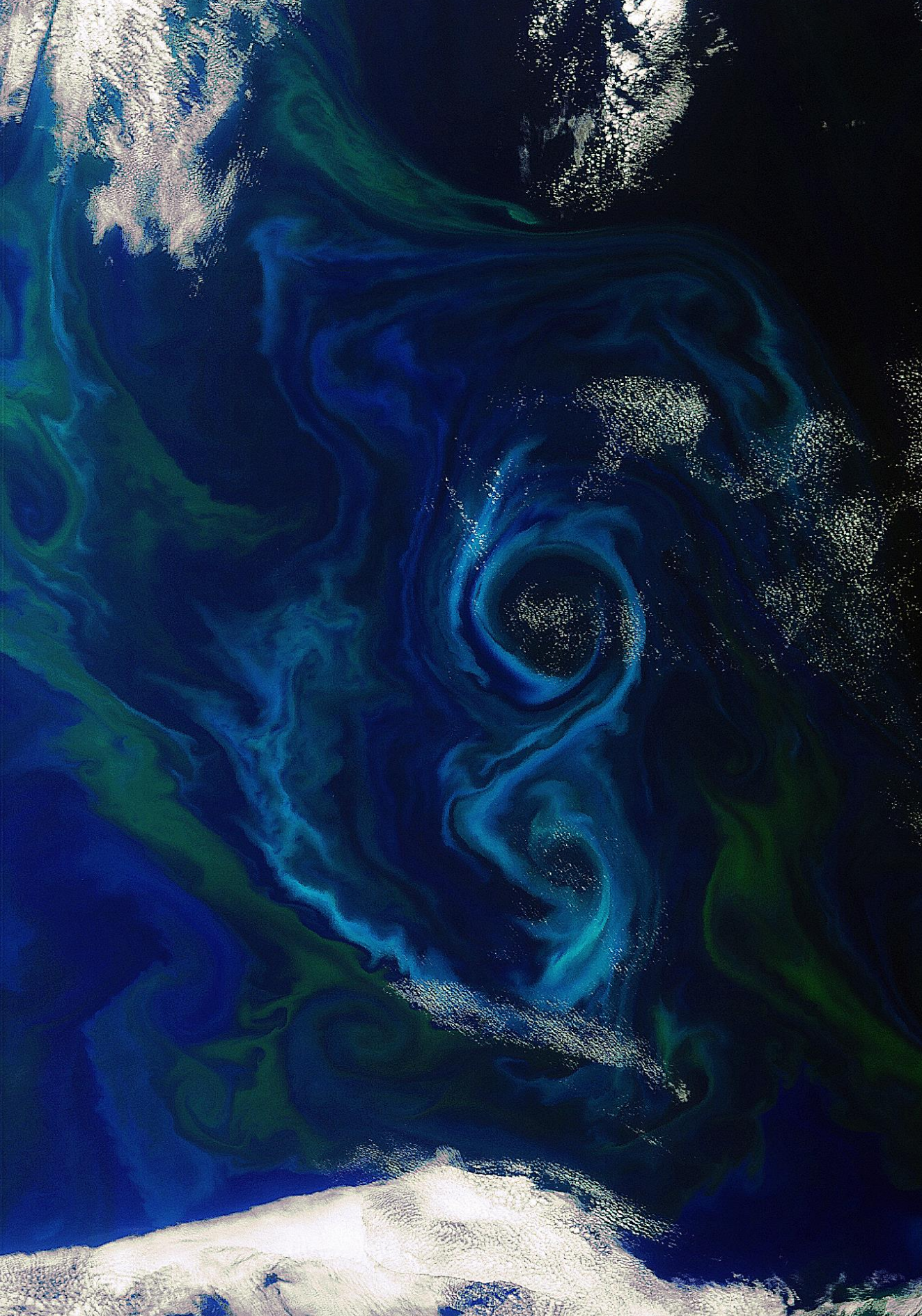

Chapter 7. Resumen en castellano

7.1 Introducción

Metales traza en el océano

El océano absorbe cerca del 26% del dióxido de carbono (CO_2) emitido por la actividad humana y desempeña un papel fundamental en la regulación de las concentraciones atmosféricas de este gas (Friedlingstein et al., 2023). Una parte significativa de esta asimilación y secuestro de carbono la realiza el fitoplancton marino y para ello requiere múltiples nutrientes, incluyendo numerosos metales traza. La biodisponibilidad en el agua de mar de metales traza como el hierro (Fe) y el cobre (Cu) afecta a la productividad del océano, ya que las especies disueltas de estos metales (dFe y dCu) son esenciales para el desarrollo del fitoplancton (Sunda, 1989; Morel and Price, 2003; Morel et al., 2008; Boyd and Ellwood, 2010; Bruland et al., 2014; Tagliabue et al., 2017).

El dFe y el dCu en el océano se encuentran en concentraciones subnanomolares, siendo en el caso del dFe debido a su baja solubilidad en aguas óxicas (Liu and Millero, 2002). El dFe es esencial para la realización de la fotosíntesis, la respiración y los procesos de fijación de nitrato (Hutchins and Bruland, 1998; Boyd et al., 2007), mientras que el dCu es necesario además para la asimilación de Fe y la desnitrificación (Twining and Baines, 2013). Hoy en día, el dFe está ampliamente reconocido como factor limitante de la producción primaria en el océano abierto y en las regiones de afloramiento (Martin and Fitzwater, 1988; Hutchins and Bruland, 1998; Boyd et al., 2000; de Baar et al., 2005). Por otro lado, las altas concentraciones de dCu pueden ser tóxicas y limitar o inhibir el crecimiento del fitoplancton,

aunque su tolerancia varía entre especies (Morel et al., 1978; Sunda and Lewis, 1978; Brand et al., 1986).

Especiación del hierro y el cobre en agua de mar

El Fe y el Cu en el agua de mar se encuentran en diferentes estado físicos y químicos, que se ven afectados por la temperatura, el pH, la salinidad, la concentración de oxígeno y la complejación con compuestos orgánicos (Millero, 2013).

En cuanto a la **especiación física** de un metal traza (M), se considera que la concentración total del metal traza (M_{total}) incluye metales particulados (pM, partículas recogidas en filtros de 0.45 µm o 0.2 µm de tamaño de poro) y disueltos (dM, partículas menores a 0.2 µm). Estos últimos se dividen en la fracción coloidal (cM, tamaños de partículas entre 0.02 y 0.2 µm) y soluble (sM, partículas menores a 0.02 µm).

$$M_{total} = pM + dM = pM + cM + sM \quad (7.1)$$

La fracción disuelta de los metales traza (<0.2 µm, Cutter et al., 2017) puede ser asimilada por el fitoplancton marino y su concentración en el agua de mar varía con el pH, la formación de complejos con la materia orgánica, la concentración de oxígeno disuelto, la salinidad y la formación de precipitados de hidróxidos (Millero et al., 1995; Millero, 2013).

Según la **especiación química**, los metales traza pueden clasificarse en especies orgánicas e inorgánicas y se ve afectada por el pH, el potencial redox, la fuerza iónica y la presencia de compuestos orgánicos, entre otros. De acuerdo con Gledhill and Buck (2012), los metales traza pueden clasificarse

en complejos lábiles inorgánicos (M', incluyendo el metal libre), complejos con ligandos orgánicos (ML) y metales no lábiles (M_{inert}).

$$M_{total} = M' + ML + M_{inert} \quad (7.2)$$

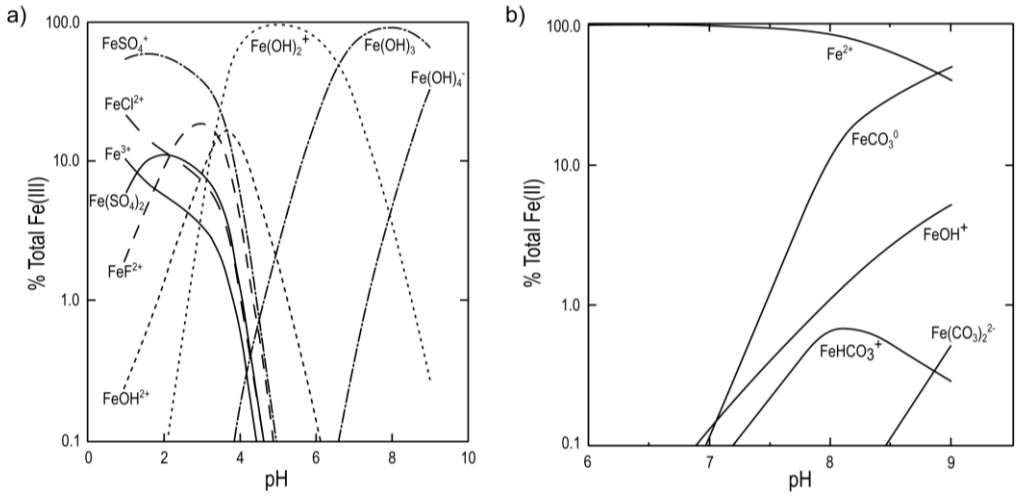

Figura 7.1. Especiación en el agua de mar de a) Fe(III) y b) Fe(II), determinada a T=25ºC y S=35. Figuras tomadas de Millero et al. (1995).

Sobre el estado redox de los metales, el Fe existe en el agua de mar como Fe(II) y Fe(III). El Fe(III) es la forma dominante y termodinámicamente estable del Fe en agua de mar, ya que en aguas óxicas el Fe(II) se oxida rápidamente (Kuma et al., 1996; Millero, 1998). La velocidad de esta oxidación depende de las propiedades físico-químicas del agua (Figura 7.1, Millero et al., 1987; González-Dávila et al., 2005; Santana-Casiano et al., 2005; González-Dávila et al., 2006; González et al., 2010a; Samperio-Ramos et al., 2018a, 2018b). No obstante, en el agua de mar se pueden detectar bajas concentraciones de Fe(II) debido a los procesos *in situ* de reducción de Fe(III) (Sarthou et al., 2011; González-Santana et al., 2023), la interacción con los ligandos (Santana-Casiano et al., 2000, 2010, 2014; Rose and Waite, 2003;

Samperio-Ramos et al., 2018a, 2018b; González et al., 2019; Arreguin et al., 2021) y las reacciones fotoquímicas (Waite and Morel, 1984; Miller et al., 1995). El Fe(III) tiende a precipitar y sufrir *scavenging*, pero la presencia de ligandos orgánicos en el agua mantiene el Fe en disolución por más tiempo (Millero et al., 1995; González et al., 2019; Arreguin et al., 2021). De hecho, más del 99% del dFe forma complejos con ligandos orgánicos (Gledhill and van den Berg, 1994), lo que puede acelerar, retrasar o no afectar a la oxidación del Fe(II) (Santana-Casiano et al., 2000).

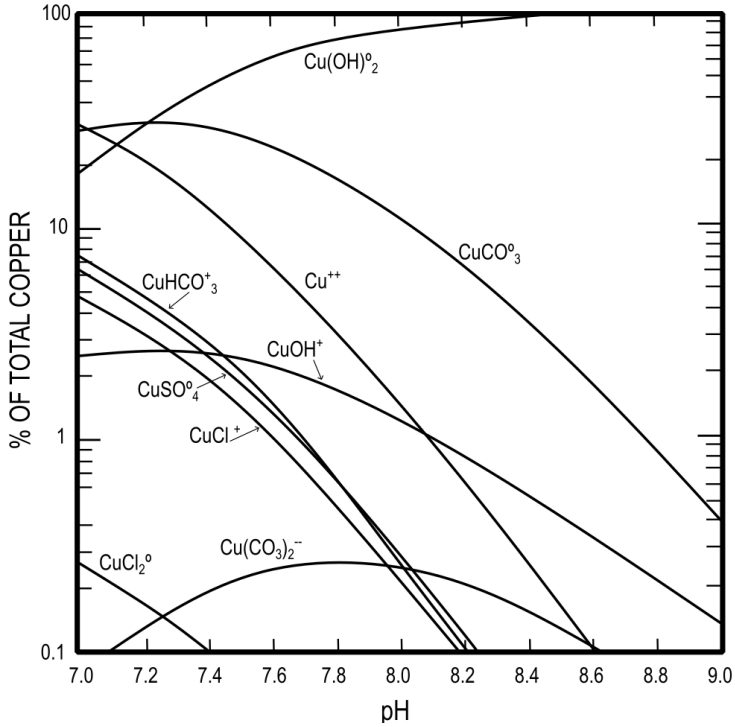

Figura 7.2. Especiación del Cu en agua de mar, determinada a T=25ºC. Figura tomada de Zirino and Yamamoto (1972).

En el agua de mar el Cu puede encontrarse como Cu(I) y Cu(II), siendo el Cu(II) la especie más abundante y estable. En el agua de mar el Cu(I) se oxida

rápidamente debido al contenido en oxígeno del agua, su temperatura, la concentración de bicarbonatos y la interacción con los iones mayoritarios como el Ca^{2+} y el Mg^{2+} (Moffett and Zika, 1983; González-Dávila et al., 2009; Pérez-Almeida et al., 2013). El Cu(II) también puede reducirse a Cu(I) por la fotooxidación de la materia orgánica disuelta (DOM) en aguas superficiales (Zika, 1981), y por la interacción del Cu(II) con iones como OH^-, Cl^-, SO_4^{2-} y CO_3^{2-} (Figura 7.2, Zirino and Yamamoto, 1972). Sin embargo, la complejación del Cu(II) inhibe los procesos de reducción (Moffett and Zika, 1983). En el agua de mar más del 99% del dCu se encuentra formando complejos con ligandos orgánicos y sólo el 1% del dCu existe como cationes de Cu^{2+} libres, que a concentraciones altas es tóxico para los microorganismos. Los estudios realizados con cianobacterias, cocolitofóridos y diatomeas indican que el límite de toxicidad del Cu^{2+} es de 10 pM (Sunda and Lewis, 1978; Brand et al., 1986), mientras que concentraciones inferiores a 0.002 pM pueden limitar el crecimiento del fitoplancton por déficit (Annett et al., 2008). A su vez, el Cu complejado puede ser asimilado por el fitoplancton y sostener el crecimiento de las comunidades que viven en condiciones de Cu^{2+} limitantes (Annett et al., 2008; Semeniuk et al., 2015).

También existe una interacción redox entre el Fe y el Cu (Figura 7.3, González et al., 2016; Pérez-Almeida et al., 2019). La presencia de Cu(II) y Cu(I) en disolución acelera la oxidación del Fe(II) en el agua de mar, debido a la interacción de ambos metales con los grupos hidroxilo, H_2O_2 y $O_2^{\bullet-}$. Por otro lado, el Cu(II) se reduce rápidamente a Cu(I) en presencia de Fe(II), mientras que la tasa de oxidación del Cu(I) aumenta en presencia de Fe(III). A su vez, se pueden formar especies de Fe y Cu, como la ferrita cúprica y cuprosa.

Tal como se ha mencionado anteriormente, la formación de complejos entre el dFe y dCu y los compuestos orgánicos (llamados ligandos) controla la especiación de estos metales. La complejación evita la formación y precipitación de oxihidróxidos de Fe y aumenta el tiempo de residencia del dFe en el agua de mar (Rue and Bruland, 1995; Liu and Millero, 2002). Para el Cu, la formación de complejos limita las tasas de *scavenging* y disminuye la concentración de Cu^{2+}, controlando su toxicidad para el fitoplancton (Brand et al., 1986). A su vez, el fitoplancton puede asimilar los metales complejados a través de mecanismos celulares específicos (Morel et al., 2008; Semeniuk et al., 2009; Walsh et al., 2015; Sutak et al., 2020).

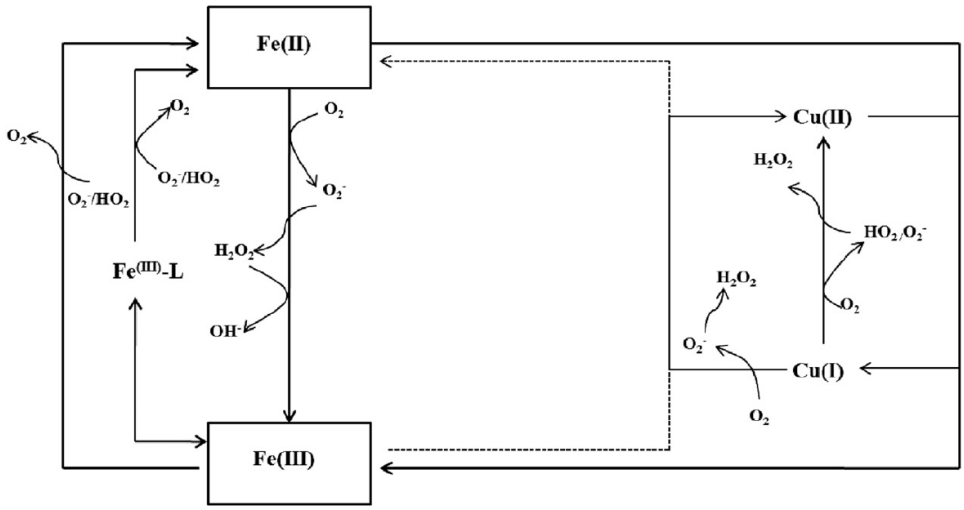

Figura 7.3. Reacciones redox y de interacción entre el Fe y el Cu en agua de mar. Figura tomada de González et al. (2016).

Los ligandos son un grupo heterogéneo de compuestos que contienen diversos grupos funcionales, algunos de los cuales son específicos para el Fe o el Cu, mientras otros son capaces de complejar ambos metales traza presentando diferentes afinidades (Rue and Bruland, 2001; Abualhaija et al.,

2015). En la práctica se sabe poco sobre la identidad de los ligandos y sólo algunos grupos funcionales han sido estudiados y reconocidos, como son: los sideróforos (McKnight and Morel, 1980; Rue and Bruland, 1995; Vraspir and Butler, 2009), los tioles (Leal et al., 1999; Tang et al., 2000; Dupont et al., 2004, 2006; Dryden et al., 2007; Sander et al., 2007; Laglera and Monticelli, 2017), las sustancias húmicas (Laglera et al., 2007, 2019; Laglera and van den Berg, 2009; Muller and Batchelli, 2013; Abualhaija et al., 2015; Gao and Guéguen, 2018), los fenoles (Munin and Edwards-Lévy, 2011; Rico et al., 2013; Santana-Casiano et al., 2014; López et al., 2015; Samperio-Ramos et al., 2018c; González et al., 2019; Arreguin et al., 2021), las metanobactinas (Choi et al., 2006; Ruacho et al., 2022), el ácido domoico (Rue and Bruland, 2001), las porfirinas (Hutchins et al., 1999) y los exopolisacáridos (González et al., 2010b; Hassler et al., 2011; Norman et al., 2015).

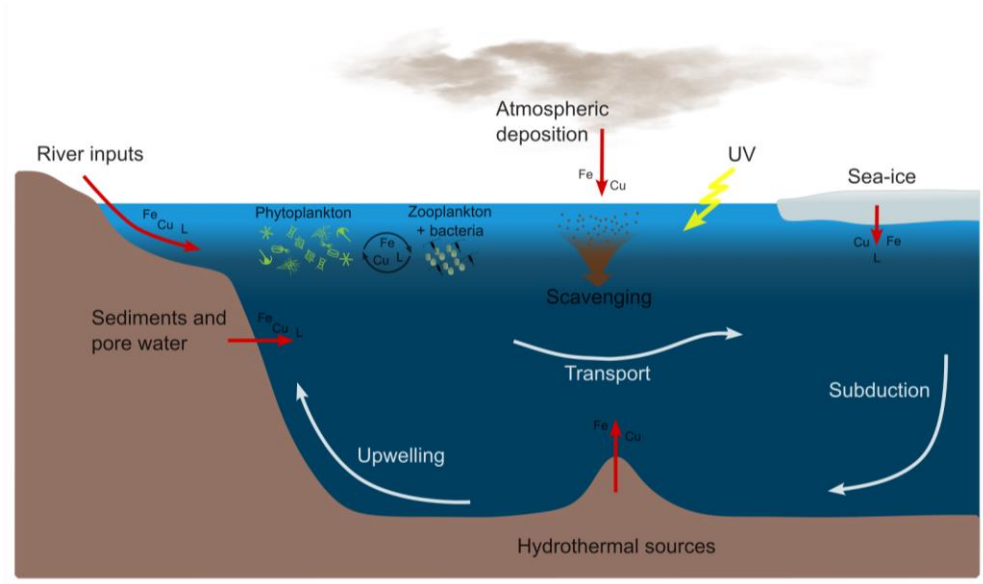

Figura 7.4. Ciclo biogeoquímico marino del hierro (Fe), el cobre (Cu) y los ligandos (L). Las flechas rojas indican los mecanismos que actúan como fuente, mientras las flechas blancas representan los mecanismos físicos de transporte. Figura modificada de Tagliabue et al. (2017) y Ruacho et al. (2022).

Ciclos biogeoquímicos del hierro y el cobre

La distribución y la abundancia de los metales traza en el océano depende de diferentes mecanismos fisicoquímicos, la circulación oceánica, las fuentes y los sumideros (Bruland et al., 2014). En términos generales, la variabilidad del dFe y del dCu depende de la ubicación y de las fuentes presentes (Figura 7.4). Dada su importancia también deben considerarse las fuentes alóctonas o autóctonas de los ligandos (Gledhill and Buck, 2012; Ruacho et al., 2022). Entre las principales fuentes de metales traza y/o ligandos se encuentran: los aportes fluviales (Sholkovitz, 1978; Kogut and Voelker, 2001; Jickells et al., 2005; Buck et al., 2007; Richon and Tagliabue, 2019; Hollister et al., 2021); los glaciares y el hielo (Sholkovitz, 1978; Kogut and Voelker, 2001; Krembs et al., 2002; Jickells et al., 2005; Buck et al., 2007; Tovar-Sánchez et al., 2010; Anderson and Amon, 2015; Richon and Tagliabue, 2019; Hawkings et al., 2020, 2020; Lin et al., 2020; Hollister et al., 2021); la deposición atmosférica (Jickells et al., 2005; Bruland et al., 2014; Little et al., 2014; Richon and Tagliabue, 2019); los sedimentos marinos (Heggie et al., 1987; Bowie et al., 2002; Gerringa et al., 2008; Ruacho et al., 2020); y las fuentes hidrotermales (German et al., 1991; German and Von Damm, 2004; Bennett et al., 2008; Tagliabue et al., 2010; Sander and Koschinsky, 2011; González-Santana et al., 2020; Dulaquais et al., 2023). Mientras que los mecanismos de eliminación son: la asimilación biológica (Sunda, 1989; Sato et al., 2007; Poorvin et al., 2011); la sedimentación de partículas (Little et al., 2013; Bruland et al., 2014; Völker and Tagliabue, 2015; Cheize et al., 2019; Richon and Tagliabue, 2019); y los procesos fotoquímicos (Barbeau et al., 2001; Barbeau, 2006; Laglera and van den Berg, 2006; Shank et al., 2006).

Caracterización de los ligandos orgánicos

La voltametría catódica de redisolución adsorptiva con intercambio competitivo de ligandos (CLE-ACSV, del inglés "competitive ligand exchange adsorptive cathodic stripping voltammetry") es una técnica que permite cuantificar la concentración de los metales disueltos, de sus ligandos y determinar las constantes de estabilidad condicional (K^{cond}_{ML}), que caracterizan la unión entre los metales traza y sus ligandos (Campos and van den Berg, 1994; Croot and Johansson, 2000; Pižeta et al., 2015). Esta técnica no proporciona información molecular sobre los ligandos y sus resultados están condicionados a las condiciones experimentales aplicadas pero, gracias a su alta sensibilidad, permite medir concentraciones bajas de metales y ligandos sin necesidad de preconcentrar la muestra (Middag et al., 2023).

$$M' + L' \rightleftharpoons ML \tag{7.3}$$

$$K^{cond}_{M'L} = \frac{[ML]}{[M']+[L']} \tag{7.4}$$

Debido a la heterogeneidad de la DOM del agua de mar y la compleja asociación que se establece con los metales traza, la identidad de los ligandos de dFe y dCu sigue siendo desconocida (Vraspir and Butler, 2009). De esta forma, se considera que los ligandos son un continuo de compuestos con diferentes capacidades complejantes, que vienen determinadas por los sitios de complejación. Por ello, los ligandos disueltos se clasifican en función de su capacidad de complejación, determinada por la K^{cond}_{ML}, que caracteriza la fuerza aparente de los sitios de complejación de los ligandos. Esta constante se utiliza para dividir operativamente los ligandos en compuestos fuertes y débiles, también denominados L_1 y L_2. En el caso de los ligandos de dFe (L_{Fe}) el log K^{cond}_{Fe3+L} =22 es el valor que diferencia las dos clases, mientras que

para los ligandos de dCu (L_{Cu}) es log K^{cond}_{Cu2+L}=13 (Bruland et al., 2000; Gledhill and Buck, 2012).

Efectos del cambio climático en la biogeoquímica del Fe y el Cu en agua de mar

La especiación, distribución y concentración del Fe y del Cu en el agua de mar dependen de los mecanismos que los suministran y eliminan, las reacciones redox y las condiciones ambientales. Las propiedades de los metales traza y los ligandos en el agua de mar dependen de muchos factores, como son la temperatura, el pH, la fuerza iónica, la salinidad y la luz. Debido al cambio climático estas condiciones ambientales están variando de forma significativa (IPCC, 2022), con importantes consecuencias para la biogeoquímica de los metales traza (Hoffmann et al., 2012; Millero et al., 2009).

El aumento de las concentraciones de CO_2 atmosférico produce un aumento de la temperatura del océano, intensificando la estratificación de las aguas y favoreciendo el derretimiento del hielo, lo que modifica la circulación oceánica y atmosférica, afectando al clima y modificando tanto la deposición atmosférica como los aportes fluviales (Doney et al., 2012). Además, disminuye el pH del agua, así como de las concentraciones de hidróxidos (OH^-) y carbonatos (CO^{2-}_3), con importantes consecuencias biogeoquímicas.

En términos de especiación inorgánica**,** la disminución del pH producida por la acidificación oceánica favorece las formas libres del Fe y el Cu, aumenta la solubilidad del Fe(III) y disminuye la tasa de oxidación del Fe(II) (Millero and Hawke, 1992; Millero et al., 1995, 2009; Millero, 2013). El aumento de las temperaturas en las aguas superficiales y la estratificación oceánica incrementa las tasas de oxidación del Fe(II) y favorece las reacciones de fotorreducción del

Fe(III) (Kuma et al., 1995). Sin embargo, la disminución de la cantidad de O_2 disuelto puede ralentizar la oxidación del Fe(II) (Keeling et al., 2010).

Los efectos de la acidificación oceánica sobre los ligandos no han sido exhaustivamente estudiados y los resultados obtenidos no son claros debido a la heterogeneidad de la materia orgánica (Millero et al., 2009). Algunos estudios sugieren que la disminución del pH produce una menor complejación del Cu y favorece las formas de metales libres (Gledhill et al., 2015; Millero et al., 2009). Otros estudios indican que la acidificación del agua puede aumentar la complejación del Fe (Hirose, 2011; Stockdale et al., 2016). Finalmente, la mayor exposición solar de las aguas superficiales, asociada al incremento en la estratificación de las aguas, produce la fotólisis de los ligandos (Barbeau, 2006; Laglera and van den Berg, 2006).

Algunas zonas del océano son más vulnerables a los efectos del cambio climático, como las islas y las regiones polares (IPCC, 2022). Las islas se ven afectadas por cambios en el clima, la circulación oceánica, la estratificación del agua y el nivel del mar (Gove et al., 2016; Veron et al., 2019). Además, en las islas tropicales y subtropicales, se espera una menor disponibilidad de nutrientes en el futuro debido a cambios en sus ciclos biogeoquímicos y en la dinámica oceánica (Doney, 2010). Por otro lado, el aumento de la temperatura está afectando significativamente a las regiones polares (IPCC, 2022). Enl Océano Ártico se espera una mayor entrada de agua dulce por el derretimiento del hielo marino y del permafrost (Peterson et al., 2002; Schuur et al., 2015, 2013), asociado a una mayor entrada de metales traza y materia orgánica (Charette et al., 2020; Frey y McClelland, 2009; Guieu et al., 1996; Stedmon et al., 2011). Sin embargo, los estudios que investigan la especiación orgánica del Fe y el Cu en islas oceánicas y regiones polares son limitados, por tanto los modelos de

predicción generan resultados inciertos. Es por ello necesario seguir investigando sobre la especiación orgánica de estos metales traza en el océano y en especial en las regiones vulnerables al cambio del clima.

7.2 Objetivos

Como ya se ha señalado, el estudio de la especiación del Fe y el Cu en el agua de mar es clave para comprender su distribución en el medio marino. Mejorar nuestros conocimientos sobre la especiación orgánica aumentará nuestra comprensión de la biodisponibilidad del dFe y dCu, arrojando luz sobre cómo la distribución de estos micronutrientes podría estar relacionada con la producción primaria y el secuestro de CO_2.

Esta tesis tiene como objetivo proporcionar una visión de la especiación orgánica de dFe y dCu en regiones poco estudiadas y potencialmente afectadas por el cambio climático. Para ello se han estimado las concentraciones de dFe y dCu, junto con las respectivas concentraciones de ligandos y las constantes de estabilidad condicional, en regiones oceánicas y costeras de los océanos Atlántico y Ártico. Este objetivo general se ha estructurado en tres objetivos específicos.

Objetivo 1. Determinar los efectos que puedan tener las islas oceánicas sobre la especiación orgánica del dFe y dCu en las aguas superficiales circundantes. Para ello se realizó una cuantificación y caracterización del dFe y dCu junto con la de los ligandos naturales que complejan cada metal traza en las aguas costeras de las islas de la Macaronesia.

El desarrollo de este objetivo constituye el Capítulo 2, donde se evaluó la especiación orgánica en torno a los archipiélagos de Cabo Verde, Canarias y Madeira. Este estudio evaluó la distribución y la fuerza de la unión de los

ligandos de Fe y Cu, indicando los posibles procesos (físicos y biológicos) que afectan a las características observadas.

Objetivo 2. Caracterizar la distribución de los ligandos de Cu en una región influenciada por procesos costeros y oceánicos. Este objetivo incluye la cuantificación de los ligandos de Cu y la determinación de las respectivas constantes de estabilidad condicional en la columna de agua.

Este objetivo se aborda en el Capítulo 3, que describe los ligandos de Cu en la zona de la plataforma de Groenlandia y la región del Estrecho de Fram. Además, se evalúa la influencia de la exportación de ligandos desde el Océano Ártico y las entradas procedentes de las zonas costeras de Groenlandia.

Objetivo 3. Caracterizar la distribución de los ligandos de Cu en una región oceánica. Este objetivo implica la cuantificación de los ligandos de Cu y la determinación de las respectivas constantes de estabilidad condicional en la columna de agua.

Este objetivo se aborda en el Capítulo 4 en un estudio sobre la especiación orgánica del Cu en el Océano Ártico. A lo largo de la región de estudio se cuantificaron los ligandos de Cu en el agua de mar en zonas cubiertas o no por el hielo. La distribución observada se relacionó con fuentes fluviales de materia orgánica y fue asociada con la exportación de materiales a través del Estrecho de Fram hacia el Mar del Norte y el Atlántico Norte.

7.3 Conclusiones

Esta Tesis muestra resultados significativos acerca de la complejación orgánica del Fe y el Cu en diversos entornos oceánicos y costeros, en regiones donde la especiación orgánica de los metales traza había sido poco estudiada.

En primer lugar, en el **Capítulo 2** analizamos el impacto potencial de las islas oceánicas de la Macaronesia sobre la complejación del Fe y el Cu en las aguas superficiales. Los principales resultados fueron los siguientes:

- Las zonas costeras que rodean las islas oceánicas del archipiélago de la Macaronesia (Cabo Verde, Canarias y Madeira) presentan concentraciones superficiales de dFe y dCu más elevadas que las aguas oceánicas circundantes, así como de sus ligandos. Esto reveló que las regiones insulares costeras podrían actuar como fuente de estos elementos hacia el océano abierto.

- La hidrodinámica de la región de investigación afecta a la dispersión del dFe y el dCu, así como a su especiación orgánica. Se postulan la actividad biológica y la resuspensión de sedimentos como los principales mecanismos que actúan como fuente de estos elementos, vinculados a la influencia del viento y las corrientes oceánicas.

- Los análisis realizados por voltametría indicaron el predominio de ligandos fuertes, los cuales controlan la especiación tanto del dFe como del dCu, así como la toxicidad del Cu^{2+}.

- El desarrollo de una ecuación lineal permitió relacionar la distribución de los ligandos de dCu con la concentración de nitratos y nitritos, la fluorescencia y la turbidez del agua.

En el **Capítulo 3** se estudió la complejación orgánica del Cu en las aguas costeras y oceánicas del Estrecho de Fram y la plataforma de Groenlandia. Esta área tiene una gran importancia biogeoquímica ya que conecta el Océano Ártico con el Atlántico Norte. En ella interactúan distintas dinámicas costeras

y oceánicas y se ve afectada por la variabilidad medioambiental producida por el cambio climático. Las principales conclusiones de este estudio son:

- La concentración de los ligandos de Cu presenta una tendencia longitudinal, con concentraciones que aumentan desde la zona de océano abierto del Estrecho de Fram hacia la costa de Groenlandia. Esto sugiere la presencia de una fuente de ligandos asociada al glaciar y a los procesos costeros.

- La constante de estabilidad condicional de los ligandos indica la presencia de ligandos fuertes que mantienen la concentración de Cu^{2+} por debajo de los límites de toxicidad. Las constantes muestran valores decrecientes desde la zona de océano abierto del Estrecho de Fram hacia la costa de Groenlandia, asociados a la degradación de la materia orgánica y/o remineralización bacteriana, y a la descarga de agua de deshielo en la costa.

- El perfil vertical de los ligandos de Cu sobre la plataforma de Groenlandia difiere de la distribución observada en otras zonas costeras y de plataforma no afectadas por las descargas fluviales, y del agua del océano abierto, incluido del Estrecho de Fram. Las concentraciones superficiales máximas se observaron en las Aguas Polares Superficiales. Esto sugiere una combinación entre el aporte costero de ligandos y su entrada desde el Océano Ártico central a través la Deriva Transpolar.

- Las altas concentraciones de dCu complejado con ligandos fuertes en las Aguas Polares Superficiales sobre la plataforma de Groenlandia permiten el transporte de dCu hacia las regiones meridionales del Mar

del Norte y el Atlántico Norte. Esto favorece el crecimiento del fitoplancton en regiones que presentan condiciones limitantes de Fe.

Finalmente, el **Capítulo 4** describe la complejación orgánica del dCu en el Océano Ártico central y el Mar de Barents, unas regiones que no había sido estudiada anteriormente. Se encontró que:

- Las cuencas de Makárov y Amundsen mostraron concentraciones superficiales de ligandos de Cu más altas que las observadas en el Mar de Barents y en otras regiones de océano abierto. Las concentraciones máximas se registraron en las Aguas Polares Superficiales y se asociaron con el transporte de aguas desde las plataformas siberianas, debido a la Deriva Transpolar.

- La estratificación y la mezcla limitada de las aguas impiden el transporte de los ligandos de Cu desde la superficie hacia el océano profundo, permitiendo el transporte de los ligandos hacia el Estrecho de Fram a través de la Deriva Transpolar.

- En las aguas superficiales se detectaron ligandos fuertes, asociados a la materia orgánica terrestre y las sustancias húmicas liberadas por los ríos. Sin embargo, parte de los ligandos detectados podría ser exudados del fitoplancton presente en el hielo y producidos por la degradación bacteriana. La presencia de estos ligandos fuertes mantiene al Cu^{2+} a concentraciones no tóxicas.

- En las Aguas Polares Superficiales de las cuencas de Amundsen y Makárov se estableció una relación entre la concentración de los ligandos de Cu con la salinidad y con la concentración de silicato y

nitrato. Esta ecuación lineal permite cuantificar los ligandos de Cu en las aguas superficiales del Océano Ártico central.

Image: USGS/ESA/ Landsat-8 satellite's Operational Land Imager (2014).

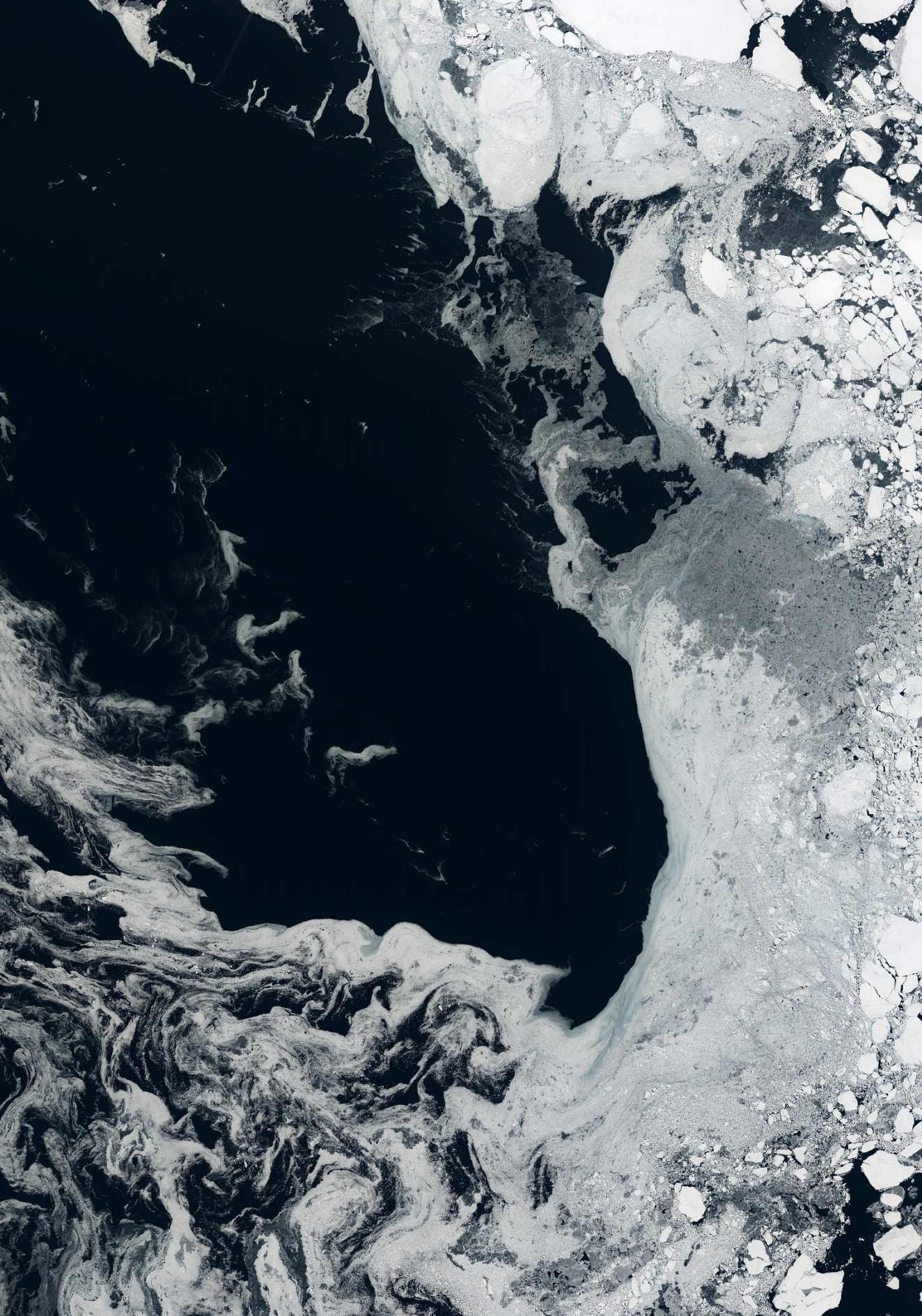

Appendices

Appendix A – Chapter 3

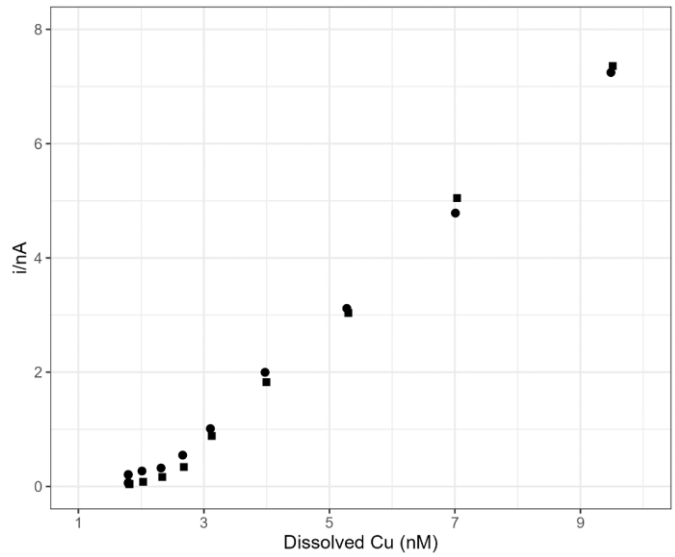

Figure A.1. Example of titration curve of two seawater samples from station 9 (square) and 22 (dots).

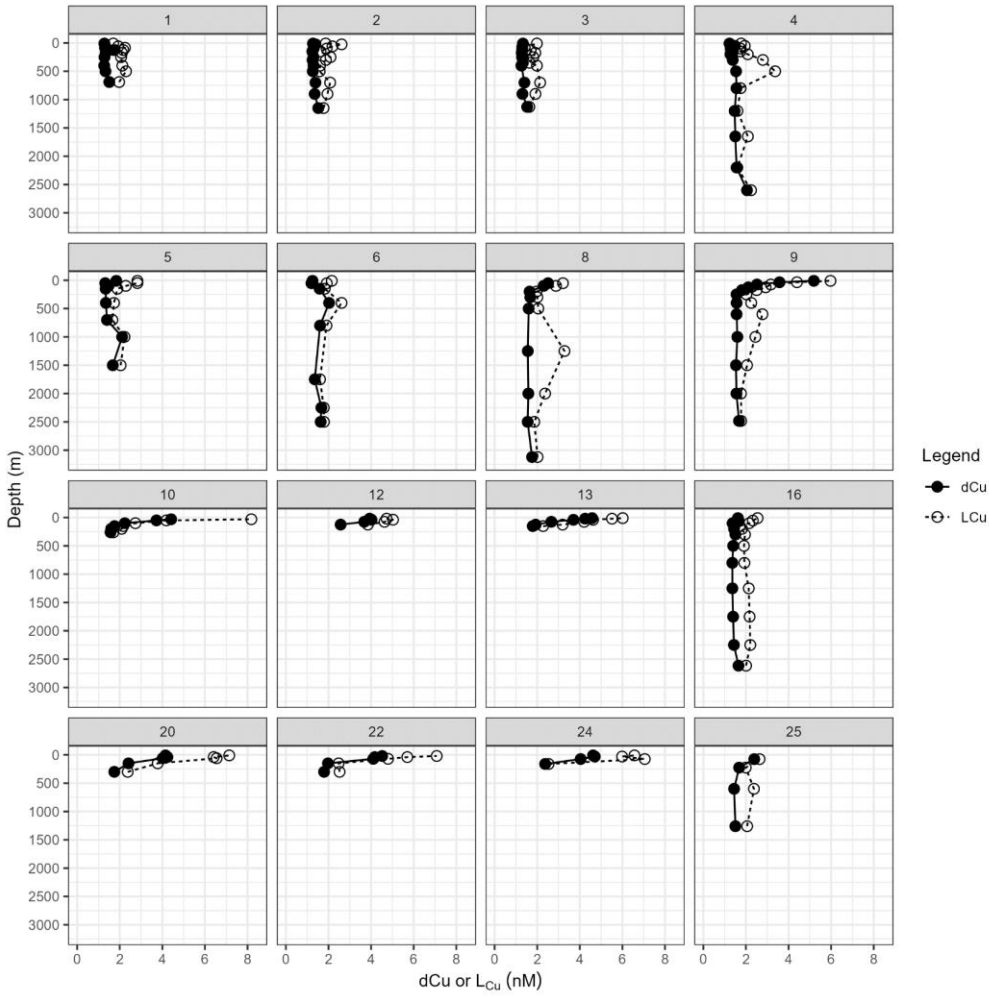

Figure A.2. Depth profiles of dissolved Cu (dCu) in nM (solid line with filled circles) and Cu-binding ligands (L_{Cu}) in nM (dashed line with open circles) obtained at each station.

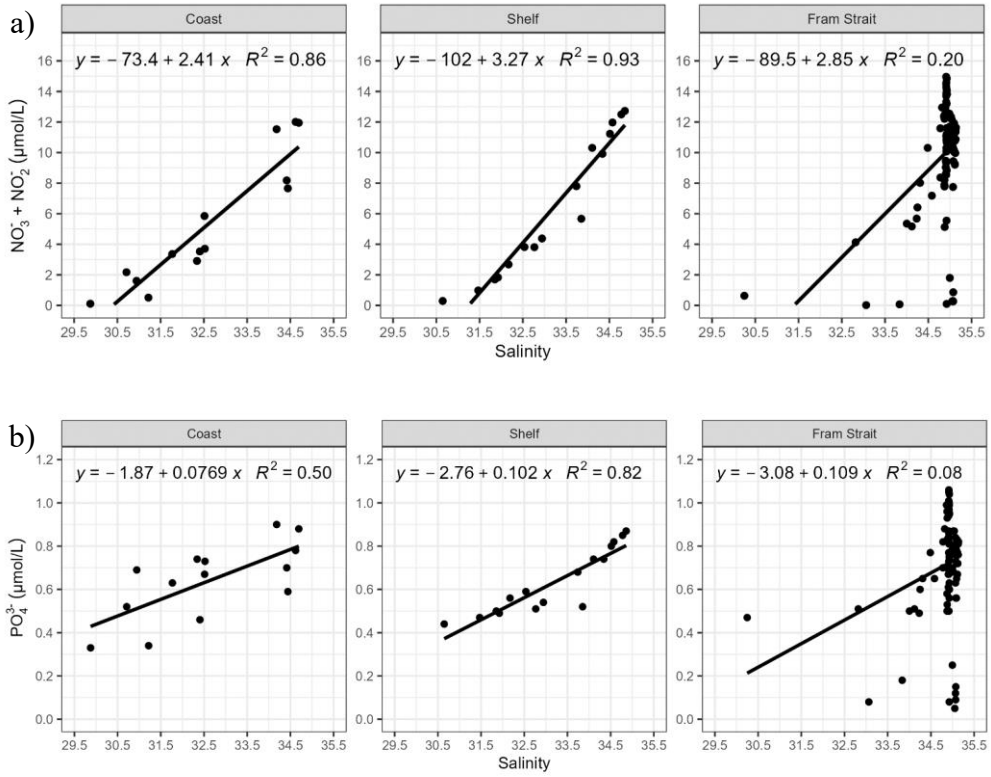

Figure A.3. Variability of (a) nitrate and nitrate, and (b) phosphate concentrations (µmol/L) with respect to salinity. The number of samples (n) vary by region: 14 observations on the coast, 16 above the shelf and 95 in Fram Strait.

Table A.1. Mean dissolved copper binding ligand parameters estimated for surface water (<100 m depth).

Region	Stations		dCu (nM)	L_{Cu} (nM)	eL_{Cu} (nM)	log K^{cond}_{Cu2+L}	log α_{Cu2+L}	Cu^{2+} (fM)	Cu' (pM)	%CuL	L_{Cu}/dCu
Coast	20, 22, 24	Min	4.0	4.8	0.7	14.5	6.3	1.4	0.04	99.99	1.2
		Max	4.7	7.1	3.0	15.3	7.1	12.5	0.36	100	1.8
		Mean	4.3 ± 0.3	6.4 ± 0.8	2.0 ± 0.8	14.8 ± 0.3	6.6 ± 0.3	4.3 ± 3.4	0.12 ± 0.1	100 ± 0.01	1.5 ± 0.2
		Median	4.2	6.6	2.2	14.9	6.7	3.3	0.09	100	1.5
Shelf	10, 12, 13	Min	2.7	4.2	0.5	14.8	6.6	1.2	0.03	100	1.1
		Max	4.6	8.2	3.8	15.7	7.3	4.7	0.14	100	1.9
		Mean	3.9 ± 0.6	5.2 ± 1.3	1.4 ± 1.0	15.2 ± 0.3	6.9 ± 0.3	2.6 ± 1.4	0.07 ± 0.04	100 ± 0.01	1.4 ± 0.2
		Median	3.9	4.7	1.0	15.0	6.8	2.0	0.06	100	1.3
Fram Strait	1, 2, 3, 4, 5, 6, 8, 9, 16, 25	Min	1.2	1.4	0.1	14.8	6.4	0.1	0.003	99.99	1.1
		Max	5.2	6.0	1.5	16.1	7.4	11.7	0.33	100	2.1
		Mean	1.8 ± 1.0	2.6 ± 1.0	0.7 ± 0.3	15.6 ± 0.3	6.9 ± 0.3	1.51± 2.7	0.04 ± 0.08	100 ± 0.01	1.5 ± 0.3
		Median	1.3	2.3	0.7	15.7	6.9	0.6	0.02	100	1.5

Table A.2. Mean dCu binding ligand parameters estimated for deep water (>100 m depth).

Region	Stations		dCu (nM)	L_{Cu} (nM)	eL_{Cu} (nM)	log K^{cond}_{Cu2+L}	log α_{Cu2+L}	Cu^{2+} (fM)	Cu' (pM)	%CuL	L_{Cu}/dCu
Coast	20, 22, 24	Min	1.7	2.4	0.4	14.7	6.2	2.0	0.06	99.99	1.2
		Max	2.4	3.8	1.4	15.3	6.7	4.0	0.12	100	1.6
		Mean	2.1 ± 0.3	2.7 ± 0.6	0.7 ± 0.4	15.0 ± 0.2	6.5 ± 0.2	3.0 ± 0.9	0.09 ± 0.03	100 ±0.01	1.4 ± 0.2
		Median	2.0	2.5	0.6	15.1	6.5	3.2	0.1	100	1.4
Shelf	10, 12, 13	Min	1.6	1.7	0.1	14.8	6.4	1.3	0.04	99.98	1.1
		Max	2.6	3.9	1.3	15.5	6.8	7.9	0.24	100	1.7
		Mean	1.92± 0.4	2.6 ± 0.7	0.7 ± 0.4	15.2 ± 0.2	6.6 ± 0.2	2.9 ± 2.4	0.09 ± 0.07	100 ± 0.01	1.3 ± 0.2
		Median	1.8	2.3	0.5	15.2	6.6	1.5	0.05	100	1.3
Fram Strait	1, 2, 3, 4, 5, 6, 8, 9, 16, 25	Min	1.2	1.6	0.03	14.3	5.8	0.2	0.01	99.96	1.0
		Max	2.3	3.4	1.8	16.3	7.7	21.1	0.63	100	2.2
		Mean	1.5 ± 0.2	2.1 ± 0.37	0.5 ± 0.3	15.5 ± 0.3	6.8 ± 0.3	1.8 ± 3.03	0.05 ± 0.09	100 ± 0.01	1.4 ± 0.2
		Median	1.5	2.0	0.5	15.6	6.9	0.8	0.03	100	1.3

Table A.3. Summary of results for dCu binding ligand parameters by region (coast, shelf and Fram Strait) and water masses (Polar Surface Water, PSW, Atlantic Water, AW, Recirculated Atlantic Water, RAW, Arctic Atlantic Water, AAW, Arctic Intermediate Water, AIW, and Deep Water, DW). Minimum, maximum, mean with standard deviation (±1σ) and median were reported.

Region	Stations	Water masses		dCu (nM)	L_{Cu} (nM)	eL_{Cu} (nM)	log K^{cond}_{Cu2+L}	log α_{Cu2+L}	Cu^{2+} (fM)	Cu' (pM)	%CuL	L_{Cu}/dCu
Coast	20,22,24	PSW	Min	2.0	2.5	0.4	14.5	6.3	1.4	38.07	99.99	1.2
			Max	4.7	7.1	3.0	15.3	7.1	12.5	361.17	100	1.8
			Mean	3.8 ± 1.0	5.5 ± 1.7	1.8 ± 0.9	14.9 ± 0.3	6.6 ± 0.2	4.0 ± 3.0	113.96 ± 86.18	100.00 ± 0.00	1.5 ± 0.2
			Median	4.1	6.2	1.7	14.9	6.6	3.3	95.16	100	1.5
		AAW	Min	1.7	2.4	0.6	14.8	6.2	2.2	66.58	99.99	1.4
			Max	1.8	2.5	0.7	15.1	6.5	4.0	120.91	100	1.4
			Mean	1.8 ± 0.0	2.5 ± 0.1	0.7 ± 0.1	14.94± 0.1	6.3 ± 0.2	3.1 ± 1.3	93.75 ± 38.41	99.99 ± 0.00	1.4 ± 0.03
			Median	1.8	2.5	0.7	14.9	6.3	3.1	93.75	99.99	1.4
Shelf	10, 12, 13	PSW	Min	1.9	2.7	0.5	14.8	6.4	1.2	33.93	100	1.1
			Max	4.6	8.2	3.8	15.7	7.3	4.7	137.37	100	1.9
			Mean	3.5 ± 0.9	4.7 ± 1.4	1.3 ± 0.9	15.1 ± 0.3	6.8 ± 0.3	2.6 ± 1.3	73.93 ± 36.53	100.00 ± 0.00	1.4 ± 0.2
			Median	3.7	4.6	1.1	15.1	6.7	2.0	58.24	100	1.3
		AAW	Min	1.6	1.7	0.1	15.2	6.4	1.5	44.3	99.98	1.1
			Max	1.8	2.3	0.6	15.5	6.8	7.9	237.01	100	1.4
			Mean	1.7 ± 0.1	2.1 ± 0.25	0.4 ± 0.2	15.3 ± 0.1	6.6 ± 0.2	3.10± 3.2	93.01 ± 96.01	99.99 ± 0.01	1.3 ± 0.1
			Median	1.7	2.1	0.5	15.3	6.6	1.5	45.36	100	1.3

Table A.3. Continued.

Region	Stations	Water masses		dCu (nM)	L_{Cu} (nM)	eL_{Cu} (nM)	$logK_{Cu2+L}$	log α_{Cu2+L}	Cu^{2+} (fM)	Cu' (pM)	%CuL	L_{Cu}/dCu
Fram Strait	1, 2, 3, 4, 5, 6, 8, 9, 16, 25	AAW	Min	1.5	1.9	0.3	15.3	6.6	0.3	9.65	99.99	1.2
			Max	1.7	2.3	0.7	16.0	7.3	2.9	88.14	100	1.4
			Mean	1.6 ± 0.1	2.0 ± 0.1	0.4 ± 0.1	15.6 ± 0.3	6.9 ± 0.3	1.3 ± 0.9	39.66 ± 28.25	100.00 ± 0.00	1.3 ± 0.1
			Median	1.6	2	0.4	15.5	6.8	1.1	33.24	100	1.3
		AIW	Min	1.3	1.6	0.1	14.9	6.4	0.2	5.53	99.99	1.1
			Max	2.1	3.3	1.7	16.3	7.7	3.1	91.39	100	2.1
			Mean	1.5 ± 0.2	2.1 ± 0.4	0.6 ± 0.4	15.5 ± 0.4	6.9 ± 0.4	1.3 ± 0.9	37.74 ± 25.48	100.00 ± 0.00	1.4 ± 0.3
			Median	1.5	2.0	0.5	15.5	6.8	1.1	33.27	100	1.4
		AW	Min	1.2	1.4	0.1	15.0	6.3	0.1	3.9	99.99	1.1
			Max	1.8	2.8	1.5	16.1	7.3	2.7	81.05	100	2.1
			Mean	1.4 ± 0.1	2.0 ± 0.3	0.6 ± 0.3	15.6 ± 0.3	6.9 ± 0.3	0.7 ± 0.6	22.27 ± 17.61	100.00 ± 0.00	1.5 ± 0.2
			Median	1.3	1.9	0.6	15.6	6.9	0.6	17.05	100	1.5
		DW	Min	1.4	1.6	0.03	14.8	6.1	0.6	18.64	99.96	1.0
			Max	2.1	2.4	0.8	16.2	7.5	21.1	633.81	100	1.6
			Mean	1.6 ± 0.2	1.9 ± 0.2	0.3 ± 0.3	15.4 ± 0.4	6.7 ± 0.4	4.2 ± 5.6	127.15 ± 167.77	99.99 ± 0.01	1.2 ± 0.2
			Median	1.6	1.9	0.3	15.5	6.8	2.1	62.29	100	1.2
		PSW	Min	1.25	2.2	0.3	14.8	6.5	0.3	7.5	99.99	1.1
			Max	5.2	6.0	0.9	15.9	7.4	11.7	328.66	100	1.7
			Mean	2.5 ± 1.1	3.2 ± 1.1	0.7 ± 0.2	15.5 ± 0.4	7.0 ± 0.3	2.3 ± 3.6	65.63 ± 101.26	100.00 ± 0.00	1.3 ± 0.2
			Median	2.3	2.9	0.7	15.6	7.0	0.7	21.32	100	1.3
		RAW	Min	1.4	1.7	0.3	14.3	5.8	0.4	11.49	99.99	1.2
			Max	2.0	3.4	1.8	15.8	7.2	4.7	140.62	100	2.2
			Mean	1.5 ± 0.2	2.3 ± 0.5	0.8 ± 0.5	15.4 ± 0.5	6.7 ± 0.4	1.34± 1.3	40.30 ± 39.76	100.00 ± 0.00	1.5 ± 0.3
			Median	1.4	2.1	0.6	15.5	6.8	0.8	23.45	100	1.5

Table A.4. Statistical analysis. A Kruskal-Wallis was applied to determine if there are significant differences among regions. To understand which regions are different a Conover test was used. The analysis was carried out considering all data (a), surface data at less than 100m depth (b) and for deeper (>100m) simples (c). P-values higher than 0.05 indicate non-significant differences.

a)

Global	Kruskal-Wallis test			Conover's test		
Parameter	χ^2	df	p-value	Fram Strait-Coast	Shelf-Coast	Shelf-Fram Strait
Temperature (°C)	22.969	2	1.03E-05	0.00089	0.73636	0.00011
Salinity	55.539	2	8.71E-13	3.00E-11	0.6865	3.40E-11
Fluorescence (au)	8.5034	2	1.42E-02	0.1108	0.6192	0.0235
O_2 (µM)	16.738	2	2.32E-04	0.0047	0.905	0.0023
NO^-_3+NO^-_2 (µM)	14.608	2	6.73E-04	0.0031	0.5164	0.017
PO^{3-}_4 (µM)	6.1809	2	0.05	-	-	-
$Si(OH)_4$ (µM)	2.7585	2	0.25	-	-	-
dCu (nM)	53.919	2	1.96E-12	2.40E-11	0.4491	3.30E-10
L_{Cu} (nM)	45.326	2	1.44E-10	8.20E-10	0.2282	2.20E-07
eL_{Cu} (nM)	21.858	2	1.79E-05	4.90E-05	0.2015	0.0062
Cu' (fM)	33.242	2	6.05E-08	6.70E-07	0.3363	3.00E-05
Cu^{2+} (fM)	33.904	2	4.34E-08	4.80E-07	0.3326	2.30E-05
log K^{cond}_{Cu2+L}	39.38	2	2.81E-09	5.10E-09	0.0932	2.00E-05
log α_{Cu2+L}	14.033	2	8.97E-04	0.00095	0.13715	0.13715

b)

Surface waters	Kruskal-Wallis test			Conover's test		
Parameter	χ^2	df	p-value	Fram Strait-Coast	Shelf-Coast	Shelf-Fram Strait
Temperature (°C)	11.444	2	3.27E-03	0.0073	0.886	0.0077
Salinity	22.954	2	1.04E-05	3.50E-07	0.2573	1.50E-05
Fluorescence (au)	0.50533	2	0.777	-	-	-
O_2 (µM)	20.15	2	4.21E-05	7.50E-06	0.4165	9.80E-05
NO^-_3+NO^-_2 (µM)	0.60768	2	0.738	-	-	-
PO^{3-}_4 (µM)	1.4204	2	0.49	-	-	-
$Si(OH)_4$ (µM)	11.922	2	0.0026	0.042	0.2231	0.0013
dCu (nM)	23.69	2	7.17E-06	1.20E-07	0.177	1.20E-05
L_{Cu} (nM)	26.684	2	1.61E-06	1.10E-09	0.0334	1.90E-06
eL_{Cu} (nM)	17.532	2	1.56E-04	1.70E-05	0.0705	0.0072
Cu' (fM)	15.296	2	4.77E-04	0.00022	0.32917	0.00432
Cu^{2+} (fM)	15.798	2	3.71E-04	0.00015	0.29938	3.63E-03
log K^{cond}_{Cu2+L}	19.354	2	6.27E-05	2.70E-06	0.0293	5.20E-03
log α_{Cu2+L}	6.9448	2	0.031	0.02	0.1458	0.5241

c)

Deep waters	Kruskal-Wallis test			Conover's test		
Parameter	χ^2	df	p-value	Fram Strait-Coast	Shelf-Coast	Shelf-Fram Strait
Temperature (°C)	1.1883	2	0.5520	-	-	-
Salinity	27.112	2	1.30E-06	0.00013	0.98348	1.50E-05
Fluorescence (au)	1.2003	2	0.5487	-	-	-
O_2 (µM)	2.5199	2	0.2837	-	-	-
NO^-_3+NO^-_2 (µM)	0.55953	2	0.7560	-	-	-
PO^{3-}_4 (µM)	0.01224	2	0.9939	-	-	-
$Si(OH)_4$ (µM)	2.5273	2	0.2826	-	-	-
dCu (nM)	21.286	2	2.39E-05	0.00057	0.60636	0.00057
L_{Cu} (nM)	13.358	2	1.26E-03	0.0042	0.3166	0.0405
eL_{Cu} (nM)	1.7164	2	0.4239	-	-	-
Cu' (fM)	14.581	2	6.82E-04	0.0071	0.6223	0.0087
Cu^{2+} (fM)	14.561	2	6.89E-04	0.0076	0.6401	0.0084
log K^{cond}_{Cu2+L}	16.818	2	2.23E-04	0.0031	0.6093	3.70E-03
log α_{Cu2+L}	13.462	2	1.19E-03	0.0112	0.6427	0.0128

Table A.5. A Kruskal-Wallis was applied to determine if there are significant differences between the water masses in Fram Strait (a), shelf (b) and coast (c). To understand which water masses are different a Conover test was used. P-values higher than 0.05 indicate non-significant differences.

a)

Fram Strait	Kruskal-Wallis test			Conover's test													
Parameter	χ^2	df	p-value	AIW-AAW	AW-AAW	DW-AAW	PSW-AAW	RAW-AAW	AW-AIW	DW-AIW	PSW-AIW	RAW-AIW	DW-AW	PSW-AW	RAW-AW	PSW-DW	RAW-DW	RAW-PSW
Temperature (°C)	80.60	5	6.43E-16	4.80E-03	1.20E-05	6.10E-08	1.60E-07	5.01E-01	2.00E-16	2.40E-03	3.20E-03	4.15E-02	2.00E-16	2.00E-16	4.10E-11	8.17E-01	1.60E-07	6.40E-07
Salinity	78.20	5	1.99E-15	2.24E-02	2.00E-16	2.50E-05	4.55E-01	4.70E-03	2.00E-16	8.28E-02	8.00E-06	4.55E-01	1.10E-13	2.00E-16	1.80E-13	4.90E-11	4.55E-01	9.10E-07
Fluorescence (au)	3.49	4	4.79E-01	-	-	-	-	-	-	-	-	-	-	-	-	-	-	-
O_2 (µM)	47.70	5	4.17E-09	5.58E-02	1.59E-01	8.98E-01	8.50E-07	1.24E-01	8.98E-01	3.40E-05	1.42E-03	9.20E-01	2.30E-05	6.30E-07	9.20E-01	3.70E-13	3.50E-04	9.50E-04
NO^-_3+NO^-_2 (µM)	24.20	5	1.99E-04	1	1	7.24E-01	1.18E-01	1	1	1	1.10E-03	1	6.40E-02	4.20E-03	1	9.20E-06	6.46E-01	2.55E-02
PO^{3-}_4 (µM)	22.70	5	3.92E-04	1	1	1	8.23E-02	1	3.53E-01	1	1.40E-03	1	4.41E-02	4.41E-02	1	9.10E-05	1	1.89E-02
$Si(OH)_4$ (µM)	56.30	5	6.96E-11	6.45E-02	3.67E-01	1.70E-04	3.67E-01	4.44E-01	1.40E-07	1.68E-01	1.00E-05	4.44E-01	3.20E-15	5.95E-01	8.80E-04	1.60E-10	3.58E-03	3.58E-03
dCu (nM)	50.10	5	1.30E-09	7.84E-01	2.90E-05	1	8.44E-01	6.97E-01	3.40E-04	7.86E-01	2.03E-02	1	2.30E-08	3.40E-11	2.55E-03	2.91E-01	7.84E-01	1.75E-02
L_{Cu} (nM)	26.80	5	6.26E-05	1	1	1	5.62E-02	1	1	1	5.60E-03	1	1	6.60E-06	3.00E-01	2.40E-05	2.83E-01	1.58E-01
eL_{Cu} (nM)	20.40	5	1.04E-03	1	7.45E-01	1	2.67E-01	6.39E-01	1	6.39E-01	4.77E-01	9.55E-01	2.80E-03	1	1	1.70E-03	1.38E-02	1
Cu' (fM)	26.80	5	6.37E-05	1	4.28E-01	1	1	1	3.61E-02	1	1	1	3.60E-06	1	4.51E-01	3.61E-02	3.14E-01	1
Cu^{2+} (fM)	26.80	5	6.22E-05	1	4.22E-01	1	1	1	3.53E-02	1	1	1	3.40E-06	1	4.45E-01	3.57E-02	3.14E-01	1
log K^{cond}_{Cu2+L}	7.26	5	2.02E-01	-	-	-	-	-	-	-	-	-	-	-	-	-	-	-
log α_{Cu2+L}	8.12	5	1.50E-01	-	-	-	-	-	-	-	-	-	-	-	-	-	-	-

b)

Shelf	Kruskal-Wallis test			Conover's test
Parameter	χ^2	df	p-value	AAW-PSW
Temperature (°C)	8.47	1	3.61E-03	7.90E-04
Salinity	8.47	1	3.61E-03	7.90E-04
Fluorescence (au)	-	-	-	-
O_2 (µM)	8.47	1	3.61E-03	7.90E-04
NO^-_3+NO^-_2 (µM)	8.47	1	3.61E-03	7.90E-04
PO^{3-}_4 (µM)	8.48	1	3.59E-03	7.80E-04
$Si(OH)_4$ (µM)	6.19	1	1.29E-02	7.30E-03
dCu (nM)	8.47	1	3.61E-03	7.90E-04
L_{Cu} (nM)	8.47	1	3.61E-03	7.90E-04
eL_{Cu} (nM)	6.49	1	1.09E-02	5.60E-03
Cu' (fM)	0.01	1	9.04E-01	-
Cu^{2+} (fM)	0.13	1	7.16E-01	-
log K^{cond}_{Cu2+L}	1.78	1	1.82E-01	-
log α_{Cu2+L}	0.53	1	4.67E-01	-

c)

Coast	Kruskal-Wallis test			Conover's test
Parameter	χ^2	df	p-value	AAW-PSW
Temperature (°C)	4.80	1	2.85E-02	2.12E-02
Salinity	4.80	1	2.85E-02	2.12E-02
Fluorescence (au)	0.50	1	4.80E-01	-
O_2 (µM)	4.80	1	2.85E-02	2.12E-02
NO^-_3+NO^-_2 (µM)	4.80	1	2.85E-02	2.12E-02
PO^{3-}_4 (µM)	3.33	1	6.79E-02	-
$Si(OH)_4$ (µM)	4.80	1	2.85E-02	2.12E-02
dCu (nM)	4.80	1	2.85E-02	2.12E-02
L_{Cu} (nM)	4.03	1	4.46E-02	3.85E-02
eL_{Cu} (nM)	1.63	1	2.01E-01	-
Cu' (fM)	0.00	1	1.00E+00	-
Cu^{2+} (fM)	0.00	1	1.00E+00	-
log K^{cond}_{Cu2+L}	0.13	1	7.15E-01	-
log α_{Cu2+L}	2.13	1	1.44E-01	-

Appendix B – Chapter 4

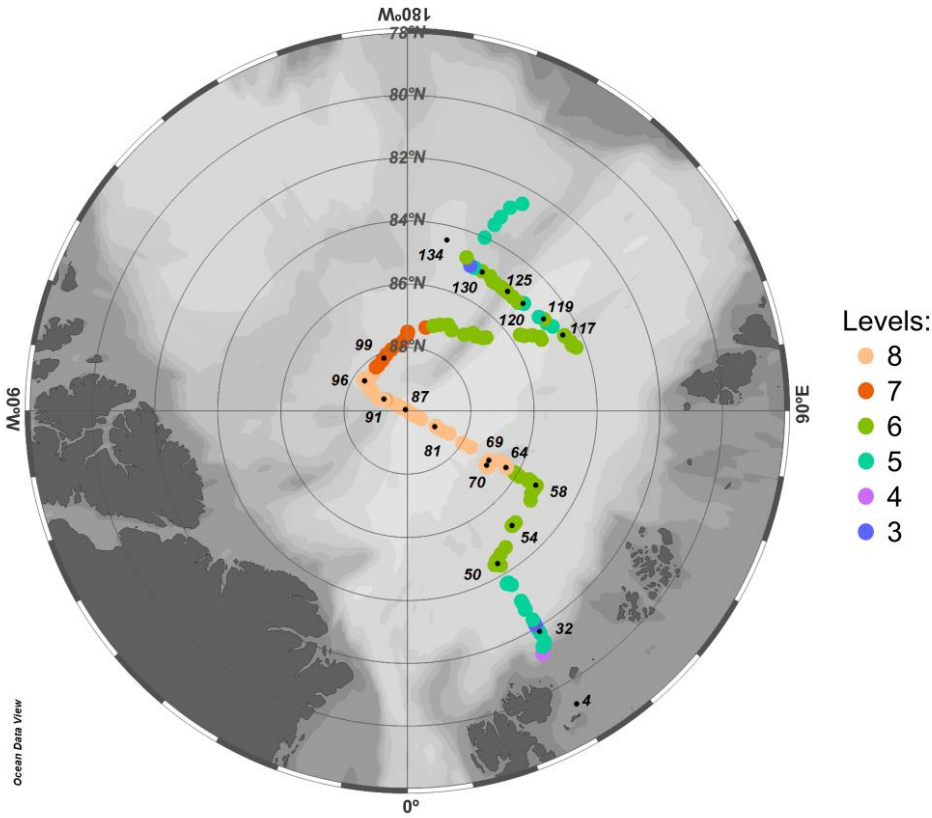

Figure B.1. Sea-ice stage development based on synoptic observations made onboard, according to the definitions of the Word Meteorological Organization WMO (König-Langlo, 2015). Description of levels of sea-ice stage. 3) Predominantly new and/or young ice with some first-year ice. 4) Predominantly thin first-year ice with some new and/or young ice. 5) All thin first-year ice (30-70 cm thick). 6) Predominantly medium first-year ice (70-120 cm thick) and thick first-year ice (more than 120 cm thick) with some thinner (younger) first-year ice. 7) All medium and first-year ice. 8) Predominantly medium and thick first-year ice with some old ice (usually more than 2 meters thick).

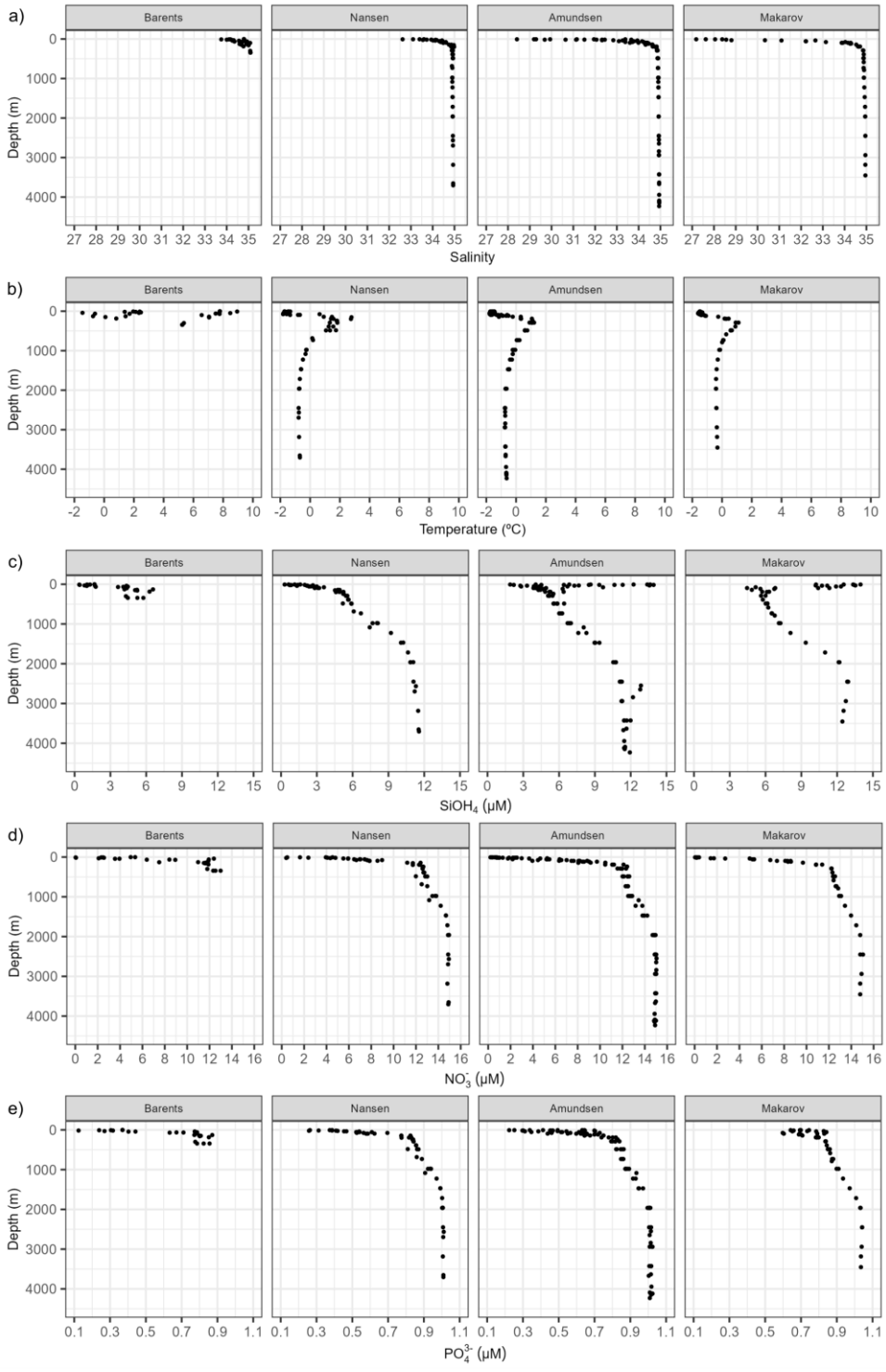
a)
Barents
Nansen
Amundsen
Makarov
Depth (m)
0
1000
2000
3000
4000
27 28 29 30 31 32 33 34 35
Salinity
b)
-2 0 2 4 6 8 10
Temperature (°C)
c)
0 3 6 9 12 15
SiOH4 (µM)
d)
0 2 4 6 8 10 12 14 16
NO3- (µM)
e)
0.1 0.3 0.5 0.7 0.9 1.1
PO43- (µM)

Figure B.2. Depth profiles of (a) salinity, (b) temperature (in ºC), (c) silicate ($SiOH^4$, in µM), (d) nitrate (NO_3^-, in µM), (e) phosphate (PO_4^{3-}, in µM) depicted per basins. Nutrient data was reported by van Ooijen et al. (2016). Barents Sea (St. 4, 147, 169 and 173), Nansen Basin (St. 32, 50 54, 58, 64), Amundsen Basin (St. 69, 70, 81, 87, 91, 117, 119, 121, 125) and Makarov Basin (St. 96, 99, 130, 134).

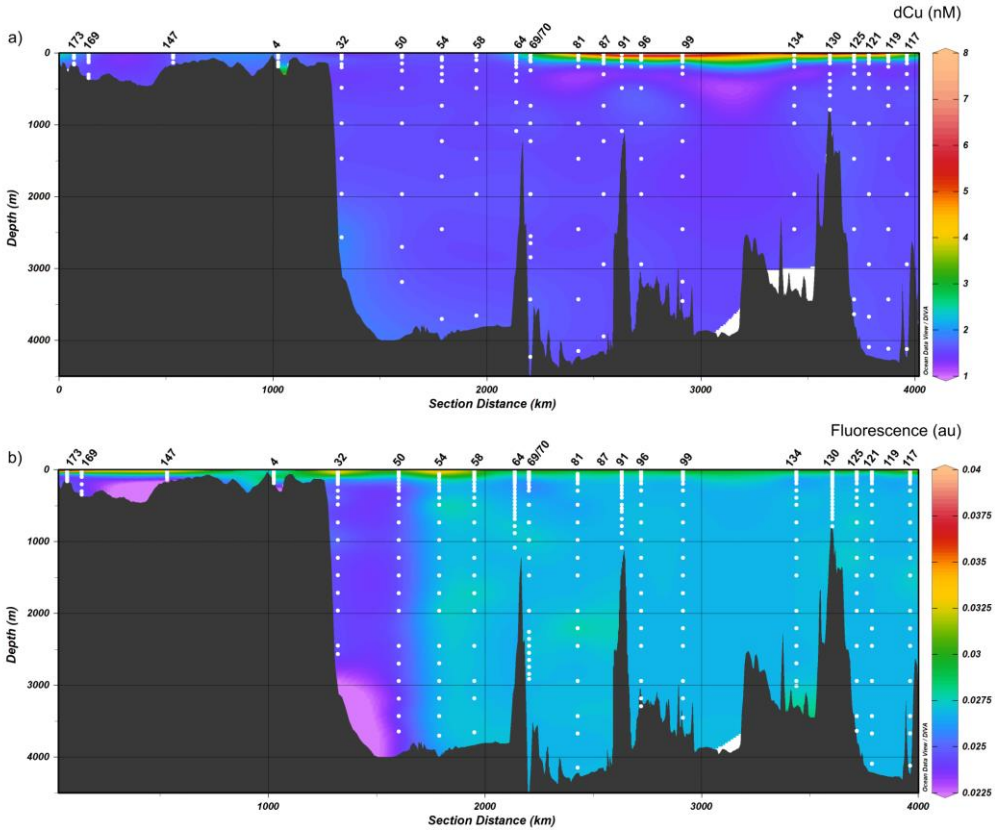

Figure B.3. Distribution of (a) dissolved Cu (in nM, data reported by Gerringa et al. (2021b) and (b) fluorescence (in arbitrary units, data reported by Rabe et al. (2016) in the Arctic Ocean, including all stations and basins. Note that the purple colour in figure b represents zones with missing data.

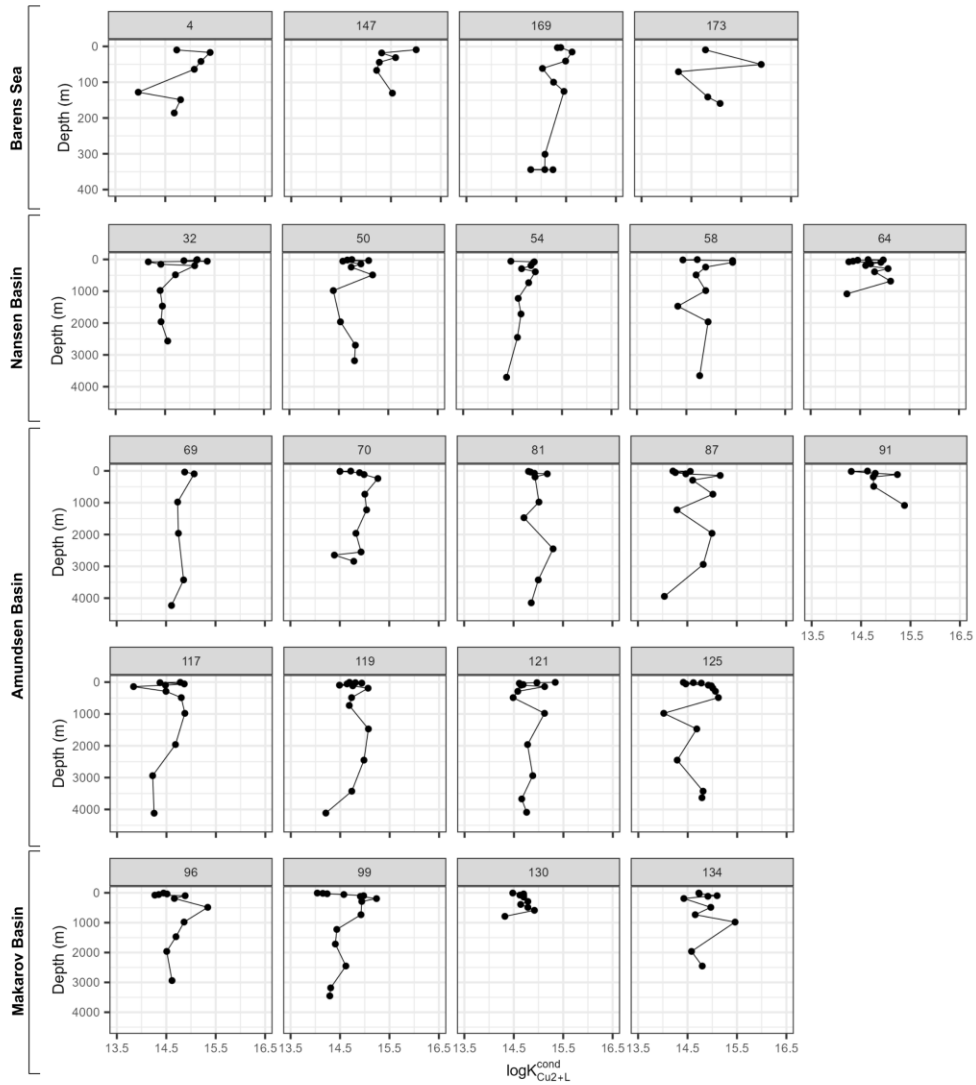

Figure B.4. Depth profile of Cu-binding ligand conditional stability constant (log K^{cond}_{Cu2+L}) represented by station and grouped by seas and basins. Barents Sea profiles represented with a different vertical scale.

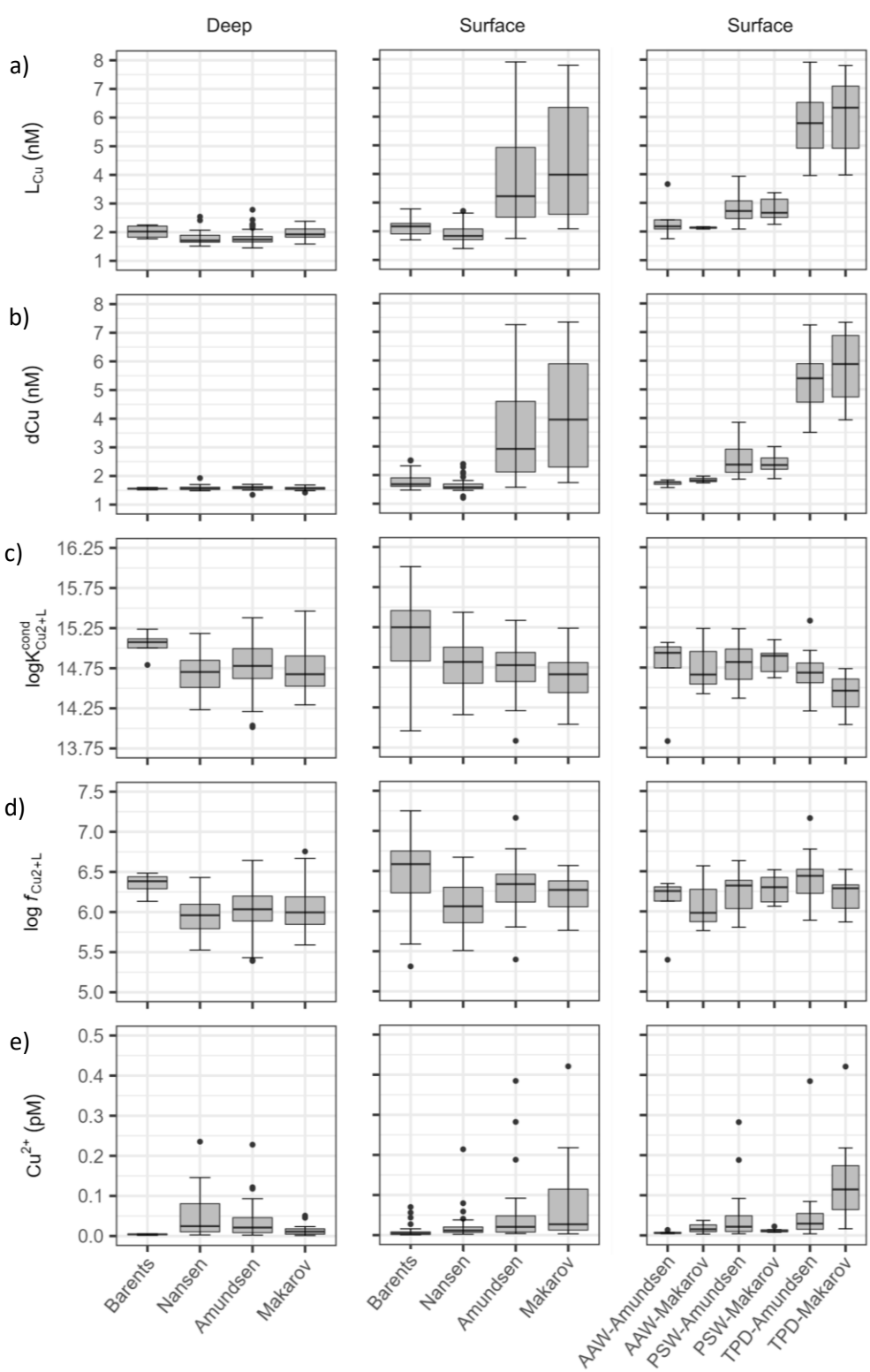
Deep
Surface
Surface
a)
L_{Cu} (nM)
b)
dCu (nM)
c)
$\log K^{cond}_{Cu2+L}$
d)
$\log f_{Cu2+L}$
e)
Cu^{2+} (pM)
Barents
Nansen
Amundsen
Makarov
Barents
Nansen
Amundsen
Makarov
AAW-Amundsen
AAW-Makarov
PSW-Amundsen
PSW-Makarov
TPD-Amundsen
TPD-Makarov

Figure B.5. Boxplot of Cu-binding ligands (L_{Cu}) and dissolved Cu (dCu) concentrations in nM (a-b), conditional stability constant (log K^{cond}_{Cu2+L}, c), side reaction coefficient (log α_{Cu2+L}, d), and the concentration of free cupric ion in pM (Cu^{2+}, e). Dots indicate outliers. The left column depict data from deep waters (>200m depth) per basin, the central column represents surface samples (≤200m depth) per basin, while the right column shows data from surface waters (≤200m depth) of Amundsen and Makarov Basins per basin and water masses (AAW: Arctic Atlantic Water, PSW: Polar Surface Water). The label TPD indicate surface waters inside the flow path, while PSW indicates surface waters outside the TPD. Dissolved Cu data were reported by Gerringa et al. (2021b).

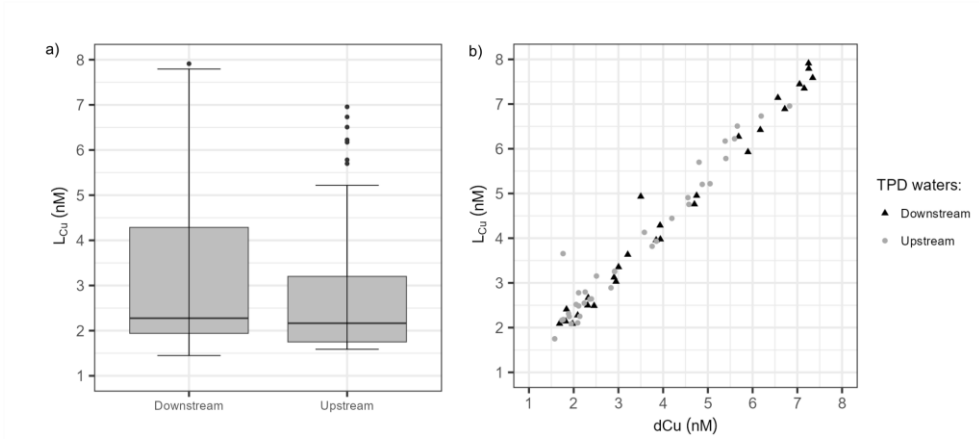

Figure B.6. Representation of surface waters located inside the Transpolar Drift (TPD) classified into downstream (St. 81 – 99) and upstream (St. 119 – 134) sections. a) Boxplot of Cu-binding ligand (L_{Cu}) in nM. b) Relationship between dissolved Cu (dCu) and L_{Cu} concentrations in nM.

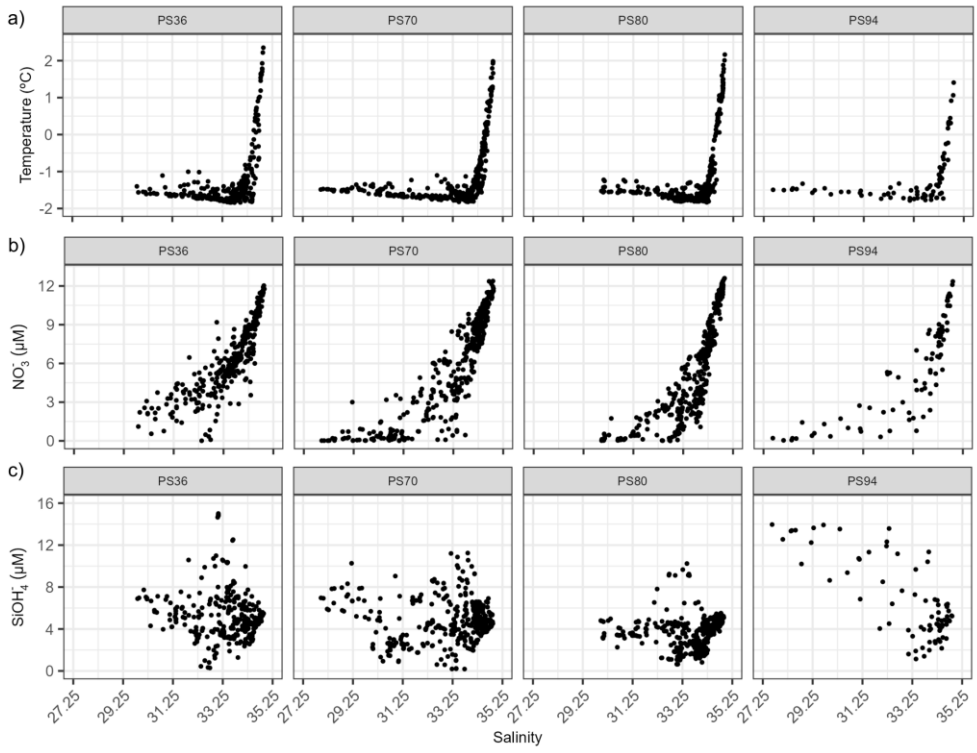

Figure B.7. Comparison of the properties recorded in the different cruises used as an example in the application of the linear model for the estimation of the concentration of copper-binding ligands. Four cruises were included: the PS36 took place in 1995 (Kattner, 2011), the PS70 in 2007 (Wisotzki and Bakker, 2008), the PS80 in 2012 (Bakker, 2014) and the PS94 (the study at hand). The properties represented against salinity were: a) temperature (ºC), b) nitrate concentration (NO3-, µM), and c) silicate concentration (SiOH4, µM).

Table B.1. Summary of range (minimum and maximum), mean and standard deviation (SD) and median of Cu speciation parameters for surface samples (≤ 200 m) of different basins and water masses. Barents Sea (BS, St. 4, 147, 169 and 173), Nansen Basin (NB, St. 32, 50 54, 58, 64), Amundsen Basin (AB, St. 69, 70, 81, 87, 91, 117, 119, 121, 125) and Makarov Basin (MB, St. 91, 96, 99, 130, 134). The surface water masses were: Polar Surface Water (PSW), Atlantic Water (AW) and Arctic Atlantic Water (AAW). Dissolved Cu data were reported by Gerringa et al. (2021b). The number of samples for each water mass inside the respective basin (n) was included in the second column.

Surface	Water mass		dCu (nM)	L_{Cu} (nM)	$\log K^{cond}_{Cu2+L}$	$\log f_{Cu2+L}$	eL_{Cu} (nM)	L_{Cu}/dCu	%CuL	Cu' (pM)	Cu^{2+} (pM)
BS	PSW (n=3)	Min	1.57	1.82	13.96	5.31	0.25	1.16	99.88	0.12	0.004
		Max	1.95	2.25	15.22	6.48	0.33	1.18	99.99	2.24	0.07
		Mean±SD	1.77±0.19	2.06±0.22	14.75±0.69	6.06±0.65	0.30±0.04	1.17±0.02	99.96±0.06	0.84±1.22	0.03±0.04
		Median	1.78	2.11	15.08	6.41	0.31	1.16	99.99	0.14	0.004
BS	AW (n=18)	Min	1.48	1.7	14.24	5.59	0.04	1.02	99.89	0.03	0.001
		Max	2.52	2.78	16.01	7.25	0.82	1.45	100	1.8	0.056
		Mean±SD	1.78±0.29	2.10±0.31	15.26±0.43	6.58±0.42	0.32±0.22	1.19±0.13	99.98±0.03	0.31±0.49	0.01±0.01
		Median	1.67	2.11	15.32	6.67	0.29	1.17	99.99	0.14	0.004
BS	AAW (n=4)	Min	1.61	2.22	14.68	6.11	0.19	1.08	99.97	0.03	0.001
		Max	2.51	2.7	15.53	6.88	0.75	1.46	100	0.87	0.027
		Mean±SD	1.93±0.41	2.46±0.21	15.06±0.39	6.45±0.35	0.53±0.24	1.30±0.16	99.99±0.02	0.27±0.40	0.01± 0.01
		Median	1.79	2.46	15.01	6.40	0.60	1.33	99.99	0.09	0.003
NB	PSW (n=21)	Min	1.2	1.4	14.27	5.65	0.02	1.01	99.57	0.07	0.002
		Max	2.39	2.71	15.44	6.67	0.54	1.34	100	6.85	0.214
		Mean±SD	1.70±0.33	1.94± 0.38	14.84±0.35	6.12± 0.31	0.24± 0.15	1.15± 0.09	99.95± 0.09	0.78± 1.45	0.02± 0.04
		Median	1.58	1.82	14.88	6.15	0.22	1.14	99.98	0.39	0.012
NB	AW (n=2)	Min	1.46	1.71	14.41	5.76	0.25	1.17	99.98	0.15	0.005
		Max	1.52	2.23	15.1	6.33	0.71	1.47	99.99	0.26	0.008
		Mean±SD	1.49±0.04	1.97± 0.37	14.76±0.48	6.05± 0.40	0.48± 0.33	1.32± 0.21	99.99± 0.00	0.21± 0.08	0.01± 0.00
		Median	1.49	1.97	14.76	6.05	0.48	1.32	99.99	0.21	0.006
NB	AAW (n=5)	Min	1.53	1.58	14.16	5.51	0.05	1.03	99.88	0.3	0.009
		Max	2.05	2.23	14.95	6.19	0.35	1.23	99.98	2.55	0.08
		Mean±SD	1.67± 0.22	1.88± 0.24	14.66± 0.31	5.93± 0.26	0.21± 0.11	1.13± 0.07	99.95± 0.05	0.97± 0.97	0.03± 0.03
		Median	1.56	1.92	14.71	6	0.19	1.12	99.98	0.37	0.012

Table B.1. Continued.

Surface	Water mass		dCu (nM)	L_{Cu} (nM)	$logK^{cond}_{Cu2+L}$	$log\ f_{Cu2+L}$	eL_{Cu} (nM)	L_{Cu}/dCu	%CuL	Cu' (pM)	Cu^{2+} (pM)
AM	PSW (n=41)	Min	1.87	2.09	14.21	5.8	0.02	1.01	99.57	0.13	0.004
		Max	7.25	7.91	15.34	7.16	1.43	1.41	100	12.31	0.385
		Mean±SD	3.67±1.59	4.02±1.69	14.75±0.27	6.32±0.27	0.35±0.29	1.10±0.09	99.95±0.07	1.57±2.39	0.05±0.07
		Median	3.09	3.26	14.78	6.36	0.34	1.09	99.98	0.82	0.026
AM	AAW (5)	Min	1.58	1.75	13.83	5.4	0.17	1.11	99.98	0.13	0.004
		Max	1.84	3.65	15.06	6.35	1.89	2.07	99.99	0.44	0.014
		Mean±SD	1.73±0.10	2.42±0.73	14.72±0.51	6.09±0.39	0.69±0.69	1.39±0.39	99.99±0.01	0.23±0.12	0.01±0.00
		Median	1.76	2.18	14.93	6.25	0.41	1.24	99.99	0.19	0.006
MB	PSW (n=20)	Min	1.89	2.25	14.04	5.87	0.04	1.01	99.66	0.25	0.008
		Max	7.34	7.79	15.1	6.52	0.64	1.26	99.99	13.47	0.421
		Mean±SD	4.44±1.95	4.74±1.96	14.60±0.29	6.24±0.20	0.29±0.17	1.08±0.07	99.94±0.08	2.72±3.33	0.08±0.10
		Median	4.45	4.6	14.66	6.29	0.25	1.06	99.97	0.97	0.03
MB	AAW (n=3)	Min	1.74	2.09	14.43	5.76	0.11	1.06	99.94	0.11	0.003
		Max	1.97	2.16	15.24	6.57	0.43	1.25	99.99	1.19	0.037
		Mean±SD	1.84±0.12	2.13±0.04	14.78±0.42	6.10±0.42	0.29±0.16	1.16±0.10	99.97±0.03	0.59±0.55	0.02±0.02
		Median	1.82	2.14	14.66	5.98	0.32	1.18	99.97	0.49	0.015

Table B.2. Three different linear regression model were developed to determine the relationship between Cu-binding ligand concentration (L_{Cu} in nM), physical water properties (temperature in ºC, or salinity) and nutrient concentrations (µM). Different nutrients were considered: nitrate (NO_3^-), silicate ($SiOH_4$) and phosphate (PO_4^{3-}). These equations were developed considering surface waters (≤ 200 m depth) from station 58 to 134. The parameters included were chosen according to the Bayesian Information Criterion (Sakamoto et al., 1986).

EQ	Formula
1	$L_{Cu} = 10.87321 - 0.244 \cdot Salinity - 0.1519 \cdot NO_3^- + 0.25263 \cdot SiOH_4$
2	$L_{Cu} = 3.93719 + 0.44556 \cdot Temperature - 0.31863 \cdot NO_3^- + 0.30287 \cdot SiOH_4$
3	$L_{Cu} = 16.45641 + 0.404 \cdot Salinity + 0.29444 \cdot SiOH_4 - 2.38481 \cdot PO_4^{3-}$
4	$L_{Cu} = 3.78431 + 0.430 \cdot Temperature - 0.34127 \cdot NO_3^- + 0.27951 \cdot SiOH_4 + 0.68346 \cdot PO_4^{3-}$
5	$L_{Cu} = 12.63534 - 0.2932 \cdot Salinity - 0.09855 \cdot NO_3^- + 0.27274 \cdot SiOH_4 - 0.95829 \cdot PO_4^{3-}$
6	$L_{Cu} = 16.61124 - 0.40326 \cdot Salinity + 0.06208 \cdot Temperature + 0.30187 \cdot SiOH_4 - 2.64021 \cdot PO_4^{3-}$
7	$L_{Cu} = 2.88253 - 0.24144 \cdot NO_3^- + 0.31985 \cdot SiOH_4$
8	$L_{Cu} = 2.66181 - 0.28919 \cdot NO_3^- + 0.27465 \cdot SiOH_4 + 1.29088 \cdot PO_4^{3-}$
9	$L_{Cu} = 18.39616 - 0.49585 \cdot Salinity - 0.21479 \cdot Temperature + 0.20122 \cdot SiOH4$
10	$L_{Cu} = 20.38904 - 0.54619 \cdot Salinity + 0.18718 \cdot SiOH_4$

Table B.3. Values of the linear regression models reported in Table B.2, which include the relation between the model parameters and coefficients. This table include the value of each parameter and statistical information corresponding to the equation (EQ) reported in Table B.2. The coefficients p-values (<0.05) indicate that in each equation all parameters included are significant. The model column includes the residual standard error (RSE) in terms of degrees of freedom (df), the adjusted R^2 and p-value of the model.

EQ	Coefficients				Coefficients p-values					Model		
	A	B	C	D	Intercept	A	B	C	D	RSE	Adjusted R^2	p-value
1	Salinity	NO_3^-	$SiOH_4$		1.27E-04	3.71E-03	4.96E-05	1.22E-12		0.4734 on 60 df	0.936	<2.2e-16
2	Temperature	NO_3^-	$SiOH_4$		<2e-16	4.84E-04	<2e-16	<2e-16		0.4587 on 60 df	0.9399	<2.2e-16
3	Salinity	$SiOH_4$	PO_4^{3-}		4.77E-13	4.31E-10	1.01E-11	8.31E-05		0.4773 on 60 df	0.9349	< 2.2e-16
4	Temperature	NO_3^-	$SiOH_4$	PO_4^{3-}	4.48E-13	9.12E-04	4.95E-11	5.95E-10	0.4887	0.4607 on 59 df	0.9394	<2.2e-16
5	Salinity	NO_3^-	$SiOH_4$	PO_4^{3-}	7.40E-04	6.57E-03	0.2180	2.77E-09	0.4557	0.4751 on 59 df	0.9355	< 2.2e-16
6	Salinity	Temperature	$SiOH_4$	PO_4^{3-}	8.01E-13	5.98E-10	0.6078	7.31E-11	8.82E-04	0.4802 on 59 df	0.9341	< 2.2e-16
7	NO_3^-	$SiOH_4$			<2e-16	<2e-16	<2e-16			0.5039 on 61 df	0.9274	< 2.2e-16
8	NO_3^-	$SiOH_4$	PO_4^{3-}		8.54E-14	9.25E-09	9.16E-09	0.2240		0.5019 on 60 df	0.928	< 2.2e-16
9	Salinity	Temperature	$SiOH_4$		9.06E-14	1.31E-13	3.38E-02	5.56E-10		0.5234 on 60 df	0.9217	< 2.2e-16
10	Salinity	$SiOH_4$			<2e-16	<2e-16	3.98E-09			0.5392 on 61 df	0.917	< 2.2e-16

References

Abualhaija, M. M., Whitby, H., and van den Berg, C. M. G. (2015). Competition between copper and iron for humic ligands in estuarine waters. *Mar Chem* 172, 46–56. doi: 10.1016/j.marchem.2015.03.010.

Aciego, S. M., Stevenson, E. I., and Arendt, C. A. (2015). Climate versus geological controls on glacial meltwater micronutrient production in southern Greenland. *Earth Planet Sci Lett* 424, 51–58. doi: 10.1016/j.epsl.2015.05.017.

Amon, R. M. W. (2003). Dissolved organic carbon distribution and origin in the Nordic Seas: Exchanges with the Arctic Ocean and the North Atlantic. *J Geophys Res* 108, 3221. doi: 10.1029/2002JC001594.

Anderson, L. G., and Amon, R. M. W. (2015). "Chapter 14 - DOM in the Arctic Ocean," in *Biogeochemistry of Marine Dissolved Organic Matter (Second Edition)*, eds. D. A. Hansell and C. A. Carlson (Boston: Academic Press), 609–633. doi: https://doi.org/10.1016/B978-0-12-405940-5.00014-5.

Annett, A. L., Lapi, S., Ruth, T. J., and Maldonado, M. T. (2008). The effects of Cu and Fe availability on the growth and Cu:C ratios of marine diatoms. *Limnol Oceanogr* 53, 2451–2461. doi: 10.4319/lo.2008.53.6.2451.

Apte, S. C., Gardner, M. J., and Ravenscroft, J. E. (1988). An evaluation of voltammetric titration procedures for the determination of trace metal complexation in natural waters by use of computers simulation. *Anal Chim Acta* 212, 1–21. doi: 10.1016/S0003-2670(00)84124-0.

Ardiningsih, I., Krisch, S., Lodeiro, P., Reichart, G. J., Achterberg, E. P., Gledhill, M., et al. (2020). Natural Fe-binding organic ligands in Fram Strait and over the northeast Greenland shelf. *Mar Chem* 224, 103815. doi: 10.1016/j.marchem.2020.103815.

Ardiningsih, I., Zhu, K., Lodeiro, P., Gledhill, M., Reichart, G. J., Achterberg, E. P., et al. (2021). Iron speciation in Fram Strait and over the Northeast Greenland Shelf: an inter-comparison study of voltammetric methods. *Front Mar Sci* 7. doi: 10.3389/fmars.2020.609379.

Ardyna, M., and Arrigo, K. R. (2020). Phytoplankton dynamics in a changing Arctic Ocean. *Nat Clim Chang* 10, 892–903. doi: 10.1038/s41558-020-0905-y.

Arístegui, J., and Montero, M. F. (2005). Temporal and spatial changes in plankton respiration and biomass in the Canary Islands region: the effect of mesoscale

variability. *Journal of Marine Systems* 54, 65–82. doi: 10.1016/j.jmarsys.2004.07.004.

Arístegui, J., Tett, P., Hernández-Guerra, A., Basterretxea, G., Montero, M. F., Wild, K., et al. (1997). The influence of island-generated eddies on chlorophyll distribution: a study of mesoscale variation around Gran Canaria. *Deep Sea Research Part I: Oceanographic Research Papers* 44, 71–96. doi: 10.1016/S0967-0637(96)00093-3.

Arnone, V., González-Santana, D., González-Dávila, M., González, A. G., and Santana-Casiano, J. M. (2022). Iron and copper complexation in Macaronesian coastal waters. *Mar Chem* 240, 104087. doi: 10.1016/j.marchem.2022.104087.

Arnone, V., Santana-Casiano, J. M., González-Dávila, M., Sarthou, G., Krisch, S., Lodeiro, P., et al. (2023). Distribution of copper-binding ligands in Fram Strait and influences from the Greenland Shelf (GEOTRACES GN05). *Science of The Total Environment*, 168162. doi: https://doi.org/10.1016/j.scitotenv.2023.168162.

Arreguin, M. L., González, A. G., Pérez-Almeida, N., Arnone, V., González-Dávila, M., and Santana-Casiano, J. M. (2021). The role of gentisic acid on the Fe(III) redox chemistry in marine environments. *Mar Chem* 234, 104003. doi: 10.1016/j.marchem.2021.104003.

Arrigo, K. R., van Dijken, G., and Pabi, S. (2008). Impact of a shrinking Arctic ice cover on marine primary production. *Geophys Res Lett* 35, L19603. doi: 10.1029/2008GL035028.

Baker, A. R., Jickells, T. D., Witt, M., and Linge, K. L. (2006). Trends in the solubility of iron, aluminium, manganese and phosphorus in aerosol collected over the Atlantic Ocean. *Mar Chem* 98, 43–58. doi: 10.1016/j.marchem.2005.06.004.

Bakker, K. (2014). Nutrients measured on water bottle samples during POLARSTERN cruise ARK-XXVII/3 (IceArc) in 2012. doi: 10.1594/PANGAEA.834081.

Barbeau, K. (2006). Photochemistry of Organic Iron(III) Complexing Ligands in Oceanic Systems. *Photochem Photobiol* 82, 1505. doi: 10.1562/2006-06-16-IR-935.

Basterretxea, G., Barton, E. D., Tett, P., Sangrá, P., Navarro-Perez, E., and Arístegui, J. (2002). Eddy and deep chlorophyl maximum response to wind-shear in the lee of Gran Canaria. *Deep Sea Research Part I: Oceanographic Research Papers* 49, 1087–1101. doi: 10.1016/S0967-0637(02)00009-2.

Bélanger, S., Xie, H., Krotkov, N., Larouche, P., Vincent, W. F., and Babin, M. (2006). Photomineralization of terrigenous dissolved organic matter in Arctic coastal waters from 1979 to 2003: Interannual variability and implications of climate change. *Global Biogeochem Cycles* 20, n/a-n/a. doi: 10.1029/2006GB002708.

Belter, H. J., Krumpen, T., von Albedyll, L., Alekseeva, T. A., Birnbaum, G., Frolov, S. V., et al. (2021). Interannual variability in Transpolar Drift summer sea ice thickness and potential impact of Atlantification. *Cryosphere* 15, 2575–2591. doi: 10.5194/tc-15-2575-2021.

Benner, R. (2011). Loose ligands and available iron in the ocean. *Proceedings of the National Academy of Sciences* 108, 893–894. doi: 10.1073/pnas.1018163108.

Benner, R., Louchouarn, P., and Amon, R. M. W. (2005). Terrigenous dissolved organic matter in the Arctic Ocean and its transport to surface and deep waters of the North Atlantic. *Global Biogeochem Cycles* 19. doi: 10.1029/2004GB002398.

Bennett, S. A., Achterberg, E. P., Connelly, D. P., Statham, P. J., Fones, G. R., and German, C. R. (2008). The distribution and stabilisation of dissolved Fe in deep-sea hydrothermal plumes. *Earth Planet Sci Lett* 270, 157–167. doi: 10.1016/j.epsl.2008.01.048.

Blain, S., Quéguiner, B., Armand, L., Belviso, S., Bombled, B., Bopp, L., et al. (2007). Effect of natural iron fertilization on carbon sequestration in the Southern Ocean. *Nature* 446, 1070–1074. doi: 10.1038/nature05700.

Blain, S., Sarthou, G., and Laan, P. (2008). Distribution of dissolved iron during the natural iron-fertilization experiment KEOPS (Kerguelen Plateau, Southern Ocean). *Deep Sea Research Part II: Topical Studies in Oceanography* 55, 594–605. doi: 10.1016/j.dsr2.2007.12.028.

Blain, S., Tréguer, P., Belviso, S., Bucciarelli, E., Denis, M., Desabre, S., et al. (2001). A biogeochemical study of the island mass effect in the context of the iron hypothesis: Kerguelen Islands, Southern Ocean. *Deep Sea Research Part I: Oceanographic Research Papers* 48, 163–187. doi: 10.1016/S0967-0637(00)00047-9.

Bluhm, B. A., Kosobokova, K. N., and Carmack, E. C. (2015). A tale of two basins: An integrated physical and biological perspective of the deep Arctic Ocean. *Prog Oceanogr* 139, 89–121. doi: 10.1016/j.pocean.2015.07.011.

Bowie, A. R., van der Merwe, P., Quéroué, F., Trull, T., Fourquez, M., Planchon, F., et al. (2015). Iron budgets for three distinct biogeochemical sites around the

Kerguelen Archipelago (Southern Ocean) during the natural fertilisation study, KEOPS-2. *Biogeosciences* 12, 4421–4445. doi: 10.5194/bg-12-4421-2015.

Bowie, A. R., Whitworth, D. J., Achterberg, E. P., Mantoura, R. F. C., and Worsfold, P. J. (2002). Biogeochemistry of Fe and other trace elements (Al, Co, Ni) in the upper Atlantic Ocean. *Deep Sea Research Part I: Oceanographic Research Papers* 49, 605–636. doi: 10.1016/S0967-0637(01)00061-9.

Boyd, P. W., and Ellwood, M. J. (2010). The biogeochemical cycle of iron in the ocean. *Nat Geosci* 3, 675–682. doi: 10.1038/ngeo964.

Boyd, P. W., Jickells, T., Law, C. S., Blain, S., Boyle, E. A., Buesseler, K. O., et al. (2007). Mesoscale iron enrichment experiments 1993-2005: Synthesis and future directions. *Science* 315, 612–617. doi: 10.1126/science.1131669.

Boyd, P. W., Watson, A. J., Law, C. S., Abraham, E. R., Trull, T., Murdoch, R., et al. (2000). A mesoscale phytoplankton bloom in the polar Southern Ocean stimulated by iron fertilization. *Nature* 407, 695–702. doi: 10.1038/35037500.

Boye, M., Aldrich, A., Berg, C. M. G. Van Den, Jong, J. T. M. De, Nirmaier, H., Veldhuis, M., et al. (2006). The chemical speciation of iron in the north-east Atlantic Ocean. *Deep-Sea Research I* 53, 667–683. doi: 10.1016/j.dsr.2005.12.015.

Boye, M., Aldrich, A. P., Berg, C. M. G. Van Den, Jong, J. T. M. De, Veldhuis, M., and Baar, H. J. W. De (2003). Horizontal gradient of the chemical speciation of iron in surface waters of the northeast Atlantic Ocean. *Mar Chem* 80, 129–143. doi: 10.1016/S0304-4203(02)00102-0.

Brand, L. E., Sunda, W. G., and Guillard, R. R. L. (1986). Reduction of marine phytoplankton reproduction rates by copper and cadmium. *J Exp Mar Biol Ecol* 96, 225–250. doi: 10.1016/0022-0981(86)90205-4.

Bruland, K. W., Franks, R. P., Knauer, G. A., and Martin, J. H. (1979). Sampling and analytical methods for the determination of copper, cadmium, zinc, and nickel at the nanogram per liter level in sea water. *Anal Chim Acta* 105, 233–245. doi: https://doi.org/10.1016/S0003-2670(01)83754-5.

Bruland, K. W., Middag, R., and Lohan, M. C. (2014). "Controls of Trace Metals in Seawater," in *Treatise on Geochemistry* (Elsevier), 19–51. doi: 10.1016/B978-0-08-095975-7.00602-1.

Bruland, K. W., Rue, E. L., Donat, J. R., Skrabal, S. A., and Moffett, J. W. (2000). Intercomparison of voltammetric techniques to determine the chemical

speciation of dissolved copper in a coastal seawater sample. *Anal Chim Acta* 405, 99–113. doi: http://dx.doi.org/10.1016/S0003-2670(99)00675-3.

Buck, K. N., and Bruland, K. W. (2005). Copper speciation in San Francisco Bay: A novel approach using multiple analytical windows. *Mar Chem* 96, 185–198. doi: 10.1016/j.marchem.2005.01.001.

Buck, K. N., Lohan, M. C., Berger, C. J. M., and Bruland, K. W. (2007). Dissolved iron speciation in two distinct river plumes and an estuary: Implications for riverine iron supply. *Limnol Oceanogr* 52, 843–855. doi: 10.4319/lo.2007.52.2.0843.

Buck, K. N., Moffett, J., Barbeau, K. A., Bundy, R. M., Kondo, Y., and Wu, J. (2012). The organic complexation of iron and copper: An intercomparison of competitive ligand exchange-adsorptive cathodic stripping voltammetry (CLE-ACSV) techniques. *Limnol Oceanogr Methods* 10, 496–515. doi: 10.4319/lom.2012.10.496.

Buck, K. N., Selph, K. E., and Barbeau, K. A. (2010). Iron-binding ligand production and copper speciation in an incubation experiment of Antarctic Peninsula shelf waters from the Bransfield Strait, Southern Ocean. *Mar Chem* 122, 148–159. doi: 10.1016/j.marchem.2010.06.002.

Buck, K. N., Sohst, B., and Sedwick, P. N. (2015). The organic complexation of dissolved iron along the U.S. GEOTRACES (GA03) North Atlantic Section. *Deep Sea Res 2 Top Stud Oceanogr* 116, 152–165. doi: 10.1016/j.dsr2.2014.11.016.

Buckley, P. J. M., and van den Berg, C. M. G. (1986). Copper complexation profiles in the Atlantic Ocean. *Mar Chem* 19, 281–296. doi: 10.1016/0304-4203(86)90028-9.

Bundy, R. M., Barbeau, K. A., and Buck, K. N. (2013). Sources of strong copper-binding ligands in Antarctic Peninsula surface waters. *Deep Sea Research Part II: Topical Studies in Oceanography* 90, 134–146. doi: 10.1016/j.dsr2.2012.07.023.

Bundy, R. M., Boiteau, R. M., McLean, C., Turk-Kubo, K. A., McIlvin, M. R., Saito, M. A., et al. (2018). Distinct siderophores contribute to iron cycling in the mesopelagic at station ALOHA. *Front Mar Sci* 5, 1–15. doi: 10.3389/fmars.2018.00061.

Cai, W. J., Chen, L., Chen, B., Gao, Z., Lee, S. H., Chen, J., et al. (2010). Decrease in the CO_2 uptake capacity in an ice-free Arctic Ocean basin. *Science* 329, 556–559. doi: 10.1126/science.1189338.

Caldeira, R. M. A., Groom, S., Miller, P., Pilgrim, D., and Nezlin, N. P. (2002). Sea-surface signatures of the island mass effect phenomena around Madeira Island, Northeast Atlantic. *Remote Sens Environ* 80, 336–360. doi: 10.1016/S0034-4257(01)00316-9.

Caldeira, R. M. A., and Sangrà, P. (2012). Complex geophysical wake flows. *Ocean Dyn* 62, 683–700. doi: 10.1007/s10236-012-0528-6.

Campos, M. L. A. M., and van den Berg, C. M. G. (1994). Determination of copper complexation in sea water by cathodic stripping voltammetry and ligand competition with salicylaldoxime. *Anal Chim Acta* 284, 481–496. doi: 10.1016/0003-2670(94)85055-0.

Cape, M. R., Straneo, F., Beaird, N., Bundy, R. M., and Charette, M. A. (2019). Nutrient release to oceans from buoyancy-driven upwelling at Greenland tidewater glaciers. *Nat Geosci* 12, 34–39. doi: 10.1038/s41561-018-0268-4.

Cauwet, G., and Sidorov, I. (1996). The biogeochemistry of Lena River: organic carbon and nutrients distribution. *Mar Chem* 53, 211–227. doi: 10.1016/0304-4203(95)00090-9.

Charette, M. A., Kipp, L. E., Jensen, L. T., Dabrowski, J. S., Whitmore, L. M., Fitzsimmons, J. N., et al. (2020). The Transpolar Drift as a source of riverine and shelf-derived trace elements to the Central Arctic Ocean. *J Geophys Res Oceans* 125, 1–34. doi: 10.1029/2019JC015920.

Cheize, M., Planquette, H. F., Fitzsimmons, J. N., Pelleter, E., Sherrell, R. M., Lambert, C., et al. (2019). Contribution of resuspended sedimentary particles to dissolved iron and manganese in the ocean: An experimental study. *Chem Geol* 511, 389–415. doi: 10.1016/j.chemgeo.2018.10.003.

Chen, X., Krisch, S., Al-Hashem, A., Hopwood, M. J., Rutgers van der Loeff, M. M., Huhn, O., et al. (2022). Dissolved, labile, and total particulate trace metal dynamics on the Northeast Greenland Shelf. *Global Biogeochem Cycles* 36. doi: 10.1029/2022GB007528.

Choi, D. W., Zea, C. J., Do, Y. S., Semrau, J. D., Antholine, W. E., Hargrove, M. S., et al. (2006). Spectral, kinetic, and thermodynamic properties of Cu(I) and Cu(II) binding by methanobactin from *Methylosinus trichosporium* OB3b. *Biochemistry* 45, 1442–1453. doi: 10.1021/bi051815t.

Clayton, T. D., and Byrne, R. H. (1993). Spectrophotometric seawater pH measurements: total hydrogen ion concentration scale calibration of m-cresol purple and at-sea results. *Deep Sea Research Part I: Oceanographic Research Papers* 40, 2115–2129. doi: 10.1016/0967-0637(93)90048-8.

Coale, K. H., and Bruland, K. W. (1990). Spatial and temporal variability in copper complexation in the North Pacific. *Deep Sea Research Part A. Oceanographic Research Papers* 37, 317–336. doi: 10.1016/0198-0149(90)90130-N.

Colombo, M., Brown, K. A., De Vera, J., Bergquist, B. A., and Orians, K. J. (2019). Trace metal geochemistry of remote rivers in the Canadian Arctic Archipelago. *Chem Geol* 525, 479–491. doi: 10.1016/j.chemgeo.2019.08.006

Conover, W., and Iman, R. (1979). Multiple-comparisons procedures. Informal report. Los Alamos, NM (United States). doi: 10.2172/6057803.

Conway, T. M., and John, S. G. (2014). Quantification of dissolved iron sources to the North Atlantic Ocean. *Nature* 511, 212–215. doi: 10.1038/nature13482.

Croot, P. L., and Johansson, M. (2000). Determination of Iron Speciation by Cathodic Stripping Voltammetry in Seawater Using the Competing Ligand 2-(2-Thiazolylazo)-p-cresol (TAC). *Electroanalysis* 12, 565–576. doi: 10.1002/(SICI)1521-4109(200005)12:8<565::AID-ELAN565>3.0.CO;2-L

Cutter, G. A., Casciotti, K., Croot, P., Geibert, W., Heimbürger, L. E., Lohan, M. C., et al. (2017). Sampling and sample-handling protocols for GEOTRACES Cruises, Version 3.0.

Cutter, G., Andersson, P., Codispoti, L., Croot, P., Francois, R., Lohan, M., et al. (2010). Sampling and Sample-handling Protocols for GEOTRACES Cruises.

Cutter, G., Andersson, P., Codispoti, L., Croot, P., Francois, R., Lohan, M., et al. (2014). Sampling and sample-handing protocols for GEOTRACES cruises. Available at: http://www.geotraces.org/images/stories/documents/intercalibration/Cookbook_v2.pdf.

Damm, E., Bauch, D., Krumpen, T., Rabe, B., Korhonen, M., Vinogradova, E., et al. (2018). The Transpolar Drift conveys methane from the Siberian Shelf to the central Arctic Ocean. *Sci Rep* 8, 4515. doi: 10.1038/s41598-018-22801-z.

Davis, J., and Benner, R. (2005). Seasonal trends in the abundance, composition and bioavailability of particulate and dissolved organic matter in the Chukchi/Beaufort Seas and western Canada Basin. *Deep Sea Research Part II: Topical Studies in Oceanography* 52, 3396–3410. doi: 10.1016/j.dsr2.2005.09.006.

de Baar, H. J. W., Boyd, P. W., Coale, K. H., Landry, M. R., Tsuda, A., Assmy, P., et al. (2005). Synthesis of iron fertilization experiments: from the iron age in the

age of enlightenment. *J Geophys Res Oceans* 110. doi: https://doi.org/10.1029/2004JC002601

Dethleff, D., Rachold, V., Tintelnot, M., and Antonow, M. (2000). Sea-ice transport of riverine particles from the Laptev Sea to Fram Strait based on clay mineral studies. *International Journal of Earth Sciences* 89, 496–502. doi: 10.1007/s005310000109.

Devez, A., Achterberg, E., and Gledhill, M. (2015). "15 Metal Ion-Binding Properties of Phytochelatins and Related Ligands," in *Metallothioneins and Related Chelators* (De Gruyter), 441–482.

Doney, S. C. (2010). The growing human footprint on coastal and open-ocean biogeochemistry. *Science* 328, 1512–1516. doi: 10.1126/science.1185198.

Doney, S. C., Ruckelshaus, M., Emmett Duffy, J., Barry, J. P., Chan, F., English, C. A., et al. (2012). Climate change impacts on marine ecosystems. *Ann Rev Mar Sci* 4, 11–37. doi: 10.1146/annurev-marine-041911-111611.

Dryden, C. L., Gordon, A. S., and Donat, J. R. (2007). Seasonal survey of copper-complexing ligands and thiol compounds in a heavily utilized, urban estuary: Elizabeth River, Virginia. *Mar Chem* 103, 276–288. doi: 10.1016/j.marchem.2006.09.003.

Duce, R. a, and Tindale, N. W. (1991). Atmospheric transport of iron and its deposition in the ocean. *Limnol Oceanogr* 36, 1715–1726. doi: 10.4319/lo.1991.36.8.1715

Dulaquais, G., Fourrier, P., Guieu, C., Mahieu, L., Riso, R., Salaun, P., et al. (2023). The role of humic-type ligands in the bioavailability and stabilization of dissolved iron in the Western Tropical South Pacific Ocean. *Front Mar Sci* 10. doi: 10.3389/fmars.2023.1219594.

Dupont, C. L., Moffett, James. W., Bidigare, R. R., and Ahner, B. A. (2006). Distributions of dissolved and particulate biogenic thiols in the subartic Pacific Ocean. *Deep Sea Research Part I: Oceanographic Research Papers* 53, 1961–1974. doi: 10.1016/j.dsr.2006.09.003.

Dupont, C. L., Nelson, R. K., Moffett, J. W., and Ahner, B. A. (2004). Novel copper-binding and nitrogen-rich thiols produced and exuded by Emiliania huxleyi. *Limnol Oceanogr* 49, 1754–1762. doi: doi.org/10.4319/lo.2004.49.5.1754.

Elrod, V. A., Berelson, W. M., Coale, K. H., and Johnson, K. S. (2004). The flux of iron from continental shelf sediments: A missing source for global budgets. *Geophys Res Lett* 31. doi: 10.1029/2004GL020216.

Evans, L. K., and Nishioka, J. (2019). Accumulation processes of trace metals into Arctic sea ice: distribution of Fe, Mn and Cd associated with ice structure. *Mar Chem* 209, 36–47. doi: 10.1016/j.marchem.2018.11.011.

Feng, D., Gleason, C. J., Lin, P., Yang, X., Pan, M., and Ishitsuka, Y. (2021). Recent changes to Arctic river discharge. *Nat Commun* 12, 6917. doi: 10.1038/s41467-021-27228-1.

Fransner, F., Fröb, F., Tjiputra, J., Goris, N., Lauvset, S. K., Skjelvan, I., et al. (2022). Acidification of the Nordic Seas. *Biogeosciences* 19, 979–1012. doi: 10.5194/bg-19-979-2022.

Frey, K. E., and McClelland, J. W. (2009). Impacts of permafrost degradation on arctic river biogeochemistry. *Hydrol Process* 23, 169–182. doi: 10.1002/hyp.7196.

Friedlingstein, P., O'Sullivan, M., Jones, M. W., Andrew, R. M., Bakker, D. C. E., Hauck, J., et al. (2023). Global Carbon Budget 2023. *Earth Syst Sci Data* 15, 5301–5369. doi: 10.5194/essd-15-5301-2023.

Gamrani, M., Eert, J., Williams, W. J., and Guéguen, C. (2023). A river of terrestrial dissolved organic matter in the upper waters of the central Arctic Ocean. *Deep Sea Research Part I: Oceanographic Research Papers* 196, 104016. doi: 10.1016/j.dsr.2023.104016.

Gao, Z., and Guéguen, C. (2018). Distribution of thiol, humic substances and colored dissolved organic matter during the 2015 Canadian Arctic GEOTRACES cruises. *Mar Chem* 203, 1–9. doi: 10.1016/j.marchem.2018.04.001.

Garnier, C., Pižeta, I., Mounier, S., Benaïm, J. Y., and Branica, M. (2004). Influence of the type of titration and of data treatment methods on metal complexing parameters determination of single and multi-ligand systems measured by stripping voltammetry. *Anal Chim Acta* 505, 263–275. doi: 10.1016/j.aca.2003.10.066.

Gelado-Caballero, M. D., López-García, P., Prieto, S., Patey, M. D., Collado, C., and Hérnández-Brito, J. J. (2012). Long-term aerosol measurements in Gran Canaria, Canary Islands: Particle concentration, sources and elemental composition. *Journal of Geophysical Research: Atmospheres* 117. doi: 10.1029/2011JD016646.

German, C. R., Campbell, A. C., and Edmond, J. M. (1991). Hydrothermal scavenging at the Mid-Atlantic Ridge: Modification of trace element dissolved fluxes. *Earth Planet Sci Lett* 107, 101–114. doi: 10.1016/0012-821X(91)90047-L.

German, C. R., and Von Damm, K. L. (2004). “Hydrothermal processes,” in *Treatise on geochemistry*, eds. H. D. Holland, K. K. Turekian, and H. Elderfield (Oxford, UK.: Elsevier-Pergamon), 182–216.

Gerringa, L. J. A., Blain, S., Laan, P., Sarthou, G., Veldhuis, M. J. W., Brussaard, C. P. D., et al. (2008). Fe-binding dissolved organic ligands near the Kerguelen Archipelago in the Southern Ocean (Indian sector). *Deep Sea Research Part II: Topical Studies in Oceanography* 55, 606–621. doi: 10.1016/j.dsr2.2007.12.007.

Gerringa, L. J. A., Rijkenberg, M. J. A., Thuróczy, C. E., and Maas, L. R. M. (2014). A critical look at the calculation of the binding characteristics and concentration of iron complexing ligands in seawater with suggested improvements. *Environmental Chemistry* 11, 114–136. doi: 10.1071/EN13072.

Gerringa, L. J. A., Rijkenberg, M. J. A., Wolterbeek, H. T., Verburg, T. G., Boye, M., and de Baar, H. J. W. (2007). Kinetic study reveals weak Fe-binding ligand, which affects the solubility of Fe in the Scheldt estuary. *Mar Chem* 103, 30–45. doi: 10.1016/j.marchem.2006.06.002.

Gerringa, L. J. A., Slagter, H. A., Bown, J., van Haren, H., Laan, P., de Baar, H. J. W., et al. (2017). Dissolved Fe and Fe-binding organic ligands in the Mediterranean Sea – GEOTRACES G04. *Mar Chem* 194, 100–113. doi: 10.1016/j.marchem.2017.05.012.

Gerringa, L. J. A., Veldhuis, M. J. W., Timmermans, K. R., Sarthou, G., and de Baar, H. J. W. (2006). Co-variance of dissolved Fe-binding ligands with phytoplankton characteristics in the Canary Basin. *Mar Chem* 102, 276–290. doi: 10.1016/j.marchem.2006.05.004

Gerringa, L. J. A., Rijkenberg, M. J. A., Slagter, H. A., Laan, P., Paffrath, R., Bauch, D., et al. (2021a). Dissolved Cd, Co, Cu, Fe, Mn, Ni, and Zn in the Arctic Ocean. *J Geophys Res Oceans* 126. doi: 10.1029/2021JC017323.

Gerringa, L. J. A., Rijkenberg, M., Laan, P., Middag, R., and Rutgers van der Loeff, M. M. (2021b). Dissolved trace metals cadmium (Cd), cobalt (Co), copper (Cu), iron (Fe), manganese (Mn), nickel (Ni), zinc (Zn) measured in samples from the Polarstern cruise PS94 to the Arctic Ocean from August to October 2015. Available at: https://doi.pangaea.de/10.1594/PANGAEA.932797.

Gledhill, M., Achterberg, E. P., Li, K., Mohamed, K. N., and Rijkenberg, M. J. A. (2015). Influence of ocean acidification on the complexation of iron and copper by organic ligands in estuarine waters. *Mar Chem* 177, 421–433. doi: 10.1016/j.marchem.2015.03.016.

Gledhill, M., and Buck, K. N. (2012). The organic complexation of iron in the marine environment: a review. *Front Microbiol* 3, 1–17. doi: 10.3389/fmicb.2012.00069.

Gledhill, M., and Gerringa, L. J. A. (2017). The Effect of Metal Concentration on the Parameters Derived from Complexometric Titrations of Trace Elements in Seawater—A Model Study. *Front Mar Sci* 4, 1–15. doi: 10.3389/fmars.2017.00254.

Gledhill, M., and van den Berg, C. M. G. (1994). Determination of complexation of iron(III) with natural organic complexing ligands in seawater using cathodic stripping voltammetry. *Mar Chem* 47, 41–54. doi: 10.1016/0304-4203(94)90012-4.

Goñi, M. A., O'Connor, A. E., Kuzyk, Z. Z., Yunker, M. B., Gobeil, C., and Macdonald, R. W. (2013). Distribution and sources of organic matter in surface marine sediments across the North American Arctic margin. *J Geophys Res Oceans* 118, 4017–4035. doi: 10.1002/jgrc.20286.

González, A. G., Cadena-Aizaga, M. I., Sarthou, G., González-Dávila, M., and Santana-Casiano, J. M. (2019). Iron complexation by phenolic ligands in seawater. *Chem Geol* 511, 380–388. doi: 10.1016/j.chemgeo.2018.10.017.

González, A. G., Pérez-Almeida, N., Magdalena Santana-Casiano, J., Millero, F. J., and González-Dávila, M. (2016). Redox interactions of Fe and Cu in seawater. *Mar Chem* 179, 12–22. doi: 10.1016/j.marchem.2016.01.004.

González, A. G., Santana-Casiano, J. M., Pérez, N., and González-Dávila, M. (2010a). Oxidation of Fe(II) in natural waters at high nutrient concentrations. *Environ Sci Technol* 44, 8095–8101. doi: 10.1021/es1009218.

González, A. G., Shirokova, L. S., Pokrovsky, O. S., Emnova, E. E., Martínez, R. E., Santana-Casiano, J. M., et al. (2010b). Adsorption of copper on Pseudomonas aureofaciens: Protective role of surface exopolysaccharides. *J Colloid Interface Sci* 350, 305–314. doi: 10.1016/j.jcis.2010.06.020.

González-Dávila, M., Santana-Casiano, J. M., González, A. G., Pérez, N., and Millero, F. J. (2009). Oxidation of copper(I) in seawater at nanomolar levels. *Mar Chem* 115, 118–124. doi: 10.1016/j.marchem.2009.07.004.

González-Dávila, M., Santana-Casiano, J. M., and Millero, F. J. (2005). Oxidation of iron(II) nanomolar with H_2O_2 in seawater. *Geochim Cosmochim Acta* 69, 83–93. doi: 10.1016/j.gca.2004.05.043.

González-Dávila, M., Santana-Casiano, J. M., and Millero, F. J. (2006). Competition between O_2 and H_2O_2 in the oxidation of Fe(II) in natural waters. *J Solution Chem* 35, 95–111. doi: 10.1007/s10953-006-8942-3.

González-Dávila, M., Santana-Casiano, J. M., Rueda, M. J., Llinás, O., and González-Dávila, E. F. (2003). Seasonal and interannual variability of sea-surface carbon dioxide species at the European Station for Time Series in the Ocean at the Canary Islands (ESTOC) between 1996 and 2000. *Global Biogeochem Cycles* 17. doi: 10.1029/2002GB001993.

González-Santana, D., Lough, A. J. M., Planquette, H., Sarthou, G., Tagliabue, A., and Lohan, M. C. (2023). The unaccounted dissolved iron(II) sink: Insights from dFe(II) concentrations in the deep Atlantic Ocean. *Science of The Total Environment* 862, 161179. doi: 10.1016/j.scitotenv.2022.161179.

González-Santana, D., Planquette, H., Cheize, M., Whitby, H., Gourain, A., Holmes, T., et al. (2020). Processes Driving Iron and Manganese Dispersal From the TAG Hydrothermal Plume (Mid-Atlantic Ridge): Results From a GEOTRACES Process Study. *Front Mar Sci* 7. doi: 10.3389/fmars.2020.00568

Gordienko, P. A., and Laktionov, A. F. (1969). "Circulation and physics of the Arctic Basin waters," in *Oceanography*, eds. A. L. Gordon and F. W. G. Baker (London: Pergamon), 94–112.

Gordon, R. M., Johnson, K. S., and Coale, K. H. (1998). The behaviour of iron and other trace elements during the IronEx-I and PlumEx experiments in the Equatorial Pacific. *Deep Sea Research Part II: Topical Studies in Oceanography* 45, 995–1041. doi: 10.1016/S0967-0645(98)00012-5.

Gordon, R. M., Martin, J. H., and Knauer, G. A. (1982). Iron in north-east Pacific waters. *Nature* 299, 611–612. doi: 10.1038/299611a0.

Gourain, C. G. (2020). Copper biogeochemical cycle and the organic complexation of dissolved copper in the North Atlantic. University of Liverpool. doi: 10.17638/03083646.

Gove, J. M., McManus, M. A., Neuheimer, A. B., Polovina, J. J., Drazen, J. C., Smith, C. R., et al. (2016). Near-island biological hotspots in barren ocean basins. *Nat Commun* 7, 1–8. doi: 10.1038/ncomms10581.

Graeve, M., Ludwichowski, K.-U., and Krisch, S. (2019). Inorganic nutrients measured on water bottle samples from ultra clean CTD/Water sampler-system during POLARSTERN cruise PS100 (ARK-XXX/2), version 2. doi: 10.1594/PANGAEA.905347.

Granskog, M. A., Stedmon, C. A., Dodd, P. A., Amon, R. M. W., Pavlov, A. K., de Steur, L., et al. (2012). Characteristics of colored dissolved organic matter (CDOM) in the Arctic outflow in the Fram Strait: Assessing the changes and fate of terrigenous CDOM in the Arctic Ocean. *J Geophys Res Oceans* 117, n/a-n/a. doi: 10.1029/2012JC008075.

Grasshoff, K., Kremling, K., and Ehrhardt, M. (1999). *Methods of Seawater Analysis*. Third, eds. K. Grasshoff, K. Kremling, and M. Ehrhardt Germany: Wiley. doi: 10.1002/9783527613984.

Guéguen, C., Guo, L., Yamamoto-Kawai, M., and Tanaka, N. (2007). Colored dissolved organic matter dynamics across the shelf-basin interface in the western Arctic Ocean. *J Geophys Res* 112, C05038. doi: 10.1029/2006JC003584.

Guieu, C., Huang, W. W., Martin, J. M., and Yong, Y. Y. (1996). Outflow of trace metals into the Laptev Sea by the Lena River. *Mar Chem* 53, 255–267. doi: 10.1016/0304-4203(95)00093-3.

Hart, T. J. (1934). On the phytoplankton of the southeast Atlantic and the Bellingshausen Sea, 1929-1931. *Discovery Reports* 8, 1–268.

Hassler, C. S., Schoemann, V., Nichols, C. M., Butler, E. C. V., and Boyd, P. W. (2011). Saccharides enhance iron bioavailability to Southern Ocean phytoplankton. *Proc Natl Acad Sci U S A* 108, 1076–1081. doi: 10.1073/pnas.1010963108.

Hatta, M., Measures, C. I., Wu, J., Roshan, S., Fitzsimmons, J. N., Sedwick, P., et al. (2015). An overview of dissolved Fe and Mn distributions during the 2010 – 2011 U.S. GEOTRACES north Atlantic cruises: GEOTRACES GA03. *Deep-Sea Research Part II* 116, 117–129. doi: 10.1016/j.dsr2.2014.07.005.

Hawkings, J. R., Skidmore, M. L., Wadham, J. L., Priscu, J. C., Morton, P. L., Hatton, J. E., et al. (2020). Enhanced trace element mobilization by Earth's ice sheets. *Proceedings of the National Academy of Sciences* 117, 31648–31659. doi: 10.1073/pnas.2014378117.

Heggie, D., Klinkhammer, G., and Cullen, D. (1987). Manganese and copper fluxes from continental margin sediments. *Geochim Cosmochim Acta* 51, 1059–1070. doi: 10.1016/0016-7037(87)90200-6.

Heller, M. I., and Croot, P. L. (2015). Copper speciation and distribution in the Atlantic sector of the Southern Ocean. *Mar Chem* 173, 253–268. doi: 10.1016/j.marchem.2014.09.017.

Hirose, K. (2011). Chemical modeling of marine trace metals: Effects of ocean acidification to marine ecosystem. in *2011 Seventh International Conference on Natural Computation* (IEEE), 2023–2026. doi: 10.1109/ICNC.2011.6022426.

Ho, T., Quigg, A., Finkel, Z. V., Milligan, A. J., Wyman, K., Falkowski, P. G., et al. (2003). The elemental composition of some marine phytoplankton. *J Phycol* 39, 1145–1159. doi: 10.1111/j.0022-3646.2003.03-090.x.

Hoffmann, L., Breitbarth, E., Boyd, P., and Hunter, K. (2012). Influence of ocean warming and acidification on trace metal biogeochemistry. *Mar Ecol Prog Ser* 470, 191–205. doi: 10.3354/meps10082.

Hoffmann, S. R., Shafer, M. M., and Armstrong, D. E. (2007). Strong colloidal and dissolved organic ligands binding copper and zinc in rivers. *Environ Sci Technol* 41, 6996–7002. doi: 10.1021/es070958v.

Hollister, A. P., Whitby, H., Seidel, M., Lodeiro, P., Gledhill, M., and Koschinsky, A. (2021). Dissolved concentrations and organic speciation of copper in the Amazon River estuary and mixing plume. *Mar Chem* 234, 104005. doi: 10.1016/j.marchem.2021.104005.

Hopwood, M. J., Carroll, D., Browning, T. J., Meire, L., Mortensen, J., Krisch, S., et al. (2018). Non-linear response of summertime marine productivity to increased meltwater discharge around Greenland. *Nat Commun* 9, 3256. doi: 10.1038/s41467-018-05488-8.

Hopwood, M. J., Carroll, D., Dunse, T., Hodson, A., Holding, J. M., Iriarte, J. L., et al. (2020). Review article: How does glacier discharge affect marine biogeochemistry and primary production in the Arctic? *Cryosphere* 14, 1347–1383. doi: 10.5194/tc-14-1347-2020.

Hudson, R. J. M., Covault, D. T., and Morel, F. M. M. (1992). Investigations of iron coordination and redox reactions in seawater using ^{59}Fe radiometry and ion-pair solvent extraction of amphiphilic iron complexes. *Mar Chem* 38, 209–235. doi: 10.1016/0304-4203(92)90035-9.

Hutchins, D. A., and Bruland, K. W. (1998). Iron-limited diatom growth and Si:N uptake ratios in a coastal upwelling regime. *Nature* 393, 561–564. doi: 10.1038/31203.

Hutchins, D. A., Witter, A. E., Butler, A., and Luther, G. W. (1999). Competition among marine phytoplankton for different chelated iron species. *Nature* 400, 858–861. doi: 10.1038/23680.

IPCC (2021). “Climate Change 2021: The Physical Science Basi” in *Contribution of Working Group I to the Sixth Assessment Report of the Intergovernmental Panel on Climate Change,* eds. V. Masson-Delmotte, P. Zhai, A. Pirani, S.L. Connors, C. Péan, S. Berger, et al. (Cambridge University Press), doi:10.1017/9781009157896.

IPCC (2022). “Impacts of 1.5°C Global Warming on Natural and Human Systems,” in *Global Warming of 1.5°C: IPCC Special Report on Impacts of Global Warming of 1.5°C above Pre-industrial Levels in Context of Strengthening Response to Climate Change, Sustainable Development, and Efforts to Eradicate Poverty*. Cambridge: Cambridge University Press. doi: 10.1017/9781009157940

Jacquot, J. E., and Moffett, J. W. (2015). Copper distribution and speciation across the International GEOTRACES Section GA03. *Deep Sea Research Part II: Topical Studies in Oceanography* 116, 187–207. doi: 10.1016/j.dsr2.2014.11.013.

Jakobsson, M. (2002). Hypsometry and volume of the Arctic Ocean and its constituent seas. *Geochemistry, Geophysics, Geosystems* 3, 1–18. doi: 10.1029/2001GC000302.

Jensen, L. T., Cullen, J. T., Jackson, S. L., Gerringa, L. J. A., Bauch, D., Middag, R., et al. (2022). A refinement of the processes controlling dissolved copper and nickel biogeochemistry: insights from the Pan-Arctic. *J Geophys Res Oceans* 127. doi: 10.1029/2021JC018087.

Jensen, L. T., Lanning, N. T., Marsay, C. M., Buck, C. S., Aguilar-Islas, A. M., Rember, R., et al. (2021). Biogeochemical cycling of colloidal trace metals in the Arctic cryosphere. *J Geophys Res Oceans* 126. doi: 10.1029/2021JC017394.

Jickells, T. D., An, Z. S., Andersen, K. K., Baker, A. R., Bergametti, C., Brooks, N., et al. (2005). Global iron connections between desert dust, ocean biogeochemistry, and climate. *Science* 308, 67–71. doi: 10.1126/science.1105959.

Johnson, K. S., Chavez, F. P., and Friederich, G. E. (1999). Continental-shelf sediment as a primary source of iron for coastal phytoplankton. *Nature* 398, 697–700. doi: 10.1038/19511.

Kanzow, T. (2016). The Expedition PS100 of the Research Vessel POLARSTERN to the Fram Strait in 2016. doi: 10.2312/BzPM_0705_2017.

Kattner, G. (2011). Inorganic nutrients measured on water bottle samples during POLARSTERN cruise ARK-XI/1. doi: 10.1594/PANGAEA.761680.

Kattner, G., Lobbes, J. M., Fitznar, H. P., Engbrodt, R., Nöthig, E.M., and Lara, R. J. (1999). Tracing dissolved organic substances and nutrients from the Lena River through Laptev Sea (Arctic). *Mar Chem* 65, 25–39. doi: 10.1016/S0304-4203(99)00008-0.

Keeling, R. F., Körtzinger, A., and Gruber, N. (2010). Ocean deoxygenation in a warming world. *Ann Rev Mar Sci* 2, 199–229. doi: 10.1146/annurev.marine.010908.163855.

Klunder, M. B., Laan, P., Middag, R., De Baar, H. J. W., and Bakker, K. (2012). Dissolved iron in the Arctic Ocean: Important role of hydrothermal sources, shelf input and scavenging removal. *J Geophys Res Oceans* 117, 1–17. doi: 10.1029/2011JC007135.

Kogut, M. B., and Voelker, B. M. (2001). Strong copper-binding behavior of terrestrial humic substances in seawater. *Environ Sci Technol* 35, 1149–1156. doi: 10.1021/es0014584.

Kogut, M. B., and Voelker, B. M. (2003). Kinetically Inert cu in coastal waters. *Environ Sci Technol* 37, 509–518. doi: 10.1021/es020723d.

Kondo, Y., Takeda, S., and Furuya, K. (2007). Distribution and speciation of dissolved iron in the Sulu Sea and its adjacent waters. *Deep Sea Research Part II: Topical Studies in Oceanography* 54, 60–80. doi: 10.1016/j.dsr2.2006.08.019.

Kong, L., and Price, N. M. (2020). A reduction-dependent copper uptake pathway in an oceanic diatom. *Limnol Oceanogr* 65, 601–611. doi: 10.1002/lno.11329.

König-Langlo, G. (2015). Meteorological observations during POLARSTERN cruise PS94 (ARK-XXIX/3). *Alfred Wegener Institute, Helmholtz Centre for Polar and Marine Research, Bremerhaven*. doi: https://doi.org/10.1594/PANGAEA.854304.

König-Langlo, G. (2016). Meteorological observations during POLARSTERN cruise PS100 (ARK-XXX/2). doi: 10.1594/PANGAEA.868103.

Kramer, C. J. M. (1986). Apparent copper complexation capacity and conditional stability constants in north Atlantic waters. *Mar Chem* 18, 335–349. doi: 10.1016/0304-4203(86)90016-2.

Krause, J., Hopwood, M. J., Höfer, J., Krisch, S., Achterberg, E. P., Alarcón, E., et al. (2021). Trace element (Fe, Co, Ni and Cu) dynamics across the salinity gradient in Arctic and Antarctic glacier fjords. *Front Earth Sci (Lausanne)* 9. doi: 10.3389/feart.2021.725279.

Krembs, C., Eicken, H., Junge, K., and Deming, J. W. (2002). High concentrations of exopolymeric substances in Arctic winter sea ice: implications for the polar ocean carbon cycle and cryoprotection of diatoms. *Deep Sea Research Part I: Oceanographic Research Papers* 49, 2163–2181. doi: 10.1016/S0967-0637(02)00122-X.

Kremling, K. (1985). The distribution of cadmium, copper, nickel, manganese, and aluminium in surface waters of the open Atlantic and European shelf area. *Deep Sea Research Part A. Oceanographic Research Papers* 32, 531–555. doi: 10.1016/0198-0149(85)90043-3.

Krisch, S., Browning, T. J., Graeve, M., Ludwichowski, K. U., Lodeiro, P., Hopwood, M. J., et al. (2020). The influence of Arctic Fe and Atlantic fixed N on summertime primary production in Fram Strait, North Greenland Sea. *Sci Rep* 10, 15230. doi: 10.1038/s41598-020-72100-9.

Krisch, S., Hopwood, M. J., Roig, S., Gerringa, L. J. A., Middag, R., Rutgers van der Loeff, M. M., et al. (2022). Arctic – Atlantic exchange of the dissolved micronutrients iron, manganese, cobalt, nickel, copper and zinc with a focus on Fram Strait. *Global Biogeochem Cycles* 36. doi: 10.1029/2021GB007191.

Krisch, S., Hopwood, M. J., Schaffer, J., Al-Hashem, A., Höfer, J., Rutgers van der Loeff, M. M., et al. (2021). The 79°N glacier cavity modulates subglacial iron export to the NE Greenland Shelf. *Nat Commun* 12, 3030. doi: 10.1038/s41467-021-23093-0.

Krumpen, T., Belter, H. J., Boetius, A., Damm, E., Haas, C., Hendricks, S., et al. (2019). Arctic warming interrupts the Transpolar Drift and affects long-range transport of sea ice and ice-rafted matter. *Sci Rep* 9, 5459. doi: 10.1038/s41598-019-41456-y.

Kruskal, W. H., and Wallis, W. A. (1952). Use of ranks in one-criterion variance analysis. *J Am Stat Assoc* 47, 583–621. doi: 10.1080/01621459.1952.10483441.

Kuma, K., Nakabayashi, S., and Matsunaga, K. (1995). Photoreduction of Fe(III) by hydroxycarboxylic acids in seawater. *War. Res* 29, 1559–1569. doi: 10.1016/0043-1354(94)00289-J.

Kuma, K., Nishioka, J., and Matsunaga, K. (1996). Controls on iron(III) hydroxide solubility in seawater: The influence of pH and natural organic chelators. *Limnol Oceanogr* 41, 396–407. doi: 10.4319/lo.1996.41.3.0396

Laglera, L. M., Battaglia, G., and van den Berg, C. M. G. (2007). Determination of humic substances in natural waters by cathodic stripping voltammetry of their complexes with iron. *Anal Chim Acta* 599, 58–66. doi: 10.1016/j.aca.2007.07.059

Laglera, L. M., Battaglia, G., and van den Berg, C. M. G. (2011). Effect of humic substances on the iron speciation in natural waters by CLE/CSV. *Mar Chem* 127, 134–143. doi: 10.1016/j.marchem.2011.09.003.

Laglera, L. M., and Monticelli, D. (2017). Iron detection and speciation in natural waters by electrochemical techniques: A critical review. *Curr Opin Electrochem* 3, 123–129. doi: 10.1016/j.coelec.2017.07.007.

Laglera, L. M., Sukekava, C., Slagter, H. A., Downes, J., Aparicio-Gonzalez, A., and Gerringa, L. J. A. (2019). First quantification of the controlling role of humic substances in the transport of iron across the surface of the Arctic Ocean. *Environ Sci Technol* 53, 13136–13145. doi: 10.1021/acs.est.9b04240.

Laglera, L. M., and van den Berg, C. M. G. (2003). Copper complexation by thiol compounds in estuarine waters. *Mar Chem* 82, 71–89. doi: 10.1016/S0304-4203(03)00053-7.

Laglera, L. M., and van den Berg, C. M. G. (2006). Photochemical oxidation of thiols and copper complexing ligands in estuarine waters. *Mar Chem* 101, 130–140. doi: 10.1016/j.marchem.2006.01.006.

Laglera, L. M., and van den Berg, C. M. G. (2009). Evidence for geochemical control of iron by humic substances in seawater. *Limnol Oceanogr* 54, 610–619. doi: 10.4319/lo.2009.54.2.0610.

Landing, W. M., and Bruland, K. W. (1987). The contrasting biogeochemistry of iron and manganese in the Pacific Ocean. *Geochim Cosmochim Acta* 51, 29–43. doi: https://doi.org/10.1016/0016-7037(87)90004-4.

Laukert, G., Frank, M., Bauch, D., Hathorne, E. C., Rabe, B., von Appen, W. J., et al. (2017). Ocean circulation and freshwater pathways in the Arctic Mediterranean based on a combined Nd isotope, REE and oxygen isotope section across Fram Strait. *Geochim Cosmochim Acta* 202, 285–309. doi: 10.1016/j.gca.2016.12.028.

Leal, M. F. C., Vasconcelos, M. T. S. D., and van den Berg, C. M. G. (1999). Copper-induced release of complexing ligands similar to thiols by *Emiliania huxleyi* in seawater cultures. *Limnol Oceanogr* 44, 1750–1762. doi: 10.4319/lo.1999.44.7.1750.

Lester, C. W., Wagner, T. J. W., McNamara, D. E., and Cape, M. R. (2021). The influence of meltwater on phytoplankton blooms near the sea-ice edge. *Geophys Res Lett* 48. doi: 10.1029/2020GL091758.

Liguori, B. T. P., Ehlert, C., and Pahnke, K. (2020). The influence of water mass mixing and particle dissolution on the silicon cycle in the Central Arctic Ocean. *Front Mar Sci* 7. doi: 10.3389/fmars.2020.00202.

Lin, H., Wang, C., Zhao, H., Chen, G., and Chen, X. (2020). A subcellular level study of copper speciation reveals the synergistic mechanism of microbial cells and EPS involved in copper binding in bacterial biofilms. *Environmental Pollution* 263, 114485. doi: 10.1016/j.envpol.2020.114485.

Little, S. H., Vance, D., Siddall, M., and Gasson, E. (2013). A modeling assessment of the role of reversible scavenging in controlling oceanic dissolved Cu and Zn distributions. *Global Biogeochem Cycles* 27, 780–791. doi: 10.1002/gbc.20073.

Little, S. H., Vance, D., Walker-Brown, C., and Landing, W. M. (2014). The oceanic mass balance of copper and zinc isotopes, investigated by analysis of their inputs, and outputs to ferromanganese oxide sediments. *Geochim Cosmochim Acta* 125, 673–693. doi: 10.1016/j.gca.2013.07.046.

Liu, X., and Millero, F. J. (1999). The solubility of iron hydroxide in sodium chloride solutions. *Geochim Cosmochim Acta* 63, 3487–3497. doi: 10.1016/S0016-7037(99)00270-7.

Liu, X., and Millero, F. J. (2002). The solubility of iron in seawater. *Mar Chem* 77, 43–54. doi: 10.1016/S0304-4203(01)00074-3.

Lombardi, A. T., Hidalgo, T. M. R., and Vieira, A. A. H. (2005). Copper complexing properties of dissolved organic materials exuded by the freshwater microalgae Scenedesmus acuminatus (Chlorophyceae). *Chemosphere* 60, 453–459. doi: 10.1016/j.chemosphere.2004.12.071.

López, A., Rico, M., Santana-Casiano, J. M., González, A. G., and González-Dávila, M. (2015). Phenolic profile of Dunaliella tertiolecta growing under high levels of copper and iron. *Environmental Science and Pollution Research* 22, 14820–14828. doi: 10.1007/s11356-015-4717-y.

López-García, P., Gelado-Caballero, M. D., Patey, M. D., and Hernández-Brito, J. J. (2021). Atmospheric fluxes of soluble nutrients and Fe: More than three years of wet and dry deposition measurements at Gran Canaria (Canary Islands). *Atmos Environ* 246, 118090. doi: 10.1016/j.atmosenv.2020.118090.

Lorenzo, J. I., Nieto-Cid, M., Álvarez-Salgado, X. A., Pérez, P., and Beiras, R. (2007). Contrasting complexing capacity of dissolved organic matter produced during the onset, development and decay of a simulated bloom of the marine diatom Skeletonema costatum. *Mar Chem* 103, 61–75. doi: 10.1016/j.marchem.2006.05.009.

Maldonado, M., and Price, N. (1996). Influence of N substrate on Fe requirements of marine centric diatoms. *Mar Ecol Prog Ser* 141, 161–172. doi: 10.3354/meps141161.

Maldonado, M. T., Allen, A. E., Chong, J. S., Lin, K., Leus, D., Karpenko, N., et al. (2006). Copper-dependent iron transport in coastal and oceanic diatoms. *Limnol Oceanogr* 51, 1729–1743. doi: 10.4319/lo.2006.51.4.1729.

Maldonado, M. T., and Price, N. M. (1999). Utilization of iron bound to strong organic ligands by plankton communities in the subarctic Pacific Ocean. *Deep Sea Res 2 Top Stud Oceanogr* 46, 2447–2473. doi: 10.1016/S0967-0645(99)00071-5

Martin, J. H. (1990). Glacial-interglacial CO_2 change: The Iron Hypothesis. *Paleoceanography* 5, 1–13. doi: 10.1029/PA005i001p00001.

Martin, J. H., and Fitzwater, S. E. (1988). Iron deficiency limits phytoplankton growth in the north-east Pacific subarctic. *Nature* 331, 341–343. doi: 10.1038/331341a0.

Martin, J. H., Gordon, R. M., and Fitzwater, S. E. (1990). Iron in Antarctic waters. *Nature* 345, 156–158. doi: 10.1038/345156a0.

McDonough, W. F., and Sun, S. S. (1995). The composition of the Earth. *Chem Geol* 120, 223–253. doi: 10.1016/0009-2541(94)00140-4.

McKnight, D. M., and Morel, F. M. M. (1980). Copper complexation by siderophores from filamentous blue-green algae. *Limnol Oceanogr* 25, 62–71. doi: 10.4319/lo.1980.25.1.0062.

Mehlmann, M., Quack, B., Atlas, E., Hepach, H., and Tegtmeier, S. (2020). Natural and anthropogenic sources of bromoform and dibromomethane in the oceanographic and biogeochemical regime of the subtropical North East

Atlantic. *Environ Sci Process Impacts* 22, 679–707. doi: 10.1039/C9EM00599D.

Meiners, K., Gradinger, R., Fehling, J., Civitarese, G., and Spindler, M. (2003). Vertical distribution of exopolymer particles in sea ice of the Fram Strait (Arctic) during autumn. *Mar Ecol Prog Ser* 248, 1–13. doi: 10.3354/meps248001.

Meire, L., Meire, P., Struyf, E., Krawczyk, D. W., Arendt, K. E., Yde, J. C., et al. (2016). High export of dissolved silica from the Greenland Ice Sheet. *Geophys Res Lett* 43, 9173–9182. doi: 10.1002/2016GL070191.

Mellett, T., and Buck, K. N. (2020). Spatial and temporal variability of trace metals (Fe, Cu, Mn, Zn, Co, Ni, Cd, Pb), iron and copper speciation, and electroactive Fe-binding humic substances in surface waters of the eastern Gulf of Mexico. *Mar Chem* 227, 103891. doi: 10.1016/j.marchem.2020.103891.

Middag, R., de Baar, H. J. W., Laan, P., and Klunder, M. B. (2011). Fluvial and hydrothermal input of manganese into the Arctic Ocean. *Geochim Cosmochim Acta* 75, 2393–2408. doi: 10.1016/j.gca.2011.02.011.

Middag, R., Zitoun, R., and Conway, T. (2023). "Trace Metals," in *Marine Analytical Chemistry* (Cham: Springer International Publishing), 103–198. doi: 10.1007/978-3-031-14486-8_3.

Miller, L. A., and Bruland, K. W. (1997). Competitive equilibration techniques for determining transition metal speciation in natural waters: Evaluation using model data. *Anal Chim Acta* 343, 161–181. doi: 10.1016/S0003-2670(96)00565-X.

Miller, W. L., King, D. W., Lin, J., and Kester, D. R. (1995). Photochemical redox cycling of iron in coastal seawater. *Mar Chem* 50, 63–77. doi: 10.1016/0304-4203(95)00027-O.

Millero, F. J. (1998). Solubility of Fe(III) in seawater. *Earth Planet Sci Lett* 154, 323–329. doi: 10.1016/S0012-821X(97)00179-9.

Millero, F. J. (2013). *Chemical Oceanogaphy*. 4th Edition. CRC Press.

Millero, F. J., and Hawke, D. J. (1992). Ionic interactions of divalent metals in natural waters. *Mar Chem* 40, 19–48. doi: 10.1016/0304-4203(92)90046-D.

Millero, F. J., Sotolongo, S., and Izaguirre, M. (1987). The oxidation kinetics of Fe(II) in seawater. *Geochim Cosmochim Acta* 51, 793–801. doi: 10.1016/0016-7037(87)90093-7.

Millero, F. J., Woosley, R., Ditrolio, B., and Waters, J. (2009). Effect of ocean acidification on the speciation of metals in seawater. 22, 72–85. doi: 10.2307/24861025.

Millero, F. J., Yao, W., and Aicher, J. (1995). The speciation of Fe(II) and Fe(III) in natural waters. *Mar Chem* 50, 21–39. doi: 10.1016/0304-4203(95)00024-L.

Mills, M. M., Ridame, C., Davey, M., La Roche, J., and Geider, R. J. (2005). Erratum: Iron and phosphorus co-limit nitrogen fixation in the eastern tropical North Atlantic. *Nature* 435, 232. doi: 10.1038/nature03632.

Moffett, J. W., and Dupont, C. (2007). Cu complexation by organic ligands in the sub-arctic NW Pacific and Bering Sea. *Deep-Sea Research I* 54, 586–595. doi: 10.1016/j.dsr.2006.12.013.

Moffett, J. W., and Zika, R. G. (1983). Oxidation kinetics of Cu(I) in seawater: implications for its existence in the marine environment. *Mar Chem* 13, 239–251. doi: 10.1016/0304-4203(83)90017-8.

Moffett, J. W., and Zika, R. G. (1987). "Photochemistry of Copper Complexes in Sea Water," in *Photochemistry of Environmental Aquatic Systems*, eds. R. G. Zika and W. J. Cooper, 116–130. doi: 10.1021/bk-1987-0327.ch009.

Moffett, J. W., Zika, R. G., and Brand, L. E. (1990). Distribution and potential sources and sinks of copper chelators in the Sargasso Sea. *Deep Sea Research Part A. Oceanographic Research Papers* 37, 27–36. doi: 0198-0149(90)90027-S.

Monteiro, P. M. S., and Orren, M. J. (1985). Trace metals in the Southern Ocean: on the geochemistry of copper. *Mar Chem* 15, 345–355. doi: 10.1016/0304-4203(85)90045-3.

Moore, C. M., Mills, M. M., Arrigo, K. R., Berman-Frank, I., Bopp, L., Boyd, P. W., et al. (2013). Processes and patterns of oceanic nutrient limitation. *Nat Geosci* 6, 701–710. doi: 10.1038/ngeo1765.

Moore, J. K., Doney, S. C., Glover, D. M., and Fung, I. Y. (2001). Iron cycling and nutrient-limitation patterns in surface waters of the world ocean. *Deep Sea Res 2 Top Stud Oceanogr* 49, 463–507. doi: 10.1016/S0967-0645(01)00109-6.

Morel, F. M. M., Kustka, A. B., and Shaked, Y. (2008). The role of unchelated Fe in the iron nutrition of phytoplankton. *Limnol Oceanogr* 53, 400–404. doi: 10.4319/lo.2008.53.1.0400.

Morel, F. M. M., and Price, N. M. (2003). The Biogeochemical Cycles of Trace Metals in the Oceans. *Science* 300, 944–947. doi: 10.1126/science.1083545.

Morel, N. M. L., Rueter, J. C., and Morel, F. M. M. (1978). Copper toxicity to Skeletonema Costatum (Bacillariophyceae) 1, 2. *J Phycol* 14, 43–48. doi: 10.1111/j.1529-8817.1978.tb00629.x.

Muller, F. L. L., and Batchelli, S. (2013). Copper binding by terrestrial versus marine organic ligands in the coastal plume of River Thurso, North Scotland. *Estuar Coast Shelf Sci* 133, 137–146. doi: 10.1016/j.ecss.2013.08.024.

Munin, A., and Edwards-Lévy, F. (2011). Encapsulation of natural polyphenolic compounds; a review. *Pharmaceutics* 3, 793–829. doi: 10.3390/pharmaceutics3040793.

Nguyen, H. T., Lee, Y. M., Hong, J. K., Hong, S., Chen, M., and Hur, J. (2022). Climate warming-driven changes in the flux of dissolved organic matter and its effects on bacterial communities in the Arctic Ocean: A review. *Front Mar Sci* 9. doi: 10.3389/fmars.2022.968583.

Nixon, R. L., Jackson, S. L., Cullen, J. T., and Ross, A. R. S. (2019). Distribution of copper-complexing ligands in Canadian Arctic waters as determined by immobilized copper(II)-ion affinity chromatography. *Mar Chem*, 103673. doi: 10.1016/j.marchem.2019.103673.

Norman, L., Worms, I. A. M., Angles, E., Bowie, A. R., Nichols, C. M., Ninh Pham, A., et al. (2015). The role of bacterial and algal exopolymeric substances in iron chemistry. *Mar Chem* 173, 148–161. doi: 10.1016/j.marchem.2015.03.015

Ober, S., Rijkenberg, M. J. A., and Gerringa, L. J. A. (2016). Physical oceanography measured on water bottle samples with ultra clean CTD/Water sampler-system during POLARSTERN cruise PS94 (ARK-XXIX/3). doi: 10.1594/PANGAEA.859561.

Oldham, V. E., Swenson, M. M., and Buck, K. N. (2014). Spatial variability of total dissolved copper and copper speciation in the inshore waters of Bermuda. *Mar Pollut Bull* 79, 314–320. doi: 10.1016/j.marpolbul.2013.12.016.

Omanović, D., Garnier, C., and Pižeta, I. (2015). ProMCC: An all-in-one tool for trace metal complexation studies. *Mar Chem* 173, 25–39. doi: 10.1016/j.marchem.2014.10.011.

Opsahl, S., Benner, R., and Amon, R. M. W. (1999). Major flux of terrigenous dissolved organic matter through the Arctic Ocean. *Limnol Oceanogr* 44, 2017–2023. doi: 10.4319/lo.1999.44.8.2017.

Paffrath, R., Laukert, G., Bauch, D., Rutgers van der Loeff, M., and Pahnke, K. (2021). Separating individual contributions of major Siberian rivers in the Transpolar Drift of the Arctic Ocean. *Sci Rep* 11, 8216. doi: 10.1038/s41598-021-86948-y.

Paulsen, M. L., Müller, O., Larsen, A., Møller, E. F., Middelboe, M., Sejr, M. K., et al. (2019). Biological transformation of Arctic dissolved organic matter in a NE Greenland fjord. *Limnol Oceanogr* 64, 1014–1033. doi: 10.1002/lno.11091.

Peers, G., Quesnel, S. A., and Price, N. M. (2005). Copper requirements for iron acquisition and growth of coastal and oceanic diatoms. *Limnol Oceanogr* 50, 1149–1158. doi: 10.4319/lo.2005.50.4.1149.

Pelegrí, J. L., Peña-Izquierdo, J., Machín, F., Meiners, C., and Presas-Navarro, C. (2017). "Oceanography of the Cape Verde Basin and Mauritanian Slope Waters," in *Deep-Sea Ecosystems Off Mauritania*, eds. A. Ramos, F. Ramil, and J. L. Sanz (Dordrecht: Springer Netherlands), 119–153. doi: 10.1007/978-94-024-1023-5_3.

Peña-Izquierdo, J., Pelegrí, J. L., Pastor, M. V., Castellanos, P., Emelianov, M., Gasser, M., et al. (2012). The continental slope current system between Cape Verde and the Canary Islands. *Sci Mar* 76, 65–78. doi: 10.3989/scimar.03607.18C.

Pérez-Almeida, N., González, A. G., Santana-Casiano, J. M., and González-Dávila, M. (2019). Iron and copper redox interactions in UV-seawater: A kinetic model approach. *Chem Geol* 506, 149–161. doi: 10.1016/j.chemgeo.2018.12.041.

Pérez-Almeida, N., González-Dávila, M., Santana-Casiano, J. M., González, A. G., and Suárez de Tangil, M. (2013). Oxidation of Cu(I) in Seawater at Low Oxygen Concentrations. *Environ Sci Technol* 47, 1239–1247. doi: 10.1021/es302465d.

Peterson, B. J., Holmes, R. M., McClelland, J. W., Vörösmarty, C. J., Lammers, R. B., Shiklomanov, A. I., et al. (2002). Increasing River Discharge to the Arctic Ocean. *Science* 298, 2171–2173. doi: 10.1126/science.1077445.

Pfirman, S. L., Kögeler, J. W., and Rigor, I. (1997). Potential for rapid transport of contaminants from the Kara Sea. *Science of The Total Environment* 202, 111–122. doi: 10.1016/S0048-9697(97)00108-3.

Pižeta, I., Sander, S. G., Hudson, R. J. M., Omanović, D., Baars, O., Barbeau, K. A., et al. (2015). Interpretation of complexometric titration data: An intercomparison of methods for estimating models of trace metal complexation

by natural organic ligands. *Mar Chem* 173, 3–24. doi: 10.1016/j.marchem.2015.03.006.

Planquette, H., Statham, P. J., Fones, G. R., Charette, M. A., Moore, C. M., Salter, I., et al. (2007). Dissolved iron in the vicinity of the Crozet Islands, Southern Ocean. *Deep Sea Research Part II: Topical Studies in Oceanography* 54, 1999–2019. doi: 10.1016/j.dsr2.2007.06.019.

Poorvin, L., Sander, S. G., Velasquez, I., Ibisanmi, E., LeCleir, G. R., and Wilhelm, S. W. (2011). A comparison of Fe bioavailability and binding of a catecholate siderophore with virus-mediated lysates from the marine bacterium Vibrio alginolyticus PWH3a. *J Exp Mar Biol Ecol* 399, 43–47. doi: 10.1016/j.jembe.2011.01.016.

Raapoto, H., Martinez, E., Petrenko, A., Doglioli, A., Gorgues, T., Sauzède, R., et al. (2019). Role of iron in the Marquesas Island mass effect. *J Geophys Res Oceans* 124, 7781–7796. doi: 10.1029/2019JC015275.

Rabe, B., Schauer, U., Ober, S., Horn, M., Hoppmann, M., Korhonen, M., et al. (2016). Physical oceanography during POLARSTERN cruise PS94 (ARK-XXIX/3). doi: 10.1594/PANGAEA.859558.

Rapp, I., Schlosser, C., Rusiecka, D., Gledhill, M., and Achterberg, E. P. (2017). Automated preconcentration of Fe, Zn, Cu, Ni, Cd, Pb, Co, and Mn in seawater with analysis using high-resolution sector field inductively-coupled plasma mass spectrometry. *Anal Chim Acta* 976, 1–13. doi: 10.1016/j.aca.2017.05.008.

Raven, J. A., Evans, M. C. W., and Korb, R. E. (1999). The role of trace metals in photosynthetic electron transport in O_2-evolving organisms. *Photosynth Res* 60, 111–150. doi: 10.1023/a:1006282714942.

Richon, C., and Tagliabue, A. (2019). Insights into the major processes driving the global distribution of copper in the ocean from a global model. *Global Biogeochem Cycles* 33, 1594–1610. doi: 10.1029/2019GB006280.

Rico, M., López, A., Santana-Casiano, J. M., González, A. G., and González-Dávila, M. (2013). Variability of the phenolic profile in the diatom Phaeodactylum tricornutum growing under copper and iron stress. *Limnol Oceanogr* 58, 144–152. doi: 10.4319/lo.2013.58.1.0144.

Riedel, A., Michel, C., and Gosselin, M. (2006). Seasonal study of sea-ice exopolymeric substances on the Mackenzie shelf: implications for transport of sea-ice bacteria and algae. *Aquatic microbial ecology* 45, 195–206.

Rignot, E., and Mouginot, J. (2012). Ice flow in Greenland for the International Polar Year 2008-2009. *Geophys Res Lett* 39, n/a-n/a. doi: 10.1029/2012GL051634.

Rijkenberg, M. J. A., de Baar, H. J. W., Bakker, K., Gerringa, L. J. A., Keijzer, E., Laan, M., et al. (2015). "PRISTINE", a new high volume sampler for ultraclean sampling of trace metals and isotopes. *Mar Chem* 177, 501–509. doi: 10.1016/j.marchem.2015.07.001.

Rijkenberg, M. J. A., Powell, C. F., Dall'Osto, M., Nielsdottir, M. C., Patey, M. D., Hill, P. G., et al. (2008). Changes in iron speciation following a Saharan dust event in the tropical North Atlantic Ocean. *Mar Chem* 110, 56–67. doi: 10.1016/j.marchem.2008.02.006.

Rijkenberg, M. J. A., Slagter, H. A., van der Loeff, M. R., van Ooijen, J., and Gerringa, L. J. A. (2018). Dissolved Fe in the deep and upper Arctic Ocean with a focus on Fe Limitation in the Nansen Basin. *Front Mar Sci* 5. doi: 10.3389/fmars.2018.00088.

Rijkenberg, M. J. A., Steigenberger, S., Powell, C. F., Haren, H., Patey, M. D., Baker, A. R., et al. (2012). Fluxes and distribution of dissolved iron in the eastern (sub-) tropical North Atlantic Ocean. *Global Biogeochem Cycles* 26. doi: 10.1029/2011GB004264.

Robinson, J., Popova, E. E., Srokosz, M. A., and Yool, A. (2016). A tale of three islands: Downstream natural iron fertilization in the Southern Ocean. *J Geophys Res Oceans* 121, 3350–3371. doi: 10.1002/2015JC011319.

Rose, A. L., and Waite, T. D. (2003). Effect of Dissolved Natural Organic Matter on the Kinetics of Ferrous Iron Oxygenation in Seawater. *Environ Sci Technol* 37, 4877–4886. doi: 10.1021/es034152g.

Roshan, S., and Wu, J. (2015). The distribution of dissolved copper in the tropical-subtropical north Atlantic across the GEOTRACES GA03 transect. *Mar Chem* 176, 189–198. doi: 10.1016/j.marchem.2015.09.006.

Ruacho, A., Bundy, R. M., Till, C. P., Roshan, S., Wu, J., and Barbeau, K. A. (2020). Organic dissolved copper speciation across the U.S. GEOTRACES equatorial Pacific zonal transect GP16. *Mar Chem* 225. doi: 10.1016/j.marchem.2020.103841.

Ruacho, A., Richon, C., Whitby, H., and Bundy, R. M. (2022). Sources, sinks, and cycling of dissolved organic copper binding ligands in the ocean. *Commun Earth Environ* 3, 263. doi: 10.1038/s43247-022-00597-1.

Rudels, B. (2012). Arctic Ocean circulation and variability – advection and external forcing encounter constraints and local processes. *Ocean Science* 8, 261–286. doi: 10.5194/os-8-261-2012.

Rudels, B. (2019). "Arctic Ocean Circulation," in *Encyclopedia of Ocean Sciences* (Elsevier), 262–277. doi: 10.1016/B978-0-12-409548-9.11209-6.

Rudels, B., Björk, G., Nilsson, J., Winsor, P., Lake, I., and Nohr, C. (2005). The interaction between waters from the Arctic Ocean and the Nordic Seas north of Fram Strait and along the East Greenland Current: results from the Arctic Ocean-02 Oden expedition. *Journal of Marine Systems* 55, 1–30. doi: 10.1016/j.jmarsys.2004.06.008.

Rue, E., and Bruland, K. (2001). Domoic acid binds iron and copper: a possible role for the toxin produced by the marine diatom Pseudo-nitzschia. *Mar Chem* 76, 127–134. doi: 10.1016/S0304-4203(01)00053-6.

Rue, E. L., and Bruland, K. W. (1995). Complexation of iron(III) by natural organic ligands in the Central North Pacific as determined by a new competitive ligand equilibration/adsorptive cathodic stripping voltammetric method. *Mar Chem* 50, 117–138. doi: 10.1016/0304-4203(95)00031-L.

Saager, P. M., de Baar, H. J. W., de Jong, J. T. M., Nolting, R. F., and Schijf, J. (1997). Hydrography and local sources of dissolved trace metals Mn, Ni, Cu, and Cd in the northeast Atlantic Ocean. *Mar Chem* 57, 195–216. doi: 10.1016/S0304-4203(97)00038-8.

Sakamoto, Y., Ishiguro, M., and Kitagawa, G. (1986). Akaike information criterion statistics. *Dordrecht, The Netherlands: D. Reidel* 81, 26853..

Samperio-Ramos, G., González-Dávila, M., and Santana-Casiano, J. M. (2018a). Impact on the Fe redox cycling of organic ligands released by *Synechococcus* PCC 7002, under different iron fertilization scenarios. Modeling approach. *Journal of Marine Systems* 182, 67–78. doi: 10.1016/j.jmarsys.2018.01.009.

Samperio-Ramos, G., Santana-Casiano, J. M., and González-Dávila, M. (2018b). Effect of organic Fe-ligands, released by *Emiliania huxleyi*, on Fe(II) oxidation rate in seawater under simulated ocean acidification conditions: A modeling approach. *Front Mar Sci* 5. doi: 10.3389/fmars.2018.00210.

Samperio-Ramos, G., Santana-Casiano, J. M., and González-Dávila, M. (2018c). Variability in the production of organic ligands, by Synechococcus PCC 7002, under different iron scenarios. *J Oceanogr* 74, 277–286. doi: 10.1007/s10872-017-0457-6.

Sander, S. G., and Koschinsky, A. (2011). Metal flux from hydrothermal vents increased by organic complexation. *Nat Geosci* 4, 145–150. doi: 10.1038/ngeo1088.

Sander, S. G., Koschinsky, A., Massoth, G., Stott, M., and Hunter, K. A. (2007). Organic complexation of copper in deep-sea hydrothermal vent systems. *Environmental Chemistry* 4, 81. doi: 10.1071/EN06086.

Sangrà, P., Pascual, A., Rodríguez-Santana, Á., Machín, F., Mason, E., McWilliams, J. C., et al. (2009). The Canary Eddy Corridor: A major pathway for long-lived eddies in the subtropical North Atlantic. *Deep Sea Research Part I: Oceanographic Research Papers* 56, 2100–2114. doi: 10.1016/j.dsr.2009.08.008.

Sangrà, P., Pelegrí, J. L., Hernández-Guerra, A., Arregui, I., Martín, J. M., Marrero-Díaz, A., et al. (2005). Life history of an anticyclonic eddy. *J Geophys Res Oceans* 110, 1–19. doi: 10.1029/2004JC002526.

Santana-Casiano, J. M., González-Dávila, M., González, A. G., and Millero, F. J. (2010). Fe(III) reduction in the presence of Catechol in seawater. *Aquat Geochem* 16, 467–482. doi: 10.1007/s10498-009-9088-x.

Santana-Casiano, J. M., González-Dávila, M., González, A. G., Rico, M., López, A., and Martel, A. (2014). Characterization of phenolic exudates from Phaeodactylum tricornutum and their effects on the chemistry of Fe(II)-Fe(III). *Mar Chem* 158, 10–16. doi: 10.1016/j.marchem.2013.11.001.

Santana-Casiano, J. M., González-Dávila, M., and Millero, F. J. (2005). Oxidation of nanomolar level of Fe(II) with oxygen in natural waters. *Environ Sci Technol* 39, 2073–2079. doi: 10.1021/es049748y.

Santana-Casiano, J. M., González-Dávila, M., Rodríguez, Ma. J., and Millero, F. J. (2000). The effect of organic compounds in the oxidation kinetics of Fe(II). *Mar Chem* 70, 211–222. doi: 10.1016/S0304-4203(00)00027-X.

Santana-Casiano, J. M., and Quack, B. (2021). Metal (iron and copper) complexation from water samples during POSEIDON cruise POS533 (AIMAC). *PANGAEA*. doi: 10.1594/PANGAEA.933690.

Sarthou, G., Bucciarelli, E., Chever, F., Hansard, S. P., González-Dávila, M., Santana-Casiano, J. M., et al. (2011). Labile Fe(II) concentrations in the Atlantic sector of the Southern Ocean along a transect from the subtropical domain to the Weddell Sea Gyre. *Biogeosciences* 8, 2461–2479. doi: 10.5194/bg-8-2461-2011.

Sato, M., Takeda, S., and Furuya, K. (2007). Iron regeneration and organic iron(III)-binding ligand production during in situ zooplankton grazing experiment. *Mar Chem* 106, 471–488. doi: 10.1016/j.marchem.2007.05.001.

Schaffer, J., von Appen, W. J., Dodd, P. A., Hofstede, C., Mayer, C., de Steur, L., et al. (2017). Warm water pathways toward Nioghalvfjerdsfjorden Glacier, Northeast Greenland. *Journal of Geophysical Research: Oceans RESEARCH* 122, 4004–4020. doi: 10.1002/2016JC012462.

Schauer, U. (2004). Arctic warming through the Fram Strait: Oceanic heat transport from 3 years of measurements. *J Geophys Res* 109, C06026. doi: 10.1029/2003JC001823.

Schauer, U. (2016). The Expedition PS94 of the Research Vessel POLARSTERN to the central Arctic Ocean in 2015. *Berichte zur Polar-und Meeresforschung= Reports on polar and marine research* 703. doi: http://doi.org/10.2312/BzPM_0703_2016.

Schlosser, P., Kromer, B., Ekwurzel, B., Bönisch, G., McNichol, A., Schneider, R., et al. (1997). The first trans-Arctic 14C section: comparison of the mean ages of the deep waters in the Eurasian and Canadian basins of the Arctic Ocean. *Nucl Instrum Methods Phys Res B* 123, 431–437. doi: 10.1016/S0168-583X(96)00677-5.

Schuur, E. A. G., Abbott, B. W., Bowden, W. B., Brovkin, V., Camill, P., Canadell, J. G., et al. (2013). Expert assessment of vulnerability of permafrost carbon to climate change. *Clim Change* 119, 359–374. doi: 10.1007/s10584-013-0730-7.

Schuur, E. A. G., McGuire, A. D., Schädel, C., Grosse, G., Harden, J. W., Hayes, D. J., et al. (2015). Climate change and the permafrost carbon feedback. *Nature* 520, 171–179. doi: 10.1038/nature14338.

Semeniuk, D. M., Bundy, R. M., Payne, C. D., Barbeau, K. A., and Maldonado, M. T. (2015). Acquisition of organically complexed copper by marine phytoplankton and bacteria in the northeast subarctic Pacific Ocean. *Mar Chem* 173, 222–233. doi: 10.1016/j.marchem.2015.01.005.

Semeniuk, D. M., Cullen, J. T., Johnson, W. K., Gagnon, K., Ruth, T. J., and Maldonado, M. T. (2009). Plankton copper requirements and uptake in the subarctic Northeast Pacific Ocean. *Deep Sea Research Part I: Oceanographic Research Papers* 56, 1130–1142. doi: 10.1016/j.dsr.2009.03.003.

Shank, G. C., Skrabal, S. A., Whitehead, R. F., and Kieber, R. J. (2004). Strong copper complexation in an organic-rich estuary: the importance of

allochthonous dissolved organic matter. *Mar Chem* 88, 21–39. doi: 10.1016/j.marchem.2004.03.001.

Shank, G. C., Whitehead, R. F., Smith, M. L., Skrabal, S. A., and Kieber, R. J. (2006). Photodegradation of strong copper-complexing ligands in organic-rich estuarine waters. *Limnol Oceanogr* 51, 884–892. doi: 10.4319/lo.2006.51.2.0884.

Sholkovitz, E. R. (1978). The flocculation of dissolved Fe, Mn, Al, Cu, Ni, Co and Cd during estuarine mixing. *Earth Planet Sci Lett* 41, 77–86. doi: 10.1016/0012-821X(78)90043-2.

Slagter, H. A., Laglera, L. M., Sukekava, C., and Gerringa, L. J. A. (2019). Fe-binding organic ligands in the humic-rich Transpolar Drift in the surface Arctic Ocean using multiple voltammetric methods. *J Geophys Res Oceans* 124, 1491–1508. doi: 10.1029/2018JC014576.

Slagter, H. A., Reader, H. E., Rijkenberg, M. J. A., Rutgers van der Loeff, M., de Baar, H. J. W., and Gerringa, L. J. A. (2017). Organic Fe speciation in the Eurasian Basins of the Arctic Ocean and its relation to terrestrial DOM. *Mar Chem* 197, 11–25. doi: 10.1016/j.marchem.2017.10.005.

Søndergaard, J., and Mosbech, A. (2022). Mining pollution in Greenland - the lesson learned: A review of 50 years of environmental studies and monitoring. *Science of The Total Environment* 812, 152373. doi: 10.1016/j.scitotenv.2021.152373.

Stedmon, C. A., Amon, R. M. W., Rinehart, A. J., and Walker, S. A. (2011). The supply and characteristics of colored dissolved organic matter (CDOM) in the Arctic Ocean: Pan Arctic trends and differences. *Mar Chem* 124, 108–118. doi: 10.1016/j.marchem.2010.12.007.

Stockdale, A., Tipping, E., Lofts, S., and Mortimer, R. J. G. (2016). Effect of Ocean Acidification on Organic and Inorganic Speciation of Trace Metals. *Environ Sci Technol* 50, 1906–1913. doi: 10.1021/acs.est.5b05624.

Sunda, W. G. (1989). Trace metal interactions with marine phytoplankton. *Biological Oceanography* 6, 411–442.

Sunda, W. G., and Lewis, J. A. M. (1978). Effect of complexation by natural organic ligands on the toxicity of copper to a unicellular alga, Monochrysis lutheri. *Limnol Oceanogr* 23, 870–876. doi: 10.4319/lo.1978.23.5.0870.

Sutak, R., Camadro, J.-M., and Lesuisse, E. (2020). Iron uptake mechanisms in marine phytoplankton. *Front Microbiol* 11. doi: 10.3389/fmicb.2020.566691.

Tagliabue, A., Bopp, L., Dutay, J. C., Bowie, A. R., Chever, F., Jean-Baptiste, P., et al. (2010). Hydrothermal contribution to the oceanic dissolved iron inventory. *Nat Geosci* 3, 252–256. doi: 10.1038/ngeo818.

Tagliabue, A., Bowie, A. R., Boyd, P. W., Buck, K. N., Johnson, K. S., and Saito, M. A. (2017). The integral role of iron in ocean biogeochemistry. *Nature* 543, 51–59. doi: 10.1038/nature21058.

Tang, D., Hung, C.-C., Warnken, K. W., and Santschi, P. H. (2000). The distribution of biogenic thiols in surface waters of Galveston Bay. *Limnol Oceanogr* 45, 1289–1297. doi: 10.4319/lo.2000.45.6.1289.

Thomas, D. N., Lara, R. J., Hajo, E., Kattner, G., Skoog, A., and Skoog Alfred Wegener, A. (1995). Dissolved organic matter in Arctic multi-year sea ice during winter: major components and relationship to ice characteristics. *Polar Biol* 15, 477–483. doi: 10.1007/BF00237461.

Thuróczy, C. E., Gerringa, L. J. A., Klunder, M. B., Laan, P., and de Baar, H. J. W. (2011a). Observation of consistent trends in the organic complexation of dissolved iron in the Atlantic sector of the Southern Ocean. *Deep Sea Res 2 Top Stud Oceanogr* 58, 2695–2706. doi: 10.1016/j.dsr2.2011.01.002..

Thuróczy, C. E., Gerringa, L. J. A., Klunder, M., Laan, P., Le Guitton, M., and de Baar, H. J. W. (2011b). Distinct trends in the speciation of iron between the shallow shelf seas and the deep basins of the Arctic Ocean. *J Geophys Res* 116, C10009. doi: 10.1029/2010JC006835.

Thuróczy, C.E., Gerringa, L. J. A., Klunder, M. B., Middag, R., Laan, P., Timmermans, K. R., et al. (2010). Speciation of Fe in the Eastern North Atlantic Ocean. *Deep Sea Research Part I: Oceanographic Research Papers* 57, 1444–1453. doi: 10.1016/j.dsr.2010.08.004.

Tomczak, M., and Godfrey, J. S. (2001). "Arctic oceanography; the path of North Atlantic Deep Water," in *Regional Oceanography: An Introduction*, eds. M. Tomczak and J. S. Godfrey, 83–103.

Tovar-Sánchez, A., Duarte, C. M., Alonso, J. C., Lacorte, S., Tauler, R., and Galbán-Malagón, C. (2010). Impacts of metals and nutrients released from melting multiyear Arctic sea ice. *J Geophys Res* 115, C07003. doi: 10.1029/2009JC005685.

Tuerena, R. E., Hopkins, J., Buchanan, P. J., Ganeshram, R. S., Norman, L., Appen, W., et al. (2021). An Arctic strait of two halves: the changing dynamics of nutrient uptake and limitation across the Fram Strait. *Global Biogeochem Cycles* 35. doi: 10.1029/2021GB006961.

Twining, B. S., and Baines, S. B. (2013). The Trace Metal Composition of Marine Phytoplankton. *Ann Rev Mar Sci* 5, 191–215. doi: 10.1146/annurev-marine-121211-172322.

Uhlig, C., Damm, E., Peeken, I., Krumpen, T., Rabe, B., Korhonen, M., et al. (2019). Sea ice and water mass influence dimethylsulfide concentrations in the central Arctic Ocean. *Front Earth Sci* 7. doi: 10.3389/feart.2019.00179.

van den Berg, C. M. G. (1982). Determination of copper complexation with natural organic ligands in seawater by equilibration with MnO_2 II. Experimental procedures and application to surface seawater. *Mar Chem* 11, 323–342. doi: 10.1016/0304-4203(82)90029-9.

van den Berg, C. M. G., Merks, A. G. A., and Duursma, E. K. (1987). Organic complexation and its control of the dissolved concentrations of copper and zinc in the Scheldt estuary. *Estuar Coast Shelf Sci* 24, 785–797.

van Ooijen, J. C., Rijkenberg, M. J. A., Gerringa, L. J. A., Rabe, B., and Rutgers van der Loeff, M. M. (2016). Inorganic nutrients measured on water bottle samples during POLARSTERN cruise PS94 (ARK-XXIX/3). doi: 10.1594/PANGAEA.868396.

Vernet, M., Ellingsen, I. H., Seuthe, L., Slagstad, D., Cape, M. R., and Matrai, P. A. (2019). influence of phytoplankton advection on the productivity along the Atlantic Water inflow to the Arctic Ocean. *Front Mar Sci* 6. doi: 10.3389/fmars.2019.00583.

Veron, S., Mouchet, M., Govaerts, R., Haevermans, T., and Pellens, R. (2019). Vulnerability to climate change of islands worldwide and its impact on the tree of life. *Sci Rep* 9, 14471. doi: 10.1038/s41598-019-51107-x.

Völker, C., and Tagliabue, A. (2015). Modeling organic iron-binding ligands in a three-dimensional biogeochemical ocean model. *Mar Chem* 173, 67–77. doi: 10.1016/j.marchem.2014.11.008.

Vraspir, J. M., and Butler, A. (2009). Chemistry of Marine Ligands and Siderophores. *Ann Rev Mar Sci* 1, 43–63. doi: 10.1146/annurev.marine.010908.163712.

Waite, T. David., and Morel, F. M. M. (1984). Photoreductive dissolution of colloidal iron oxides in natural waters. *Environ Sci Technol* 18, 860–868. doi: 10.1021/es00129a010.

Walsh, M. J., and Ahner, B. A. (2013). Determination of stability constants of Cu(I), Cd(II) & Zn(II) complexes with thiols using fluorescent probes. *J Inorg Biochem* 128, 112–123. doi: 10.1016/j.jinorgbio.2013.07.012.

Walsh, M. J., Goodnow, S. D., Vezeau, G. E., Richter, L. V., and Ahner, B. A. (2015). Cysteine enhances bioavailability of copper to marine phytoplankton. *Environ Sci Technol* 49, 12145–12152. doi: 10.1021/acs.est.5b02112.

Wang, Q., Wekerle, C., Wang, X., Danilov, S., Koldunov, N., Sein, D., et al. (2020). Intensification of the Atlantic water supply to the Arctic Ocean through Fram Strait induced by Arctic sea ice decline. *Geophys Res Lett* 47. doi: 10.1029/2019GL086682.

Wells, M. L., and Mayer, L. M. (1991). Variations in the chemical lability of iron in estuarine, coastal and shelf waters and its implications for phytoplankton. *Mar Chem* 32, 195–210. doi: 10.1016/0304-4203(91)90038-X.

Whitby, H., Hollibaugh, J. T., and van den Berg, C. M. G. (2017). Chemical Speciation of Copper in a Salt Marsh Estuary and Bioavailability to Thaumarchaeota. *Front Mar Sci* 4. doi: 10.3389/fmars.2017.00178.

Whitby, H., Posacka, A. M., Maldonado, M. T., and van den Berg, C. M. G. (2018). Copper-binding ligands in the NE Pacific. *Mar Chem* 204, 36–48. doi: 10.1016/j.marchem.2018.05.008.

Whitby, H., and van den Berg, C. M. G. (2015). Evidence for copper-binding humic substances in seawater. *Mar Chem* 173, 282–290. doi: 10.1016/j.marchem.2014.09.011.

Williford, T., Amon, R. M. W., Kaiser, K., Benner, R., Stedmon, C., Bauch, D., et al. (2022). Spatial complexity in dissolved organic matter and trace elements driven by hydrography and freshwater input across the Arctic Ocean during 2015 Arctic GEOTRACES expeditions. *J Geophys Res Oceans* 127. doi: 10.1029/2022JC018917.

Wilson, N., Straneo, F., and Heimbach, P. (2017). Satellite-derived submarine melt rates and mass balance (2011–2015) for Greenland's largest remaining ice tongues. *Cryosphere* 11, 2773–2782. doi: 10.5194/tc-11-2773-2017.

Wisotzki, A., and Bakker, K. (2008). "Hydrochemistry measured on water bottle samples during POLARSTERN cruise ARK-XXII/2," in (PANGAEA). doi: 10.1594/PANGAEA.759286.

Witter, A. E., Hutchins, D. A., Butler, A., and Luther, G. W. (2000). Determination of conditional stability constants and kinetic constants for strong model Fe-

binding ligands in seawater. *Mar Chem* 69, 1–17. doi: 10.1016/S0304-4203(99)00087-0.

Wiwit, Wong, K. H., Fukuda, H., Ogawa, H., Mashio, A. S., Kondo, Y., et al. (2021). Wide-range detection of Cu-binding organic ligands in seawater using reverse titration. *Mar Chem* 230, 103927. doi: 10.1016/j.marchem.2021.103927.

Wolfe-Simon, F., Grzebyk, D., Schofield, O., and Falkowski, P. G. (2005). The role and evolution of superoxide dismutases in algae. *J Phycol* 41, 453–465. doi: 10.1111/j.1529-8817.2005.00086.x.

Wong, K. H., Obata, H., Kim, T., Kondo, Y., and Nishioka, J. (2021). New insights into the biogeochemical cycling of copper in the subarctic Pacific: Distributions, size fractionation, and organic complexation. *Limnol Oceanogr* 66, 1424–1439. doi: 10.1002/lno.11695.

Wu, J., Boyle, E., Sunda, W., and Wen, L.S. (2001). Soluble and colloidal iron in the oligotrophic North Atlantic and North Pacific. *Science* 293, 847–849. doi: 10.1126/science.1059251.

Zabłocka, M., Kowalczuk, P., Meler, J., Peeken, I., Dragańska-Deja, K., and Winogradow, A. (2020). Compositional differences of fluorescent dissolved organic matter in Arctic Ocean spring sea ice and surface waters north of Svalbard. *Mar Chem* 227, 103893. doi: 10.1016/j.marchem.2020.103893.

Zika, R. G. (1981). “Chapter 10 Marine Organic Photochemistry,” in *Marine Organic Chemistry Evolution, Composition, Interactions and Chemistry of Organic Matter in Seawater*, eds. E. K. Duursma and R. Dawson, 299–325. doi: 10.1016/S0422-9894(08)70332-5.

Zirino, A., and Yamamoto, S. (1972). A pH-dependent model for the chemical speciation of copper, zind, cadmium, and lead in seawater. *Limnol Oceanogr* 17, 661–671. doi: 10.4319/lo.1972.17.5.0661.

Zuehlke, R. W., and Kester, D. R. (1983). “Copper Speciation in Marine Waters,” in *Trace Metals in Sea Water* (Boston, MA: Springer US), 773–788. doi: 10.1007/978-1-4757-6864-0_42.